NATIONAL
SCIENCE
FOUNDATION

Journal
of the
National Science Foundation
of Sri Lanka

www.nsf.gov.lk

C O N T E N T S

Guidelines for Contributors

Cover: Rediscovered *Hedyotis quinquinervia* plant from Mount Thotupola, Sri Lanka.
Left (top) - terminal inflorescence with each floret having four white petals; Left (bottom) - brownish ellipsoidal capsules arranged in fruit; Right (top and bottom) - compactly arranged curved leaves on a woody shrub.
See *J.Natn.Sci.Foundation Sri Lanka 2023 51 (3): 505 - 517*

EDITORIAL

The value of a modern science museum

The modern science museum is not merely a collection of historical artefacts and exhibits from the natural world depicting physical, chemical and biological phenomena. It is also a science center, which creates a space for learning about and understanding science mainly through interactive exhibits. Working with interactive exhibits can play an important role in the educational process of young people interested in science. It can provide an opportunity to actively engage in making observations, analyze information and draw conclusions, in an enjoyable setting. The incorporation of these ideas in science education is reflected in the commonly used phrases, "learning science by doing science" and "science is fun".

At a time when developing an educational system relevant for Sri Lanka in the 21st century is being discussed at various levels of policy making, undue importance is given sometimes to changing syllabi and course contents. In keeping with world-wide trends, a more important aspect of reforms should be to shift the focus from curriculum-based teacher directed education, to one that is curiosity driven, student centred active learning, particularly in the early years. In catalyzing this shift, the access to modern science museums can play a major role. It will be difficult for a school to provide children with the experience they can have in a science centre functioning within a science museum. In addition to exhibits, the museum will provide for an information system including a library and also other resources such as an auditorium for public lectures, films and demonstrations. The learning experience in a science museum is often a social experience, shared by family, friends and other visitors to the museum.

Thus, science museums will also serve to spread scientific knowledge and the culture of science among the general population which will help in creating an informed population, better able to take rational decisions on issues facing society.

Ajit Abeysekera

RESEARCH ARTICLE

Plant Microbiology

Probiotic potential of bacterial endophytes isolated from leaves of *Murraya koenigii* L.

AC Bandara[1*], CL Abayasekara[1], AM Karunaratne[1] and GJ Panagoda[2]

[1] *Department of Botany, Faculty of Science, University of Peradeniya, Peradeniya, Sri Lanka.*
[2] *Division of Microbiology, Department of Oral Medicine and Periodontology, Faculty of Dental Sciences, University of Peradeniya, Peradeniya, Sri Lanka.*

Abstract: Probiotics are live microorganisms which confer health benefits to the host when administered in adequate amounts. Endophytes, which live in plant tissues between the plant cells, can act as potential probiotic bacteria. The leaves of *Murraya koenigii* L. is a common cuisine and herbal ingredient used in indigenous medicine. The main objective of the current study was to assess probiotic characteristics of isolated bacterial endophytes of *M. koenigii* leaves. Young and mature leaves of *M. koenigii* were collected from sites in the wet and dry zones of Sri Lanka. The endophytes were isolated using three techniques: placing leaf segments, leaf macerations and preparation of pour plates on three different media *viz*., nutrient agar, Luria-Bertani (LB), and De Man, Rogosa and Sharpe agar (MRS). They were identified from morphological characteristics and preliminary biochemical tests. Probiotic characterization of the isolates was carried out by using a series of standard tests including resistance to low pH, tolerance of bile salts, antimicrobial activity (*Escherichia coli* and *Pseudomonas aeruginosa*), antibiotic resistance (Gentamycine), anti-haemolytic activity, and non-DNase activity. Ten endophytic bacteria (two bacilli, eight cocci including two Gram positive cocci, and eight Gram negative cocci and bacilli) were isolated from the young and mature leaf samples collected. While probiotic characterization tests were positive, four isolates showed antibiotic susceptibility. These results indicate the possibility that *M. koenigii* leaves possess bacterial endophytes with probiotic potential.

Keywords: Antibiotic resistance, antimicrobial activity, endophytes, *Murraya koenigii* L., probiotics.

INTRODUCTION

Probiotics have been referred to as 'live microorganisms, which when administered in adequate amounts confer a health benefit on the host' (Shuhadha *et al.*, 2017). Probiotic bacteria can be broadly categorized as plant probiotics and human probiotics depending on their potential host (Oh, 2017), and this study focuses mainly on human probiotics. Human probiotics are mostly Gram-positive microorganisms, which comprise a wide range of the genera *Lactobacillus*, *Bifidobacterium* and *Enterococcus*, including the mostly studied species *Lactobacillus acidophilus, L. casei* group, *L. reuteri/, L. fermentum, Bifidobacterium* spp. (*B. animalis*) and *Enterococcus faecium* (Holzapfel *et al.*, 2015; Shuhadha *et al.*, 2017).

However, there are a few gram-negative bacteria that are considered as probiotics, *viz: Escherichia coli* strain Nissle 1917, *Bacteroides fragilis*, and *Akkermansia muciniphila* (Bhensen *et al.*, 2013; Wang *et al.*, 2017; Zhai *et al.*, 2018).

The most important criteria for a probiotic are that it should have a history of being non-pathogenic, not being associated with diseases such as infective endocarditis or gastrointestinal disorders, ability to survive passage through the digestive tract by exhibiting acid and bile tolerance, ability to proliferate in the gut, and ability to exert their benefits on the host through growth and/or activity in the human body (Kimoto *et al.*, 2004; Pineiro & Stanton, 2007). Probiotic characterization is done by considering the major characters of probiotics in the human gastrointestinal tract. Being of human origin, the major criteria considered for probiotic characterization are antimicrobial activity against pathogenic bacteria, acid tolerance, bile salt

* Corresponding author (adheeshachamodini@gmail.com; https://orcid.org/0009-0009-6379-1405)

tolerance, resistance to antibiotic compounds, anti- haemolytic activity, anti- hydrolysing of DNA, adherence to human epithelial cells, and persistence in the human gastrointestinal tract (Shuhadha *et al.*, 2017). Auto-aggregation, hydrophobicity, cholesterol removal, and conjugated linoleic acid (CLA) conversion are some additional probiotic characterization tests (Alkalbani *et al.*, 2019)

However, among these criteria, being of human origin has not been a highly required character to be a probiotic because there are probiotics of dairy and plant, which serve as efficient and safe probiotics in humans (Da Sesto, 2008).

Of the microorganisms associated with plants, endophytes are a variety of bacteria and fungi that reside inside the internal tissues of living plants (collectively known as endophytic microorganisms), which do not cause any symptoms and obvious harm to the host plants (Yiing & Ting, 2015). Most of the probiotics extracted from plants live as endophytes though a very few species live as epiphytes and rhizobacteria that are inhabitants of the rhizosphere (Ruiza *et al.*, 2011). These plant endophytic probiotics synthesize bioactive compounds, which improve stress tolerance of plants and their medicinal potential (Anand 2023).

Murraya koenigii L. or curry leaf plant [Karapincha (Sinhala), Karuvapillai (Tamil)] of the family Rutaceae is a small deciduous tree with highly pungent aromatic leaves and characteristic taste (Yankuzo *et al.*, 2011). The plant is recorded to have various ethnobotanical, pharmacognostic, phytochemical and pharmacological properties (Gahlawat *et al.*, 2014). A scrutiny of specific literature reveals some notable pharmacological activities of the plant such as on the heart through cholesterol reducing properties, and in addition it is recorded to have antimicrobial activity, and anti-cancer activity (Balakrishnan *et al.*, 2020). Its medicinal values include, antioxidative properties, cytotoxic and anti-diarrhoea activity (Chaudhary, 2020; Rautela & Katiyar, 2023), and additionally it is considered to be anti-diabetic (Habbu *et al.*, 2014). The plant possess various health beneficial properties due to the presence of secondary metabolites such as polyphenols (reduce oxidative stress and prevent degenerative diseases such as cardiovascular disease and cancers), flavonoids (regulation of cholesterol levels), flavonoid compounds such as myricetin, quercetin and epicatechin (effective in the growth inhibition of breast cancer cells), minerals (maintenance of normoglycemia or normal glucose content of blood), and antioxidants as well as presence of beneficial probiotic endophytic microorganisms (Abeysinghe *et al.*, 2021). It has been found that the leaves, stems and roots of *M. koenigii* L. have both bacterial and fungal endophytes including endophytic Bacilli (Khan et *al.*, 2022). Fungal endophytes isolated from *M. koenigii* L. includes *Aspergillus niger, Aspergillus flavus, Candida albicans, Penicillium sublateritium* and *Phoma hedericola* (Soundappan *et al.*, 2018). Since *M. koenigii* has various medicinal properties viz., anti- cancer, anti- diabetic ability etc., the presence of potential probiotic endophytes in *M. koenigii* leaves would be an added feature that could be exploited either for the leaves to be consumed raw (paste) or produce probiotics as a commercial product. Therefore, the objectives of the current study were to isolate bacterial endophytes from leaves of *M. koenigii* and to investigate their probiotic potential.

MATERIALS AND METHODS

Sample collection

Samples of leaves were collected from Gampaha, Kandy and Jaffna districts covering the wet and dry zones in Sri Lanka, for the isolation of endophytic bacteria. Young and mature leaves were used separately for testing. Young leaves and mature leaves were distinguished as young leaves with pale green colour occurred at the distal end of the branch while mature leaves with dark green colour located below the distal end of branches.

Surface sterilization of leaves

The leaves were sterilized by washing with running tap water, followed by soaking in 70% ethanol for 30 s, and sodium hypochlorite solution (5 %) for 3 min, and finally rinsing thrice with distilled water (Habbu *et al.*, 2014).

Isolation of endophytic bacteria from leaves of *M. koenigii*

The bacteria were isolated by placing cut leaf sections (1 cm²) on the solid medium (Mohamad *et al*., 2020), placing leaf macerations on the solid medium (Habbu *et al*., 2014), and preparing pour plates with leaf extract (Costa *et al*., 2012). nutrient agar (NA), Lauria-Bertani (LB) and de Man, Rogosa and Sharpe (MRS) media were used for isolation of non-fastidious endophytes, endophytic bacteria belonging to the family Enterobacteraceae, and bacterial endophytes of the genus *Lactobacillus*, respectively.

Preliminary identification and characterization of pure cultures

Morphological identification of isolated bacterial endophytes was carried out by Gram staining and endospore staining, followed by motility test and catalase test for biochemical identification (Cullimore, 2019).

Gram staining

Bacterial smears were prepared on clean microscopic slides. The heat fixed smear was then flooded with crystal violet (primary stain) and allowed to stand for 1 min. Then the excess dye was removed and the smear was flooded with Gram's iodine solution, and allowed to stand for 1 min. The smear was again washed with running tap water and dipped in 95% ethanol until the smear became decolorized. The smear was then flooded with safranin (secondary stain) and allowed to stand for 1 min. The slide was again washed with running tap water to remove excess stain and observed under the microscope using an oil immersion lens.

Endospore staining

Bacterial smears were prepared on clean microscope slides, malachite green (primary stain) was applied, and heatfixed with a steam bath. The slides were then removed from the flame, cooled, and rinsed with running tap water to decolorize bacterial cells. The slides were flooded with the counter stain (safranin) for 30 s and rinsed with water. Subsequently, the slide was air dried and observed under the light microscope.

Motility test

The hanging drop method was used to determine the motility of bacterial isolates. Using the inoculating loop a small drop of the bacterial sub culture was aseptically placed in the centre of a clean coverslip. The cavity slide was lowered, with the concavity facing down, onto the coverslip to allow the drop to protrude into the centre of the concavity of the slide. It was pressed gently to form a seal. The drop was examined under the light microscope.

Catalase test

A drop of sterile distilled water was placed on the middle of a glass slide and a small amount of the culture was picked up with a sterile inoculating loop. One or two colonies were emulsified on each drop to make a smooth suspension. Then, one drop of 3% peroxide was placed over the test smear using a Pasteur pipette. The smears were observed for rapid gas bubble formation.

Probiotic characterization of endophytic bacteria

Determination of resistance of bacterial isolates to low pH

The resistance of bacterial isolates to low pH was determined using three methods. In the first method, the pH of the nutrient broth was adjusted to pH 3. In the fasted state, the median gastric pH is 1.7 and when the meal is administered the gastric pH climbs briefly to a median peak value of 6.7 (Dressman *et al*., 1990). PH was adjusted to 3 in the current experiment as a middle value between these two states. The survival rate of each bacterial isolate was measured by enumeration of bacterial colonies on nutrient agar (NA) plates at hourly intervals, up to 6 h (Both *et al*., 2010). In the second method, spread plates were prepared on NA plates which were

adjusted to pH 3 and the survival rate was measured by enumeration of bacterial colonies on NA plates at hourly intervals up to 6 h. In the third method, a mixture of cooked rice, saliva and leaf macerations of *Murraya koenigii* L. was added to normal nutrient broth, adjusted to pH 3. The survival rate of bacterial isolates was measured by determining the absorbance of each broth inoculated with bacteria culture, using UV-VIS spectrophotometer (Camspec M02, Spectronic Campsec Ltd., UK).

Determination of bile salt tolerance of bacterial isolates

One milliliter of each overnight culture, which was adjusted similar to McFarland 0.5 turbidity were aseptically transferred to 10 mL of 0.3% bile containing broth, and streak plates were prepared on NA plates at hourly intervals for 4 h (Bassyouni *et al*., 2012). Semi-quantitative screening streak method was used to prepare streak plates to obtain isolated colonies (Furgason *et al*., 1995; Croxatto *et al*., 2015). Plates were incubated at 37 °C for 24 h.

Determination of antimicrobial activity of bacterial isolates

Antimicrobial activity of the bacterial strains was determined using the disc diffusion method on Muller Hinton agar (MHA) against the pathogenic strains of *Pseudomonas aeruginosa* and *Escherichia coli*. The pathogenic strains, which were adjusted similar to McFarland 0.5 turbidity, were inoculated on MHA plates using sterilized cotton swabs. Sterile filter paper discs of 9 mm diameter were dipped in fresh overnight cultures of endophytic bacterial isolates and placed on the surface of an agar plate. The petri plates were kept at 4 °C for 30 min to permit diffusion on the assay material, and incubated at 37 °C for 24 h, and the zone of inhibition was measured in millimetres. The assay was repeated 3 times. Discs dipped in sterile distilled water and gentamycin discs (10 mg) served as negative and positive controls respectively (Abeysinghe *et al*., 2021).

Determination of antibiotic resistance

Fresh overnight endophytic bacterial cultures, which were adjusted similar to McFarland 0.5 turbidity were spread evenly on the surface of MHA plates using sterile cotton swabs. One Petri plate was used for spreading one endophytic bacterial isolate and each Petri plate was divided into two equal halves. In one half, a 6 mm diameter Gentamicin disc (10 mg/mL) was placed, and in other half, a filter paper impregnated with distilled water was placed that served as the negative control. The plates were then incubated at 37 °C for 24 h, and the diameter of the zone of inhibition was measured (Fallah *et al*., 2013).

Determination of haemolytic activity of bacterial isolates

Haemolytic activity of endophytic bacterial isolates was tested using blood agar base with 10% human blood. A loop full of each fresh overnight culture was aseptically transferred to the blood agar plates separately and incubated at 37 °C for 24 h. After incubation, agar plates were observed for clear zones around the colonies. Freshly subcultured *Streptococcus* sp. was used as the positive control and *Lactobacillus* sp. was used as the negative control (Bassyouni *et al*., 2012).

Determination of DNAse activity of bacterial isolates

DNase activity of bacterial isolates was tested by aseptically transferring a loop full of fresh overnight broth cultures on DNase agar plates separately. Plates were incubated at 37 °C for 24 h. After incubation, DNase agar plates were flooded with conc. HCl and the excess was removed. After 5 min, agar plates were observed for the appearance of a 'halo' surrounding the strains. Freshly sub cultured *Staphylococcus aureus* was used as the positive control and *Lactobacillus* sp. was used as the negative control (Gündoğan *et al*., 2006).

RESULTS AND DISCUSSION

Sample collection and isolation of bacterial endophytes

Endophytes are microorganisms living inter or intra cellularly in most of plant tissues without causing any disease symptoms while producing plant growth promoting compounds (Nair & Padmawathy, 2014). Ten morphologically different endophytic bacterial strains were isolated on NA and LB media and none were isolated from leaves inoculated on MRS Medium (Table 1). In this study, samples of leaves were collected from different maturity stages and environments. According to Ullah *et al.*, (2018), abundance and composition of endophytic communities can vary depending on plant genotype, colonizing tissue type, plant developmental stage, soil type and environmental conditions. Due to this reason both mature and young leaf samples were taken from three districts covering the wet and dry zones. Out of the ten isolates, eight were isolated from leaf samples taken from the wet zone and six were isolated from young leaves (Table 1).

Plants that are adapted to live in dry climatic conditions (i.e., xerophytes) usually have a high number of plant endophytes (Yadav & Meena, 2021). However, in the current study, there was a high number of endophyte isolates from leaves sampled from the wet zone. In the current study, young leaves had a higher number of endophytes than mature leaves (Table 1).

Probable reasons could be that young leaves are more prone for herbivory than mature leaves because of their lower fragility due to thinner cell walls, and some endophytic bacteria secrete allelopathic chemical compounds, which reduce competition from pathogenic bacteria for colonization of intercellular tissues of plants and reduce herbivore attacks (Milute *et al.*, 2015). Further, nutritional composition is higher in young leaves when compared with mature leaves due to nutrient sequestration, which probably facilitates an abundant endophytic bacteria community when compared to mature leaves (Kandel *et al.*, 2017).

MRS medium was specifically used for isolation of *Lactobacillus* spp. (Shuhadha *et al.*, 2017). The isolated bacteria did not grow on MRS medium although they grew on NA and LB media (Table 1) probably indicating the isolated strains do not belong to the genus *Lactobacillus*. Out of the three methods used to isolate endophytes from leaves, pour plates with the addition of leaf extracts resulted in most isolations, probably as all the endophytic bacteria had an equal chance of being released from the leaf tissue, which were thoroughly macerated.

Table 1:   Isolate, location, maturity status of the leaf sample, isolated medium and inoculation method of isolates.

Isolate	Location (Dry zone/wet zone)	Maturity status of the leaf sample	Isolated medium	Inoculation method
1	Jaffna (DZ)	Mature	LB	C
2	Jaffna (DZ)	Mature	NA	C
3	Gampaha (WZ)	Young	LB	A
4	Gampaha (WZ)	Young	LB	A
5	Kandy (WZ)	Young	NA	A
6	Kandy (WZ)	Young	NA	A
7	Kandy (WZ)	Mature	LB	B
8	Kandy (WZ)	Young	LB	B
9	Kandy (WZ)	Young	NA	B
10	Kandy (WZ)	Mature	NA	B

NA - nutrient agar; LB – Lauria-Bertani medium; A - placing 1 cm^2 square particles of leaves on the medium; B - placing leaf macerations on the medium; C -preparing pour plate with leaf extraction; WZ - wet zone; DZ - dry zone.

Preliminary identification and characterization of pure cultures

The ten bacterial isolates were categorized based on their morphological characteristics such as cell shape, Gram staining results, presence/absence of spores, motility and catalase activity (Table 2, Figure 1). All the isolates were non- motile, catalase negative, non- endospore forming bacteria including eight cocci strains and two bacilli strains. According to the Gram staining results, two isolates were Gram positive while the other eight isolates were Gram negative. Previous studies done on endophytic bacteria isolated from plant parts of *M. koenigii* L. reveal that there are Gram positive endophytes in the plant, and according to literature Gram positive bacilli isolated from leaves could be *Bacillus* sp. (Khan *et al.*, 2022). Furthermore, Habbu *et al.*, 2014 states that Gram positive *Exiguobacterium indicum* endophytes are present in various plant parts of *M. koenigii*. As the 10 isolates were Gram positive, there is a possibility for that *Exiguobacterium indicum* is also included among them.

Table 2: Results obtained from preliminary identification tests.

Isolate	Gram stain	Shape/ arrangement	Catalase test	Endospore staining	Motility test
1	Gram negative	Cocci	-	-	-
2	Gram positive	Cocci	-	-	-
3	Gram negative	Cocci	-	-	-
4	Gram negative	Bacilli	-	-	-
5	Gram negative	Streptococci	-	-	-
6	Gram negative	Cocci	-	-	-
7	Gram negative	Cocci	-	-	-
8	Gram negative	Cocci	-	-	-
9	Gram negative	Bacilli	-	-	-
10	Gram negative	Cocci	-	-	-
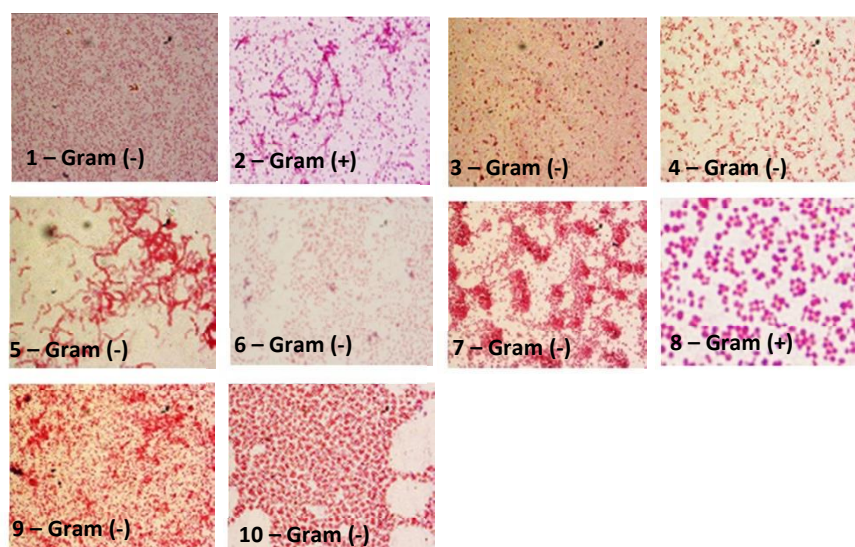
Figure 1: Microscopic images of isolated bacterial endophytes (×10 ×100).

Probiotic characterization of endophytic bacteria

Probiotics are viable, non-pathogenic microorganisms (bacteria or yeast) that, when ingested, are able to reach the intestines in sufficient numbers to confer health benefits to the host (Wong *et al.*, 2015). Probiotic characterization tests, which were carried out with isolated endophytic bacteria reveal their potential as probiotics.

Determination of resistance of isolated bacteria to low pH

The ability of a certain isolate to survive in an acidic pH and high levels of bile enable their probiotic potential by ensuring their transit through the stomach to reach the intestine. The results showed that no colonies could survive at pH 3, either on nutrient broth or NA plates (Figures 2, 3 and 4). Absorbance in nutrient broth cultures containing additional nutrients was slightly increased six hours after inoculation (Figures 2, 3 and 4), in each set of isolates indicating their survival in low pH. Nutrient Broth treated with a mixture of macerated *M. koenigii* leaves, rice and saliva showed a higher increase in absorbance (higher survival rate of isolates) than nutrient agar broth without the mixture (Figures 2, 3 and 4). Tolerance to acidic pH conditions was measured using three protocols (Hassanzadazar, 2012; Shuhadha *et al*., 2017); the most effective method, which indicated the survival of isolates in low pH, was nutrient broth at pH 3 with the additional components of rice, saliva and *M. koenigii* leaf macerations (Figure 1, 2 and 3) to simulate the environmental conditions as inside the gut. In the first two methods, the non-appearance of bacterial colonies at any of the time intervals on the NA plates may be due to the very low survival in an acidic environment, which were not sufficient to make a visible colony on the medium. This test was carried out for all 10 isolates as 3 different sets. Therefore, controls are different for each set of isolates. Hence, it is difficult to do a comparison of values for all 10 isolates at once and decide on the isolates with the highest and lowest pH tolerance. But, as an overall result, isolates 1-10 were susceptible to low pH.
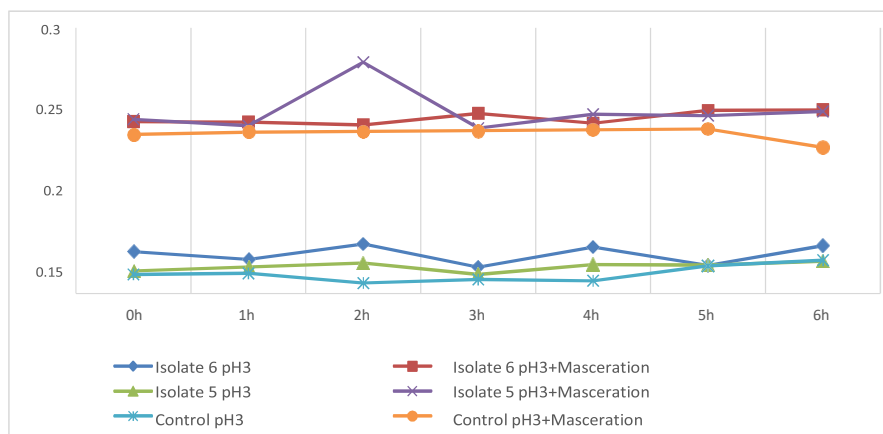
Figure 2: Survival in acidic media. Absorbance (λ = 600 nm) vs time for isolates 5 and 6
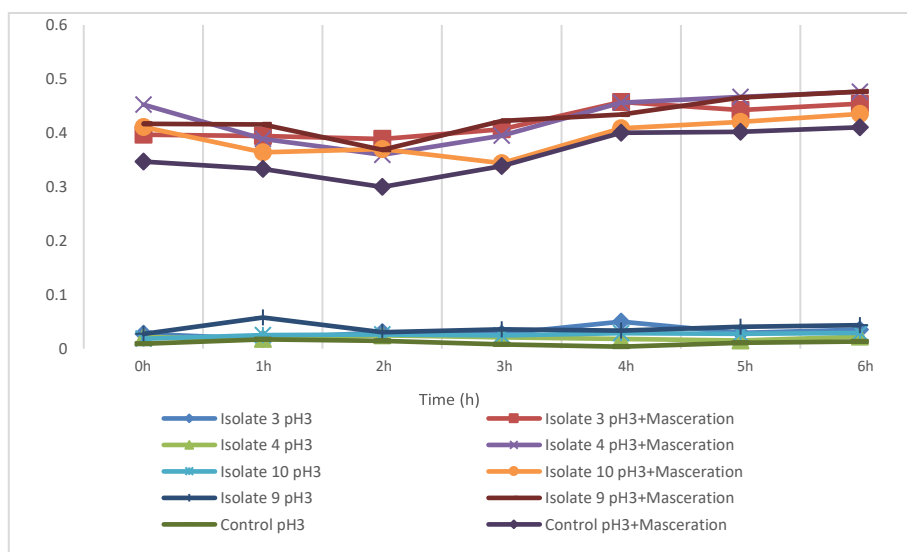
Figure 3: Absorbance (λ = 600 nm) vs time for isolates 3, 4, 9 and 10
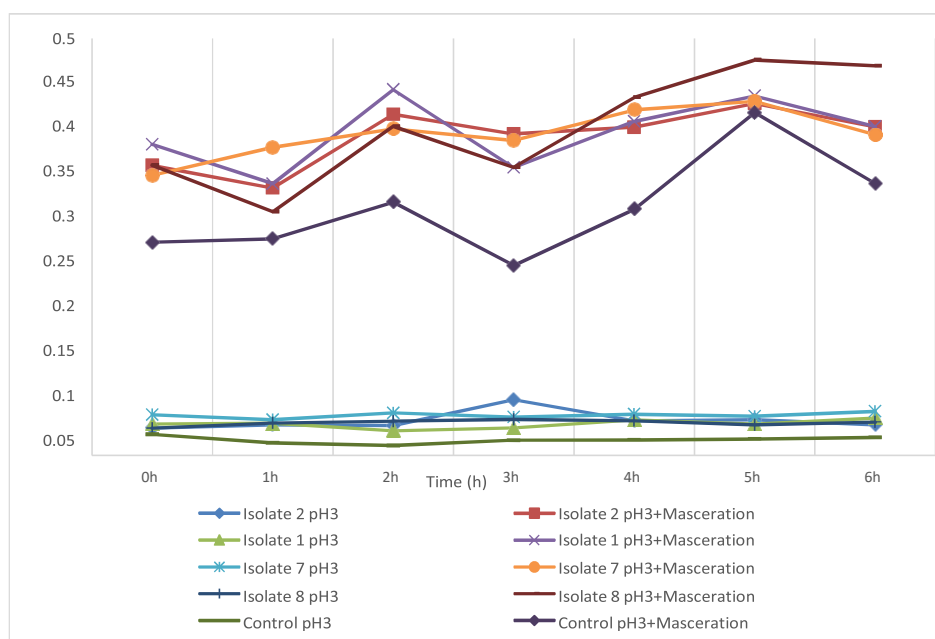
Figure 4: Absorbance (λ = 600 nm) vs time for isolates 1, 2, 7 and 8

Determination of bile salt tolerance

After bacterial exposure to bile salts, disruptions of cellular homeostasis cause the dissociation of the lipid bilayer and integral protein of their cell membranes, resulting in leakage of bacterial contents and finally cell death (Hassanzadazar, 2012). Even four hours after inoculation, considerable number of colonies were observed on the solid medium indicating their ability to survive in the bile salt medium. Isolates 2, 3, 6 and 7 showed a considerable increase in colony count three hours after inoculation (Table 3). According to the number of colonies formed after four hours of incubation, isolates 4 and 5 showed the highest ability to survive in the presence of bile salts and the lowest bile salt tolerance was detected in isolate 9. When compared with the initial values, bacterial growth was drastically decreased after four hours; however, they survived even after this time period.

Table 3: Number of colonies of bacterial isolates counted at 1-hour intervals for 4 hours

Number of colonies × 1000 (CFU/mL)	T1			T2			T3			T4		
	R1	R2	Average	R1	R2	Average	R1	R2	Average	R1	R2	Average
1	TNTC	TNTC	-	TNTC	TNTC	-	216	187	201.5	126	143	134.5
2	TNTC	TNTC	-	TNTC	TNTC	-	94	87	90.5	112	131	121.5
3	TNTC	TNTC	-	TNTC	TNTC	-	114	123	118.5	143	152	147.5
4	TNTC	260	-	TNTC	TNTC	-	272	264	268	250	274	262
5	TNTC	TNTC	-	TNTC	TNTC	-	204	212	208	182	171	176.5
6	TNTC	TNTC	-	TNTC	TNTC	-	108	121	114.5	119	131	125
7	TNTC	TNTC	-	TNTC	TNTC		103	136	119.5	121	127	124
8	TNTC	TNTC	-	155	133	144	126	109	117.5	91	96	93.5
9	TNTC	TNTC	-	TNTC	TNTC	-	84	93	88.5	86	81	83.5
10	TNTC	TNTC	-	164	173	168.5	127	134	130.5	95	89	92

T1 - one hour after inoculation; T2 - two hours after inoculation; T3 - three hours after inoculation; T4 - four hours after inoculation; R1 - replicate one for taking colony count; R2 - replicate two for taking colony count; TNTC- too numerous to count

Determination of antimicrobial activity
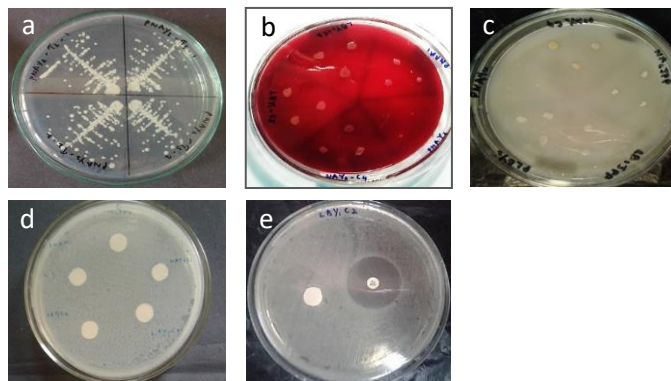
Figure 5: Isolated bacterial endophytes showing (a) Bile salt tolerance with colonies grown on NA medium after 4 hours incubation in bile salt; (b) non-haemolytic activity without forming clear zones around isolates; (c) non-DNase activity without forming clear zones around isolates; (d) negative antimicrobial activity with no inhibition zones around the filter paper discs impregnated with the isolates; (e) antibiotic susceptibility with isolate forming inhibition zone around gentamycin disc.

Antimicrobial activity was tested against two potential pathogenic strains in the gut microbiota, *E. coli* and *P. aeruginosa*. None of the bacterial isolates (1-10) formed inhibition zones in the spread plates of *E. coli* and *P. aeruginosa*, although Gentamicin discs formed inhibition zones of 20.12 mm and 16.31 mm, respectively with these pathogenic strains (Figure 5), indicating that the endophytic bacterial isolates do not possess antimicrobial activity. The ability of the isolates to inhibit the colonization of gut epithelial cells by pathogenic bacteria through mechanisms other than antagonism (i.e., blocking the colonization sites on epithelial cells, inhibiting the ability of pathogens to adhere to the epithelial cells) cannot be ruled out (Candela *et al*., 2008). However, the results obtained in this *in vitro* study may not completely reflect their performance *in situ*. This is because there are number of other physiological conditions, which may possibly affect the survival of the bacteria (Hassanzadazar, 2012). The current research did not look into the anti-adherence property. It is suggested that further testing should be done to assess the isolates for anti-adherence property, as according to literature there are some microorganisms which have the ability to block the adherence of pathogenic microorganisms to gut epithelial cells.

Determination of antibiotic resistance

According to recent studies, some probiotics in dietary supplements possess antibiotic resistant properties (Wong *et al*., 2017) while most of the potential probiotics do not contribute to the spread of antibiotic resistance and may even reduce it (Ouwehand *et al*., 2016). There is a negative aspect of antibiotic resistance strains because horizontal gene transfer can deliver the antibiotic resistance genes to pathogenic bacteria (Imperial & Ibana, 2016), which can act as Multidrug Resistant Strains that are resistant to more than one common antibiotic (Gueimunde *et al*., 2013). Isolates 1, 2, 7, 8, 9 and 10 showed antibiotic resistance while isolates 3, 4, 5 and 6 showed antibiotic susceptibility. The highest antibiotic susceptibility (lowest antibiotic resistance) was showed by isolate 3. However, the potential of horizontal gene transfer of the antibiotic resistance genes of bacteria strains, which were antibiotic resistant (bacterial isolates 1, 2, 7, 8, 9, 10) should be studied before considering them as safe probiotics.

Table 4: The antibiotic resistance and diameters of zones of inhibition for antibiotic susceptible bacterial isolates.

Name of the isolate	Antibiotic resistant / susceptible	Diameter of the zone of inhibition (mm)
1	Resistant	-
2	Resistant	-
3	Susceptible	28 ± 0.57
4	Susceptible	10 ± 1.25
5	Susceptible	24 ± 0.57
6	Susceptible	24 ± 0.57
7	Resistant	-
8	Resistant	-
9	Resistant	-
10	Resistant	-

Determination of haemolytic activity and DNase activity

Detection of non-haemolytic activity and non-DNase activity is considered as a safety prerequisite for characterizing a certain bacterium as a probiotic organism (Shuhadha *et al.*, 2017). According to the results obtained, none of the bacterial isolates (1-10) showed either haemolytic or DNase activity (Figure 5), which concludes that they have potential probiotic properties.

CONCLUSION

Composition and abundance of endophytic bacteria colonizing *M. koenigii* vary depending on climatic conditions and the maturity of leaves. Leaves of *M. koenigii* possessed Gram positive and Gram-negative endophytic bacteria. All the endophytic bacteria isolated showed most of the potential probiotic characters, while four isolates did not show antibiotic resistance. None of the isolates exhibited antimicrobial activity. Future studies include testing of anti- adherence ability of isolates on pathogenic bacteria and further identification of isolates using molecular techniques.

REFERENCES

Abeysinghe D.T., Kumara K.A.H., Kaushalya K.A.D., Chandrika U.G. & Alwis D.D.D.H. (2021). Phytochemical screening, total polyphenol, flavonoid content, in vitro antioxidant and antibacterial activities of Sri Lankan varieties of *Murraya koenigii* and *Micromelum minutum* leaves. *Heliyon* **7**(7): e07449.
DOI: https://doi.org/10.1016/j.heliyon.2021.e07449

AlKalbani N.S., Turner M.S. & Ayyash M.M. (2019). Isolation, identification, and potential probiotic characterization of isolated lactic acid bacteria and in vitro investigation of the cytotoxicity, antioxidant, and antidiabetic activities in fermented sausage. *Microbial Cell Factories* **18**(1): 1–12.
DOI: https://doi.org/10.1186/s12934-019-1239-1

Anand U. *et al.* (13 authors) (2023). Current scenario and future prospects of endophytic microbes: promising candidates for abiotic and biotic stress management for agricultural and environmental sustainability. *Microbial Ecology* 1–32.
DOI: https://doi.org/10.1007/s00248-023-02190-1

Balakrishnan R., Vijayraja D., Jo S.H., Ganesan P., Su-Kim I. & Choi D.K. (2020). Medicinal profile, phytochemistry, and pharmacological activities of *Murraya koenigii* and its primary bioactive compounds. *Antioxidants* **9**(2): 101.
DOI: https://doi.org/10.3390/antiox9020101

Bassyouni R.H., Abdel-all W.S., Abdel-all M.G.F.S. & Kamel Z. (2012). Characterization of lactic acid bacteria isolated from dairy products in Egypt as a probiotic. *Life Science Journal* **9**(4): 2924–2933.

Behnsen J., Deriu E., Sassone-Corsi M. & Raffatellu M. (2013). Probiotics: properties, examples, and specific applications. *Cold Spring Harbor Perspectives in Medicine* **3**(3): a010074.
DOI: https://doi.org/10.1101/cshperspect.a010074

Both E., Gyorgy E., Kibedi-Szabo C.Z., Tamas E., Abraham B., Miklossy I. & Lanyi S. (2010). Acid and bile tolerance, adhesion to epithelial cells of probiotic microorganisms. *UPB Buletin Stiintific, Series B: Chemistry and Materials Science* **72**(2): 37–44.

Candela M., Perna F., Carnevali P., Vitali B., Ciati R., Gionchetti P. & Brigidi P. (2008). Interaction of probiotic Lactobacillus and Bifidobacterium strains with human intestinal epithelial cells: adhesion properties, competition against enteropathogens and modulation of IL-8 production. *International Journal of Food Microbiology* **125**(3): 286–292.
DOI: https://doi.org/10.1016/j.ijfoodmicro.2008.04.012 s

Chaudhary A. (2020). A review on the culinary uses and therapeutic properties of *Murraya koenigii*. *Journal of Advancement in Pharmacognosy* **1**(1): 1–8.

Chow Y. & Ting A.S. (2015). Endophytic L-asparaginase-producing fungi from plants associated with anticancer properties. *Journal of Advanced Research* **6**(6): 869–876.
DOI: https://doi.org/10.1016/j.jare.2014.07.005

Costa L.E.D.O., Queiroz M.V.D., Borges A.C., Moraes C.A.D. & Araújo E.F.D. (2012). Isolation and characterization of endophytic bacteria isolated from the leaves of the common bean (Phaseolus vulgaris). *Brazilian Journal of Microbiology* **43**(4): 1562–1575.
DOI: https://doi.org/10.1590/S1517-83822012000400041

Croxatto A., Dijkstra K., Prod'hom G. & Greub G. (2015). Comparison of the InoqulA and the WASP automated systems with manual inoculation. *Journal of Clinical Microbiology* **53**(7): %P 2298–2307.
DOI: https://doi.org/10.1128/JCM.03076-14

Cullimore D.R. (2019). *Practical Atlas for Bacterial Identification*. CRC Press, USA.

da sesto VC. (2008). The (non-) sense of human origin of probiotics. In *Prebiotics/probiotics* pp. 8-10. Milano, Italy.

Dressman J.B., Berardi R.R., Dermentzoglou L.C., Russell T.L., Schmaltz S.P., Barnett J.L. & Jarvenpaa K.M. (1990). Upper gastrointestinal (GI) pH in young, healthy men and women. *Pharmaceutical Research* **7**(7): 756–761.
DOI: https://doi.org/10.1023/A:1015827908309

Fallah S.H., Asgharpour F., Naderian Z. & Moulana Z. (2013). Isolation and determination of antibiotic resistance patterns in nontyphoid *Salmonella* spp. isolated from chicken. *International Journal of Enteric Pathogens* **1**(1): 17–21.
DOI: https://doi.org/10.17795/ijep9416

Ferguson J., Tanner J. & Miller J.M. (1995). Evaluation of a new, semi quantitative screening culture device for urine specimens. *Journal of Clinical Microbiology* **33**(5): 1351–1353.
DOI: https://doi.org/10.1128/jcm.33.5.1351-1353.1995

Gahlawat D.K., Jakhar S. & Dahiya P. (2014). *Murraya koenigii* (L.) Spreng: an ethnobotanical, phytochemical and pharmacological review. *Journal of Pharmacognosy and Phytochemistry* **3**(3): 109-119.

Gueimonde M., Sánchez B., de los Reyes-Gavilán C.G. & Margolles A. (2013). Antibiotic resistance in probiotic bacteria. *Frontiers in Microbiology* **4**: 202.
DOI: https://doi.org/10.3389/fmicb.2013.00202

Gündoğan N., Citak S.U.M.R.U. & Turan E. (2006). Slime production, DNase activity and antibiotic resistance of Staphylococcus aureus isolated from raw milk, pasteurised milk and ice cream samples. *Food Control* **17**(5): 389–392.
DOI: https://doi.org/10.1016/j.foodcont.2005.01.006

Habbu P.V., Patil B.S., Salagare M.V., Madagundi S.D., Vankudri R.V., Shukla S.T. & Kulkarni V.H. (2014). Antidiabetic potential of endophytic bacterial fraction of *Murraya koenigii* (L.) Spreng. in rats. *Spatula DD* **4**(3): 139–150.
DOI: http://doi.org/10.5455/spatula.20140826011114

Hassanzadazar H., Ehsani A., Mardani K. & Hesari J. (2012). Investigation of antibacterial, acid and bile tolerance properties of *lactobacilli* isolated from Koozeh cheese. *Veterinary Research Forum* **3**(3): 181.

Holzapfel W.H., Haberer P., Geisen R., Björkroth J. & Schillinger U. (2001). Taxonomy and important features of probiotic microorganisms in food and nutrition. *The American Journal of Clinical Nutrition* **73**(2): 365s–373s.
DOI: https://doi.org/10.1093/ajcn/73.2.365s

Imperial I.C. & Ibana J.A. (2016). Addressing the antibiotic resistance problem with probiotics: reducing the risk of its double-edged sword effect. *Frontiers in Microbiology* **7**: 1983.
DOI: https://doi.org/10.3389/fmicb.2016.01983

Kandel S., Joubert P. & Doty S. (2017). Bacterial endophyte colonization and distribution within plants. *Microorganisms* **5**(4): 77.
DOI: https://doi.org/10.3390/microorganisms5040077

Khan S.S., Zargar S.A., Gupta V.K., Verma V. & Rasool S. (2022). Isolation and identification of bacterial and fungal endophytes from selected plants of Western Himalayas in prospect for bioactivities of economic importance. *Biology Bulletin* **49**(5): 444–457.
DOI: https://doi.org/10.1134/S1062359022050090

Kimoto H., Nomura M., Kobayashi M., Okamoto T. & Ohmomo S. (2004). Identification and probiotic characteristics of *Lactococcus* strains from plant materials. *Japan Agricultural Research Quarterly* **38**(2): 111–117.
DOI: https://doi.org/10.6090/jarq.38.111

Miliute I., Buzaite O., Baniulis D. & Stanys V. (2015). Bacterial endophytes in agricultural crops and their role in stress tolerance: a review. *Zemdirbyste-Agriculture* **102**(4): 465–478.
    DOI: https://doi.org/10.13080/z-a.2015.102.060

Mohamad A.O.A., Ma J.B., Liu Y.H., Zhang D., Hua S., Bhute S. & Li L. (2020). Beneficial endophytic bacterial populations associated with medicinal plant *Thymus vulgaris* alleviate salt stress and confer resistance to *Fusarium oxysporum*. *Frontiers in plant Science* **11**: 47.
    DOI: https://doi.org/10.3389/fpls.2020.00047

Nair D.N. & Padmavathy S. (2014). Impact of endophytic microorganisms on plants, environment and humans. *The Scientific World Journal* **2014**: 250693.
    DOI: https://doi.org/10.1155/2014/250693

Oh S. (2017). Animal- origin probiotics vs plant- origin probiotics. *Food and Beverages* **8**(8): 30.
    DOI: https://doi.org/10.4172/2157-7110-C1-065

Ouwehand A.C., Forssten S., Hibberd A.A., Lyra A. & Stahl B. (2016). Probiotic approach to prevent antibiotic resistance. *Annals of Medicine* **48**(4): 246–255.
    DOI: https://doi.org/10.3109/07853890.2016.1161232

Pineiro M. & Stanton C. (2007). Probiotic bacteria: legislative framework—requirements to evidence basis. *The Journal of Nutrition* **137**(3): 850S–853S.
    DOI: https://doi.org/10.1093/jn/137.3.850S

Rautela R. & Katiyar R. (2023). *Aegle marmelos* and *Murraya koenigii*: The wonder plants against bovine infertility. *Indian Journal of Animal Sciences* **93**(1): 6.
    DOI: https://doi.org/10.56093/ijans.v93i1.115512

Ruiza D., Agaras B., de Werrab P., Wall L.G. & Valverde C. (2011). Characterization and screening of plant probiotic traits of bacteria isolated from rice seeds cultivated in Argentina. *The Journal of Microbiology* **49**(6): 902–912.
    DOI: http://doi.org/10.1007/s12275-011-1073-6

Soundappan K., Bajaj R., Vaidya B.N. & Joshee N. (2018). Anatomical and biochemical investigations on medicinal tree *Murraya koenigii* Spreng. *Journal of Biotech Research* **9**: 70–78.

Shuhadha M.F.F., Panagoda G.J., Madhujith T. & Jayawardana N.W.I.A. (2017). Evaluation of probiotic attributes of *Lactobacillus* sp. isolated from cow and buffalo curd samples collected from Kandy. *Ceylon Medical Journal* **62**(3): 159–166.
    DOI: http://doi.org/10.4038/cmj.v62i3.8519

Wang Y., Deng H., Li Z., Tan Y., Han Y., Wang X. & Bi Y. (2017). Safety evaluation of a novel strain of *Bacteroides fragilis*. *Frontiers in Microbiology* **8**: 435.
    DOI: https://doi.org/10.3389/fmicb.2017.00435

Wong A., Saint Ngu Dan D.Y., Ooi L.A. & Lim R L.H. (2015). Detection of antibiotic resistance in probiotics of dietary supplements. *Nutrition Journal* **14**(1): 1–6.
    DOI: https://doi.org/10.1186/s12937-015-0084-2

Yadav G. & Meena M. (2021). Bioprospecting of endophytes in medicinal plants of Thar Desert: An attractive resource for biopharmaceuticals. *Biotechnology Reports* **30**: e00629.
    DOI: https://doi.org/10.1016/j.btre.2021.e00629

Yankuzo H., Ahmed Q.U., Santosa R.I., Akter S.F.U. & Talib N.A. (2011). Beneficial effect of the leaves of *Murraya koenigii* (Linn.) Spreng (Rutaceae) on diabetes-induced renal damage in vivo. *Journal of Ethnopharmacology* **135**(1): 88–94.
    DOI: https://doi.org/10.1016/j.jep.2011.02.020

Zhai Q., Feng S., Arjan N. & Chen W. (2018). A next generation probiotic, *Akkermansia muciniphila*. *Critical Reviews in Food Science and Nutrition* **59**: 3227–3236.
    DOI: https://doi.org/10.1080/10408398.2018.1517725

RESEARCH ARTICLE

Coastal Ecology

Spatial distribution of heavy metals in surface sediments of the Kalametiya Lagoon in southern Sri Lanka: Insights into the pollution status and socio-economic interactions

KAS Kodikara[1*†], T Hoessein[2†], PMCS De Silva[3], P Ranasinghe[4], HPPS Somasiri[4], SK Madarasinghe[1], DUV Gunathilaka[1], D Ranawaka[1], M Danaee[5], J Andrieu[6] and F Dahdouh-Guebas[2,7]

[1] *Department of Botany, Faculty of Science, University of Ruhuna, Matara, Sri Lanka.*

[2] *Ecology and Biodiversity, Laboratory of Plant Biology and Nature Management, Biology Department, Vrije Universiteit Brussel, Brussels, Belgium.*

[3] *Department of Zoology, Faculty of Science, University of Ruhuna, Matara, Sri Lanka.*

[4] *Herbal Technology Section, Industrial Technology Institute, Colombo 7, Sri Lanka.*

[5] *Department of Social and Preventive Medicine, Faculty of Medicine, University of Malaya, 50603 Kuala Lumpur, Malaysia.*

[6] *GEOSpatial Monitoring & Information Technology (GeoSMIT) department, French Institute of Pondichery (IFP), Pondichery, India.*

[7] *Laboratory of Systems Ecology and Resource Management, Département de Biologie des Organismes, Université Libre de Bruxelles, Brussels, Belgium.*

Abstract: Heavy metal pollution has become a serious threat to coastal aquatic ecosystems. Therefore, this study, aimed to assess the spatial distribution of five selected heavy metals/metalloids, arsenic (As), cadmium (Cd), chromium (Cr), lead (Pb), and mercury (Hg), in surface sediment samples collected from the Kalametiya Lagoon in southern Sri Lanka. Sixteen (16) areas of the lagoon were sampled. The sediment samples were analysed for heavy metal content by using ICP-MS while the water samples were measured for salinity and pH. A questionnaire survey was conducted to investigate the possible sources of heavy metal pollution in the Lagoon. Water pH and salinity showed significant variations across the lagoon. The overall mean value of pH and salinity were 6.68 ± 0.17 and 2.9 ± 2.2 PSU, respectively. The spatial distribution of the heavy metals was not monotonous and showed a high spatial variation. The kernel density maps of the measured heavy metals demarcated several spatially different patches in the lagoon. The mean levels of As, Cd, Cr, Hg, and Pb were lower than the threshold effect level (TEL) although it was higher for Hg in the North inlet. Nevertheless, it was still lower than the potential effect level (PEL). Industrial sewage, river suspended sediments, and agrochemicals such as fertilizers and pesticides were identified as the possible sources for heavy metal loads. Accumulation of toxic heavy metals can be minimized by by-passing the freshwater inflow to the lagoon.

Keywords: Fertilizers, heavy metals, kernel density maps, pesticides, Sri Lanka.

INTRODUCTION

Coastal lagoons are highly productive ecosystems that provide numerous ecosystem goods and services many of which are important in terms of economic benefits. These include the provision of products for human use, efficient nutrient cycling, water regulation and flood protection, sediment trapping and water purification, lagoon fisheries, and ecotourism (Dahdouh-Guebas *et al*., 2021). However, coastal lagoons have not escaped human pressure (Ofori *et al*., 2021; 2022).

In this respect, heavy metal pollution in aquatic environments has evidently become a menace due to their high toxicity, low solubility, wide range of sources, and bioaccumulation behaviour (Yu *et al*., 2008). Heavy metal pollution is also a matter of concern because it poses a high risk to aquatic organisms at different trophic levels owing to biomagnification through the food chain (Liu *et al*., 2018). In recent decades, large amounts of

* Corresponding author (sunandaruh@gmail.com; https://orcid.org/0000-0002-2493-3580)

† First co-authors

agricultural, industrial and domestic pollutants, especially heavy metals, have accumulated in coastal aquatic ecosystems, such as lagoons and estuaries (Bandara *et al*., 2008; Wuana & Okieimen, 2011; Chandrajith *et al*., 2012; Sivanantha *et al*., 2016; Kodikara, 2021). Sediments at the bottom of the water body serve as an ideal material for monitoring of contaminants including heavy metals in aquatic ecosystems. They can also act as a sink and a transport agent for aquatic pollutants (Ulbrich *et al*., 1997). Therefore, determining the levels of heavy metals in aquatic sediments is imperative to identify sources of heavy metal pollution (Diop *et al*., 2014). Further, the spatial distribution of heavy metals in aquatic sediments can also provide valuable information regarding the impact of discharged waste on ecosystems and associated risks (Yan *et al*., 2010). This approach would assist effective management of polluted aquatic ecosystems and also serve to monitor such systems (Li *et al*., 2016).

Whereas several studies in Sri Lanka have been carried out to assess the heavy metal content in food crops, land sediments, atmospheric depositions, and drinking water (Herath *et al*., 2016; Subasinghe *et al*., 2016; Weerasundara *et al*., 2018; Kodikara *et al*., 2022). Heavy metal contents in coastal aquatic ecosystems and spatial distribution of heavy metals received less attention. Adhikaram *et al*. (2016) reported the distribution and contamination status of environmentally important elements including major heavy metals of superficial sediments in the Batticaloa Lagoon, which is situated in the northern part of the eastern coast of Sri Lanka; they concluded that discharges from agricultural channels and marine fluxes in the lagoon affects the spatial distribution of the measured elements. The Kalametiya Lagoon on the southern coast of Sri Lanka, on the other hand, has been subjected to extensive discussions as the Udawalawe irrigation scheme. This came into operation in 1967, and has severely affected the lagoon over the past decades (Dahdouh-Guebas *et al*., 2005a), and continues to do so today (Madarasinghe *et al*., 2020a). In the Udawalawe project, drainage canals with excess water from upstream paddy lands and other areas in the immediate neighbourhood including industrial, urban and domestic areas, are connected to natural tributaries discharging into the sea through the Kalametiya Lagoon. This has caused heavy silt and pollutant input and salinity reduction. Further to this, Jayatissa *et al*. (2002) and Dahdouh-Guebas *et al*. (2005a) have reported that socio-economic interactions with the lagoon have become nearly nil (i.e., drastic socioeconomic degradation) resulting from these hydrological alterations.

Taking these facts into account, this study aims to assess selected heavy metals/metalloids in the surface sediments in the Kalametiya Lagoon and their spatial distribution. The following research questions were addressed: a) what is the average content of the major heavy metals in the lagoon; b) what is the spatial distribution of HMs in the lagoon; and c) what are the possible sources of heavy metal pollution in the lagoon.

MATERIALS AND METHODS

Study site

This study was conducted on the southern coast of Sri Lanka in 2020. The Kalametiya Lagoon was selected for the study based on the fact that this coastal lagoon is highly affected by the aforementioned Udawalawe irrigation scheme, which irrigates 32,000 ha of land, particularly paddy cultivations in the dry zone of southern Sri Lanka. In this scheme, drainage canals with excess water from the paddy lands are connected to the sea through the Kalametiya Lagoon (details are extensively discussed in Madarasinghe *et al*., 2020a). Furthermore, this may have caused deposition of loads of heavy metals in the lagoon. Therefore, this coastal ecosystem on the southern coast could be considered as a model site to study heavy metal pollution. The Kalametiya Lagoon (6° 04' 26"–6° 07'19" N and 80° 54' 43"–80° 57' 25" E), located in the dry zone (annual rainfall is < 1750 mm) about 65 km east from Matara (Figure 1), is the largest lagoon on the southern coast of Sri Lanka, having an area of approximately 4.8 km^2. Several canals, streams and reservoirs feed the Kalametiya Lagoon through Kuchchigal Ara, which is the main freshwater inflow to the lagoon. At present, the lagoon is dominated by *Sonneratia caseolaris* (low saline mangrove species) and marsh vegetation. A narrow canal, reinforced by a rocky dyke, has been constructed under the Udawalawa irrigation scheme as a pathway for continuous outflow from the lagoon to the sea. After construction of this reinforced outlet, the natural mouth of the lagoon has been closed almost permanently by the formation of a sand bar. Meteorological data (2019) obtained from Hambantota – the recording station nearest to the Kalametiya Lagoon – show that mean annual rainfall and monthly temperature for the area vary from 07-164 mm (January to December) and from 29.7–32.9 °C, respectively (Figure 1). The present study was performed in five areas ('sampling regions'), as shown in the map (Figure 2): Lagoon Outlet (A), Centre (B & F-

M), Narrow West Stream (C & N-P), Wide East Stream close to the inlet after paddy lands (D), and North Inlet (E).
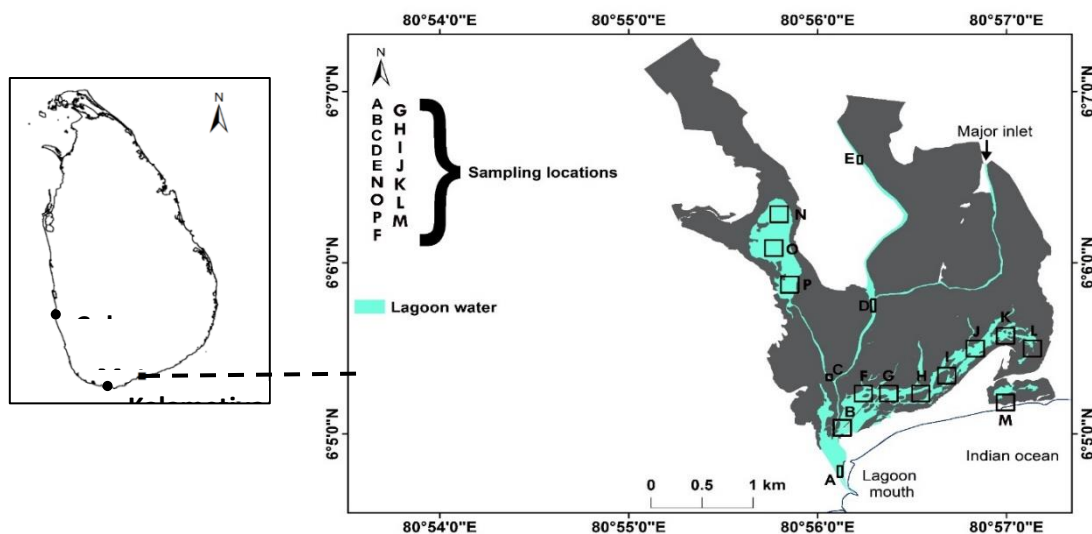
Figure 1: Map of Sri Lanka (left) and location of the Kalametiya Lagoon (right) on the southern coast of Sri Lanka, approximately 65 km to the east of Matara in the dry zone. Dark colour shows land area (silted landmass) while blue colour represents waterways.
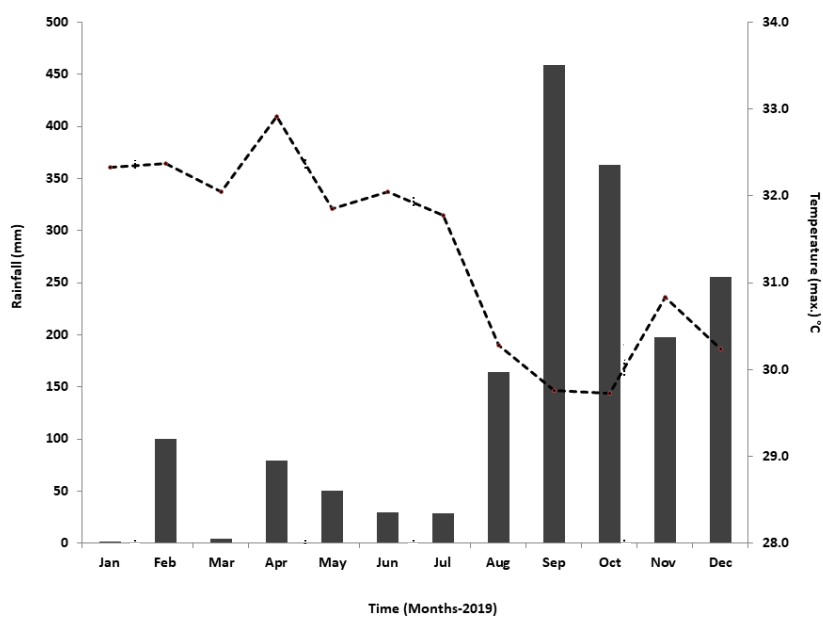
Figure 2: The graph shows the variation of rainfall (bar-graph) from January to December 2019 and the maximum temperature (line-graph) (weather station: Hambantota). Sediment and water sampling was done from February to April-2019, while the questionnaire survey was performed during July to October 2019.

Water and sediment sampling

Sediment sampling was conducted from February to mid-March in 2019, and water sampling in April-2019 (Figure 2). Water and sediment samples were collected from the five major sampling regions (sampling points A-P) shown in the map. Water sampling was done at the sub water layers (20–80 cm) with the help of a Ruttner

sampler (HYDRO-BIOS, PMMA Water Sampler, China), and water samples were taken at the middle water. In total, 84 water samples were collected covering the major sampling regions (Lagoon Outlet: n = 12; Centre: n = 36; Narrow West Stream: n = 12; Wide East Stream: n = 12, North Inlet: n = 12), and stored in the laboratory under cool conditions (at 4 °C temperature). The pH and salinity were measured by using a pH meter (STRATER300, OHAUS, USA) and refractometer (ATAGOS/Mill-E, Japan), respectively. Sediment sampling was also carried out in the major sampling areas at a depth of 0–10 cm by using a bottom dredge sampler (Ponar grab, WILDCO, New York, USA). In total, 60 sediment samples (Lagoon Outlet: n = 10; Centre: n = 26; Narrow West Stream: n = 12; Wide East Stream: n = 06; North Inlet: n = 06) were collected, placed in labelled plastic bags, and stored under cool conditions until analysis.

Acid digestion of sediment samples for heavy metal analysis

The sediment samples were digested and analysed for the selected heavy metals i.e., arsenic (As), cadmium (Cd), chromium (Cr), lead (Pb), and mercury (Hg) following the methodology described by Wathsara *et al.* (2020), with minor modifications. Approximately 0.5 g of finely powdered dried sediment sample was weighed using an electronic balance (KERNTM KB2000-2N) into an easy prep high-pressure microwave vessel, and approximately 10 mL of nitric acid was added, and the microwave digestion programme of the microwave digester (CEM MARS5, USA) was run to digest all samples. The digested samples were filtered with No.542 Whatman filter paper, washed with deionized water to a volume of 25 mL, and the metal ion content of the samples was determined by inductively coupled plasma mass spectrometry (ICP- MS, Agilent 700, USA).

Questionnaire survey

A questionnaire survey was conducted to obtain an overall view of the current human activities that led deposition of heavy metals in the lagoon, and their life experience related to lagoon pollution (mainly unsuitability of lagoon water). A standardized questionnaire (open-ended) was designed to evaluate the socio-economic status of the Kalametiya Lagoon using a preliminary field survey and interviews. The key stakeholders were identified through a combination of methods: expert knowledge elicitation and preliminary field survey. The snowball sampling technique (Atkinson & Flint, 2001) was used to identify further resource persons from whom more information could be collected. A face-to-face interview was carried out as a two-way interaction between respondent and interviewer (Kelley *et al.*, 2003). In total, 45 people (single person from a given family) including five community leaders, were interviewed individually in the survey.

Data analyses and kernel density mapping

Heavy metal content and physicochemical parameters were treated as continuous variables, and descriptive statistics were studied along with data distribution patterns. Parametric assumptions were verified for normality of the data by the Shapiro-test, and homogeneity of variances by the Levene's test. As all conditions were met for the dependent variables at a 95% confidence level, one-way ANOVA was performed to determine the level of significance of heavy metal distribution among the sampling regions. Similarly, the level of significance was tested for physicochemical parameters among the sampling regions using one-way ANOVA. The Pearson correlation test was performed to study correlation between physicochemical parameters of lagoon water and the heavy metal content. All statistical analyses were performed using R-3.2.2 statistical software. Kernel density maps were prepared using the heavy metal contents obtained from 60 sediment samples representing the total spatiality of the lagoon. The maps were processed on ArcMap v. 10.6.

RESULTS AND DISCUSSION

Physicochemical parameters

The results of the physicochemical parameters of water samples from the five regions (A-E) in Kalametiya Lagoon are presented in Table 1. The pH ranged from 6.58 to 6.92 with an overall mean value of 6.68 ± 0.17. Water acidity varied in different regions of the lagoon and water collected near the North Inlet showed the highest acidity. The water samples collected from B (Centre), D (Wide East Stream), and E (North Inlet) showed significantly higher (p < 0.05) water acidity than those collected from A (Outlet) and C (Narrow West Stream). Similarly, the

level of salinity also showed some variations across the lagoon. The highest salinity (i.e., 5.1 ± 0.06 PSU) was recorded near region A (Outlet) while the lowest (i.e., 1.1 ± 0.25 PSU) was recorded for water near region E (North Inlet). The overall mean salinity of the lagoon for the studied period was 2.9 ± 2.2 PSU. A significantly higher salinity ($p < 0.05$) was recorded in region A (Outlet) than in region E (North Inlet). The level of salinity in regions B (Centre), D (Wide East Stream), and C (Narrow West Stream) was significantly higher ($p < 0.05$) than in region E (North Inlet) while significantly lower than ($p < 0.05$) in region A (Outlet).

Table 1: Descriptive details of heavy metal content (mg/kg) in surface sediments of the study area. Values are mean ± SD.

Sites	As (mg/kg)	Cd (mg/kg)	Cr (mg/kg)	Hg (mg/kg)	Pb (mg/kg)	pH	Salinity (PSU)
Outlet (A)	0.104 ± 0.003	0.007 ± 0.001	2.635 ± 0.617	0.002 ± 0.001	0.347 ± 0.076	6.85 ± 0.07	5.1 ± 0.06
Centre (B)	0.137 ± 0.012	0.014 ± 0.005	2.723 ± 0.723	0.004 ± 0.002	0.411 ± 0.191	6.61 ± 0.03	2.4 ± 0.04
Narrow west stream (C)	0.112 ± 0.018	0.016 ± 0.002	2.926 ± 1.081	0.002 ± 0.001	0.315 ± 0.071	6.73 ± 0.02	2.7 ± 0.05
Wide east stream (D)	0.082 ± 0.022	0.004 ± 0.003	1.253 ± 0.437	0.003 ± 0.001	0.137 ± 0.045	6.60 ± 0.05	3.1 ± 0.04
North inlet (E)	0.075 ± 0.036	0.004 ± 0.003	1.849 ± 1.323	0.425 ± 0.134	0.235 ± 0.160	6.62 ± 0.04	1.1 ± 0.25
Threshold effect level (TEL)[i]	7.420	0.680	52.30	0.130	30.200		
Probable effect level (PEL) [i]	41.600	4.200	160.400	0.700	112.200		
Effect range low (ER-L) [ii]	8.200	1.200	81.000	0.150	46.700		
Effect range medium (ER-M)[ii]	70.000	9.600	370.000	0.170	218.000		

TEL: threshold effect level, represents the concentration below which adverse biological effects are rarely expected to occur; PEL: probable effect level (PEL), defines the level above which adverse effects are expected to occur frequently; ER-L: effect range-low, is interpreted with a rare biological effect; ER-M: effect range-medium, indicates frequent biological effects. i) Threshold effect level or probable effect level for marine and estuarine sediments (Long *et al.*, 1995). ii) Sediment quality guidelines for metals in the freshwater ecosystem (Macdonald *et al.*, 2000)

Spatial distribution of heavy metals

The analytical results of the heavy metals are presented in Table 1. The overall mean levels of heavy metals in descending order were Cr > Pb > As > Hg > Cd. The ranges (mg/kg) recorded for the heavy metals were 1.253–2.926 for Cr, 0.137–0.411 for Pb, 0.137–0.075 for As, 0.002–0.425 for Hg, and 0.004–0.016 for Cd. Further, according to the kernel maps (Figure 3), the following descending order was observed: A (Outlet): Cr > Pb > As > Cd > Hg; B (Centre): Cr > Pb > As > Cd > Hg; C (Narrow West Stream): Cr > Pb > As > Cd > Hg; D (Wide East Stream): Cr > Pb > As > Cd > Hg and E (North Inlet): Cr > Hg > Pb > As > Cd. The spatial distribution of the heavy metals was not monotonic and showed a considerable spatial variation. The kernel density maps based on the heavy metal levels indicated that A to E have different compositions (Figure 3). The distribution maps of Cr and Pb indicated significantly higher concentrations ($p < 0.05$) in A (Outlet), B (Centre), C (Narrow West Stream) and E (North Inlet) compared to D (Wide East Stream). The levels of As and Cd were significantly higher ($p < 0.05$) in B (Centre). The distribution of Hg was comparatively higher in E (North Inlet) than other areas.

The recorded heavy metal levels further showed that the mean levels of As, Cd, Cr, Hg, and Pb were lower than the threshold effect level (TEL). The TEL is the contaminant level below which harmful effects on organisms are not expected (MacDonald *et al.*, 2000; EC, 2018) while it was higher for Hg in E (North Inlet) (Table 1). However, it was still lower than the probable effect level (PEL) [*PEL is the contaminant level above which harmful effects on organisms are expected* ((MacDonald *et al.*, 2000; EC, 2018)]. Similarly, none of the heavy metal exceeded the effect range low (ER-L) [*ER-L is interpreted with a rare biological effect (*Long *et al.*, 2015] and effect range medium (ER-M) [*ER-M indicates frequent biological effects* (Long *et al.*, 2015)]. According to the results of the correlation analysis, Cr ($r = 0.56$) and Pb ($r = 0.45$) showed a positive correlation with water pH while Hg ($r = -0.53$) had a negative correlation with salinity. The rest of the heavy metals did not show any correlation with water pH and salinity.
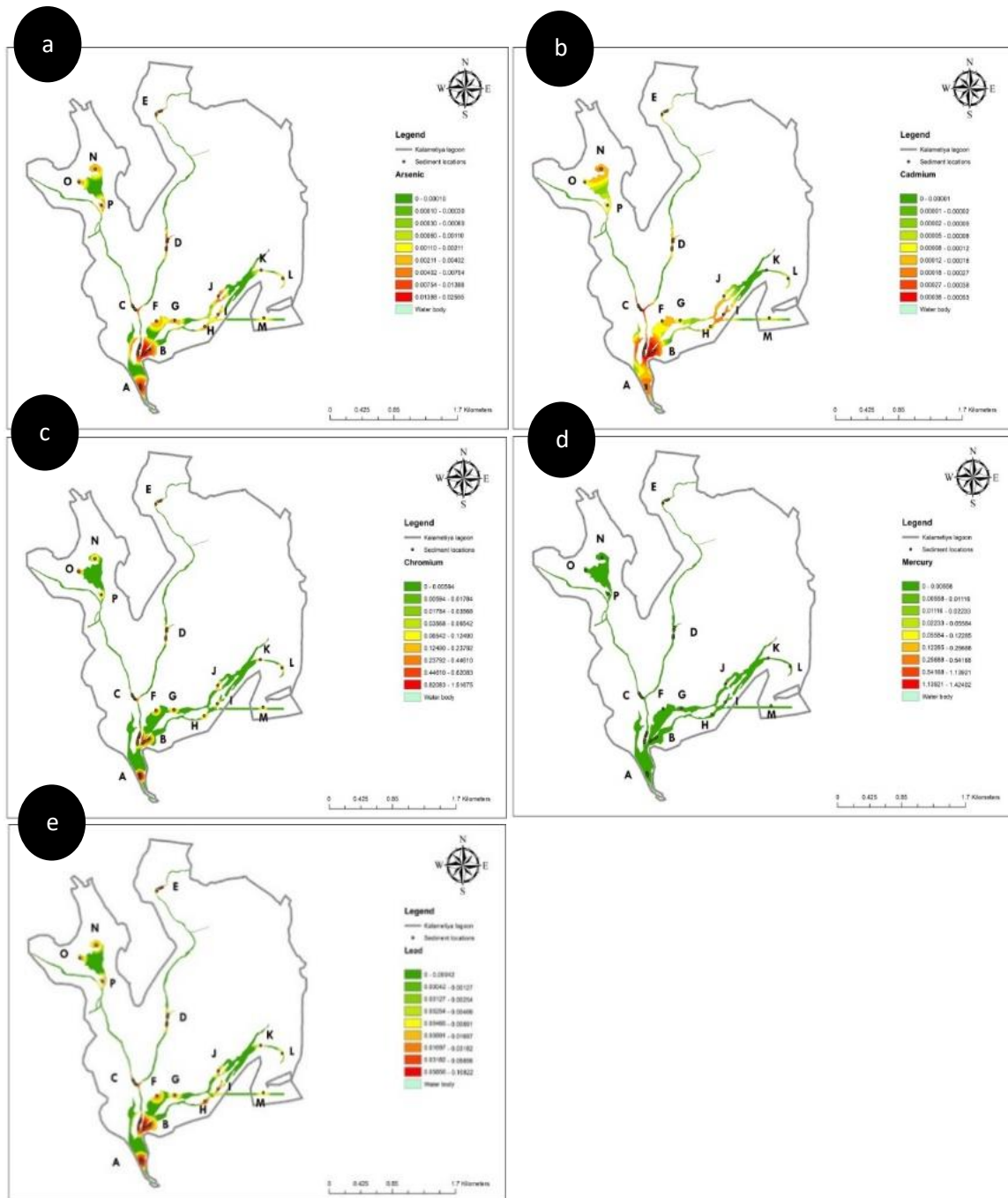
Figure 3: Kernel density maps (a-e) reflect spatial distribution of the studied heavy metals; a) As; b) Cd; c) Cr; d) Hg; e) Pb. Ranges of heavy metal contents are given in the map legends. Major sampling regions of the lagoon are A: Outlet; B: Centre; C: Narrow West Stream; D: Wide East Stream; E: North Inlet

Questionnaire survey

There were 65% male and 35% female respondents. According to the questionnaire survey, 32% of the respondents engaged in lagoon fishery for their daily subsistence; of these 16% were farmers and the rest (52%) involved in various occupations. Moreover, 53% of the farmers claimed that they had been using fertilizers such as urea, potash, rock dust fertilizer, and general fertilizers for their paddy lands to provide nitrogen (N), phosphorus (P), and potassium (K) requirements. In addition, 21% of interviewees stated that they had not used fertilizers and the rest (26%) did not clearly answer the question. Dwellers in the area mentioned the benefits that they obtained from the lagoon during 2000–2019; 79% said that the local people largely engaged in fishing in the

past, but now many of them are working in the bird sanctuary in the lagoon as tourist guides. In addition, 90% of the respondents mentioned the changes that had taken place during the past two decades: a) decrease in bird diversity and density; b) increase in mangroves and *Typha* (water sedge) plants; c) decrease in water salinity and lagoon depth; d) increase in freshwater fish species with shallow water column; and e) heavy sedimentation with the onset of the Udawalawe irrigation project. Of the respondents, 75% pointed out that the lagoon water has become unsuitable for use and hence was not using for drinking and bathing purposes. Furthermore, the respondents remarked on the managerial actions that would have been taken to conserve the Kalametiya Lagoon. The suggestions included: a) removal of excess sedimentation; b) removal of aquatic invasive plants; c) widening of the lagoon outlet; d) planting of fibrous rooted plants along the main freshwater channel that can trap excess sediments brought by freshwater; e) strengthening institutional coordination – both government and non-governmental institutions.

The Udawalawe irrigation project, which came into operation in 1967, has caused the release of excess freshwater into the Kalametiya Lagoon through Kuchchigal Ara (Dahdouh-Guebas *et al*., 2005a; Madarasinghe *et al*., 2020a) resulting in desalination. In addition, due to the fact that the natural sand bar is not seasonally opened, as a result of continuous outflow of lagoon water through the man-made canal supported by the dyke constructed during the irrigation project, the ebb-flow system of the lagoon has been disturbed. Therefore, the tidal effect has become minimal (Madarasinghe *et al*., 2020a) [Sri Lanka, anyway has a microtidal system (Kodikara *et al*., 2017)]. This scenario has eventually caused a reduction of the overall mean salinity level of the lagoon. In contrast, during the dry season, seawater intrusion becomes prominent and leads to an increase in the lagoon salinity. Owing to this fact, a spatial disparity in salinity distribution could be observed with the highest salinity at the lagoon outlet and the lowest at the inlet, particularly in the dry season. It is evident that the lagoon ecology and biology are affected with such salinity reduction (Madarasinghe *et al*., 2020b), and salinity further plays a crucial role since increased salinity results in increasing heavy metal bioavailability (Hou *et al*., 2013). In term of water pH, Ramanathan *et al*. (2005) recommended an optimum pH range of 6.8 – 8.7 for proper function of a lagoon and the mean value in this study for water pH was lower than that of the prescribed range (dry season). This directly indicates a deterioration of water quality of the Kalametiya Lagoon. In addition to pH and salinity, it is recommended to check the dissolved oxygen, total suspended materials, redox potential, and organic matter content, which may be useful in figuring out a holistic picture of the lagoon (Lawson, 2011).

Heavy metals have recently gained worldwide attention due to their high toxicity, environmental persistence, and accumulation in the environment and organisms (Zhang *et al*., 2014). Heavy metal levels are mainly attributed to lithogenic and anthropogenic inputs (Kabata-Pendias & Mukherjee, 2007). Two major causes are discussed for Cr enrichment in the lagoon. It is apparent that sediments are brought to the lagoon with excess freshwater and that heavy sedimentation taking place due to excess freshwater inflow to the lagoon, may have caused the addition of Cr into the lagoon. There is evidence which reflects that the lithogenic components, produced from the weathering of bedrocks and soils (Yunginger *et al*., 2018), in the upper areas are transported by water, which then settles at the bottom of the downstream water bodies (Tamuntuan *et al*., 2015). Cromium, in many cases, is controlled by bedrock influence (Sun *et al*., 2013) and the other probable source of Cr may be phosphate fertilizers used in agricultural fields in the area (Dissanayaka & Chandrajith, 2009). There is a high likelihood of phosphate being solubilized from phosphate fertilizers when excess freshwater flows through the agricultural lands, situated at the upstream areas whereas extensive paddy cultivation may occur in downstream areas in the area of interest. In addition, Dissanayaka & Chandrajith (2009) reported that the phosphate fertilizers used in Sri Lanka contain not only Cr, but also high amounts of other heavy metals such as Ni, and Pb. Furthermore, Zn, Cu, Cd, Pb, and As, have also been identified as widely found heavy metals in agricultural fertilizers, pesticides and fungicides (Gimeno-Garci'a *et al*., 1996; Kelepeitzis, 2014). Therefore, As, Cd and Pb could be linked with agricultural fertilizers, being used in the area. Although Adikaram *et al*. (2016) reported that most marine algae produce organo-arsenic compounds, for example in the Batticaloa Lagoon, it is unlikely to be applicable to the Kalametiya Lagoon since material exchange is minimal at the lagoon outlet (Madarasinghe *et al*., 2020a). When Hg is considered, this could be due to higher input from domestic sewage and hospital effluents (Wang *et al*., 2017). Moreover, metal processing, stainless steel welding, chromate production, tannery facilities and ferrochrome and chrome pigment production could largely contribute to heavy metal release (ATSDR, 2012; Jayawardana *et al*., 2014). (During the initial site visit, we observed homemade paint shops, metal processing and stainless steel welding). It is well-known that the pH of water directly influences the heavy metal concentrations by altering bio-availability and toxicity. Metals such as Cr and Pb had a significant correlation with water pH and are recorded

to increase detrimental environmental effects with increasing acidity (DWAF, 1996). It has been found that pH governs the methylation of elements such as Pb and Hg (van Loon, 1982) that was best reflected by significant correlation shown for Hg in this study. In general, higher water acidity (low pH) causes higher heavy metal availability in water and the opposite was obtained in our study. That could be linked with the continuous flow of freshwater into the lagoon through which heavy metals are unremittingly brought in. However, it is recommended to re-conduct the research covering both rainy and dry seasons and that will help to provide a holistic view of the levels of heavy metals in the sediments.

It is commonly observed that, except Hg, the rest of the heavy metals are largely accumulated at the Centre and Outlet of the lagoon. Higher accumulation of heavy metals at these regions is due to poor ebb-flow system of the lagoon, which was most likely enhanced by the construction of the artificial dyke, and the natural sand barrier, which obstructed the water outflow. In general, the mosaic distribution of heavy metals in the Kalametiya Lagoon could be due to the limited circulation taking place inside the lagoon (Dahdouh-Guebas *et al.*, 2005b; Madarasinghe *et al.*, 2020a). Furthermore, the increasing trend of heavy metals in the lagoon from the Inlet (E) to the Outlet (A) might be due to the sediment accumulation pattern from upstream to downstream of the lagoon (Dahdouh-Guebas *et al.*, 2005b). Although the sediment undergoes resuspension, redox reactions and biodegradation, could considerably change the affinity of the sediment, which is considered to be the deposition compartment of the marine environment. The distribution and accumulation of heavy metals depend on the grain size. Therefore, a grain size analysis of the lagoon would provide useful information on this aspect (ElNemr *et al.*, 2007).

When the current pollution status is considered, the Kalametiya Lagoon is not critical since the heavy metal contents does not exceed the TEL and PEL. In Sri Lanka, a few studies have focused on heavy metal pollution in several water bodies and lagoons including Kumbichchankulama, Alankulama, and Thuruwila, in the dry zone (Bandara *et al.*, 2008; Chandrajith *et al.*, 2012), and the Negombo Lagoon (Sivanantha *et al.*, 2016). According to their results, the Negombo Lagoon showed the highest content of heavy metals in the published data of Sri Lanka, for example As: 9.89 mg/kg; Cd: 2.63 mg/Kg; Cr: 26.1 mg/kg; and Pb: 20.26 mg/kg (sediments). In the other water bodies, Cd content was greater than 2.18 mg/kg (sediments). Thus, the pollution level of the Kalametiya Lagoon is far below the aforementioned values in the other water bodies in the country. Since an excess freshwater flow continues, higher levels of pollution can be expected soon. On the other hand, survey data clearly reflect that socio-economic interactions have become minimal and less than 5% of the dwellers now depend on lagoon fisheries. Further, the dwellers have indirectly experienced water quality changes including toxicity (sudden fish death, skin irritation). As a result, most dwellers are reluctant to use lagoon water for their daily use. However, such livelihood transformations are not uncommon in Sri Lanka as well as in other parts of the world (Schernewski *et al.*, 2018; Okello *et al.*, 2019; Madarasinghe *et al.*, 2020a, 2020b;).

To minimize the impact of heavy metal pollution at this stage, it is recommended to implement eco-sustainable remedies such as construction of a separate canal to dispose excess water coming from the Udawalawe irrigation project, introduction of a cascade system to freshwater canals before entering in to the lagoon to minimize sediment loading, periodic removal of accumulated sediments manually, and the use of phytoremediation techniques.

CONCLUSION

The Kalametiya Lagoon in southern Sri Lanka contains heavy metals such as As, Cd, Cr, Hg, and Pb. The levels recorded in descending order were Cr > Pb > As > Hg > Cd. The spatial distribution of the heavy metals was not monotonic and showed considerable spatial variation. According to the kernel maps for the regions, A (Outlet), B (Centre), C (Narrow West Stream) and D (Wide East Stream) recorded heavy metal levels in the descending order: Cr > Pb > As > Cd > Hg; this was different from E (North Inlet): Cr > Hg > Pb > As > Cd. The mean levels of As, Cd, Cr, Hg, and Pb were lower than that of Threshold Effect Level (TEL) and Potential Effect Level (PEL). Similarly, none of the studied heavy metals/metalloids exceeded the Effect Range Low (ER-L) and the Effect Range Medium (ER-M). The highest levels of Cr recorded could be due to natural weathering. Therefore, the Kalametiya Lagoon is not at risk from heavy metal pollution at present. However, there is a possibility of these levels increasing in the future with continuous freshwater input to the Kalametiya Lagoon.

Acknowledgement

REFERENCES

Adikaram M., Pitawala A., Ishiga H. & Jayawardana D. (2016). Spatial distribution, enrichment, and source of environmentally important elements in Batticaloa lagoon, Sri Lanka. *Environmental Science and Pollution Research* **24**: 2089–2099.
DOI: https://doi.org/10.1007/s11356-016-7973-6

Agency for Toxic Substances and Disease Registry (ATSDR) (2012). *Toxicological Profile for Chromium*. Agency for Toxic Substances and Disease Registry, Department of Health and Human Services, Public Health Service, Atlanta, USA.

Atkinson R. & Flint J. (2001). Accessing hidden and hard-to-reach populations: Snowball research strategies. *Social Research Update* **33**(1): 1–4.

Bambaradeniya C.N.B. (2004). Freshwater wetlands in Sri Lanka: Their conservation significance and current status. *Proceedings of the National Symposium on Wetland Conservation and Management*, pp. 19–24.
DOI: https://doi.org/10.1007/s10653-007-9129-6

Bandara J.M.R.S., Senevirathna D.M.A.N., Dasanayake D.M.R.S.B., Herath V., Bandara J.M.R. P., Abeysekara T. & Rajapaksha K.H. (2008). Chronic renal failure among farm families in cascade irrigation systems in Sri Lanka associated with elevated dietary cadmium levels in rice and freshwater fish (Tilapia). *Environmental Geochemistry and Health* **30**(5): 465–478.

Chandrajith R., Ariyaratna T. & Dissanayake C. (2012). The status of cadmium in the geo-environment of Sri Lanka. *Ceylon Journal of Science (Physical Sciences)* **16**: 47–53.

Dahdouh-Guebas F., Jayatissa L.P., Di Nitto D., Bosire J.O., Lo Seen D. & Koedam N. (2005a). How effective were mangroves as a defence against the recent tsunami? *Current Biology* **15**(12): R443–R447.
DOI: https://doi.org/10.1016/j.cub.2005.06.008

Dahdouh-Guebas F. *et al.* (17 authors) (2021). Reconciling nature, people and policy in the mangrove socialecological system through the adaptive cycle heuristic. *Estuarine, Coastal and Shelf Science* **248**: 106942.
DOI: https://doi.org/10.1016/j.ecss.2020.106942

Department of Water Affairs and Forestry (DWAF) (1996). *South African Water Quality Guidelines, Domestic Use*. volume 1, 2nd edition. Department of Water Affairs and Forestry, Pretoria, South Africa.

Diop C., Dewaele D., Diop M., Toure A., Cabral M., Cazier F., Fall M., Diouf A. & Ouddane B. (2014). Assessment of contamination, distribution and chemical speciation of trace metals in water column in the Dakar coast and the Saint Louis estuary from Senegal, West Africa. *Marine Pollution Bulletin* **86**(1–2): 539–546.
DOI: https://doi.org/10.1016/j.marpolbul.2014.06.051

Dissanayaka C.B. & Chandrajith R. (2009). Phosphate mineral fertilizers, trace metals and human health. *Journal of the National Science Foundation of Sri Lanka* **37**(3): 153–165.
DOI: https://doi.org/10.4038/jnsfsr.v37i3.1219

ElNemr A.H., El Sikaily A. & Khaled A. (2007). Total and leachable heavy metals in muddy and sandy sediments of Egyptian coast along Mediterranean Sea. *Journal of Coastal Shelf Science* **129**: 151–168.
DOI: https://doi.org/10.1007/s10661-006-9349-8

EC (European Commission) (2018). *European Technical Guidance Document (TGD) for Deriving Environmental Quality Standards No. 27, Common Implementation Strategy for the Water Framework Directive* (2000/60/EC). Guidance Document No. 27, Technical Guidance for Deriving Environmental Quality Standards; Technical Report-2011-055. Office for Official Publications in the European Communities, Brussels, Belgium.

Gimeno-Garci'a E., Andreu V. & Boluda R. (1996). Heavy metals incidence in the application of inorganic fertilizers and pesticides to rice farming soils. *Environmental Pollution* **92**: 19–25.
DOI: https://doi.org/10.1016/0269-7491(95)00090-9

Herath D., Pitawala A. & Gunatilake J. (2016). Heavy metals in road deposited sediments and road dusts of Colombo Capital, Sri Lanka. *Journal of the National Science Foundation of Sri Lanka* **44**(2): 193–202.
DOI: https://doi.org/10.4038/jnsfsr.v44i2.8000

Hou D., He J., Lu¨ C., Ren L., Fan Q., Wang J. & Xie Z. (2013). Distribution characteristics and potential ecological risk assessment of heavy metals (Cu, Pb, Zn, Cd) in water and sediments from Lake Dalinouer, China. *Ecotoxicology and Environmental Safety* **93**: 135–144.
DOI: https://doi.org/10.1016/j.ecoenv.2013.03.012

Jayatissa L.P., Guero M.C., Hettiarachchi S. & Koedam N. (2002). Changes in vegetation cover and socio-economic transitions in a coastal lagoon (Kalametiya, Sri Lanka), as observed by teledetection and ground truthing, can be attributed to an upstream irrigation scheme. *Environment, Development and Sustainability* **4**(2): 167–183.

DOI: https://doi.org/10.1023/A:1020831416827

Jayawardana D.T., Pitawala H.M.T.G.A. & Ishiga H. (2014). Assessment of soil geochemistry around some selected agricultural sites of Sri Lanka. *Environmental Earth Sciences* **71**(9): 4097–4106.
DOI: https://doi.org/10.1007/s12665-013-2798-9

Kabata-Pendias A. & Mukherjee A. B. (2007). *Trace Elements from Soil to Human*. Springer, Berlin, Germany.
DOI: https://doi.org/10.1007/978-3-540-32714-1

Kelepertzis E. (2014). Accumulation of heavy metals in agricultural soils of Mediterranean: insights from Argolida basin, Peloponnese, Greece. *Geoderma* **221–222**: 82–90.
DOI: https://doi.org/10.1016/j.geoderma.2014.01.007

Kelley K., Clark B., Brown V. & Sitzia J. (2003). Good practice in the conduct and reporting of survey research. *International Journal for Quality in Health Care* **15**(3): 261–266.
DOI: https://doi.org/10.1093/intqhc/mzg031

Kodikara K.A.S. (2021). Phytoremediation capacity of aquatic floating plants; *Salvinia molesta* and *Eichhornia crassipes* in desalinated Kalametiya Lagoon, southern coast of Sri Lanka. *WILDLANKA* **9**(1): 150–59.

Kodikara K.A.S., Lewandowski S., De Silva P.M.C.S., Gunarathna S.D., Madarasinghe S.K., Ranasinghe P., Jayatissa L.P.R., Dahdouh-Guebas F. (2022). Heavy metal pollution in selected upland tributaries of Sri Lanka: comprehension towards the localization of sources of pollution. *Journal of Water and Health* **20**(3): 505–517.
DOI: https://doi.org/10.2166/wh.2022.250

Kodikara K.A.S., Mukherjee N., Jayatissa L.P., Dahdouh-Guebas F. & Koedam, N. (2017). Have mangrove restoration projects worked? An in-depth study in Sri Lanka. *Restoration Ecology* **25**(5): 705–716.

Lawson E.O. (2011). Physico-chemical parameters and heavy metal contents of water from the mangrove swamps of Lagos Lagoon, Lagos, Nigeria. *Advances in Biological Research* **5**(1): 08–21.

Li R., Chai M. & Qiu G. Y. (2016). Distribution, fraction, and ecological assessment of heavy metals in sediment-plant system in Mangrove Forest, South China Sea. *PLoS One* **11**(1): e0147308.
DOI: https://doi.org/10.1371/journal.pone.0147308

Liu Y., Liu G., Yuan Z., Liu H. & Lam P. K. (2018). Heavy metals (As, Hg and V) and stable isotope ratios (d13C and d15N) in fish from Yellow River Estuary, China. *Science of the Total Environment* **613**: 462–471.
DOI: https://doi.org/10.1016/j.scitotenv.2017.09.088

MacDonald D.D., Ingersoll C.G. & Berger T.A. (2000). Development and evaluation of consensus-based sediment quality guidelines for freshwater ecosystems. *Archives of Environmental Contamination and Toxicology* **39**: 20–31.
DOI: https://doi.org/10.1007/s002440010075

Madarasinghe S.K., Yapa K.K.A.S., Satyanarayana B., Udayakantha P.M.P., Kodikara S. & Jayatissa L.P. (2020a). Inland irrigation project causes disappearance of coastal lagoon: the trajectory of Kalametiya Lagoon, Sri Lanka from 1956 to 2016. *Coastal Management* **48**(3): 188–209.
DOI: https://doi.org/10.1080/08920753.2020.1747914

Madarasinghe S.K. *et al*. (11 authors) (2020b). Retrospective study on changes in Dondra lagoon (2006–2017) resulting from tsunami impact and post-tsunami development. *Journal of Coastal Conservation* **24**(5): 1–11.
DOI: https://doi.org/10.1007/s11852-020-00777-1

McCartney M., Rebelo L.M., Senaratna Sellamuttu S. & De Silva S. (2010). Wetlands, agriculture and poverty reduction. *IWMI Research Report*, pp. 137–139. International Water Management Institute (IWMI), Colombo, Sri Lanka.
DOI: https://doi.org/10.5337/2010.230

Ofori S.A., Arachchilage S.K., Jayatissa L.P., Madarasinghe S.K., Gunathilaka U.V., Wijesundara I.T.D. (2021). Shrimp farming, a major threat to mangrove and lagoon ecosystem in the Pambala-Chilaw lagoon complex, Sri Lanka. In: *Book of Abstracts—VLIZ Marine Science Day, VLIZ Special Publication 85,* (eds. J. Mees & J. Seys), pp. 129. *Vlaams Instituut Voor de zee—Flanders Marine Institute* (VLIZ) Oostende, Belgium.

Ofori S.A., Kodikara K.A.S., Jayatissa, L.P., Gunathilaka U.V., Wijesundara I., Mafaziya Nijamdeen T.W.G.F., Dahdouh-Guebas F. (2022). Spatial dynamics of pollution in a tropical lagoon ecosystem and its social-ecological impacts. *Water Air Soil Pollution* **233**: 266.
DOI: https://doi.org/10.1007/s11270-022-05729-z

Okello J.A., Alati V., Kodikara S., Kairo J.G., Dahdouh-Guebas F. & Koedam N. (2019). The status of Mtwapa Creek mangroves as perceived by the local communities. *WIO Journal of Marine Science* **18**(1): 67–81.
DOI: https://doi.org/10.4314/wiojms.v18i1.7

Ramanathan N.P., Padmavathy T., Francis S., Athithian & Selvaranjitham N. (2005). *Manual on Polyculture of Tiger Shrimp and Carps in Freshwater*, pp. 1–161. Tamil Nadu Veterinary and Animal Sciences University, Fisheries College and Research Institute, Thothukudi, India.

Schernewski G., Baltranaite E., Katarzyte M., Balciunas A., Cerkasova N. & Mezine J. (2018). Establishing new bathing sites at the Curonian Lagoon coast: An ecological-social-economic assessment. *Journal of Coastal Conservation* **23**: 899–911.
DOI: https://doi.org/10.1007/s11852-017-0587-4

Sivanantha N., Wijesinghe M.R. & Wijesekara R.D. (2016). Distribution of five toxic heavy metals in biotic and abiotic constituents of the Negombo Lagoon, Sri Lanka. *Sri Lankan Journal of Biology* **1**(1): 1–14.
DOI: https://doi.org/10.4038/sljb.v1i1.1

Subasinghe S., Estoque R.C. & Murayama Y. (2016). Spatiotemporal analysis of urban growth using GIS and remote sensing: A case study of the Colombo Metropolitan Area, Sri Lanka. *International Journal of Geo-Information* **5**: 197.
   DOI: https://doi.org/10.3390/ijgi5110197

Sun C., Liu J., Wang Y., Sun L. & Yu H. (2013). Multivariate and geostatistical analyses of thespatial distribution and sources of heavy metals in agricultural soil in Dehui, Northeast China. *Chemosphere* **92**: 517–523.
   DOI: https://doi.org/10.1016/j.chemosphere.2013.02.063

Tamuntuan G., Bijaksana S., King J., Russell J., Fauzi U., Maryunani K., Aufa N. & Safiuddin L.O. (2015). Variation of magnetic properties in sediments from Lake Towuti, Indonesia, and its paleoclimate significance. *Palaeogeography Palaeoclimatology Palaeoecology* **420**: 163–172.
   DOI: https://doi.org/10.1016/j.palaeo.2014.12.008

Ulbrich K., Marsula R., Jeltsch F., Hofmann H. & Wissel C. (1997). Modelling the ecological impact of contaminated river sediments on wetlands. *Ecological Modelling* **94**(2–3): 221–230.
   DOI: https://doi.org/10.1016/S0304-3800(96)00023-3

United Nations Educational, Scientific and Cultural Organization (UNESCO) (1971). *Convention on Wetlands of International Importance especially as Waterfowl Habitat, Ramsar Iran-1971.* Available at https://www.ramsar.org/sites/default/files/documents/library/sitelist.pdf RamsarWeb, Accessed 1 September 2021.

Van Loon J.C. (1982). *Chemical Analysis of Inorganic Constituent of Water.* CRC Press, Boca Raton, Florida, USA.

Wang L., Ji B., Hu Y., Liu R. & Sun W. (2017). A review on in situ phytoremediation of mine tailings. *Chemosphere* **184**: 594–600.
   DOI: https://doi.org/10.1016/j.chemosphere.2017.06.025

Wathsara H.P.T., Weeratunge H.D., Mubarak M.N.A., Godakumbura P.I. & Ranasinghe P. (2020). *In vitro* antioxidant and antidiabetic potentials of *Syzygium caryophyllatum* L. Alston. *Evidence-Based Complementary and Alternative Medicine* **2020**: 1–15.
   DOI: https://doi.org/10.1155/2020/9529042

Weerasundara L., Magana-Arachchi D.N., Ziyath A.M., Goonetilleke A. & Vithanage M. (2018). Health risk assessment of heavy metals in atmospheric deposition in a congested city environment in a developing country: Kandy City, Sri Lanka. *Journal of Environmental Management* **220**: 198–206.
   DOI: https://doi.org/10.1016/j.jenvman.2018.04.036

Wuana R.A. & Okieimen F.E. (2011). Heavy metals in contaminated soils: a review of sources, chemistry, risks and best available strategies for remediation. *ISRN Ecology* **2011**: 402–647.
   DOI: https://doi.org/10.5402/2011/402647

Yan C., Li Q., Zhang X. & Li G. (2010). Mobility and ecological risk assessment of heavy metals in surface sediments of Xiamen Bay and its adjacent areas, China. *Environmental Earth Sciences* **60**(7): 1469–1479.
   DOI: https://doi.org/10.1007/s12665-009-0282-3

Yu R.L., Yuan X., Zhao Y.H., Hu G.R. & Tu X.L. (2008). Heavy metal pollution in intertidal sediments from Quanzhou Bay, China. *Journal of Environmental Science* **20**: 664–669.
   DOI: https://doi.org/10.1016/S1001-0742(08)62110-5

Yunginger R., Bijaksana S., Dahrin D., Zulaikah S., Hafidz A., Kirana K.H., Sudarningsih S., Mariyanto M. & Fajar S.J. (2018). Lithogenic and anthropogenic components in surface sediments from Lake Limboto as shown by magnetic mineral characteristics, trace metals, and REE geochemistry. *Geosciences* **8**(4): 116.
   DOI: https://doi.org/10.3390/geosciences8040116

Zhang C., Yu Z.G., Zeng G.M., Jiang M., Yang Z.Z., Cui F., Zhu M.Y., Shen L.Q. & Hu L. (2014). Effects of sediment geochemical properties on heavy metal bioavailability. *Environment International* **73**: 270−281.
   DOI: https://doi.org/10.1016/j.envint.2014.08.010

RESEARCH ARTICLE

Cosmeceutics

pH-dependent release properties of curcumin encapsulated alginate nanoparticles in skin and artificial sweat

IF Shakoor[1], GK Pamunuwa[1*] and DN Karunaratne[2]

[1] *Department of Horticulture and Landscape Gardening, Faculty of Agriculture and Plantation Management, Wayamba University of Sri Lanka, Makandura, Gonawila, Sri Lanka.*

[2] *Department of Chemistry, Faculty of Science, University of Peradeniya, Peradeniya, Sri Lanka.*

Abstract: Topical skin application of curcumin is challenging due to the low solubility and poor stability, including fast photodegradation, of this bioactive compound. Therefore, curcumin encapsulated alginate (CU-Al) nanoparticles were prepared by the ionic gelation method followed by freeze drying to determine the efficacy of alginate in facilitating curcumin release. Evaluation of the release of curcumin from the encapsulate in the presence of artificial sweat (pH 4.7) and skin (pH 5.5), about which the literature is meagre, was carried out after particle size characterization. CU-Al nanoparticles were in the nano-range (186.8 nm), assimilated a negative zeta-potential value (-15.4 ± 8.13 mV), and displayed a high encapsulation efficiency (94.55 ± 0.53%). The release of encapsulated curcumin at pH 5.5 (max. 64%) and at pH 4.7 (max. 27%) were significantly different. In pH 5.5 and pH 4.7, the release profiles of encapsulated curcumin fitted best with the Weibull (followed an anomalous transport mechanism) and Gompertz (followed a super case II transport mechanism) models respectively, displaying sigmoidal release patterns. Diffusion and polymer relaxation/swelling based release at pH 5.5 and rapid polymer relaxation/erosion based release at pH 4.7 have governed the encapsulated curcumin release. The results indicated that CU-Al nanoparticles may be utilized to facilitate controlled and prolonged release of curcumin in both skin and artificial sweat, thereby functioning as a promising novel delivery vehicle for curcumin. However, skin deposition or penetration may be required for yielding a satisfactory topical administration of curcumin during sweating.

Keywords: Alginate polymer, curcumin, nanoparticle formulation, release kinetic mechanisms, skin delivery.

INTRODUCTION

Skin, as a sensitive organ and as the first line of defence, is very susceptible to injuries, burns, infections, rashes, acne, and skin related disorders such as scleroderma, dermatitis, psoriasis, etc. (Chanchal & Swarnlata, 2008). Exposure to sunlight (UV radiation) and various other environmental conditions could lead to photo-aging, damaging and darkening of skin, and skin cancer problems (Svobodová *et al.*, 2003; Afaq & Mukhtar, 2006; Thangapazham *et al.*, 2013). As a remedy for the aforementioned skin related issues, development of cosmetic products in the form of nano-cosmetics has emerged (Boonme *et al.*, 2009; Saraf & Kaur, 2010; Li *et al.*, 2011; Taib *et al.*, 2015).

Curcumin, which is a polyphenolic phytoconstituent derived from the rhizome of turmeric (*Curcuma longa*), has been utilized in skin formulations since ancient times. Curcumin possesses antibacterial, anti-oxidant, anti-inflammatory, antifungal, antiproliferative, anti-viral, anticancer, and wound healing properties that are highly beneficial in addressing skin related issues. Moreover, curcumin acts as a protective agent against various chemicals and environmental pollutants that could cause skin damage (Thangapazham *et al.*, 2013). Regardless of the high functionality of curcumin, its poor solubility (Dutta & Ikiki, 2013), fast photodegradation upon exposure to sunlight (Tønnesen *et al.*, 1986; Lee *et al.*, 2013a), low bioavailability (Dutta & Ikiki, 2013) and poor stability in neutral and alkaline aqueous solutions and in hydrophilic topical formulations (Guadarrama-Acevedo *et al.*, 2019) could be considered as major drawbacks that make its direct application challenging.

---

* Corresponding author (geethip@wyb.ac.lk; ⓘD https://orcid.org/0000-0002-1156-5088)

In the recent past, many studies have been conducted to enhance the properties of curcumin for topical and transdermal delivery using alginate (Guadarrama-Acevedo *et al*., 2019), chitosan (Nair *et al*., 2019), nanoliposomes (Zhao *et al*., 2013), and solid lipid nanoparticles (Rungphanichkul *et al*., 2011; Zamarioli *et al*., 2015). Also, numerous topical formulations of curcumin have been developed and investigated for wound healing over the past years. For example, the review by Kumari *et al*. (2022) highlights the usage of different curcumin loaded nanocarriers such as liposomes, nanoparticles, nanoemulsions, quantum dots, lipid nanoparticles and polymeric micelles, and other polymeric systems of curcumin for wound healing.

Although such systems undoubtedly improve skin permeation and distribution of loaded bioactives, the mechanism by which this enhancement is achieved is unclear. When developing topical formulations, it is important to understand the effect of numerous variables including pH on the penetration and permeation of bioactives through the skin (de Oliveira *et al*., 2021). Current research on topical formulations of curcumin appears promising. However, the majority of published evidence is based on *in vitro* release in phosphate buffered saline (PBS) pH 7.4 or skin pH 5.0 with *ex vivo* skin permeation studies (Pamunuwa *et al*., 2016; Sharma *et al*., 2020). Yet, the effect of sweat on the release of curcumin has been poorly investigated. Specifically, the release of curcumin in the absence of sweat (at skin pH 5.5) and in the presence of sweat (pH 4.7) from alginate nanoparticles pertinent for cosmetic formulations has not been studied so far or has been rarely evaluated, although alginate and curcumin are frequently investigated for skin applications (Zakerikhoob *et al*., 2021; Kumari *et al*., 2022; Sahu & Mallick, 2022). However, gaining an understanding of the release mechanism of encapsulated curcumin, especially during sweating, is very important in order to comprehend the skin penetration ability and longevity of bioactive agents once administered topically.

For this purpose, alginate (derived from seaweed) was utilized in this study to formulate curcumin encapsulated nanoparticles which were then evaluated for release properties in media pertinent to skin. Biodegradability, biocompatibility, and non-toxicity, along with other remarkable properties of alginate beneficial for skin application, were considered in selecting this matrix. Hydrophilicity, high absorption capacity, haemostatic nature, swelling and gelling capabilities, ability to be crosslinked, bio similarity to extracellular matrices, controllable porosity, bio adhesivity, and affordability, which are properties of alginate important in wound healing, are beneficial for skin applications as well (Aderibigbe & Buyana, 2018; Guadarrama-Acevedo *et al*., 2019; Sahu & Mallick, 2022).

After characterizing the freeze-dried curcumin encapsulated alginate particles for encapsulation efficiency, loading capacity, particle size, polydispersity index, zeta-potential, and morphology, *in vitro* release at skin pH 5.5 and in artificial sweat (pH 4.7) was carried out for release model fitting and elucidation of the release mechanism, which have not been reported previously. Importantly, the release model of best fit for the release profiles and the release transport mechanism of curcumin from the nanoparticle system were determined to obtain a thorough understanding of the release of curcumin from alginate nanoparticles in media pertaining to skin conditions. The findings of this study may contribute to the development and formulation of curcumin encapsulated nano-cosmetic formulations.

MATERIALS AND METHODS

Materials

Curcumin ($\geq$ 65% purity), sodium alginate, sorbitan monooleate (Span 80) and dialysis tubing cellulose membrane (avg. flat width 43 mm/12,000 MWCO) were purchased from Sigma Aldrich Company (St. Louis, MO, USA). All other chemicals were of analytical grade.

Synthesis of curcumin encapsulated alginate (CU-Al) nanoparticles

Curcumin encapsulated alginate (CU-Al) nanoparticles were prepared using the ionic gelation method followed by centrifugation and freeze drying as described by Pamunuwa *et al*. (2021) with modifications as follows.

Initially, alginate (1.0 g) was dissolved in distilled water in order to obtain a solution of 1.0% (w/v) and the pH was adjusted to 5. After stirring the solution, span 80 (0.4% v/v) was added to the solution which was then

stirred for 2 h. Next, 5 mg of curcumin (CU) dissolved in ethanol (5 mL) was added to the solution, which was stirred well to obtain a homogeneous solution. Then, 50 mL of CaCl$_2$ (1.5% w/v) was added dropwise as a crosslinker to the mixture and stirring was continued for 1 h. Finally, the solution was refrigerated overnight, and was then centrifuged (12, 000 RPM for 45 min) and freeze dried to obtain a free-flowing powder of CU-Al nanoparticles. The stirring speed and the temperature of the solution were maintained at 1200 RPM and 60 ºC, respectively, throughout the study. Plain alginate particles were prepared similarly without incorporating CU. All the experiments were carried out under dark conditions.

Determination of encapsulation efficiency (% EE) and loading capacity (% LC)

EE and LC (%) were determined by measuring absorbance at wavelength (λ_{max}) 425 nm using a UV-Vis spectrophotometer (Evolution 220 / Thermo Fisher Scientific, USA). The amount of CU in the supernatants obtained by centrifuging the particle suspensions was determined. The experiments were carried out in triplicate under dark conditions.

% EE and % LC were calculated using the equations (1 and 2) shown below, respectively (Pamunuwa *et al*., 2016).

$$\% \ EE = \frac{\text{Mass of total amount of CU used} - \text{Mass of CU in supernatant}}{\text{Mass of total amount of CU used}} \times 100$$

...(01)

$$\% \ LC = \frac{\text{Mass of CU entrapped}}{\text{Mass of particles used}} \times 100 \qquad \qquad \text{...(02)}$$

where, CU stands for curcumin.

Particle characterization

Determination of particle size (D$_{50}$), polydispersity index (PDI) and zeta- potential

The particle size of CU-Al particles dispersed in distilled water was measured using a particle size analyzer (Cilas Nano DS, France). The dynamic light scattering (DLS) technique was utilized in order to obtain the particle size and the PDI of the particles. The zeta-potential of CU-Al particles dispersed in distilled water was measured using a Zeta-Potential Analyzer (Zetasizer Nano ZS, Malvern Instruments, UK) that uses the laser doppler electrophoresis technique.

Fourier transform infrared spectroscopy (FTIR) analysis

Infrared spectra of free CU, freeze dried free alginate nanoparticles and CU-Al nanoparticles were obtained in the range of 500-4000 cm^{-1} wavenumber under the absorbance mode, using the attenuated total reflection (ATR) (Alpha, Bruker, Germany) technique in order to verify the encapsulation of CU in the alginate matrix.

Scanning electron microscopic (SEM) imaging

To evaluate the surface morphology of the CU-Al nanoparticles, freeze dried CU-Al nanoparticles were scanned using SEM (ZEISS EVO/LS15). Nanoparticles were sprinkled on a conductive double adhesive tape supported by an aluminum stub followed by gold sputtering. Finally, the sample was scanned with an acceleration voltage and a magnification of 5.0 kV and 50.00 K X, respectively, to obtain a SEM image.

In vitro **release study at skin pHs**

In vitro release of CU from alginate nanoparticles at the average skin pH of 5.5 and artificial sweat pH of 4.7 was carried out as described by previous studies using the dialysis bag method (Pamunuwa *et al*., 2015; Ariyarathna & Karunaratne, 2016) with slight modifications as follows.

First, a known quantity of CU-Al nanoparticles was suspended in pH 5.5 phosphate buffer solution (10 mL) in a dialysis bag which was then submerged in the same buffer solution (100 mL). The temperature of the medium and the speed of stirring were maintained at 37 ± 2 °C and 400 RPM, respectively, throughout the 8 h of release study. Next, an aliquot from the release medium was removed to quantify the amount of CU at one-hour intervals. The release medium was replenished with the same volume of fresh buffer solution each time an aliquot was removed. The amount of CU released was determined using a UV-Vis spectrophotometer by measuring the absorbance at 421.1 nm wavelength (pH 5.5 $\lambda_{max} = 421.1$ nm). A similar study was carried out using artificial sweat of pH 4.7 as the release medium (pH 4.7 $\lambda_{max} = 437.1$ nm). Also, parallel experiments were carried out using free CU.

The cumulative release percentage was calculated by using the following equation (3) (Ariyarathna & Karunaratne, 2016).

$$\text{Cumulative release (\%)} = \frac{\text{Total amount of CU released to the medium}}{\text{Total encapsulated CU used}} \times 100 \qquad \ldots(3)$$

where, CU stands for curcumin.

Phosphate buffer of pH 5.5 (European Pharmacopoeia 7.0) and artificial sweat (Randin, 1987; Pamunuwa *et al.*, 2015) of pH 4.7 were prepared according to the procedures stated briefly as follows.

Phosphate buffer solution: 96.4 mL of KH_2PO_4 (13.61 g L^{-1}) was mixed with 3.6 mL of Na_2HPO_4 (35.8 g L^{-1}) and the solution was diluted to 1 L using distilled water.

Artificial sweat solution: NaCl (20 g), NH_4Cl (17.5 g), urea (5 g), acetic acid (2.5 g) and *d,l*-lactic acid (15 g) were added to 1 L of distilled water and pH of the solution was brought to 4.7 using $NaOH_{(aq)}$.

Release model fitting and transport mechanism

The data of CU release from CU-Al nanoparticles were fitted into different drug release kinetic models (Dash *et al.*, 2010; Pamunuwa *et al.*, 2020) to determine the kinetic model of best fit and the release transport mechanisms of CU. The model with the highest R-square value was considered as the model of best fit. The equations (equations 4-10) of the release kinetic models are indicated below.

Zero Order: $Q_t = Q_0 + K_0 t$ $\qquad \ldots(4)$

where, Q_t - Amount of curcumin (CU) dissolved in time t
       Q_0 - Initial amount of CU in the solution
       K_0 - Zero order release constant

First Order: $\log C = \log C_0 - Kt/2.303$ $\qquad \ldots(5)$

where, C_0 - Initial concentration of curcumin (CU)
       C - Concentration of CU at time t
       K - First order rate constant

Higuchi: $Q_t = K_H \times t^{1/2}$ $\qquad \ldots (6)$

where, Qt - Amount of curcumin (CU) released in time t
       K_H - Higuchi dissolution constant

Hixson-Crowell: $M_0^{1/3} - M_t^{1/3} = \kappa_{HC} t$ $\qquad \ldots(7)$

where, M_0 - Initial amount of curcumin (CU) in the matrix
       M_t - Remaining amount of CU in the matrix at time t
       κ_{HC} - Hixson-Crowell constant

Baker-Lonsdale: $f = \frac{3}{2}\left[1 - (\frac{M_t}{M_\alpha})^{2/3}\right] - \frac{M_t}{M_\alpha} = kt$ ...(8)

where, M_t/M_α - Fraction of curcumin (CU) released at time t

       k - Release constant

Weibull: $M = M_0\left[1 - e^{\left\{-\frac{(t-T)^b}{a}\right\}}\right]$ ...(9)

where, M - Amount of curcumin (CU) dissolved as a function of time t

     M_0 - Total amount of CU being released

      T - Lag time

      b - Shape parameter

      a - Scale parameter

Gompertz: $X(t) = X_{max}x\, e^{\{-\alpha\, e^{\beta\log t}\}}$ ...(10)

where, $X(t)$ - Percentage of curcumin (CU) dissolved at time t

     X_{max} - Maximum dissolution

       α - Undissolved proportion at time t (location/scale parameter)

       β - Dissolution rate per unit of time (shape parameter)

To evaluate the release transport mechanisms of the release of CU from CU-Al nanoparticles at pH 5.5 and pH 4.7, the semi-empirical model 'Power Law' (equation 11) described by Korsmeyer *et al*. (1983) was utilized.

$\frac{M_t}{M_\infty} = \kappa t^n$ ...(11)

where, M_t / M_∞ is the fraction of curcumin (CU) released at time t, κ is the release rate constant and n is the diffusional exponent.

The diffusional exponent (n) for each trial was determined by fitting the first 60% of the CU release data in the linearized power law equation (equation 12) which is shown below to obtain a linear plot of $M_t/M_\infty \leq 0.6$ versus log t.

$log\left(\frac{M_t}{M_\infty}\right) = log\,\kappa + n\,log\,t$ ...(12)

where, Mt / M∞ is the fraction of curcumin (CU) released at time t, κ is the release rate constant and n is the diffusional exponent.

Next, the release transport mechanisms of CU-Al nanoparticles showing spherical shaped geometry were evaluated based on different (n) values obtained for the release of CU from CU-Al nanoparticles at pH 5.5 and pH 4.7. The n values corresponding to different release mechanisms are stated in Table 1 (Korsmeyer *et al*., 1983; Peppas & Sahlin, 1989; Azad *et al*., 2020).

Table 1: Diffusional exponent ('n') values from power law corresponding to different release mechanisms for spherical particles

'n' value (Diffusional Exponent)	Release mechanism
n < 0.43	Quasi – Fickian (diffusion controlled release)
n = 0.43	Fickian (diffusion controlled release)
0.43 < n < 0.85	Anomalous transport-non Fickian diffusion (diffusion and polymer relaxation controlled release)
n = 0.85	Case II transport mechanism (release based on relaxation of the polymeric chains or swelling)
n > 0.85	Super case II transport mechanism (release based on polymer chain expansion or relaxation)

Statistical analysis

All data are presented as mean ± standard deviation (SD) of parallel experiments. Origin 6 and Origin Pro (9.1) software were used for curve fitting. One-way ANOVA with a significance value of $p \leq 0.05$ was carried out using Minitab 16 software. Microsoft Office Excel (2010) was used for producing graphs.

RESULTS AND DISCUSSION

Synthesis of CU-Al nanoparticles

Synthesis of CU-Al nanoparticles was completed successfully by using the ionic gelation method, which is one of the most common methods of alginate hydrogel preparation (Kim *et al.*, 2000). The utilization of the ionic gelation method under very mild conditions has avoided any toxic chemical involvements (Usmiati *et al.*, 2014) during nanoparticle preparation, making these particles safe for topical use. Also, enhanced protection from light and temperature may be provided to CU by encapsulation in alginate according to another study carried out by our group (Shakoor *et al*, 2023).

%EE and %LC

Encapsulation of CU in alginate displayed a high %EE of $94.55 \pm 0.53\%$ and was similar to those values reported in the literature (Nguyen *et al.*, 2015). However, the %LC was moderate and was $0.47 \pm 0.00\%$. The reason for obtaining only a moderate loading capacity may be the utilization of low CU to alginate ratio (Ji *et al.*, 2012). However, the increment of the amount of CU further led to adsorption of CU on the surface of the alginate polymer which in turn may lead to higher agglomeration of the particles. Therefore, the CU to alginate ratio was maintained at 1:200 (w/w) to enhance encapsulation and avoid/reduce adsorption of CU on the surface of alginate particles.

Particle size, PDI and zeta-potential

The stratum corneum (SC), which is the outermost layer of the epidermis of the skin, acts as a barrier against the penetration of numerous substances, including therapeutic formulations, through the skin (Kim *et al.*, 2020). The size of the particles usually has an influence on skin barrier penetration, and thus particle size determination of formulations designed for topical application is mandatory (Uchechi *et al.*, 2014). Explicitly, the smaller the particles become, the easier it is for deep skin infiltration (Hoet *et al.*, 2004). In this study, the median (D50) value of the hydrodynamic diameter of CU-Al nanoparticles was 186.8 nm. The utilization of $CaCl_2$ as a crosslinker along with Span 80 as a non-ionic surfactant may have affected the particle size (Paradee *et al.*, 2012; Suhail *et al.*, 2019). Evidently, biopolymeric nanoparticles tend to have low stability leading to a broad particle size distribution via agglomeration. However, crosslinking increases the stability of nanoparticles while decreasing particle agglomeration (Paradee *et al.*, 2012; Suhail *et al.*, 2019). Figure 1 shows the distribution of the particle size (hydrodynamic diameter) of the CU-Al nanoparticles in aqueous medium.

It is highlighted in the literature that nanocarriers developed for cosmetics or dermatology need to be sufficiently small to allow efficient penetration in to the skin owing to their high surface area and mechanical strength (Nguyen *et al.*, 2015). Nanoparticles with diameters below 500 nm guarantee direct contact with the stratum corneum due to their larger surface area to volume ratio. Therefore, CU-Al particles of nano size are expected to enhance dermal permeation, as a result of skin barrier passage including intracellular passage, making it more appropriate for topical application (Krausz *et al.*, 2015; Guadarrama-Acevedo *et al.*, 2019). However, the particles should not be too small since they tend to diffuse into the blood stream. Also, particles of diameter ~200 nm have been considered suitable for topical applications (Nguyen *et al.*, 2015). Thus, it is clearly evident that the particle sizes obtained in this study are suitable for skin delivery. Try *et al.* (2016) showed, using nanocarriers of two different sizes (*i.e.*, 70 nm and ~300 nm), that particles of sizes in this range exhibit skin penetration and that the depth of skin penetration of the smaller particles is greater than that of larger particles. Hence, CU-Al particles fabricated in this study may show skin penetration, in addition to release of CU, on topical application.
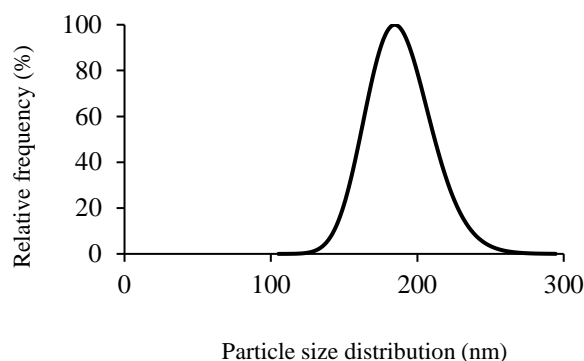
Figure 1: Particle size distribution of CU-Al nanoparticles in aqueous medium

The PDI value of the CU-Al nanoparticles was 0.292 which suggests a monodispersed and uniform distribution of particle size which is favorable for developing skin formulations. In the case of a polymeric nanoparticle system, maintaining the PDI value as low as possible (≤ 0.2) is important to obtain a monodispersed particle size distribution (Danaei *et al*., 2018).

The zeta-potential value of CU-Al nanoparticles was -15.4 ± 8.1 mV, indicating an incipient instability in aqueous medium. Zeta potential values around -30 mV generally ensure colloidal stability due to strong electrostatic repulsion between the nanoparticles (Nguyen *et al*., 2015). Yet, according to the literature, a zeta potential of -10 mV could be adequate in order to maintain the stability of nano-systems in suspensions (Nguyen *et al*., 2015). According to the zeta-potential reported in this study, -15.4 ± 8.1 mV, the fabricated CU-Al particles may show only incipient instability, and may exhibit adequate stability for the development of a skin formulation. Interestingly, charged drug carriers have caused increased diffusion of the drugs through the skin. Further, negatively charged carriers have shown a higher flux of drugs than positively charged carriers in numerous instances (Sinico *et al*., 2005; Lee *et al*., 2013b). Also, electrostatic interactions between the positively charged nanoparticles with negatively charged molecules in the matrix have caused a slowing down of particle diffusion (Lee *et al*., 2013b). However, the influence of nanoparticle charge on skin permeation is quite inconsistent according to the literature.

Overall, improved skin permeation, while protecting the encapsulated bioactive compound, may be expected according to the particle size, PDI, and zeta potential of CU-Al nanoparticles synthesized in this study.

FTIR analysis

Evaluation of the functional groups of pure CU, lyophilized plain alginate nanoparticles, and CU-Al nanoparticles was carried out by using FTIR-ATR technique, in order to confirm the interactions of the alginate polymer matrix with CU in CU-Al nanoparticles. Figure 2 displays the FTIR spectra of free CU, freeze dried alginate and CU-Al nanoparticles.

The characteristic peaks of the IR spectrum of pure CU closely aligned with the literature values (Ismail *et al*., 2014; Chen *et al*., 2015; Pecora *et al*., 2016; Okagu *et al*., 2020). A prominent broad peak corresponding to the stretching vibrations of phenolic OH groups at 3504.6 cm^{-1}, sharp narrow peaks corresponding to aromatic C=C stretching vibrations at 1507.2 cm^{-1} and C=O stretching of the keto group at 1626.7 cm^{-1} were observed. Peaks at 1274.2 cm^{-1} and 1424.9 cm^{-1} corresponding to the C-O stretching vibration of phenolic group and bending vibration of C-H (alkane), respectively, were also observed. In addition, the peak at 1231.3 cm^{-1} is attributable to asymmetric C-O-C stretching vibrations, while the peak at 1025.4 cm^{-1} is attributable to symmetric C-O-C stretching vibrations. The characteristic peaks at 856.9 cm^{-1} and 809.2 cm^{-1} represent the C-H out of plane bending mode of the meta- and para-substituted aromatic moiety.

Encapsulation of CU in alginate has caused shifting of certain peaks and revealed the distinct absorption peaks of CU indicating a mixture of signals in the spectrum of CU-Al particles. The shifting of the peaks of alginate on encapsulation of CU is indicated in Table 2 (Nastaj *et al.*, 2010; Larosa *et al.*, 2018).

Table 2: Shifted FTIR peaks of plain alginate and curcumin encapsulated alginate nanoparticles

Vibration/ functional group	Peak (cm^{-1})	
	Alginate	CU-Al nanoparticles
Stretching vibrations of O-H group (broad peak)	3267.7	3259.5
Stretching vibrations of aliphatic C-H	2923.9	2921.8
Shoulder peak corresponding to the stretching vibrations of the C-O group of the un-dissociated carboxylic group	1737.8	1746.1
Splitting of COO- stretching into asymmetric C=O vibrations	1412.5	1418.6
C-O stretching vibrations	1299.3	1293.1
C-O, C-C, and COC stretching vibrations	1085.3	1081.0
C-C and COC vibrations	1029.5	1025.4
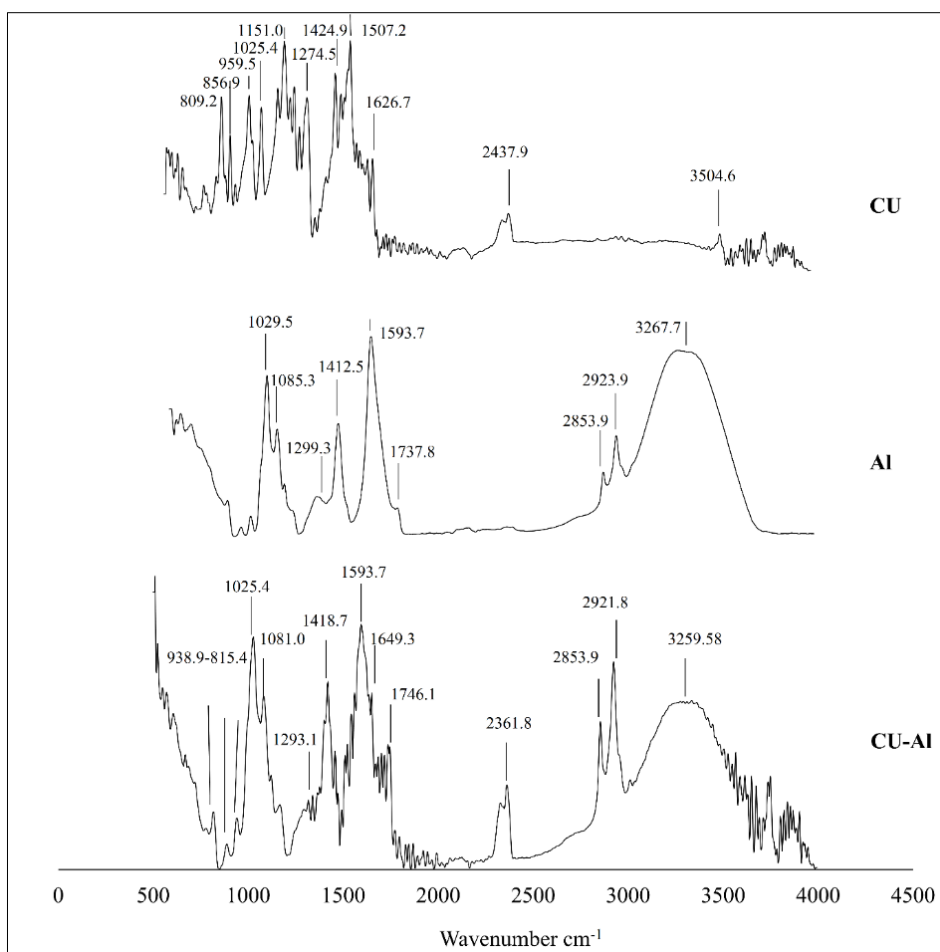
Figure 2: FTIR of pure CU, freeze dried alginate and CU-Al nanoparticles, respectively.
(CU : curcumin, Al : Alginate, CU-Al : Curcumin encapsulated alginate particles)

Further, especially, the appearance of characteristic peak of pure CU at 2437.9 cm^{-1} in the functional group region of CU-Al nanoparticles at 2361.8 cm^{-1} and the observation of peaks related to pure CU in the finger print region of CU-Al encapsulate indicated that the CU was loaded into the alginate matrix of the nanoparticles successfully.

SEM Imaging

Figure 3 shows the SEM image of freeze-dried CU-Al nanoparticles. According to the SEM image, CU-Al nanoparticles displayed a spherical shape and diameters mostly below 200 nm. As expected, the diameter of the freeze-dried particles was smaller than the hydrodynamic diameter. Even though the homogeneity of CU-Al particle sizes is not clear in the SEM image, obtaining a single peak in DLS data close to 186 nm proved a uniform particle size distribution. However, the appearance of lump structure in the background of the SEM image may be probably due to agglomeration and cluster formation of the freeze-dried particles during the time of sample preparation. Depending on the type of skin formulation, either freeze dried particles or wet particles may be used since the particle size may have a significant influence on the efficacy of the skin formulation (Uchechi *et al.*, 2014).
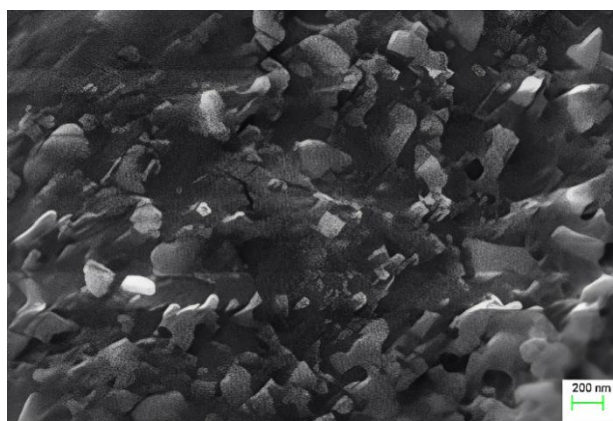
Figure 3: SEM image of CU-Al particles (CU-Al : Curcumin encapsulated alginate)

***In vitro* release of CU from CU-Al nanoparticles at skin pHs**

An *in vitro* release study was performed to determine the release models and mechanisms of release of CU from CU-Al nanoparticles at average skin pH 5.5 and in sweat at pH 4.7. Figure 4 shows the comparative release of free CU and CU from CU-Al nanoparticles at pH 5.5 and in artificial sweat.

At pH 5.5, release of free CU was significantly higher than that from the CU encapsulated nanoparticles. Free CU displayed a burst release of around 40% during the very first hour of the release time. The highest release of free CU was approximately 93%. However, release of CU from CU-Al nanoparticles displayed a much controlled and slower release and the highest release, shown at 8 h of release time, was approximately 65%. Prolonged release of encapsulated CU may increase the resident time of CU on the skin surface. Also, encapsulation of CU has mostly avoided burst release of CU and avoided high amounts of CU in contact with skin. This property is very significant as any direct contact of the skin with CU that exceeds its toxic limit would be harmful (Krausz *et al.*, 2015). Moreover, controlled release of encapsulated CU may avoid the bright yellow pigmentation leading to skin discoloration caused by free CU accumulating on the skin surface.

The release of CU from CU-Al nanoparticles at pH 4.7 was significantly different from the release of CU from CU-Al at pH 5.5. In fact, the maximum release of CU from CU-Al nanoparticles at pH 4.7 was much lower (approx. 27%) than that at pH 5.5 (approx. 65%). This is in accordance with the literature that has shown lower release of encapsulated material in artificial sweat than media of higher pH (Pamunuwa *et al.*, 2015). Interestingly, free CU displayed a release pattern almost similar to CU-Al in artificial sweat (pH 4.7). The maximum release of free CU was nearly 35%. Low release of free CU and CU from CU-Al nanoparticles at pH 4.7 may be due to the low solubility of CU in aqueous media of low pH that lead to crystallization and sedimentation of CU (Zheng & McClements, 2020).
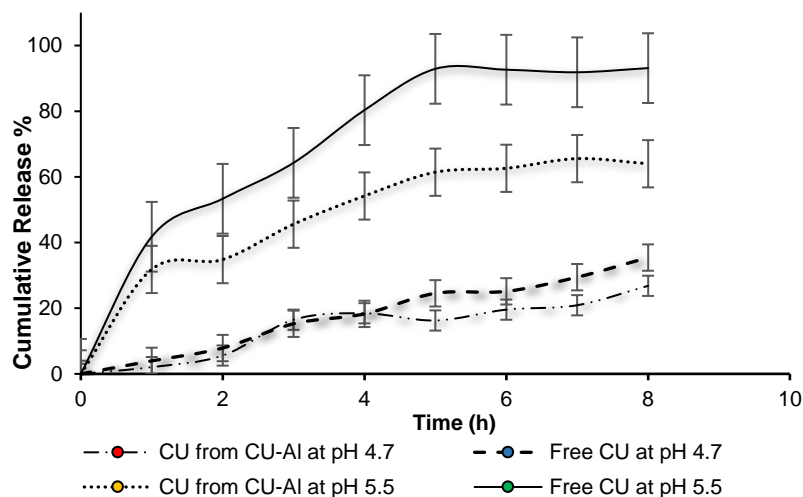
Figure 4: Release of free CU and CU from CU-Al nanoparticles at pH 5.5 and artificial sweat
pH 4.7 (CU – free curcumin, CU-Al – Curcumin encapsulated alginate particles)

Further evaluation of the pharmacokinetics of CU release from CU-Al nanoparticles was carried out at skin pH 5.5 and artificial sweat pH 4.7. Table 3 shows the adjusted R^2 values of the release profiles fitted to different kinetic models and the model of best fit was selected based on these values.

At pH 5.5, the Weibull model fitted well with the release profile of CU from the CU-Al spherical nanoparticles confirming that the best release model for swellable polymeric matrix is the Weibull model (Azadi *et al.*, 2017). At pH 4.7, the Gompertz and Weibull models described the release of CU from the nanoparticles. Both Weibull and Gompertz models infer a sigmoidal pattern of release of encapsulated CU.

Table 3: Correlation coefficients (adjusted R^2 values) of release kinetic model fitting for CU release from CU-Al nanoparticles at pH 5.5 and pH 4.7 (artificial sweat)

Models n = 3	Release of CU from CU-Al nanoparticles at pH 5.5 Adjusted R^2 values Mean ± SD	Release of CU from CU-Al nanoparticles at pH 4.7 Adjusted R^2 values Mean ± SD
Zero order	0.769 ± 0.040[b]	0.846 ± 0.011[a]
First order	0.383 ± 0.026[c]	0.744 ± 0.029[a]
Higuchi	0.914 ± 0.022[a]	0.828 ± 0.052[a]
Hixson-Crowell	0.360 ± 0.037[c]	0.476 ± 0.008[b]
Baker-Lonsdale	0.410 ± 0.070[c]	0.094 ± 0.348[c]
Weibull	0.916 ± 0.048[a]	0.851 ± 0.083[a]
Gompertz	0.830 ± 0.090[a, b]	0.869 ± 0.084[a]

Means that do not share the same superscript in the same column are significantly different ($p < 0.05$).
n: number of trials; CU: curcumin; CU-Al: curcumin encapsulated alginate

Alginate is a water-soluble polymer showing pH-dependent behavior. The release of a bioactive compound from alginate occurs after alginate undergoes hydration, swelling, relaxation of the chains, or erosion. At low pH levels, alginate chains tend to shrink considerably, and with the increase of the pH level, the chains undergo relaxation followed by swelling of the alginate matrix, with an enhancement of the porosity of the structure (Tønnesen & Karlsen, 2002). Considering the aforementioned phenomena, the release of CU from the nanoparticles at pH 5.5 and pH 4.7 could take place due to either pure diffusion, swelling, or polymer erosion/degradation controlled mechanisms. In this regard, obtaining the diffusional coefficient (n value) using the linearized power law equation (equation 12) is essential for a better understanding of the release mechanisms of encapsulated CU at those pHs.

At pH 5.5, the diffusional coefficient (n) value obtained for CU release from nanoparticles was 0.61, which indicated an anomalous transport mechanism. This mechanism is a non-Fickian transport mechanism of which release is governed by a combination of diffusion and chain relaxation (Azad *et al*., 2020). Therefore, the alginate polymer must have undergone a considerable amount of chain relaxation and solvent diffusion to the same extent, leading to polymer swelling, thereby releasing CU at the skin pH of 5.5. Previous studies on alginate hydrogels have concluded that the release of lipophilic bioactive agents (such as curcumin) were controlled by swelling of the hydrogel and diffusion of the bioactives (Xu *et al.,* 2019).

At pH 4.7, the n value was 1.16, which displayed a super case II transport mechanism of encapsulated CU, which indicated a release of CU due to the expansion or relaxation/erosion of alginate chains (El-Houssiny *et al*., 2017; Azad *et al*., 2020). This observation may probably be due to the high NaCl concentration present in artificial sweat medium, which affected the solubility of alginate. That is, Ca^{2+} ions involved in hardening of the alginate matrix via crosslinking, forming a hydrogel structure (Reddy & Nagabhushanam, 2019), may have undergone ion exchange with Na^+ ions in the solution. During the ion exchange, partial disintegration of the previously insoluble structure may have occurred due to the destabilization of the egg-box structure, leading to higher solubility of the matrix (Segale *et al*., 2016). Despite the fact that rapid release of CU was expected due to rapid polymer relaxation/erosion, the reason for a lower CU release from the nanoparticles at pH 4.7 may be due to the low solubility of CU in the acidic medium. Besides, the similar release pattern observed for free CU at pH 4.7 indicates that the reduced rate of CU release from CU-Al at pH 4.7 may be due to low solubility of CU. It has been found that increased salt (NaCl) concentrations (2-500 mM) influences CU decomposition (Mondal *et al*., 2016). Therefore, poor acidic solubility of CU supported by NaCl concentration of artificial sweat (pH 4.7) may have affected CU solubility and stability in the release medium.

Therefore, considering the overall outcomes, further improvements in engineering of CU-Al nanoparticles may be essential to enhance the solubility of CU, especially in the presence of sweat. However, utilization of nano-encapsulation to facilitate slow release of CU at both skin pH and artificial sweat, could result in enhancement of both skin deposition and skin penetration.

CONCLUSION

Nanoparticles of CU-Al showed properties, especially particle size, PDI, and encapsulation efficiency, favorable for topical skin application. Encapsulation of CU in alginate provided slow controlled release of CU, thus, enabling prolonged release of CU from the nanoparticles so that sustained topical or skin delivery may take place. Also, photodegradation of CU occurring on exposure to sun light (UV rays) could be avoided, especially, when the active ingredient CU encapsulated in alginate is applied on the skin via nanocosmetic formulations. Therefore, encapsulated CU is expected to exhibit greater activity and photo-stability once applied on the skin. However, improving the activity of CU during sweating may require skin deposition or skin penetration of nanoparticles encapsulated with CU mainly due to poor solubility of free CU. Evaluation of both the release model and release mechanism indicated that release of CU at the skin pH and in artificial sweat occurs due to diffusion and polymer expansion respectively, along with chain relaxation and swelling of the particles. However, the extent of skin penetration of free CU and nanoencapsulated CU needs to be evaluated for a better understanding of the overall skin delivery process. Therefore, *in vivo* experiments leading to human clinical trials should be conducted to evaluate the therapeutic effect of curcumin-alginate formulations fabricated in this study for topical application especially during sweating conditions.

REFERENCES

Aderibigbe B.A. & Buyana B. (2018). Alginate in wound dressings. *Pharmaceutics* **10**(2): 42.
    DOI: https://doi.org/10.3390/pharmaceutics10020042

Afaq F. & Mukhtar H. (2006). Botanical antioxidants in the prevention of photocarcinogenesis and photoaging. *Experimental Dermatology* **15**: 678–84.
    DOI: https://doi.org/10.1111/j.1600-0625.2006.00466.x

Ariyarathna I.R. & Karunaratne D.N. (2016). Microencapsulation stabilizes curcumin for efficient delivery in food applications. *Food Packaging and Shelf Life* **10**:79–86.
    DOI: https://doi.org/10.1016/j.fpsl.2016.10.005

Azad A.K., Al-Mahmood S.M., Chatterjee B., Wan Sulaiman W.M., Elsayed T.M. & Doolaanea A.A. (2020). Encapsulation of black seed oil in alginate beads as a pH-sensitive carrier for intestine-targeted drug delivery: In vitro, in vivo and ex vivo study. *Pharmaceutics* **12**(3):219.
    DOI: https://doi.org/10.3390/pharmaceutics12030219

Azadi S., Ashrafi H., & Azadi A. (2017). Mathematical modeling of drug release from swellable polymeric nanoparticles. *Journal of Applied Pharmaceutical Science* **7**:125–133.
    DOI: https://doi.org/10.7324/JAPS.2017.70418

Boonme P., Junyaprasert V.B., Suksawad N. & Songkro S. (2009). Microemulsions and nanoemulsions: Novel vehicles for whitening cosmeceuticals. *Journal of Biomedical Nanotechnology* **5**:373–383.
    DOI: https://doi.org/10.1166/jbn.2009.1046

Chanchal D. & Swarnlata S. (2008). Novel approaches in herbal cosmetics. *Journal of Cosmetic Dermatology* **7**:89–95.
    DOI: https://doi.org/10.1111/j.1473-2165.2008.00369.x

Chen X., Zou L.Q., Niu J., Liu W., Peng S.F. & Liu C.M. (2015). The stability, sustained release and cellular antioxidant activity of curcumin nanoliposomes. *Molecules* **20**: 14293–14311.
    DOI: https://doi.org/10.3390/molecules200814293

Danaei M., Dehghankhold M., Ataei S., Hasanzadeh Davarani F., Javanmard R., Dokhani A., Khorasani S. & Mozafari M. R. (2018). Impact of Particle Size and Polydispersity Index on the Clinical Applications of Lipidic Nanocarrier Systems. *Pharmaceutics* **10**(2): 57.
    DOI: https://doi.org/10.3390/pharmaceutics10020057

Dash S., Murthy P.N., Nath L. & Chowdhury P. (2010). Kinetic modeling on drug release from controlled drug delivery systems. *Acta Poloniae Pharmaceutica* **67**: 217–23.

De Oliveira R.S., Fantaus S.S., Guillot A.J., Melero A. & Beck R.C.R. (2021). 3D-printed products for topical skin applications: from personalized dressings to drug delivery. *Pharmaceutics* **13**(11): 1946.
    DOI: https://doi.org/10.3390/pharmaceutics13111946

Dutta A.K. & Ikiki E. (2013). Novel drug delivery systems to improve bioavailability of curcumin. *Journal of Bioequivalence and Bioavailability* **6**:001–9.
    DOI: http://dx.doi.org/10.4172/jbb.1000172

El-Houssiny A.S., Ward A.A., Mostafa D.M., Abd-El-Messieh S.L., Abdel-Nour K.N., Darwish M.M. & Khalil W.A. (2017). Sodium alginate nanoparticles as a new transdermal vehicle of glucosamine sulfate for treatment of osteoarthritis. *European Journal of Nanomedicine* **9**:105–114.
    DOI: https://doi.org/10.1515/ejnm-2017-0008

European Pharmacopoeia 7.0 (2021). Buffer Solutions. Available at: https://www.researchgate.net/profile/Samarth_Zarad/post/How_to_prepare_20_mM_sodium_acetate_buffer_pH_46/attachment/59d6526079197b80779aa9b2/AS%3A5120 87772364801%401499102647435/download/USEPA+_BUFFER.PDF Accessed on 02 Jan 2021.

Guadarrama-Acevedo M.C. *et al.* (14 authors) (2019). Development and evaluation of alginate membranes with curcumin-loaded nanoparticles for potential wound-healing applications. *Pharmaceutics* **11**(8): 389.
    DOI: https://doi.org/10.3390/pharmaceutics11080389

Hoet P.H., Bruske-Hohlfield I. & Salata O.V. (2004). Nanoparticles-known and unknown health risks. *Journal of Nano biotechnology* **2**:12.
    DOI: https://doi.org/10.1186/1477-3155-2-12

Ismail E.H., Sabry D.Y., Mahdy H. & Khalil M.M. (2014). Synthesis and characterization of some ternary metal complexes of curcumin with 1, 10-phenanthroline and their anticancer applications. *Journal of Science Research* **6**: 509–519.
    DOI: https://doi.org/10.3329/jsr.v6i3.18750

Ji J., Wu D., Liu L., Chen J. & Xu Y. (2012). Preparation, characterization, and in vitro release of folic acid-conjugated chitosan nanoparticles loaded with methotrexate for targeted delivery. *Polymer Bulletin* **68**: 1707–1720.
    DOI: https://doi.org/10.1007/s00289-011-0674-x

Kim, B., Cho, H.E., Moon, S.H., Ahn, H.J., Bae, S., Cho, H.D. & An, S. (2020). Transdermal delivery systems in cosmetics. *Biomedical Dermatology* **4**:1–2.
    DOI: https://doi.org/10.1186/s41702-020-0058-7

Kim Y.J., Yoon K.J. & Ko S.W. (2000). Preparation and properties of alginate superabsorbent filament fibers crosslinked with glutaraldehyde. *Journal of Applied Polymer Science* **78**: 1797–804.

DOI: https://doi.org/10.1002/1097-4628(20001205)78:10<1797::AID-APP110>3.0.CO;2-M

Korsmeyer R.W., Gurny R., Doelker E., Buri P. & Peppas N.A. (1983). Mechanisms of solute release from porous hydrophilic polymers. *International Journal of Pharmaceutics* **15**: 25–35.
DOI: https://doi.org/10.1016/0378-5173(83)90064-9

Krausz A.E. *et al.* (14 authors) (2015). Curcumin-encapsulated nanoparticles as innovative antimicrobial and wound healing agent. *Nanomedicine* **11**: 195–206.
DOI: https://doi.org/10.1016/j.nano.2014.09.004

Kumari A., Raina N., Wahi A., Goh K.W., Sharma P., Nagpal R. & Gupta M. (2022). Wound-healing effects of curcumin and its nanoformulations: a comprehensive review. *Pharmaceutics* **14**(11): 2288.
DOI: https://doi.org/10.3390/pharmaceutics14112288

Larosa C., Salerno M., de Lima J.S., Meri R.M., da Silva M.F., de Carvalho L.B. & Converti A. (2018). Characterisation of bare and tannase-loaded calcium alginate beads by microscopic, thermogravimetric, FTIR and XRD analyses. *International Journal of Biological Macromolecules* **115**: 900–906.
DOI: https://doi.org/10.1016/j.ijbiomac.2018.04.138

Lee B.H., Choi H.A., Kim M.R. & Hong J. (2013a). Changes in chemical stability and bioactivities of curcumin by ultraviolet radiation. *Food Science and Biotechnology* **22**:279–282.
DOI: https://doi.org/10.1007/s10068-013-0038-4

Lee O., Jeong S.H., Shin W.U., Lee G., Oh C. & Son S.W. (2013b). Influence of surface charge of gold nanorods on skin penetration. *Skin Research and Technology* **19**: e390–e396.
DOI: https://doi.org/10.1111/j.1600-0846.2012.00656.x

Li D., Wu Z., Martini N. & Wen J. (2011). Advanced carrier systems in cosmetics and cosmeceuticals: a review. *Journal of Cosmetic Science* **62**: 549–63.

Mondal S., Ghosh S. & Moulik S.P. (2016) Stability of curcumin in different solvent and solution media: UV–visible and steady-state fluorescence spectral study. *Journal of Photochemistry and Photobiology B: Biology* **158**: 212–218.
DOI: https://doi.org/10.1016/j.jphotobiol.2016.03.004

Nair R.S., Morris A., Billa N. & Leong C.O. (2019). An evaluation of curcumin-encapsulated chitosan nanoparticles for transdermal delivery. *AAPS PharmSciTech* **20**: 1–3.
DOI: https://doi.org/10.1208/s12249-018-1279-6

Nastaj J., Przewłocka A. & Rajkowska-Myśliwiec M. (2016). Biosorption of Ni (II), Pb (II) and Zn (II) on calcium alginate beads: equilibrium, kinetic and mechanism studies. *Polish Journal of Chemical Technology* **8**: 81–7.
DOI: https://doi.org/10.1515/pjct-2016-0052

Nguyen H.T.P., Munnier E., Souce M., Perse X., David S., Bonnier F. & Chourpa I. (2015). Novel alginate-based nanocarriers as a strategy to include high concentrations of hydrophobic compounds in hydrogels for topical application. *Nanotechnology* **26**(25): 255101.
DOI: https://doi.org/10.1088/0957-4484/26/25/255101

Okagu O.D., Verma O., McClements D.J. & Udenigwe C.C. (2020). Utilization of insect proteins to formulate nutraceutical delivery systems: encapsulation and release of curcumin using mealworm protein-chitosan nano-complexes. *International Journal of Biological Macromolecules* **151**: 333–43.
DOI: https://doi.org/10.1016/j.ijbiomac.2020.02.198

Pamunuwa G., Anjalee N., Kukulewa D., Edirisinghe C., Shakoor F. & Karunaratne D.N. (2020). Tailoring of release properties of folic acid encapsulated nanoparticles via changing alginate and pectin composition in the matrix. *Carbohydrate Polymer Technologies and Applications* **1**: 100008.
DOI: https://doi.org/10.1016/j.carpta.2020.100008

Pamunuwa G., Nilakshi H., Rajapaksha G., Shakoor F. & Karunaratne D.N. (2021). Sensory and physicochemical properties and stability of folic acid in a pineapple ready-to-serve beverage fortified with encapsulated folic acid. *Journal of Food Quality* **2021**: 9913884.
DOI: https://doi.org/10.1155/2021/9913884

Pamunuwa G., Karunaratne V. & Karunaratne D. (2016). Effect of lipid composition on in vitro release and skin deposition of curcumin encapsulated liposomes. *Journal of Nanomaterials* **2016**: 4535790.
DOI: https://doi.org/10.1155/2016/4535790

Pamunuwa K.M.G.K., Bandara C.J., Karunaratne V. & Karunaratne D.N. (2015). Optimization of a liposomal delivery system for the highly antioxidant methanol extract of stem-bark of *Schumacheria castaneifolia* Vahl. *Journal of Chemical and Pharmaceutical Research* **7**: 1236–1245.

Paradee N., Sirivat A., Niamlang S. & Prissanaroon-Ouajai W. (2012). Effects of crosslinking ratio, model drugs, and electric field strength on electrically controlled release for alginate-based hydrogel. *Journal of Materials Science: Materials in Medicine* **23**: 999–1010.
DOI: https://doi.org/10.1007/s10856-012-4571-0

Pecora T.M., Cianciolo S., Catalfo A., De Guidi G., Ruozi B., Cristiano M.C., Paolino D., Graziano A.C., Fresta M. & Pignatello R. (2016). Preparation, characterization and photostability assessment of curcumin microencapsulated within methacrylic copolymers. *Journal of Drug Delivery Science and Technology* **33**: 88–97.
DOI: https://doi.org/10.1016/j.jddst.2016.03.013

Peppas N.A. & Sahlin J.J. (1989). A simple equation for the description of solute release. III. Coupling of diffusion and relaxation. *International Journal of Pharmaceutics* **57**: 169–172.
DOI: https://doi.org/10.1016/0378-5173(89)90306-2

Randin J.P. (1987). Pitting potential of stainless steels in artificial sweat. *Materials and Corrosion* **38**: 175–183.
DOI: https://doi.org/10.1002/maco.19870380404

Reddy K.V. & Nagabhushanam M. (2019). Preparation of gastro retentive mucoadhesive beads for atorvastatin by using ionic gelation method with divalence and trivalence curing agents and their characterization studies. *International Journal of Pharmaceutical Sciences and Research* **10**: 157–179.
DOI: https://doi.org/10.13040/IJPSR.0975-8232.10(1).157-79

Rungphanichkul N., Nimmannit U., Muangsiri W. & Rojsitthisak P. (2011). Preparation of curcuminoid niosomes for enhancement of skin permeation. *International Journal of Pharmaceutical Sciences* **66**: 570–575.
DOI: https://doi.org/10.1691/ph.2011.1018

Sahu S. & Mallick B.C. (2022). Curcumin-Alginate mixed nanocomposite: an evolving therapy for wound healing. In: *Properties and Applications of Alginates* (eds. E Deniz, E. Imamoglu & T.K. Gundogdu), pp. **131**. IntechOpen Limited, London, UK.
DOI: https://doi.org/10.5772/intechopen.98830

Saraf S. & Kaur C.D. (2010). Phytoconstituents as photoprotective novel cosmetic formulations. *Pharmacognosy Reviews* **4**:1.
DOI: https://dx.doi.org/10.4103%2F0973-7847.65319

Segale L., Giovannelli L., Mannina P. & Pattarino F. (2016). Calcium alginate and calcium alginate-chitosan beads containing celecoxib solubilized in a self-emulsifying phase. *Scientifica* **2016:** 5062706.
DOI: https://doi.org/10.1155/2016/5062706

Sinico C., Manconi M., Peppi M., Lai F., Valenti D. & Fadda A.M. (2005). Liposomes as carriers for dermal delivery of tretinoin: in vitro evaluation of drug permeation and vesicle–skin interaction. *Journal of Controlled Release* **103**:123–36.
DOI: https://doi.org/10.1016/j.jconrel.2004.11.020

Shakoor I.F., Pamunuwa G.K. & Karunaratne D.N. (2023). Efficacy of alginate and chickpea protein polymeric matrices in encapsulating curcumin for improved stability, sustained release and bioaccessibility. *Food Hydrocolloids for Health*, 100119.
DOI: https://doi.org/10.1016/j.fhfh.2023.100119

Sharma A., Mittal A., Puri V., Kumar P. & Singh I. (2020). Curcumin-loaded, alginate–gelatin composite fibers for wound healing applications. *3 Biotech* **10**(11): 1–13.
DOI: https://doi.org/10.1007/s13205-020-02453-5

Suhail M., Janakiraman A.K., Khan A., Naeem A., & Badshah F.S. (2019). Surfactants and their role in pharmaceutical product development: an overview. *Journal of Pharmacy and Pharmaceutics* **6:** 72–82.
DOI: https://doi.org/10.15436/2377-1313.19.2601

Svobodová A., Psotová J. & Walterová D. (2003). Natural phenolics in the prevention of UV-induced skin damage: a review. *Biomedical Papers* **147**: 137–45.
DOI: https://doi.org/10.5507/bp.2003.019

Taib S.H., Abd Gani S.S., Ab Rahman M.Z., Basri M., Ismail A. & Shamsudin R. (2015). Formulation and process optimizations of nano-cosmeceuticals containing purified swiftlet nest. *RSC Advances* **5**: 42322–42328.
DOI: https://doi.org/10.1039/C5RA03008K.

Thangapazham R.L., Sharad S. & Maheshwari R.K. (2013). Skin regenerative potentials of curcumin. *Biofactors* **39**:141–149.
DOI: https://doi.org/10.1002/biof.1078.

Try C., Moulari B., Béduneau A., Fantini O., Pin D., Pellequer Y. & Lamprecht A. (2016). Size dependent skin penetration of nanoparticles in murine and porcine dermatitis models. *European Journal of Pharmaceutics and Biopharmaceutics* **100**: 101–108.
DOI: https://doi.org/10.1016/j.ejpb.2016.01.002

Tønnesen H.H. & Karlsen J. (2002). Alginate in drug delivery systems. *Drug Development and Industrial Pharmacy* **28**: 621–630.
DOI: https://doi.org/10.1081/DDC-120003853

Tønnesen H.H., Karlsen J. & van Henegouwen G.B. (1986). Studies on curcumin and curcuminoids VIII. Photochemical stability of curcumin. *Zeitschrift für Lebensmittel-Untersuchung und Forschung* **183**:116–122.
DOI: https://doi.org/10.1007/BF01041928

Uchechi O., Ogbonna J.D. & Attama A.A. (2014). Nanoparticles for dermal and transdermal drug delivery. *Application of Nanotechnology in Drug Delivery* **4**:193–227.
DOI: http://dx.doi.org/10.5772/58672.

Usmiati S., Richana N., Mangunwidjaja D., Noor E. & Prangdimurti E. (2014). The using of ionic gelation method based on polysaccharides for encapsulating the macromolecules–a review. *Encapsulation for Protecting the Bioactive Compounds* **67**: 79–84.
DOI: http://dx.doi.org/10.7763/IPCBEE. 2014.V67.16

Xu W., Huang L., Jin W., Ge P., Shah B.R., Zhu D. & Jing, J. (2019). Encapsulation and release behavior of curcumin based on nanoemulsions-filled alginate hydrogel beads. *International Journal of Biological Macromolecules* **134**: 210–215.

DOI: https://doi.org/10.1016/j.ijbiomac.2019.04.200

Zakerikhoob M., Abbasi S., Yousefi G., Mokhtari M. & Noorbakhsh M.S. (2021). Curcumin-incorporated crosslinked sodium alginate-g-poly (N-isopropyl acrylamide) thermo-responsive hydrogel as an in-situ forming injectable dressing for wound healing: In vitro characterization and in vivo evaluation. Carbohydrate Polymers **271**: 118434.

Zamarioli C.M., Martins R.M., Carvalho E.C. & Freitas L.A. (2015). Nanoparticles containing curcuminoids (Curcuma longa): development of topical delivery formulation. *Revista Brasileira de Farmacognosia* **25**: 53–60.
DOI: https://doi.org/10.1016/j.bjp.2014.11.010

Zhao Y.Z., Lu C.T., Zhang Y., Xiao J., Zhao Y.P., Tian J.L., Xu Y.Y., Feng Z.G. & Xu C.Y. (2013). Selection of high efficient transdermal lipid vesicle for curcumin skin delivery. *International Journal of Pharmaceutics* **454**: 302–309.
DOI: https://doi.org/10.1016/j.ijpharm.2013.06.052

Zheng B. & McClements D.J. (2020). Formulation of more efficacious curcumin delivery systems using colloid science: enhanced solubility, stability, and bioavailability. *Molecules* **25**: 2791.
DOI: https://doi.org/10.3390/molecules25122791.

RESEARCH ARTICLE

Organic Synthesis

Synthesis and biological evaluation of gallic acid esters as phagocyte oxidative burst inhibitors

MAA Baheej[1,2], HM Haniffa[2*], H Siddiqui[1] and A Jabeen[3]

[1] *H.E.J. Research Institute of Chemistry, International Center for Chemical and Biological Sciences, University of Karachi, Karachi-75270, Pakistan.*

[2] *Department of Chemical Sciences, Faculty of Applied Sciences, South Eastern University, Oluvil, Sri Lanka.*

[3] *Dr. Panjwani Center for Molecular Medicine and Drug Research International Center for Chemical and Biological Sciences, University of Karachi, Karachi-75270, Pakistan.*

Abstract: Several degenerative diseases, including cancer, are caused by oxidative stress, which is caused by the overproduction and accumulation of free radicals. The purpose of the study was to synthesize gallic acid (GA or 3,4,5-trihydroxybenzoic acid) esters and evaluate their anti-inflammatory potential through the inhibition of reactive oxygen species (ROS). The compounds methyl gallate (2), s*ec*-butyl gallate (3), ethyl gallate (4), isopropyl gallate (5), 2-methoxyethyl gallate (6), 4-methoxybutyl gallate (7), 2-methylbutyl gallate (8) and pentan-3-yl gallate (9) were synthesized. ^{1}H NMR, MS and IR data are reported for compounds 2-9, and ^{13}C NMR data for compounds 2, 3, 5, and 6. The molecular formulae of compounds 3 and 7-9 were established by HREI-MS spectroscopic data. All the synthesized compounds were tested for their anti-inflammatory and cytotoxic activities by chemiluminescence and MTT cytotoxicity assay respectively. The results revealed the anti-inflammatory potential of compounds 2-8 with an IC_{50} range between (13.3 – 54.3 µM) as compared to the standard anti-inflammatory drug, Ibuprofen (IC_{50} = 54.3 ± 9.2 µM). The most potent inhibitors were found to be compound 3 (ROS IC_{50} = 15.0 ± 6.6 µM) and compound 7 (ROS IC_{50} = 13.3 ± 0.8 µM). All compounds were found to be non-cytotoxic in the NIH-3T3 fibroblast cell line. Compounds 3, 7- 9 were identified as new compounds.

Keywords: Anti-inflammatory, cytotoxicity, ester derivatives, gallic acid, ROS Inhibitors.

INTRODUCTION

Oxidative stress, is a result of an overproduction and accumulation of free radicals, and among the main source of degenerative diseases like cancer, atherosclerosis, ageing, and cardiovascular and inflammatory diseases (Badhani *et al.*, 2015). Inflammation is the body's defence system that protects it from harmful changes and speeds up the healing process. The lack of a healing process for injuries or any other dysfunction will result in chronic inflammation. It is characterized by redness, pain, warmth, swelling, and lack of function in the injured region (Krishnaraju *et al.*, 2009; Ho *et al.*, 2010; Ali *et al.*, 2019). Certain natural and synthetic drugs have been produced for the treatment of chronic inflammation and related diseases. These are classified as steroidal and non-steroidal anti-inflammatory drugs (NSAIDs) (Crofford, 2013). Short-term use of steroidal drugs is linked with side effects, including cutaneous effects, electrolyte abnormalities, hypertension, hyperglycaemia, and neuropsychological effects, while their long-term use is associated with more serious consequences, such as osteoporosis, aseptic joint necrosis, adrenal insufficiency, growth suppression, and possible congenital malformations (Brown & Chandler, 2001).

The side effects related to these drugs create a need for the development of new and powerful anti-inflammatory drugs. Antioxidants decrease oxidative stress and neutralize ROS before they damage the tissues (Roots & Okada, 1975; Thadhani *et al.*, 2011). By augmenting the natural antioxidant defence system with diverse exogenous antioxidants such as vitamins and synthetic agents, oxidative damage and disease development could be slowed down in the body (Lee *et al.*, 1998). Tissue damage can be caused by an imbalance between antioxidant defences and repair mechanisms (Davies, 2000). This imbalance can also be a factor in tissue injuries. The impact of ROS on tissues is devastating regarding oxidative stress-induced cell death (Valko *et al.*, 2007).

* Corresponding author (haroonmh@seu.ac.lk; https://orcid.org/0000-0001-7439-0724)

Some naturally occurring phenolic acids and their analogs, such as gallic acids, have a wide range of essential pharmacological effects. Gallic acid (GA, 3,4,5-trihydroxybenzoic acid) possesses anti-inflammatory capabilities and regulates many pharmacological and biochemical pathways (Kroes *et al*., 1992). It also has anti-mutagenic and anticancer effects (Gichner *et al*., 1987; Inoue *et al*., 2000), in addition to its primary antioxidant activity (Golumbic & Mattill, 1942; Heo *et al*., 2007; Kumar *et al*., 2012). GA and its esters are used in the food and pharmaceutical industries as antioxidant additives (Locatelli *et al*., 2013). E-310 (propyl gallate) and E-311 (octyl gallate) are known to protect against oxidative damage induced by reactive oxygen species (ROS), such as hydroxyl radicals or hydrogen peroxide, and reactive sulphur species (RSS) (Klein & Weber, 2001; Fiuza *et al*., 2004). Synthetic galloyl esters were found to be effective and selective enzyme inhibitors, as well as synergistic peroxyl radical protectors in membranes (Lü *et al*., 2010).

A total of eight ester derivatives of gallic acid were synthesized during this study. Among them, 3, 7, 8, and 9 were identified as new compounds. Synthesized compounds were purified and characterized by spectroscopic techniques, such as EI-MS, IR, ^{1}H-NMR, and ^{13}C-NMR spectroscopic data. The results indicated the effects of test compounds 2-9 on innate immune response phagocyte oxidative burst. All the compounds were found to be non-cytotoxic when checked against the mouse fibroblast NIH-3T3 cell line.

MATERIALS AND METHODS

General experimental conditions

Bruker Avance 400 and 500 MHz instruments were used for NMR experiments. ^{1}H NMR spectra were recorded at 400 or 500 MHz, while ^{13}C NMR spectra were recorded at 125 MHz. As per the international standard, the chemical shift (δ) was in ppm relative to tetramethylsilane (TMS) and coupling constants J in Hz. Precoated ALUGRAM, SIL G/UV254 aluminum plates (Kieselgel 60, 20 x 20, 0.5 mm thick, E. Merck, Germany) were used for thin layer chromatography (TLC) analysis. The reagents and solvents were purchased from Aldrich (St. Louis, Missouri, USA), E. Merck Darmstadt, (Germany), and Fluka (Buchs, Switzerland). They were used without purification. Developed chromatograms on TLC plates were visualized under ultraviolet light at 254 nm for fluorescence quenching spots, and 365 nm for fluorescent spots. FTIR-8900 (Shimadzu, Japan) was used to perform IR spectrophotometry of the compounds using KBr discs. Buchi 535 (Japan) melting point apparatus was used to measure melting points. JEOL JMS-600H mass spectrometer with a MASPEC data system was used to record electron impact mass spectra (EI-MS).

The general reaction for the synthesis of compounds 2–9 is given below.

Chemicals: Gallic acid purchased from Sigma Aldrich, India; Methanol, ethanol, isopropanol, 2- butanol, 4-methoxy-1-butanol, 2-methoxyethanol, 2- methyl-1-butanol, and pentane-3-ol from Aldrich, Poland.

General Reaction Procedure of Compounds 2-9

Chemical Synthesis

Concentrated sulphuric acid (0.5 mL) was carefully added to gallic acid (170 mg, 1 mmol) in the corresponding alcohols (2 mmol) in THF (5 mL) and the mixture was refluxed at 60-80 ºC for 18-20 h in an oil bath with continuous stirring. The progress of the reaction was monitored by TLC (DCM : Methanol = 9:1). Once the reaction was complete, the reaction mixture was cooled to room temperature, and excess alcohol and solvent were removed by using a rotary evaporator. The resulting mixture was then poured into cold water (25 mL), extracted with ethyl acetate (3×25 mL), and washed with a saturated sodium bicarbonate solution (10 mL). It was then dried with Na$_2$SO$_4$, the solvent evaporated off under reduced pressure and the residue purified by column chromatography [Silica-gel 60 (230–400 mesh), isocratic elution with Hex–EtOAc (65:35)].
The following scheme describes the synthesis of all of the compounds (Figure 1).
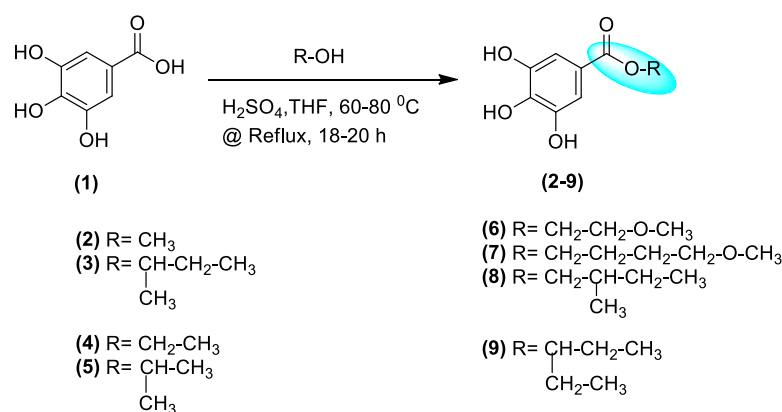
Figure 1: Synthesis of Gallic acid esters (**2-9**).

***Methyl 3,4,5-trihydroxybenzoate* (2).** Yield: 80-82%; m.p 209–210 ˚C; TLC (DCM: MeOH, 7:3 v/v) R_f = 0.80; ^{1}H-NMR (400 MHz, CD$_3$OD): δ_H 7.03 (s, 2H, H-2' /H-6'), 3.80 (s, 3H, C$\underline{H}_3$); ^{13}C-NMR (125 MHz, DMSO-d_6): δ 166.2 (C-7'), 145.5 (C-3' / C-5'), 138.4 (C-4'), 119.2 (C-1'), 108.4 (C-2' / C-6'), 51.5 (C-1); EI-MS *m/z* (% rel. abund.): 184.1 [M$^+$, 96.7], 153.0 (100).

***Sec-butyl 3,4,5-trihydroxybenzoate* (3).** Yield: 50-52 %; TLC (DCM: MeOH, 7:3 v/v) R_f = 0.70; IR (KBr, cm^{-1}): 3548 (O-H stretching), 1743 (C=O stretch, ester), 1513 (C–C stretch (in–ring), 1062 (C-O stretch); UV/Vis (MeOH): λ_{max} nm 229, 276; ^{1}H-NMR (400 MHz, DMSO-d_6): δ_H 6.92 (s, 2H, H-2' /H-6'), 4.86 (m, 1H, H-1), 1.61 (m, 2H, H-2); 1.21 (d, $J_{4,1}$ = 6.1 Hz, CH$_3$-4), 088 (t, $J_{3,2}$ = 7.4 Hz, CH$_3$-3); ^{13}C-NMR (125 MHz, DMSO-d_6): δ 165.4 (C-7'), 145.5 (C-3' / C-5'), 138.2 (C-4'), 119.8 (C-1'), 108.4 (C-2' / C-6'), 71.4 (C-1), 28.3 (C-2), 19.3 (C-4), 9.5 (C-3); EI-MS *m/z* (% rel. abund.): 226.1 [M$^+$,30], 170.0 (100), 153.0 (100); HREI-MS: Calculated for C$_{11}$H$_{14}$O$_5$: 226.0842, Observed m/z: 226.0841.

***Ethyl 3,4,5-trihydroxybenzoate* (4).** Yield: 78-80 %; m.p: 150-152 ˚C; TLC (DCM: MeOH, 7:3 v/v) R_f = 0.80; ^{1}H-NMR (500 MHz, DMSO-d_6): δ_H 6.92 (s, 2H, H-2' /H-6'), 4.18 (q, $J_{1,2}$ = 7.1 Hz, 2H, H-1), 1.25 (t, $J_{2,1}$ = 7.1 Hz, 3H, CH$_3$), EI-MS *m/z* (% rel. abund.): 198.1 [M$^+$,53], 152.9 (100).

***Isopropyl 3,4,5-trihydroxybenzoate* (5).** Yield: 75-77 %; TLC (DCM: MeOH, 6:4 v/v) R_f = 0.60 ;^{1}H-NMR (400 MHz, DMSO-d_6): δ_H 6.92 (s, 2H, H-2' /H-6'), 5.01 (septet, $J_{1,2/1,3}$ = 6.2 Hz, 1H, H-1), 1.25 (d, $J_{2,1/3,1}$ = 6.0 Hz, 2CH$_3$); ^{13}C-NMR (125 MHz, DMSO-d_6): δ 165.2 (C-7'), 145.4 (C-3' / C-5'), 138.2 (C-4'), 119.9 (C-1'), 108.4 (C-2' / C-6'), 67.1 (C-1), 21.7 (C-2 / C-3); EI-MS *m/z* (% rel. abund.): 212.1 [M$^+$,79], 170.0 (100), 153.0 (100).

***2-methoxyethyl 3,4,5-trihydroxybenzoate* (06).** Yield: 60-63 %; TLC (DCM: MeOH, 6:4 v/v) R_f = 0.60; ^{1}H-NMR (400 MHz, DMSO-d_6): δ_H 6.94 (s, 2H, H-2' /H-6'), 4.26 (t, $J_{1,2}$ = 4.6 Hz, 2H, H-1), 3.59 (t, $J_{2,1}$ = 4.7 Hz, 2H, H-2), 3.15 (s, 3H, CH$_3$); ^{13}C-NMR (125 MHz, DMSO-d_6): δ 165.7 (C-7'), 145.5 (C-3' / C-5'), 138.4 (C-4'), 119.2 (C-1'), 108.5 (C-2' / C-6'), 69.9 (C-1), 63.2 (C-2), 58.1 (C-3); EI-MS *m/z* (% rel. abund.): 228.2 [M$^+$,46], 170.0 (94), 153.0 (100).

***4-methoxybutyl 3,4,5-trihydroxybenzoate* (07).** Yield: 55-58%; TLC (DCM: MeOH, 6:4 v/v) R_f = 0.70; IR (KBr, cm^{-1}): 3394 (O-H stretching), 1685 (C=O stretch, ester), 1614 (C–C stretch (in–ring), 1248 (C–O stretch); UV/Vis (MeOH): λ_{max} nm 230, 262, 273; ^{1}H-NMR (500 MHz, DMSO-d_6): δ_H 6.93 (s, 2H, H-2' /H-6'), 4.15 (t, $J_{1,2}$ = 6.2 Hz, 2H, H-1), 3.31-3.21 (overlapped, 5H, H-4 & H-5), 1.67 (quintet, $J_{2,1/3}$ = 6.2 Hz, 2H, H-2), 1.59 (quintet, $J_{3,2/4}$ = 6.4 Hz, 2H, H-3); EI-MS *m/z* (% rel. abund.): 256.0 [M$^+$, 6], 170.0 (50), 153.0 (100); HREI-MS: Calculated for C$_{12}$H$_{16}$O$_6$: 256.0946, Observed m/z: 256.0947.

***2-methylbutyl 3,4,5-trihydroxybenzoate* (08).** Yield: 70-72%; TLC (DCM: MeOH, 7:3 v/v) R_f = 0.80; IR (KBr, cm^{-1}): 3468, 3358 (O-H stretching), 1696 (C=O stretch, ester), 1612 (C–C stretch (in–ring), 1038 (C–O stretch); UV/Vis (MeOH): λ_{max} nm 230, 273; ^{1}H-NMR (500 MHz, DMSO-d_6): δ_H 6.93 (s, 2H, H-2' /H-6'), 4.05-3.95 (m, 2H, H-1), 1.77-1.71 (m, 1H, H-2), 1.48-1.40 (m, 1H, H-3), 1.25-1.16 (m, 1H, H-3), 0.93 (d, $J_{5,2}$ = 6.7 Hz, 3H, H-5), 0.89 (t, $J_{4,3}$ = 7.4 Hz, 3H, H-4); EI-MS m/z (% rel. abund.): 240.1 [M$^+$,58], 170.0 (100), 153.0 (92); HREI-MS: Calculated for $C_{12}H_{16}O_5$: 240.0997, Observed m/z: 240.0998.

***Pentan-3-yl 3,4,5-trihydroxybenzoate* (09).** Yield: 60-63 %; TLC (DCM: MeOH, 7:3 v/v) R_f = 0.50; IR (KBr, cm^{-1}): 3358 (O-H stretching), 1680 (C=O stretch, ester), 1612 (C–C stretch (in–ring), 1032 (C–O stretch); UV/Vis (MeOH): λ_{max} nm 220, 228, 275; ^{1}H-NMR (400 MHz, DMSO-d_6): δ_H 6.92 (s, 2H, H-2' /H-6'), 4.79 (quintet, $J_{1,2/4}$ = 6.9 Hz, 1H, H-1), 1.64-1.52 (m, 4H, H-2, H-4), 0.85 (t, , $J_{3,2/5,4}$ = 7.4 Hz, 6H, H-3, H-5); EI-MS m/z (% rel. abund.): 240.2 [M$^+$,40], 170.1 (100), 153.1 (99); HREI-MS: Calculated for $C_{12}H_{16}O_5$: 240.0997, Observed m/z: 240.0998.

Anti-Inflammatory Assay

The anti-inflammatory activity of the synthesized compounds (2–8), and gallic acid (**1**) was evaluated by the following method reported by Helfand. *et al*. (Helfand *et al*., 1982; Mbiantcha *et al*., 2017). Initially all the compounds were evaluated at a single dose of 25 µg/mL, each in triplicate. The compounds having >50% inhibition were further evaluated at three different concentrations, 1, 10, and 100 µg/mL, to determine IC$_{50}$ values. A compound that failed to inhibit the production of ROS from zymosan-activated whole blood cells at the highest used dose (100 µg/mL) was considered inactive.

Cytotoxicity Assay

The cell line used for the cytotoxicity assay was obtained from the Biobank facility, The Panjwani Center for Molecular Medicine and Drug Research, International Center for Chemical and Biological Sciences, University of Karachi. It was purchased from ATCC, Manassas, USA. The cytotoxicity of the synthesized compounds (2–9), and gallic acid (1) was evaluated by the method reported by Pauwels. *et al*. (Pauwels *et al*., 1988; Choudhary *et al*., 2010). In this experiment, all the compounds were evaluated at the dose of 30 µM each, in triplicate. A compound having <50% inhibition at 30 µM was considered inactive. Cycloheximide was used as a standard drug (Siddiqui *et al*., 2021). Cycloheximide was used as a positive control in this assay. The percent inhibition was calculated by using the following formula:

$$\% \text{ inhibition} = \frac{100 - (\text{mean of O.D of test compound} - \text{mean of O.D of negative control})}{(\text{mean of O.D of positive control} - \text{mean of O.D of negative control})} \text{ X } 100$$

The results (% inhibition) were processed by using Soft- Max Pro software (Molecular Device, USA).
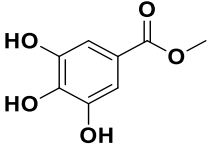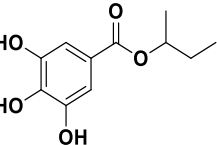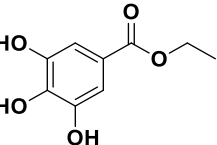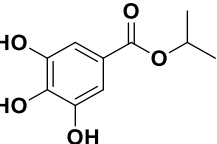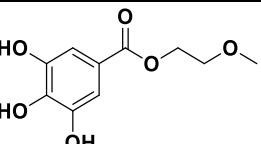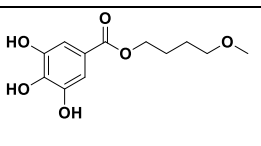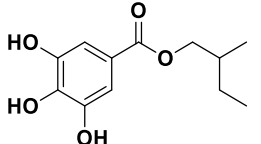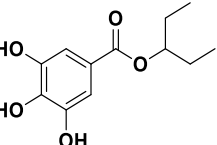
RESULTS AND DISCUSSION

The chemical structures of the synthesized gallic acid esters were deduced with the help of ^{1}H, ^{13}C NMR, IR, EI-MS, and HR-EIMS techniques. All the synthesized compounds were tested for their anti-inflammatory and cytotoxic activities by chemiluminescence and MTT cytotoxicity assay, respectively.

Anti-inflammatory activity

Oxidative burst assay was used to determine the anti-inflammatory properties of seven synthesized compounds. Among them, all the tested compounds (**2-8**) revealed potent to moderate inhibitory activity with IC$_{50}$ values in the range of 13.3-54.3 µM, when compared to the standard drug Ibuprofen (IC$_{50}$ = 54.3 ± 9.2 µM) (Table 1).

Table 1: Anti-inflammatory activity and Cytotoxicity of compounds 1-9.

Compound no	Structures	Oxidative burst inhibition IC$_{50}$ (μM)	Cytotoxicity (3T3 Cell line)
2		51.6 ± 2.1	>30
3		15.0 ± 6.6	>30
4		30.2 ± 0.5	>30
5		26.8 ± 3.2	>30
6		28.4 ± 8.5	>30
7		13.3 ± 0.8	>30
8		54.3 ± 9.2	>30
9		N/T	>30a
1	Gallic acid	N/A	>30
Ibuprofen (Standard)	-	54.3 ± 9.2	-
Cycloheximide (Standard)	-	-	0.8 ± 0.14

*SD = Standard deviation, N/A = Not active, N/T= Not tested

Structure-activity relationship of various gallic acid esters

The standard drug used was ibuprofen (IC$_{50}$ = 54.3 ± 9.2 µM). Among the test compounds, seven exhibited anti-inflammatory activities with IC$_{50}$ values in the range of 13.3-54.3 µM. The new compounds 3 (IC$_{50}$ = 15.0 ± 6.6 µM), 7 (IC$_{50}$ = 13.3 ± 0.8 µM), and 8 (IC$_{50}$ = 54.3 ± 9.2 µM) along with the known compounds 2 (IC$_{50}$ = 51.6 ±

2.1 µM), 4 (IC$_{50}$ = 30.2 ± 0.5 µM), 5 (IC$_{50}$ = 26.8 ± 3.2 µM) and 6 (IC$_{50}$ = 28.4 ± 8.5 µM) were found to be more potent inhibitors than ibuprofen (IC$_{50}$ = 54.3 ± 9.2 µM). The parent gallic acid was found to be inactive (Table 1). This implies that *sec*-butyl gallate and 4-methoxybutyl gallate, which have four carbon atoms in the aliphatic chain, are potent anti-inflammatory agents. As a result, the new compounds 3 and 7 which were esterified with *sec*-butyl and 4-methoxybutyl alcohols, respectively, possessed potent anti-inflammatory activity.

Cytotoxic activities on NIH-3T3 cell line

The tested compounds 2–9 and gallic acid (1) were tested for their cytotoxic activity on NIH-3T3 mouse fibroblast cell line where all esters were found to be inactive (Table 1).

CONCLUSION

The ester derivatives of GA were synthesized, among which compounds 3 and 7–9 were new. Our findings suggest that seven compounds showed promising anti-inflammatory activity; among them, the new compounds 3 and 7 were found to be the most potent inhibitors of ROS. Therefore, these compounds must be further investigated through detailed *in vivo* studies to evaluate their anti-inflammatory potential.

Acknowledgments

Ethical approval

The *in vitro* studies on human blood cells was conducted as per approval of the Independent Ethics Committee, UoK No: ICCBS/IEC-008-BC-2015.

REFERENCES

Ali M.S., Anuradha V., Yogananth N. & Bhuvana P. (2019). GCMS analysis and in vitro antibacterial and anti-inflammatory study on methanolic extract of *Thalassiosira weissflogii*. *Biocatalysis and Agricultural Biotechnology* **19**: 101–148.
   DOI: https://doi.org/10.1016/j.bcab.2019.101148

Badhani B., Sharma N. & Kakkar R. (2015). Gallic acid: a versatile antioxidant with promising therapeutic and industrial applications. *RCS Advances* **5**(35): 27540 –27557.
   DOI: https://doi.org/10.1039/C5RA01911G

Brown E.S. & Chandler P.A. (2001). Mood and cognitive changes during systemic corticosteroid therapy. *Primary Care Companion to the Journal of Clinical Psychiatry* **3**(1): 17.
   DOI: https://doi.org/10.4088/PCC.v03n0104

Choudhary M.I., Ismail M., Shaari K., Abbaskhan A., Sattar S.A. & Lajis N.H. (2010). *cis*-Clerodane-type furanoditerpenoids from *Tinospora crispa*. *Journal of Natural Products* **73**(4): 541–547.
   DOI: https://doi.org/10.1021/np900551u

Crofford L.J. (2013). Use of NSAIDs in treating patients with arthritis. *Arthritis Research and Therapy* **15**(3): 1–10.
   DOI: http://arthritis-research.com/content/15/S3/S2

Davies K.J. (2000). Oxidative stress, antioxidant defenses, and damage removal, repair, and replacement systems. *IUBMB Life* **50**(4-5): 279 –289.
   DOI: https://doi.org/10.1080/713803728

Fiuza S., Gomes C., Teixeira L., Da Cruz M.G., Cordeiro M., Milhazes, Borges F. & Marques M. (2004). Phenolic acid derivatives with potential anticancer properties, a structure activity relationship study. Part 1: Methyl, propyl and octyl esters of caffeic and gallic acids. *Bioorganic and Medicinal Chemistry* **12**(13): 3581–3589.
   DOI: https://doi.org/10.1016/j.bmc.2004.04.026

Gichner T., Pospíšil P., Velemínský J., Volkeová V. & Volke J. (1987). Two types of antimutagenic effects of gallic and tannic acids towards N-nitroso-compounds-induced mutagenicity in the ames *Salmonella* assay. *Folia Microbiologica* **32**(1): 55–62.
   DOI: https://doi.org/10.1007/BF02877259

Golumbic C. & Mattill H. (1942). The antioxidant properties of gallic acid and allied compounds. *Oil and Soap* **19**(8): 144 – 145.
DOI: https://doi.org/10.1007/BF02545531

Helfand S.L., Werkmeister J, & Roder J.C. (1982). Chemiluminescence response of human natural killer cells: The relationship between target cell binding, chemiluminescence, and cytolysis. *The Journal of Experimental Medicine* **156**(2): 492–505.
DOI: https://doi.org/10.1084/jem.156.2.492

Heo B.G., Park Y.S., Chon S.U., Lee S.Y., Cho J.Y. & Gorinstein S. (2007). Antioxidant activity and cytotoxicity of methanol extracts from aerial parts of Korean salad plants. *Biofactors* **30**(2): 79–89.
DOI: https://doi.org/10.1002/biof.5520300202

Ho K.J., Spite M., Owens C.D., Lancero H., Kroemer A.H., Pande R., Creager M.A., Serhan C.N. & Conte M.S. (2010). Aspirin-triggered lipoxin and resolvin E1 modulate vascular smooth muscle phenotype and correlate with peripheral atherosclerosis. *The American Journal of Pathology* **177**(4): 2116–2123.
DOI: https://doi.org/10.2353/ajpath.2010.091082

Inoue M., Sakaguchi N., Isuzugawa K., Tani H,. & Ogihara Y. (2000). Role of reactive oxygen species in gallic acid-induced apoptosis. *Biological and Pharmaceutical Bulletin* **23**(10): 1153–1157.
DOI: https://doi.org/10.1248/bpb.23.1153

Klein E. & Weber N. (2001). In vitro test for the effectiveness of antioxidants as inhibitors of thiyl radical-induced reactions with unsaturated fatty acids. *Journal of Agricultural and Food Chemistry* **49**(3): 1224–1227.
DOI: https://doi.org/10.1021/jf000725m

Krishnaraju A.V., Rao C.B., Sundararaju D., Sengupta K. & Trimurtulu G. (2009). Anti-Inflammatory activity of *Vitex leucoxylon* L. bark extracts against Freund's complete adjuvant induced arthritis in Sprague Dawley rat. *American Journal of Infectious Diseases* **5**: 68 –73.
DOI: https://www.academia.edu/download/73783665/ajidsp.2009.68.pdf

Kroes B.V., Van den Berg A., Van Ufford H.Q., Van Dijk H. & Labadie R. (1992). Anti-inflammatory activity of gallic acid. *Planta Medica* **58**(06): 499–504.
DOI: https://doi.org/10.1055/s-2006-961535

Kumar M., Kumar S. & Kaur S. (2012). Role of ROS and COX-2/iNOS inhibition in cancer chemoprevention: a review. *Phytochemistry Reviews* **11**(2-3): 309 –337.
DOI: https://doi.org/10.1007/s11101-012-9265-1

Lee S.K., Mbwambo Z., Chung H., Luyengi L., Gamez E., Mehta R., Kinghorn A. & Pezzuto J. (1998). Evaluation of the antioxidant potential of natural products. *Combinatorial Chemistry and High Throughput Screening* **1**(1): 35–46.

Locatelli C., Filippin-Monteiro F.B., Centa A. & Creczinsky-Pasa T.B. (2013). Antioxidant, antitumoral and anti-inflammatory activities of gallic acid. In: *Handbook on Gallic Acid: Natural Occurrences, Antioxidant Properties and Health Implications* (eds. M.A. Thompson & P.B. Collins), pp.1–23. Nova Science Publishers, New York, USA .

Lü J.M., Lin P.H., Yao Q. & Chen C. (2010). Chemical and molecular mechanisms of antioxidants: experimental approaches and model systems. *Journal of Cellular and Molecular Medicine* **14**(4): 840–860.
DOI: https://doi.org/10.1111/j.1582-4934.2009.00897.x

Mbiantcha M., Almas J., Shabana S.U., Nida D. & Aisha F. (2017). Anti-arthritic property of crude extracts of *Piptadeniastrum africanum* (Mimosaceae) in complete Freund's adjuvant-induced arthritis in rats. *BMC Complementary and Alternative Medicine* **17**(1): 1–16.
DOI: https://doi.org/10.1186/s12906-017-1623-5

Pauwels R., Balzarini J., Baba M., Snoeck R., Schols D., Herdewijn P., Desmyter J. & De Clercq E. (1988). Rapid and automated tetrazolium-based colorimetric assay for the detection of anti-HIV compounds. *Journal of Virological Methods* **20**(4): 309–321.
DOI: https://doi.org/10.1016/0166-0934(88)90134-6

Roots R. & Okada S. (1975). Estimation of life times and diffusion distances of radicals involved in X-ray-induced DNA strand breaks or killing of mammalian cells. *Radiation Research* **64** (2): 306–320.
DOI: https://doi.org/10.2307/3574267

Siddiqui H., Baheej M., Ullah S., Rizvi F., Iqbal S., Haniffa H.M., Wahab A.T. & Choudhary M.I. (2021). Synthesis of 1,2,3-triazole modified analogues of hydrochlorothiazide via click chemistry approach and *in vitro* α-glucosidase enzyme inhibition studies. *Molecular Diversity*: **26**: 2049–2067.
DOI: https://doi.org/10.1007/s11030-021-10314-3

Thadhani V.M., Choudhary M.I., Ali S., Omar I., Siddique H. & Karunaratne V. (2011). Antioxidant activity of some lichen metabolites. *Natural Product Research* **25**(19): 1827–1837.
DOI: https://doi.org/10.1080/14786419.2010.529546

Valko M., Leibfritz D., Moncol J., Cronin M.T., Mazur M. & Telser J. (2007). Free radicals and antioxidants in normal physiological functions and human disease. *The International Journal of Biochemistry and Cell Biology* **39**(1): 44–84.
DOI: https://doi.org/10.1016/j.biocel.2006.07.001

RESEARCH ARTICLE

Software Engineering

Secure CodeCity: 3-dimensional visualization of software security facets

C Wijesiriwardana[1*], P Wimalaratne[2], T Abeysinghe[2], S Shalika[2], N Ahmed[2] and M Mufarrij[2]

[1] *Faculty of Information Technology, University of Moratuwa, Katubedda, Sri Lanka.*

[2] *University of Colombo School of Computing, Reid Avenue, Colombo 07, Sri Lanka.*

Abstract: Over the last few decades, the software industry investigated security best practices to guide software developers in producing less vulnerable software products. As a result, security engineering has emerged as an integral part of the software development lifecycle. With the increase in the number of security vulnerabilities discovered, the software industry encountered challenges finding software security experts. Despite the availability of static code analysis tools to detect security vulnerabilities, they are underused due to several reasons such as inadequate usability and the lack of integration support. For example, such tools are deficient in providing enough information, produce faulty warning messages, and miscommunicate with developers. As a solution, this work presents a conceptual framework and a proof-of-concept visualization tool, Secure CodeCity, as an extension to the CodeCity metaphor, to facilitate security analytics. Secure CodeCity extends the CodeCity metaphor into three different granularity levels in 3-dimensional space, facilitating the vulnerability analysis in different granularities. Thus, software practitioners can use Secure CodeCity to obtain useful security-related information such as *'What is the most vulnerable class/method in a particular software project?'*. A between-subjects design-based user study was conducted with 23 subjects using a set of security-related tasks with two benchmark open-source Apache projects. The evaluation results show that Secure CodeCity surpasses the state-of-the-art security analysis tools in terms of correctness, usability, and time efficiency.

Keyword : Metaphoric visualization, security vulnerabilities, software security, static code analysis.

INTRODUCTION

Over the last few decades, software security has been recognized as an integral part of software product quality. Thus it is identified as a major quality characteristic in ISO/IEC 25010 quality model. Consequently, the paradigm shift of Build Security In has emerged with the idea of incorporating security into each phase of the Software Development Lifecycle (SDLC) (Soman *et al*., 2021). As a result, a series of security best practices threat modelling and static code analysis have been identified concerning each phase of the SDLC.

Detecting software security defects early in the lifecycle is important because security vulnerabilities are most likely to cause disturbances that affect end users. Besides, long-lingering defects are more expensive to fix. Despite the availability of static code analysis tools to detect security vulnerabilities, they are underused due to several reasons such as inadequate usability and the lack of integration support (Abeyrathna *et al*., 2020). For instance, such tools do not provide enough information (Johnson *et al*., 2013), produce faulty warning messages (Christakis & Bird, 2016), and miscommunicate with developers (Johnson *et al*., 2016). Finally, the results produced by security analysis tools must be understandable to developers who are not experts in software security (Tahaei *et al*., 2021).

Thus, it is believed that a better exploration and visualization can be performed on the data in software artifacts, to provide increased awareness of security aspects, such as vulnerability distribution, obtaining and understanding information regarding vulnerability mitigation, and monitoring the evolution of software security. Therefore, novel metaphoric software visualization models or notable extensions to the existing models are required to better comprehend the software projects (Assal *et al.*, 2016).
This paper presents a conceptual framework and a proof-of-concept implementation of a visualization framework

* Corresponding author (chaman@uom.lk; https://orcid.org/0000-0002-1124-425X

that enables software practitioners to visually observe and analyze various security-related perspectives of a software system. It facilitates drilling down the security issues into different abstraction levels. The visualization framework was built by adhering to the underlying concepts of the CodeCity metaphor. This paper, therefore, expects to address the following research questions (RQs):

RQ1: How to visualize class-level and method-level security vulnerabilities in the source code by extending the CodeCity metaphor based on a multi-layered abstraction mechanism?

RQ2: Can such a visualization give rise to an improvement over the state-of-the-art security analysis tools regarding the correctness, usability, and time efficiency when performing security-specific analysis tasks?

The remainder of the paper is organized as follows. The Materials and Methods is presented in Section 2 followed by the Results and Discussion in Section 3. Finally, the Conclusions and Future work are presented in Section 4.

MATERIALS AND METHODS

Software visualization is beneficial in the contexts of software maintenance, reverse engineering, and software evolution analysis. Literature reveals that software visualization has been effective in reducing the difficulty of understanding complex software systems (Merino *et al.*, 2018). Different visualization techniques have been proposed in the literature to represent different types of information about software systems. Thus far, techniques to visualize software attributes such as source code (Qayum *et al.*, 2022), architecture (Dashuber *et al.*, 2021), evolutionary aspects (Hammad *et al.*, 2021), dependencies (Liu *et al.*, 2021) and static aspects such as hierarchy (Caserta & Zendra, 2010) have been reported.

More than a decade ago, one of the main observations was that efforts in software visualization are not directly aligned with the needs of software developers (Reiss & Renieris, 2005). However, a few attempts have been made to address this issue and inspire developers to adopt visualization by utilizing multiple visualization techniques. It was observed that the lack of association among different visualization approaches is a significant barrier to finding the appropriate visualization technique to use in practice (Shahin *et al.*, 2014). Thus, it was noted that most of the software practitioners are unaware of existing visualization techniques. Several research attempts tried to address this issue by examining to which software engineering tasks distinct visualization techniques have been applied. Nevertheless, it was observed that most of these research attempts are still too coarse-grained to find a fitting visualization for the different needs of software practitioners (Merino *et al.*, 2018; Wijesiriwardana & Wimalaratne, 2019).

Software visualization techniques

Software visualization techniques can be categorized based on different aspects of software systems. For example, Shahin *et al.* (2014) classified visualization techniques into five groups: graph-based, notation-based, metaphor-based, metrics-based, and other techniques. Early on, the visualization techniques were purely in two-dimensional space, but later evolved into three-dimensional space and virtual/augmented reality applications.

This section attempts to provide a simple, yet useful classification based on two-dimensional and three-dimensional techniques. Furthermore, this classification summarizes the different visualization attributes of software systems such as architecture, evolution, and code structure. Figure 1 provides a taxonomy of visualization techniques together with the corresponding software attributes. This classification would facilitate software researchers in identifying a suitable visualization approach and picking the most suitable tool.

City metaphor: City metaphor (Wettel, 2008) is formulated based on the concept of cities, and it is commonly used to provide a visual overview of the entities of a software system. It allows enhancements to represent information related to these entities. In the visual representation of city metaphor, the cities correspond to packages; the buildings correspond to classes, and objects inside buildings correspond to the methods. Existing streets represent the relationship between classes among buildings. The city metaphor lets developers solve high-level programme comprehension tasks on different versions of a target programme. Further, it was used to identify possible design issues and to study the evolution of software systems (Ardigò *et al.*, 2022). The city metaphor has

also been utilized in combination with virtual reality-based interactive visualization tools in immersive 3D environments (Moreno-Lumbreras, 2021). Interactive visualization supported by navigation with the keyboard makes the City metaphor suitable for the visualization of large-scale software systems. Also, its ability to isolate elements allows focusing on different parts of the software system. However, the City metaphor is not suitable for representing complex relationships such as dependencies in a software system. Furthermore, it might encounter performance issues while increasing scalability. This research utilizes the core concepts of the city metaphor with some extensions.
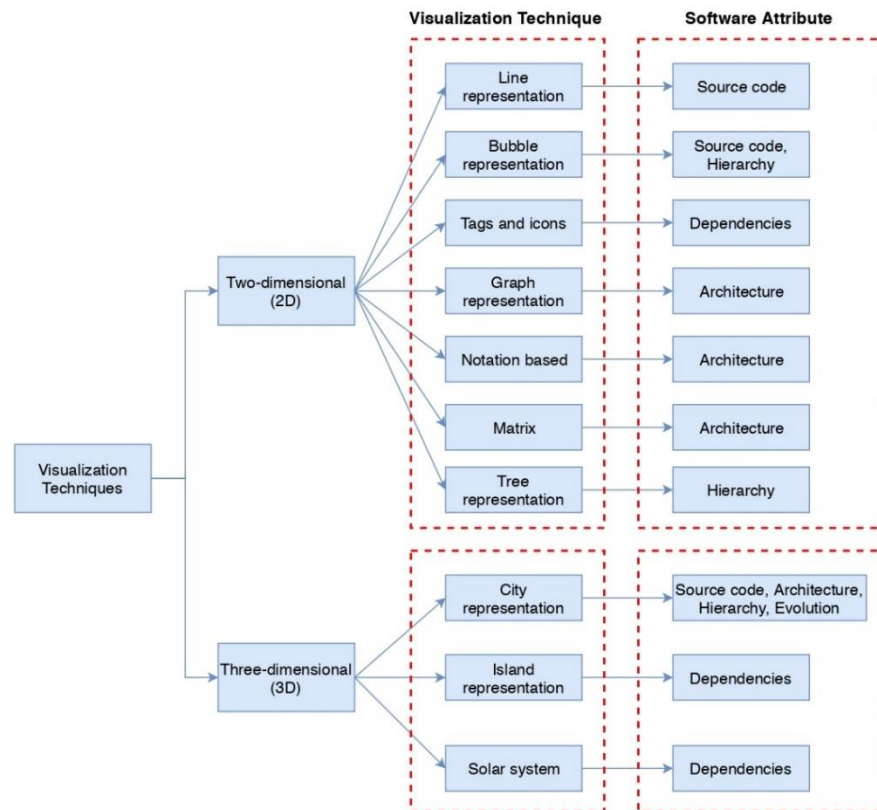
Figure 1: Taxonomy of software visualization techniques

Solar system metaphor: This technique visualizes a software system using a 3-dimensional solar system (Todorov *et al*., 2017). In this way of visualization, the software is represented by a virtual galaxy, consisting of several solar systems. This is capable of applying the consolidated knowledge of software engineers. However, for considerably large software systems that have long names for library packages, the ones placed near the core will become unreadable. Further, overlaps can be observed in the libraries that have data similarities, which could affect visibility.

Island metaphor: Island metaphor intends to visualize software entities such as classes, packages, and components. In this metaphor, an ocean with separate islands is used   to represent the software system (Misiak *et al*., 2018). A notable advantage of the island metaphor is that it shows a lot of information in a single view, which is better than displaying information in multiple views. However, in the island metaphor, the information can only be presented on a 2-dimensional space, which makes displaying relationships between components problematic.

Graph representation: This technique (Müller, 2019) is capable of displaying various types of quantitative data of a software system, which is a 2D technique that utilizes graphics according to the plotted data. It can visualize software metrics and the evolution of specific metrics. The graph visualization concept enables software architects to analyze and design changes to software systems visually. Using a consolidated view of the hierarchy and the dependencies of the software system, software architects can reorganize the modular structure interactively.

Matrix-based visualization: This is a well-known 2-dimensional approach that allows for understanding the software evolution process. It is capable of keeping track of changes made to the source code across various versions (Rufiange, 2014). Thus, it is considered a suitable technique for the real-time monitoring of constraint-oriented programmes.

Bubble metaphor: This is a two-dimensional visualization environment, where the bubbles represent the code segments of a software product. The bubble metaphor is suitable for understanding complicated behavior in software systems. Also, it is identified as efficient in comparison to a box or convex hull (Merino *et al*., 2017).

Tree technique: The tree technique visualizes entities of software systems using trees (Yu, 2020). Thus, the hierarchical structure of the source code entities such as method, classes, and packages are represented by different types of trees. The colour, height, and width represent software metrics associated with these entities. The tree-based visualizations can be grouped into two types, called explicit and implicit techniques. For example, the tree map is considered implicit, whereas the node-link diagram is considered explicit. The tree technique provides ease in laying out different information in a structured manner for effective interpretation.

Based on the literature review, it was decided to select the City metaphor as the visualization technique to be used for visualizing security facets due to three main reasons. First, researchers have formulated the city metaphor in different ways based on how the software components and their characteristics are visually described through the city metaphor. Second, the city metaphor significantly affects the users' feelings and emotions. Finally, the users' thinking about city metaphor is positive and comparable with that of other traditional 3D implementations. Apart from the above-mentioned reasons, the city metaphor provides natural support in nailing down the different aspects such as code evolution and quality improvements of software products.

Security vulnerability detection

Static code analysis tools find code vulnerabilities in the source code automatically. While most of the tools give examples of how to resolve the security flaws, some may modify the code to remove the vulnerabilities. Some of the most widely used static code analysis tools are described below.

FindBugs: FindBugs mainly searches for potential problems by matching bytecode against a list of bug patterns. Some of its strengths are that it successfully finds real defects in code, and it has a low rate of detecting false bugs. Among its weaknesses is that it needs compiled code to work, which can be difficult for developers.

Rough auditing tool for security (RATS): RATS is a tool for scanning C, C++, Perl, PHP, and Python source codes. As stated in the name, it only performs a rough analysis of the source code. This tool will not find every error in the source code, and at times produces false positives.

LAPSE+: LAPSE is developed by OWASP, which detects security vulnerabilities specifically for suspicious data injection in Java applications. LAPSE+ facilitates developers as well as auditors to detect vulnerabilities in Java EE Applications. The level of complexity of this analysis grows when the software products are having thousands of lines of code.

Flawfinder: Flawfinder is a code analysis tool that examines C/C++ code and reports possible flaws sorted by risk level. Flawfinder is continually being updated and improved, and has many resources available to help developers use this tool. Flawfinder falls short in its speed in comparison to RATS.

Yasca: Yasca is available for use with many programming languages such as Java, C/C++, JavaScript, HTML, and Visual Basic. Yasca not only detects security vulnerabilities but deviation from best practices in programming.

Proposed approach

CodeCity provides a 3D view of the source code by using a city structure, which it makes sense to manipulate by using the size, shape, and colour. Secondly, it allows using different granularity levels to visualize multiple perspectives of software security, for example, cities having buildings and buildings having rooms. By extending

the 3D space into more levels, Secure CodeCity is also able to provide a game-like environment, thereby encouraging engagement. Secure CodeCity also supports effective visualization of vulnerabilities at different granularity levels. Figure 2 presents the proposed extensions to the CodeCity metaphor.
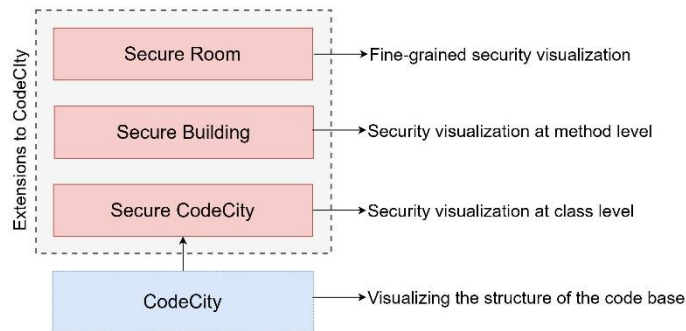
Figure 2: Proposed extensions to CodeCity

Conceptual model for Secure CodeCity

Figure 3 presents the conceptual model of the proposed visualization approach. The proposed model employs static code analysis to identify security vulnerabilities with respect to OWASP vulnerability types. Security aspects in complex software systems can be systematically categorized into different types based on the nature of the security vulnerabilities. This paper is intended to assist software developers by categorizing vulnerabilities by considering the structure of the source code, with a particular focus on object-oriented software systems. Besides, security vulnerabilities can be observed at different levels of a software product (*i.e.*, package level, class level, and method level in object-oriented software systems). Thus, different granularity levels are required to better comprehend the security issues at the aforementioned different levels. To overcome this issue, the proposed visualization model consists of three distinct visualizations namely, Secure CodeCity, Secure Building, and Secure Room.
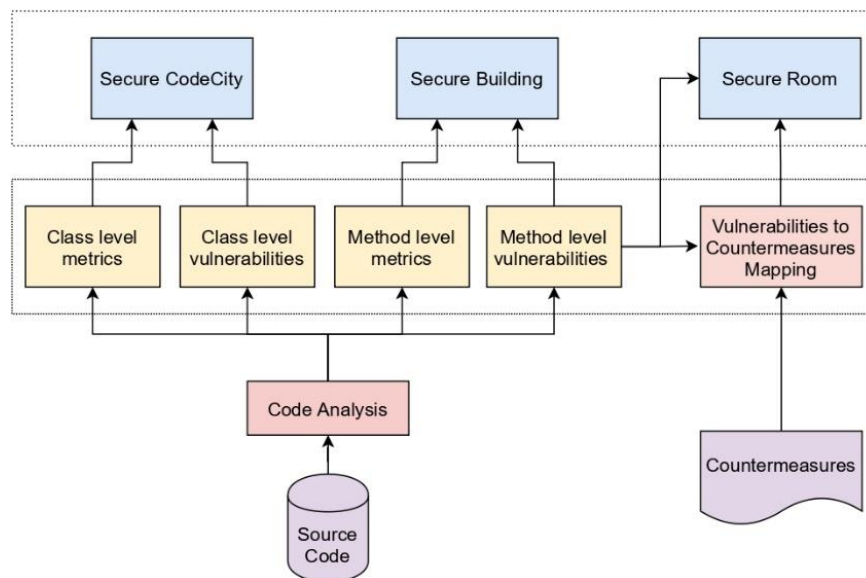
Figure 3: Architecture of visualization

Secure CodeCity : The first level view visualizes the software system as a three-dimensional city, where each building depicts a class of the software system investigated. The footprint size and the height of the building represent Cyclomatic Complexity and the Lines of Code, respectively. Once the city structure is built, the

CodeCity will be augmented with security-related information in the software project. For example, a building will be further augmented with different software metrics such as Severity level of vulnerabilities, Security Remediation Effort, Security Rating, and Cognitive Complexity. Besides, the operations such as zoom, move, and rotate could be performed on the 3D city view.

Secure building: The building view appears upon triggering a Class (*i.e.*, a building, in the city view). As stated previously, the first level is based on the CodeCity concept, where a building represents a Class in the software system. A Class consists of Methods, similar to a building consisting of rooms. Therefore, using a building view in the second level visualization allows users to generate a familiar mental model by minimizing the cognitive loads. This view can identify all the methods that have OWASP vulnerabilities. Besides, this view can share some other useful information such as the number of OWASP vulnerabilities in a particular class and vulnerability distribution among the selected class.

Secure room: Selection of a method in the second level view (*i.e.*, building view) allows navigation to the third level view. The walls of the room are used to represent different aspects of vulnerabilities. All the vulnerability details in the selected Method are shown in the third view, along with the suggested countermeasures to resolve the security bugs in the source code.

City generation and attribute mapping

Like CodeCity , in Secure CodeCity also, the classes are visualized as buildings and packages as districts. This choice is rooted in the fact that classes are the cornerstones of the object-oriented paradigm. However, the attributes mapping of Secure CodeCity is completely different from CodeCity. For example, as stated previously, the footprint size and the height of the building represent Cyclomatic Complexity and the Lines of Code, respectively. Besides, the colour of the building represents the severity level of the vulnerabilities of a particular class.

Positioning of the buildings:

An algorithm is designed to generate a 2D Grid, where the location of each package is determined by using (x,y) coordinates that are calculated based on the root level. Then the exact location of the class in a particular folder is also determined by using (x,y) coordinates that are calculated for the relevant package. Using the class ID and the folder structure, the classes that belong to each folder are separately grouped and positioned. Using the number of lines of codes and the number of attributes in each class, the space required to generate a particular class as a 3D model is calculated.

In the second level view (*i.e.*, the building view), the rooms are assigned a colour based on the following equation as depicted in OWASP risk ranking methodology.

Risk = likelihood ∗ impact

The likelihood will be calculated based on the factors such as ease of discovery, ease of exploitation, awareness, and intrusion detection.

Secure CodeCity for security visualization

This section describes Secure CodeCity that is implemented to visualize vulnerabilities in software systems. The implementation goals of Secure CodeCity are two-fold: to visualize the security bugs that lie in the codebase and to visualize the interlinked security artifacts. The implementation is based on the theoretical foundation laid in Section 3. As described previously, Secure CodeCity consists of three views: the City view, the Building view, and the Room view to analyze the security vulnerabilities in different granularity levels. The Secure CodeCity framework was developed as a standalone application that renders in the browser. How the data are extracted from different sources and pre-processed to facilitate the visualization is described below.

Data extraction and preparation for visualization

Static code analysis with SonarQube : SonarQube is a static code analysis tool as well as a code quality measuring tool which is widely used among software practitioners and researchers. The Secure CodeCity Framework requires analyzing the source code using SonarQube to identify Security vulnerabilities. Besides, SonarQube provides the required software metrics of the software system. The vulnerabilities identified as security bugs are categorized with respect to OWASP T10 by this tool. Categorization of software bugs into OWASP T10 is the additional reason for selecting SonarQube.

Metrics pre-processor: SonarQube provides an API to get metric details related to the scanned project, where the extracted details could be used to generate the project structure. To store details about the extracted details from SonarQube, TreeElement is used, which is implemented using the TypeScript Classes. However, SonarQube API does not provide a way to get method details inside a class. Therefore, the source code is fed to a Java parser and the method name, size, and method lines details are extracted.

Issues pre-processor : SonarQube provides the facility to extract vulnerability details, Security Remediation Effort, and Security Rating Details of any given File via Sonar API. It sends output details as a JSON object. Each JSON object is processed, and security-related details are stored in the tree node. The details are processed according to the various needs of the project.

Different views in secure CodeCity

As described previously, the first level view visualizes the software system as a three-dimensional city. Figure 4a shows the City view of a software system, with buildings are represented in different colours, where less vulnerable classes are shown in Green colour and highly vulnerable classes are shown in Red colour.
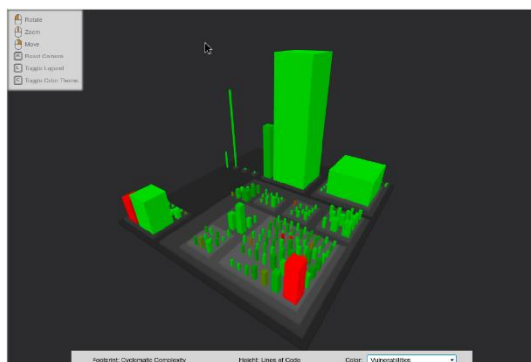
Figure 4a: Security vulnerability distribution of secure CodeCity (Less vulnerable class: Green building; Highly vulnerable class: Red colour)
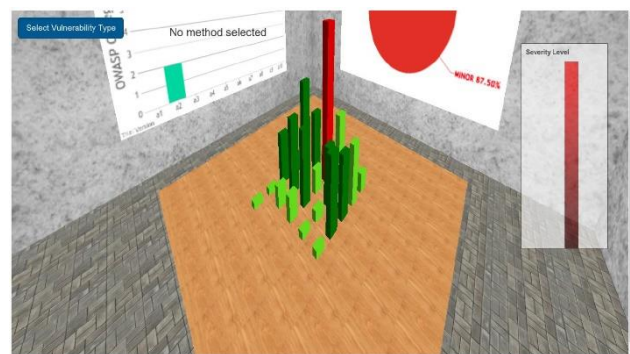
Figure 4b: Visualization of method level vulnerabilities

Upon triggering a building (*i.e*., a Class) in the City view, the next level of visualization appears. Figure 4b shows the vulnerability distribution of the Methods of the triggered Class. Moreover, the Wall view is used to provide additional security information such as vulnerability categorized according to OWASP and percentage of critical vulnerabilities. Therefore, with the conceptual framework of Secure CodeCity and the proof-of-concept implementation, RQ1 can be addressed successfully.

RESULTS AND DISCUSSION

This paper presents a novel mechanism and a proof-of- concept implementation to effectively visualize software security facets in a three-dimensional metaphor. First, the evaluation is carried out to measure the overall correctness of Secure CodeCity when compared with a state-of-the-art security analysis tool. Then, the usability

of Secure CodeCity compared with the same tool is determined. In order to evaluate the above claims, three hypotheses (see Table 2) have been formulated, such that they are expected to answer RQ2: Can such a visualization witness an improvement over the state-of-the-art security analysis tools regarding the correctness, usability, and time efficiency when performing security-specific analysis tasks?

Table 2:   Hypothesis

	Null hypothesis		Alternative hypothesis
H1o	The total correctness score for all tasks is the same across the experimental and control group.	H1	The total correctness score for all tasks is different across the experimental and control group.
H2o	The System Usability Scores are the same across the experimental and control group.	H2	The System Usability Scores are different from the experimental and control group.
H3o	The total completion time for all tasks is the same across the experimental and control group.	H3	The total completion time for all tasks is different from the experimental and control group.

Experimental design

A user study-based experiment has been designed by following the Between Subjects Design approach, which is a well-known experimental design strategy in Software Engineering (Kampenes, 2009). The goal of the experiment is to show whether Secure CodeCity's metaphoric visualizations provide better support to software practitioners in solving software security-related tasks than state-of-the-practice non-visual exploration tools. Thus, like other empirical evaluations of metaphoric software visualization approaches, the usability has been selected as one the dependent variables of the experiment along with the correctness and time efficiency.

SonarQube was selected as the baseline state-of-the-practice tool due to several reasons. Foremost, SonarQube is considered as a benchmark tool among the software engineering research community over the last decade (Wijesiriwardana & Wimalaratne, 2018; Marcilio *et al.*, 2019; Lenarduzzi *et al.*, 2020). Furthermore, SonarQube is well suited for software security-related analytics.

Two open-source benchmark Apache projects, Apache Ant and Struts 2, available in Github, are used for the experiment. It was decided to select the projects that are less than 500,000 Lines of Code (LOC) due to the time limitations in conducting the user study. The first project, Apache Ant, is an open-source project initiated by Apache Software Foundation; it is a software tool used to automate software build processes such as compile, run, test, and assemble Java-based applications. The second project, Apache Struts, is a free open-source solution to create Java web applications. It encourages developers to utilize a model-view-controller (MVC) architecture.

Table 3:   Summary of the Open-Source Projects Used for the User Study

Project Name	No: of Classes	LOC
Apache Ant	1,277	112,503
Apache Struts 2	1,649	134,155

Controlled variables

The experiment is conducted with 23 subjects who are Masters students in Computer Science and Information Technology. The inclusion criteria of the subjects were based on working experience in the software industry and awareness of SonarQube. A minimum of two years of industry experience and a minimum of two years of experience in working with SonarQube were considered as the inclusion criteria. Of the 23 participants, 12 were allocated to the experimental group, and the remaining 11 were allocated to the control group. The allocation of the subjects to both experimental and control groups was done randomly. The experimental group was instructed to perform the tasks with Secure CodeCity, whereas the control group was instructed to use SonarQube to perform the tasks. Figure 5 shows the industry experience in years among the experimental and control groups and the experience in using SonarQube in years.

The experimental group and the control group were instructed to provide answers to the tasks as per their experience with Secure CodeCity and SonarQube, respectively while performing the tasks.
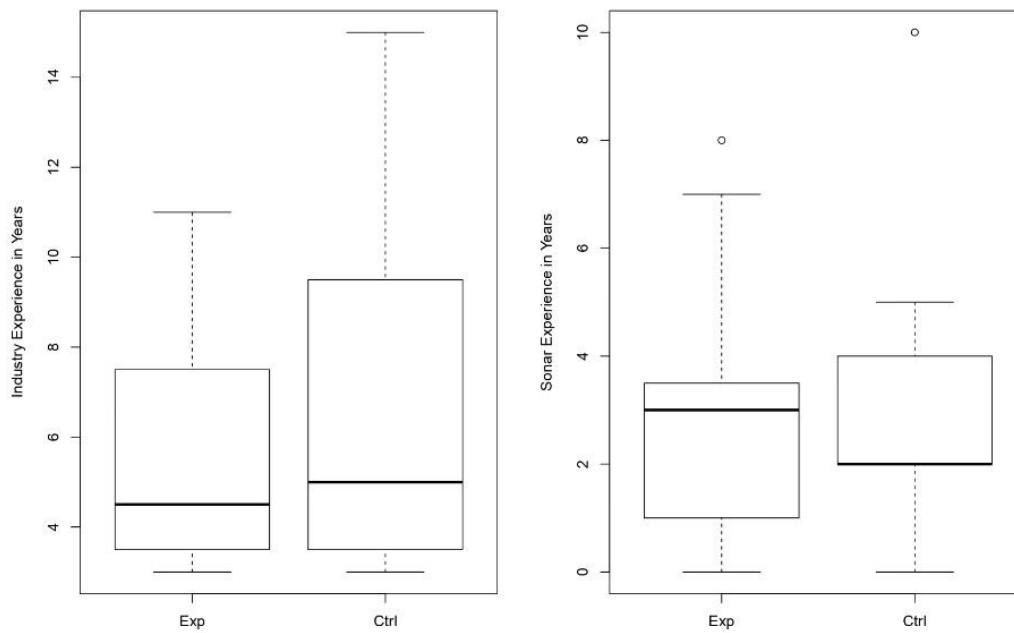
Figure 5: Industry experience (on the left) and SonarQube experience (on the right)

Selection of security-related tasks

The task selection was based on several visualization levels of the CodeCity framework. The initial focus is on the class level (first level) vulnerability information and other essential software metrics. For example, finding out "What is the most vulnerable class of a particular software project?" is a piece of useful information for a software practitioner. Then the tasks are gradually focused on the second level and third level visualizations.

Table 4: Security-related Tasks Used for the Evaluation

Task ID	Task Description
T1	What is the most vulnerable class in Apache Ant project?
T2	How many vulnerabilities are there in the ChainReadeRHelper.java class?
T3	How many security vulnerabilities are there in the verifySettings method in the DepthSelector.java class?
T4	What is the cyclomatic complexity of the DepthSelector.java class?
T5	What is the Security Remediation Effort in the DepthSelector.java class?
T6	What is the most critical method in the JakartaMultiPartRequest.java class?
T7	What is the percentage of MINOR issues in class Reg- ister.java?
T8	How many security vulnerabilities are there in the cleanUp method in the JakartaMultiPartRequest.java class?
T9	Does the system suggest countermeasures to rectify the first vulnerability in cleanUp method in the JakartaMultiPartRequest.java class?

Data analysis

This section presents the data collection and analysis process to evaluate the aforementioned two hypotheses and the experimental results gathered by the statistical analysis.

Correctness scores of the tasks for both experimental and control groups:

The correctness values for the tasks are obtained by a simple rating mechanism. For example, if the answer provided by a participant to a particular task is correct, two points are given. Thus, a maximum of 18 points can be obtained by a participant if all the tasks were correctly answered. Likewise, the wrong answers were allocated zero marks.

The mean correctness score of Secure CodeCity is 9.11 (with a standard deviation of 1.45), which is higher than the mean correctness score of 7.22 in the control group (with a standard deviation of 1.98). The correctness scores of the experimental and control groups are shown as a box plot in Figure 6. According to the Figure, the 25th percentile of the experimental group is above the 75th percentile of the control group. Thus, notable overall correctness of Secure CodeCity is observed over SonarQube in performing the security-related tasks. Besides, the non-parametric Independent Samples Mann-Whitney U (MWU) test is used with a significance level of 0.01 to test the first hypothesis. As per the experimental results, the MWU test rejects H1o at the 99 percent confidence level (with $p < 0.0001$), accepting the hypothesis H1: total correctness scores are different for the experimental and control groups.
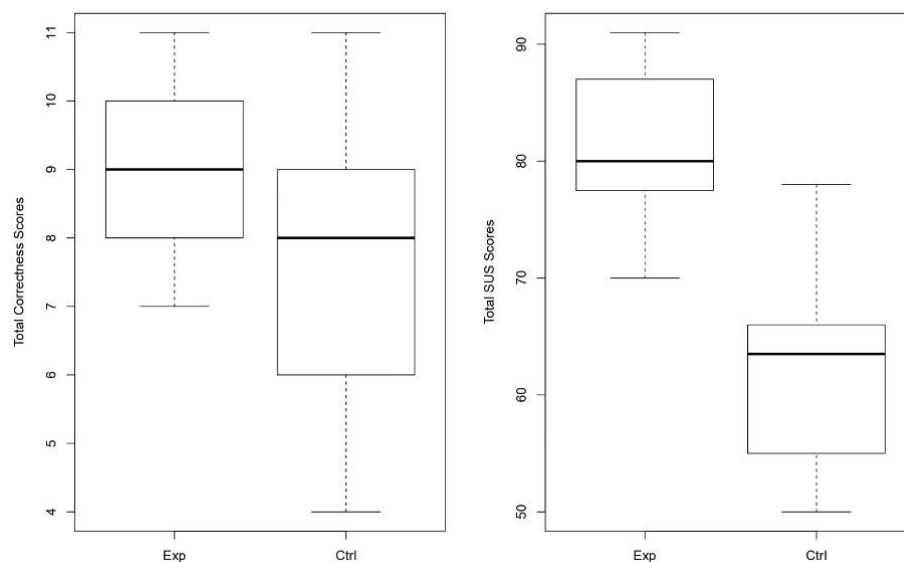
Figure 6: Total correctness score (on the left) and total SUS score (on the right)

Usability scores of the tasks for both experimental and control groups:

System usability score (SUS): 10 questions have been used to assess the usability of Secure CodeCity compared with the SonarQube in performing the aforementioned nine tasks. The subjects were requested to provide a score ranging from 1 to 5 for each of the ten SUS questions as per the level of satisfaction while performing the tasks. As per the SUS scoring mechanism, 1 point has been subtracted from the score for each odd-numbered question. For each even-numbered question, 5 points have been subtracted from the score. Then the total score was obtained by summing up the newly generated values. As the last step, the final SUS score was obtained by multiplying the total score by 2.5. However, the final SUS score is not a percentage value, instead, it gives the score out of 100, and still is considered an unambiguous method for the comparison of the results.

The mean SUS score of Secure CodeCity is 80.82 (with a standard deviation of 7.01), and it is 16.1 greater than the control group's SUS score of 64.70 (with a standard deviation of 8.02). It was observed that the 25th percentile of the experimental group is above the 75th percentile of the control group as shown in the box plots in Figure 7. Thus, it confirmed the acceptance of Secure CodeCity over the baseline tool, SonarQube used for the evaluation. Moreover, the MWU test rejects H2o at the 95 percent confidence level (with $p < 0.0001$), accepting hypothesis H2: the SUS scores are different for the experimental and control groups.

**Overall completion time of the tasks for both experimental and control groups:**

Based on the difficulty level of a few questions, study subjects were instructed not to spend more than 10 minutes on a single task. Upon the completion of each task, they were requested to note down the time spent on each task. Figure 7 presents the distribution of time across the experimental group and the control group. Based on that, it was observed that Secure CodeCity was capable of obtaining the results much faster than the baseline tools. However, a distinguishable benefit was not witnessed in Secure CodeCity in performing T2 and T5. The MWU test rejects the null hypothesis H3o at the 99 percent confidence level. The acceptance of the alternative hypothesis confirms that the distribution of the total completion times among the two groups is different.
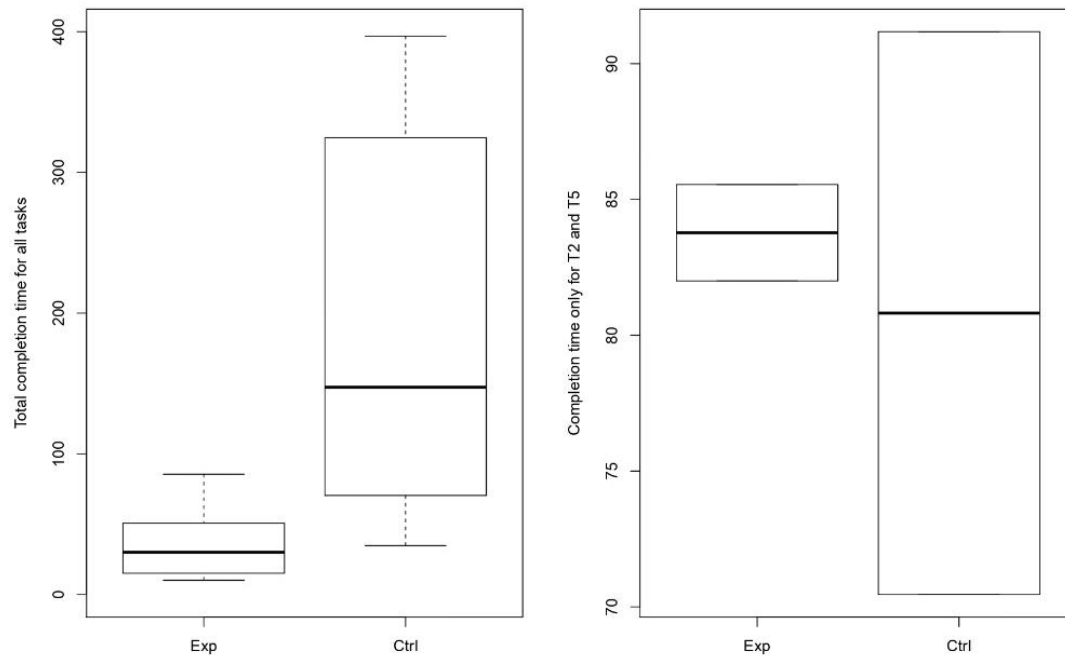
Figure 7: Overall completion time for all the tasks (on the left) and completion time only for T2 and T5 (on the right)

Thus, RQ2 can be successfully answered by accepting hypotheses H1, H2, and H3. Thus, secure CodeCity outperforms state-of-the-art tools regarding usability, accuracy, and time efficiency.

CONCLUSION

This work presents a novel mechanism and a proof-of-concept visualization tool, Secure CodeCity to facilitate security analytics in software projects. Secure CodeCity is capable of visualizing the security issues in software projects organized into different granularity levels: Secure CodeCity , Secure Building, and Secure Room. For example, Secure CodeCity presents the class-level vulnerabilities, and Secure Building presents the method-level vulnerabilities. A user study was conducted with 23 participants to evaluate Secure CodeCity in terms of correctness, usability, and time efficiency compared with the selected state-of-the-art tool SonarQube. Evaluation results confirmed the capability of Secure CodeCity in facilitating security analytics thus, this study would provide means for better software security analytics in developing less vulnerable software. More specifically, the main contributions (C1 and C2) of this paper are as follows:

C1: Metaphoric software visualization based on a multilayered abstraction mechanism.

As described in Section 3, a conceptual model of Secure CodeCity is introduced, which was organized into different abstractions to effectively visualize fine-grained security facets. Secure CodeCity is a natural extension of CodeCity, where three distinct views are provided namely Secure CodeCity, Secure Building, and Secure Room.

C2: Design, implementation, and evaluation of Secure CodeCity

As described previously, Secure CodeCity extends the CodeCity metaphor to facilitate understanding of security-related information of software projects. The evaluation results prove that Secure CodeCity is capable of addressing the limitations of existing static code analysis tools for security analysis.

As future work, it is expected to develop a security-specific positioning algorithm for Secure CodeCity. As of now, the positioning of the classes (*i.e.*, buildings) on top of a package (*i.e.*, 2D pane) is based on a positioning algorithm that avoids class overlaps and class displacements. However, a security-aware positioning algorithm would improve the usability of the Secure CodeCity by further minimizing the cognitive loads of the users. Besides, extensive pre-processing mechanisms could be investigated to facilitate the swift rendering of Secure CodeCity. However, performance is considered a common challenge that every software visualization tool needs to encounter. Therefore, a security-specific pre-processing of the source code is recommended prior to the visualization step.

Acknowledgment

REFERENCES

Abeyrathna A., Samarage C., Dahanayake B., Wijesiriwardana C. & Wimalaratne P. (2020) A security specific knowledge modelling approach for secure software engineering. *Journal of the National Science Foundation of Sri Lanka* **48**: 93–98.
    DOI: http://dx.doi.org/10.4038/jnsfsr.v48i1.8950

Ardigò S., Nagy C., Minelli R. & Lanza M. (2022). M3triCity: Visualizing evolving software and data cities. *Proceedings of the ACM/IEEE 44th International Conference on Software Engineering: Companion Proceedings*, 21 - 29 May. Pittsburgh, Pennsylvania, USA, pp. 130–133.
    DOI: http://dx.doi.org/10.1145/3510454.3516831

Assal H., Chiasson S. & Biddle R. (2016). Cesar: Visual representation of source code vulnerabilities. *Proceedings of the 2016 IEEE Symposium on Visualization for Cyber Security (VizSec)*, 24-24 October. pp. 1–8. Baltimore, MD, USA.
    DOI: http://dx.doi.org/10.1109/VIZSEC.2016.7739576

Caserta P. & Zendra O. (2010). Visualization of the static aspects of software: A survey. *IEEE Transactions on Visualization and Computer Graphics* **17**(7): 913–933.
    DOI: http://dx.doi.org/10.1109/TVCG.2010.110

Christakis M. & Bird C. (2016). What developers want and need from program analysis: an empirical study. *Proceedings of the 31st IEEE/ACM international conference on automated software engineering,* 3-7 September. Singapore, pp. 332–343.
    DOI: http://dx.doi.org/10.1145/2970276.2970347

Dashuber V., Philippsen M. & Weigend J. (2021). A Layered Software City for Dependency Visualization. *Proceedings of the 16th International Joint Conference on Computer Vision, Imaging and Computer Graphics Theory and Applications (VISIGRAPP),* 8-10 February. pp. 15–26.
    DOI: http://dx.doi.org/10.5220/0010180200150026

Hammad M., Abdul H., Jarzabek S. & Koschke R. (2021). Visualization of clones. In: *Code Clone Analysis.* (eds. K.Inoue & C.K. Roy), pp. 107–120. Springer, Singapore.
    DOI: http://dx.doi.org/10.1007/978-981-16-1927-4_8

Johnson B., Song Y., Murphy-Hill E. & Bowdidge R. (2013). Why don't software developers use static analysis tools to find bugs?. *Proceedings of the 35th IEEE International Conference on Software Engineering (ICSE)*, 18-26 May. San Francisco,USA, pp. 672–681.
    DOI: http://dx.doi.org/10.1109/ICSE.2013.6606613

Johnson B., Pandita R., Smith J., Ford D., Elder S., Murphy-Hill E. & Sadowski C. (2016). A cross-tool communication study on program analysis tool notifications. *Proceedings of the 2016 24th ACM SIGSOFT International Symposium on Foundations of Software Engineering*, 13-18 November. Seattle, USA, pp. 73–84.
    DOI: http://dx.doi.org/10.1145/2950290.2950304

Kampenes V.B., Dybå T., Hannay J.E. & Sjøberg D.I. (2009). A systematic review of quasi-experiments in software engineering. *Information and Software Technology* **51**(1): 71–82.
DOI: http://dx.doi.org/10.1016/j.infsof.2008.04.006

Lenarduzzi V., Lomio F., Huttunen H. & Taibi D. (2020). Are sonarqube rules inducing bugs?. *Proceedings of the 2020 IEEE 27th International Conference on Software Analysis, Evolution and Reengineering (SANER)*, 18-21 February. Ontario, Canada, pp. 501–511.
DOI: http://dx.doi.org/10.1109/SANER48275.2020.9054821

Liu H., Tao Y., Huang W. & Lin H. (2021). Visual exploration of dependency graph in source code via embedding-based similarity. *Journal of Visualization* **24**(3): 565–581.
DOI: http://dx.doi.org/10.1007/s12650-020-00727-x

Marcilio D., Bonifácio R., Monteiro E., Canedo E., Luz W. & Pinto G. (2019). Are static analysis violations really fixed? a closer look at realistic usage of sonarqube. *Proceedings of the 2019 IEEE/ACM 27th International Conference on Program Comprehension (ICPC)*, 25-26 May. Montreal, Canada, pp. 209–219.
DOI: http://dx.doi.org/10.1109/ICPC.2019.00040

Merino L., Ghafari M., Anslow C. & Nierstrasz O. (2017). CityVR: Gameful software visualization. *Proceedings of the 2017 IEEE International Conference on Software Maintenance and Evolution (ICSME)*, 17-22 September. Shanghai, China, pp. 633–637.
DOI: http://dx.doi.org/10.1109/ICSME.2017.70

Merino L., Ghafari M., Anslow C. & Nierstrasz O. (2018). A systematic literature review of software visualization evaluation. *Journal of Systems and Software* **144**: 165–180.
DOI: http://dx.doi.org/10.1016/j.jss.2018.06.027

Misiak M., Schreiber A., Fuhrmann A., Zur S., Seider D. & Nafeie L. (2018). IslandViz: A tool for visualizing modular software systems in virtual reality. *Proceedings of the 2018 IEEE Working Conference on Software Visualization (VISSOFT)*, Madrid, Spain, pp. 112–116.
DOI: http://dx.doi.org/10.1109/VISSOFT.2018.00020

Moreno-Lumbreras D., Minelli R., Villaverde A., González-Barahona J. M. & Lanza M. (2021). CodeCity : On-Screen or in Virtual Reality? *Proceedings of the 2021 Working Conference on Software Visualization (VISSOFT),* 27-28 September. Luxembourg, pp. 12–22.
DOI: http://dx.doi.org/10.1109/VISSOFT52517.2021.00011

Müller R. & Fischer M. (2019). Graph-based analysis and visualization of software traces. *Proceedings of the 10th Symposium on Software Performance*, 5 November. Würzburg, Germany, pp. 26–28.

Qayum A., Khan S.U.R. & Akhunzada A. (2022). FineCodeAnalyzer: Multi-perspective source code analysis support for software developer through fine-granular level interactive code visualization. *IEEE Access* **10**: 20496–20513.
DOI: http://dx.doi.org/10.1109/ACCESS.2022.3151395

Reiss S. P. & Renieris M. (2005). JOVE: Java as it happens. *Proceedings of the 2005 ACM Symposium on Software Visualization*, 14-15 May. St. Louis Missouri, USA, pp. 115–124.
DOI: http://dx.doi.org/10.1145/1056018.1056034

Rufiange S. & Melançon G. (2014). Animatrix: A matrix-based visualization of software evolution. *Proceedings of the 2014 Second IEEE Working Conference on Software Visualization*, 29-30 September. Victoria, Canada, pp. 137–146.
DOI: http://dx.doi.org/10.1109/VISSOFT.2014.30

Shahin M., Liang P. & Babar M.A. (2014). A systematic review of software architecture visualization techniques. *Journal of Systems and Software* **94**: 161–185.
DOI: http://dx.doi.org/10.1016/j.jss.2014.03.071

Soman S., Pareek P.K., Dixit S., Chethana R.M. & Kotagi V. (2021). Exploration study to study the relationships between variables of secure development lifecycle (SDL). In: *Emerging Technologies in Data Mining and Information Security (*eds. J.M.R.S.Tavares, S. Chakrabarti, A. Bhattacharya & S. Ghatak) pp. 641–649. Springer, Singapore.
DOI: http://dx.doi.org/10.1007/978-981-15-9774-9_59

Tahaei M., Vaniea K., Beznosov K. & Wolters M.K. (2021). Security notifications in static analysis tools: Developers' attitudes, comprehension, and ability to act on them. *Proceedings of the 2021 CHI Conference on Human Factors in Computing Systems*, 8-13 May. Yokohama, Japan, pp. 1–17.
DOI: http://dx.doi.org/10.1145/3411764.3445616

Todorov B., Kula R.G., Ishio T. & Inoue K. (2017). SoL Mantra: Visualizing update opportunities based on library coexistence. In *2017 IEEE Working Conference on Software Visualization (VISSOFT)*, 18-19 September. Shanghai, China, pp. 129–133.
DOI: http://dx.doi.org/10.1109/VISSOFT.2017.23

Wettel R. & Lanza M. (2008). CodeCity : 3D visualization of large-scale software. In *Companion of the 30th international conference on Software engineering*, 10-18 May. Leipzig Germany, pp. 921–922.
DOI: http://dx.doi.org/10.1145/1370175.1370188

Wijesiriwardana C. & Wimalaratne P. (2018). Fostering real-time software analysis by leveraging heterogeneous and autonomous software repositories. *IEICE Transactions on Information and Systems* **101**(11): 2730–2743.
DOI: http://dx.doi.org/10.1587/transinf.2018EDP7094

Wijesiriwardana C. & Wimalaratne P. (2019). Software engineering data analytics: a framework based on a multi-layered abstraction mechanism. *IEICE Transactions on Information and Systems* **102**(3): pp. 637–639.
 DOI: http://dx.doi.org/10.1587/transinf.2018EDL8070

Yu, G. (2020). Using ggtree to visualize data on tree-like structures. *Current Protocols in Bioinformatics* **69**(1): e96.
 DOI: http://dx.doi.org/10.1002/cpbi.96

RESEARCH ARTICLE

Computational Archeaology

Chronological attribution of Sinhalese inscriptions using deep learning approaches

HMSCR Heenkenda[*] and TGI Fernando

Department of Computer Science, University of Sri Jayewardenepura, Gangodawila, Nugegoda, Sri Lanka.

Abstract: A study of this caliber can be identified as a profound source for a wealth of knowledge as the aim of this study is to present chronological attribution of Sinhalese inscriptions based on deep learning approaches. Inscriptions shed light on a multitude of information such as chronicled civilizational thought, economic status, language evolution, cultural boundaries, details of royal officers, local rules, ethnic groups, land tenure, religious activities, beliefs, and trade and industries. Inscriptions are major assets to showcase inclusive of listed above, multitude information; hence, the benefits served by a study of high caliber, especially to the historical heritage research and to the heritage tourism. Several computer-aided solutions have been proposed to resolve the recognition of inscriptions in the Sri Lankan context. But this paper proposes an optimized classification. A dataset of five hundred images of original Sinhalese inscriptions dating from the 3rd century BC to the present was used to train and test the models. This study adopts four deep learning models to classify Sinhalese inscriptions: a newly proposed convolutional neural network model, and the pre-trained models Inception-v3, VGG-19, and ResNet-50. Palaeographical and morphological rules were adopted in the manual classification of Sinhalese inscriptions into a number of eras, namely, the Early Brahmi (3rd century BC to 1st century AD), Late Brahmi (2nd century AD to 4th century AD), Transitional Brahmi (5th century AD to 7th century AD), Medieval Sinhala (8th century AD to 14th century AD), and Modern Sinhala (15th century AD to the present). The results of the study indicate promising outcomes with accuracies of 70.66%, 85.94%, 57.44%, and 58.77% respectively for used four models. Further, the study revealed that the Inception-v3 model outperformed in classifying the Sinhalese inscriptions in respective eras.

Keywords: Convolutional neural network, deep learning, Sinhalese inscriptions, transfer learning.

INTRODUCTION

Inscriptions are documents which were inscribed by our ancestor on stone surfaces in ancient times. The Ministry of Cultural Heritage, Department of Archaeology and other relevant authorities in respective countries have identified the values of inscriptions and taken measures to preserve such inscriptions. A great number of ancient inscriptions have been discovered in Sri Lanka, revealing the rich history and culture of this fascinating country. According to the literature, 4000 stone inscriptions have been discovered and around 1,500 of them recorded (Bandara & Warnajith, 2012). In Sri Lanka, ancient inscriptions offer valuable insights into the donations and maintenance of temples, the construction of water tanks, and the establishment of rules for civilians. Some inscriptions can be observed under the drip ledges of caves, rocks, pillars, and slabs. Inscriptions belong to different categorizations based on eras. Deep learning approaches have shown remarkable performance in automating tasks, with the potential to achieve high accuracies in a wide range of classification and detection problems (Rustam *et al.*, 2021).

Several past studies focused on recognizing inscriptions in the Sri Lankan context. Some of those studies have been conducted to recognize and digitize some Brahmi and Sinhala characters found in inscriptions, but most of those studies have failed to recognize and translate the whole content of the inscriptions and classify the inscriptions based on palaeography and morphology. At present, there is no standardized classification system for Sinhalese inscriptions. According to archaeology experts, classification of inscriptions is made based on research findings of researchers in the field (Deraniyagala, 1992).

The aim of this study is to classify Sinhalese inscriptions both manually and computationally, based on the evolution of Sinhala characters as well as the palaeographical and morphological data of the Sinhalese inscriptions. Different deep learning models, including those with transfer learning techniques, were employed to classify the inscriptions based on the results of manual classification. The performance of the model was analyzed based on their accuracy.

There are few studies carried out related to this research. One of the research groups actualized a computational framework to set up the accurate characters of early Brahmi scripts of Sri Lankan inscriptions (Bandara, 2014). The study was carried out in four major steps. As an initial step, Brahmi scripts were converted to photographic data. Based on the photographic data Brahmi characters were identified. Then a database was created based on the identification results. An optical image scanner with the resolution of 300 pixels per inch was utilized to scan the image. Adobe Photoshop CS3 and MATLAB were used for primary image processing and further processing respectively, to identify the ideal shape of the Brahmi characters. The Majority algorithm was proposed in this research. The system showcases the accurate alphabet fonts of early Brahmi scripts of Sri Lankan inscriptions.

Yet another group created a computerized system to detect inscription characters and location of the inscription site. The system comprises two major modules: OCR and geological information system (GIS) consisting of two databases; one to support OCR which contains images and Sinhala interpretation of inscriptions and the other database to store geological information of inscriptions (Ruwanmini *et al.*, 2016). In the preprocessing phase, binarization, boundary detection, segmentation and thinning are involved. After the completion of the binarization phase, Ostu's method was applied. Next, feature extraction and classification are taken into consideration. The K-mean algorithm was used for clustering.

Another study reports an approach to recognize Brahmi characters in ancient inscriptions in Sri Lanka. That system comprises an artificial neural network agent, lexical agent, structure analyst agent, and semantic agent. Various image processing techniques were employed to pre-process the image dataset. The lexical, structure analyst, and semantic agents were used to correct mistakenly identified characters. The output of the system consists of relevant Sinhala Unicode characters for the recognized Brahmi character string. This system has achieved an accuracy of 84% (Peiris, 2010).

Convolutional neural network (CNN) based classification was applied to identify similarities of modern Japanese characters and Kanji characters. The study was based on two datasets Kuzushiji-Kanji and KanjiVG. The datasets were trained using both recurrent neural network (RNN) and a mixture density network (MDN) (Heenkenda & Fernando, 2020). Initially, two separate convolutional variational autoencoders were trained on the Kuzushiji-Kanji dataset and the pixel version (64*64 pixel resolution) of the KanjiVG dataset. The datasets were compressed into their own 64 dimensional latent space z_{old} and z_{new}, and an MDN with two hidden layers was trained to model the density function, which can be represented as $P(z_{new}|z_{old})$ and approximated as a mixture of Gaussians. Finally, a Sketch-RNN model was used to generate Modern Kanji based on z_{new}.

A deep neural network-based text restoration model which recovers missing characters from a damaged text input in Greek inscriptions called PYTHIA, is the first ancient text restoration model (Assael *et al.*, 2019). The dataset consists of 3.2 million words from Greek inscriptions written in the ancient Greek language dating from before the 7th century BCE to 5th century CE. The model was created based on long short term memory (LSTM). The system achieved a character error rate of the computerized system 30.1% which is significantly lower than the human recognition rate of 57.3%.

MATERIALS AND METHODS

Population and sampling technique

The population of this study consisted of a pool of inscriptions written in the Sinhala language and vetted by the subject experts in the field of archaeology. The study's inclusions consisted of images, videos, literature, text, and translations of Sinhalese inscriptions. Meanwhile inscriptions that were not accessible due to antiquities

legislation, the condition of the inscription surface and environmental factors, such as height, were excluded from the study.

Convenience sampling was employed as the sampling technique for this study. Under the guidance of archeological experts and based on the density of Sri Lankan inscriptions site maps, data were collected from various districts, including Anuradhapura, Polonnaruwa, Ampara, Kurunegala, Puttalam, Vavuniya, Trincomalee, Batticaloa, Hambantota, Kandy, Kegalle, Matale, Badulla, Monaragala, Nuwara Eliya, Gampaha, and Rathnapura. Additionally, some inscriptions were obtained from the archeological museum in Colombo and included in the study.

Data Collection

Data collection methods

The research utilized a range of data gathering techniques including interviews, field visits, observation, archeological scholarly books, and websites. In-depth interviews, both informal face-to-face and telephone, were conducted with archeological experts and museologists to capture valuable insights and perspectives. The knowledge and perceptions of these subject experts greatly enriched the research and ensured its quality. Qualitative data was primarily gathered through interviews with archeological specialists, including in-depth discussions with site officers and knowledge experts. Face-to-face interviews and online meetings were conducted with site officers at inscription sites and academic staff members to obtain comprehensive information. The data collection process utilized a variety of devices, platforms, and tools to facilitate this, including:
● Data collection sheets: Microsoft Word, Microsoft Excel, Text Analyzer
● To get photographs and videos: Android mobile phone
● Interview protocols: Semi-structured
● Recording methods: Voice recording, taking notes, taking images and videos of inscriptions

The following qualitative data were gathered:
● Images, photographs, and videos of inscriptions which were written in Sinhala language
● Archeological terms
● Paleographical and morphological data for the Sinhala language
● Translated text of inscriptions
● Sinhala language evolution related to inscriptions

The Department of Archaeology maintains a collection of inscriptions' estampages. However, for this study, the focus was on onsite images as the majority of the estampages in the collection were captured many decades ago.

Manual classification of Sinhalese inscriptions

Prior to applying machine learning approaches, the data was analyzed manually using a thematic analysis approach. Specifically, content analysis was utilized as a manual qualitative data analysis technique, given the historical nature of the data and the importance of cultural, social, and economical preservation, identifying patterns in the written text, including inscriptions, archaeological terms, and palaeographical and morphological data for the Sinhala language, as well as the evolution of the Sinhala language over time.

Thematic analysis

Sinhalese inscriptions have been categorized into different eras by researchers based on their convenience, rather than adhering to a proper set of standards. To simplify and standardize the ideas presented within the inscriptions, a thematic analysis was carried out. Additionally, voice cuts and recordings of subject experts in the field of archaeology were transcribed to identify patterns which make arguments, ultimately leading to a better understanding of the study through examination of differing expert opinions. However, it was a challenging task to compose different ideas into a coherent whole.

To ensure the accuracy of the analysis, thorough examinations were carried out with scholarly articles that were gathered to identify translations of the text on inscriptions and to classify the inscriptions themselves.

Computational classification for Sinhalese inscriptions

This section illustrates the different machine learning techniques which were used to classify Sinhalese inscriptions. CNNs became a state-of-the-art method for classification of images (Rustam *et al*., 2021). As images of inscriptions are limited, transfer learning techniques were used for this research. In this section, we describe different deep CNN models used in this research.

Dataset

The dataset comprises images obtained from the original Sinhalese inscriptions, and the number of relevant estampages of the inscriptions can be found from the Department of Archaeology and Central Cultural Fund. To increase the number of images and enhance the dataset's variability, data augmentation techniques were utilized on the original dataset. Augmentation methods such as translation, rotation, scale, and zooming were applied. Following the application of these augmenting methods, the total number of images in the dataset increased to 475 as shown in Table 1.

Table 1: Number of original Sinhalese inscriptions and number of augmented images in the dataset

Category	No of original Sinhalese inscriptions	No of augmented images
Early Brahmi	16	110
Late Brahmi	10	90
Transitional Brahmi	7	72
Medieval Sinhala	15	100
Modern Sinhala	14	103

Classification models

Figure 1 shows the classification approach of Sinhalese inscription.
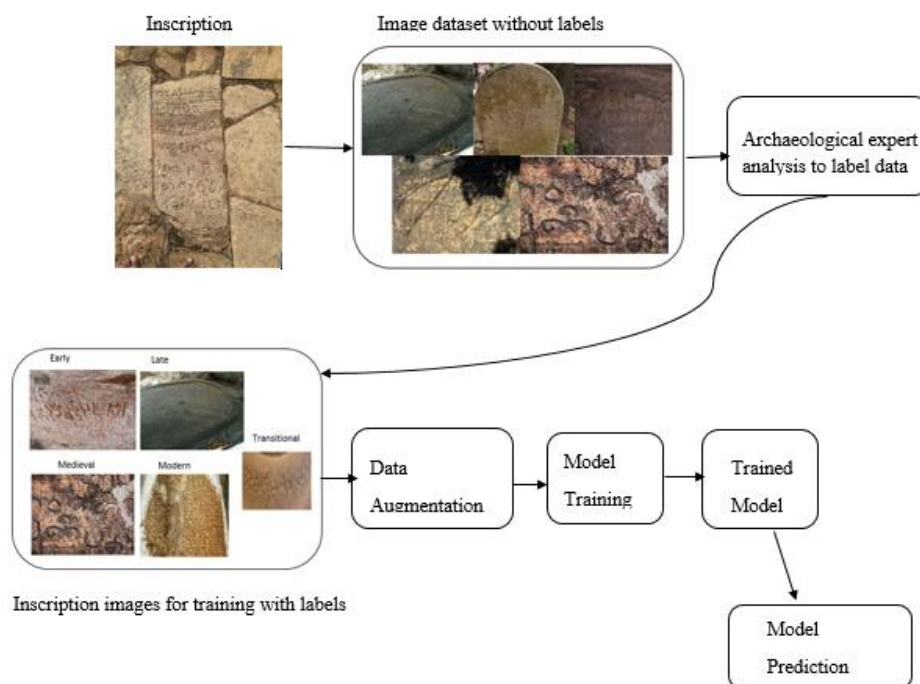
Figure 1: Classification approach of Sinhalese inscriptions

CNN model trained from the scratch

CNN is a widely used and powerful type of neural network that is particularly effective at processing complex computational data. The CNN model developed from scratch consists of seven convolutional layers, pooling layers, flattening layers, non-linear activation layer and dropout layer. The primary convolutional layer is responsible for extracting feature maps from input images, while the max pooling layer is utilized to identify sharp features within the proposed system. The activation function employed in this CNN model is the ReLU (rectified linear unit) function. Figure 2 shows the architecture of CNN model trained from the scratch.
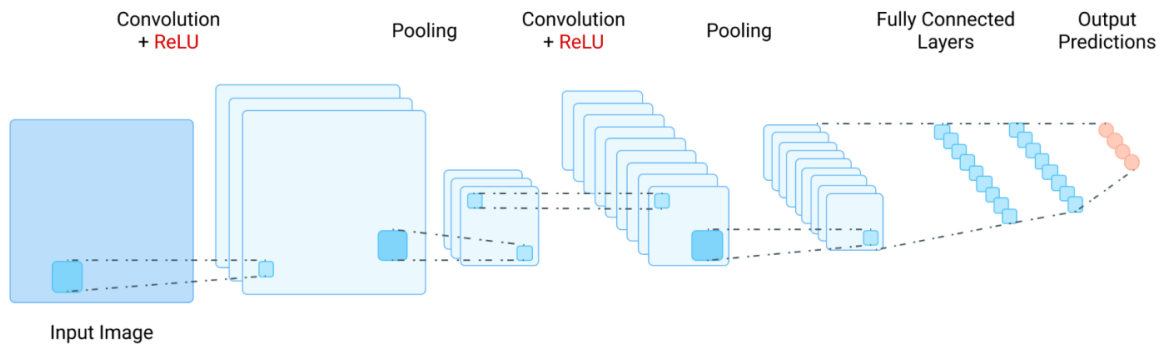
Figure 2: Architecture of CNN model developed from scratch

Inception-v3

Inception-v3 is a convolutional neural network (CNN) that builds upon the GoogLeNet (Szegedy *et al*., 2015). It is pre-trained and utilizes transfer learning for feature extraction. This approach reduces computational complexity by decreasing the number of parameters that need to be trained. The system's high-level architecture is illustrated in Figure 3.
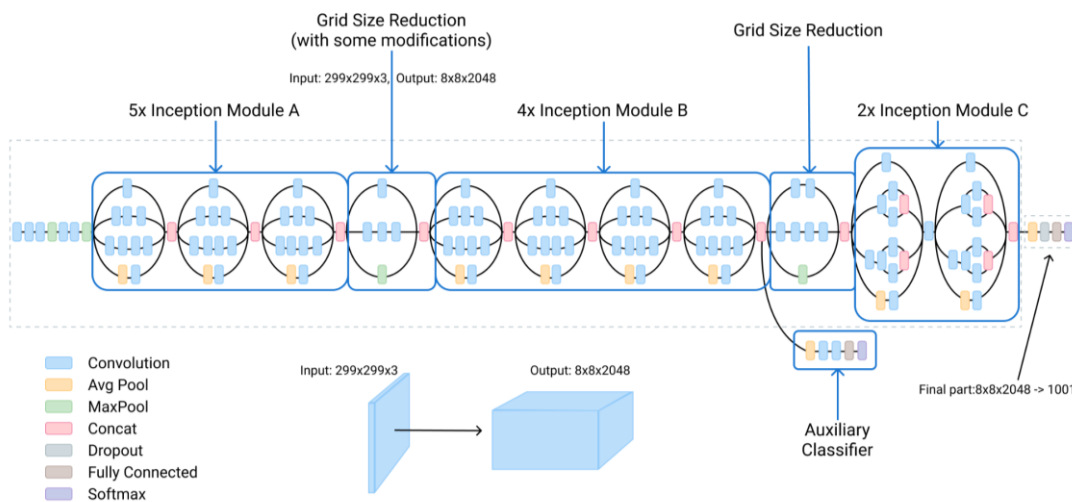
Figure 3: The high level architecture of Inception-v3 (https://cloud.google.com/tpu/docs/inception-v3-advanced)

VGG-19

The VGG-19 model, as depicted in Figure 4, is composed of six structures that incorporate multiple connected convolutional layers and fully connected layers. The convolutional kernel is fixed at 3 x 3, while the input size is 224 x 224 x 3. The model performs feature extraction on its own, and it utilizes max-pooling for down-sampling,

with the rectified linear unit (ReLU) serving as the activation function. The down-sampling layer plays a crucial role in improving the model's anti-distortion ability, while simultaneously reducing the number of parameters, as stated by Jian Xiao *et al.* (2020).
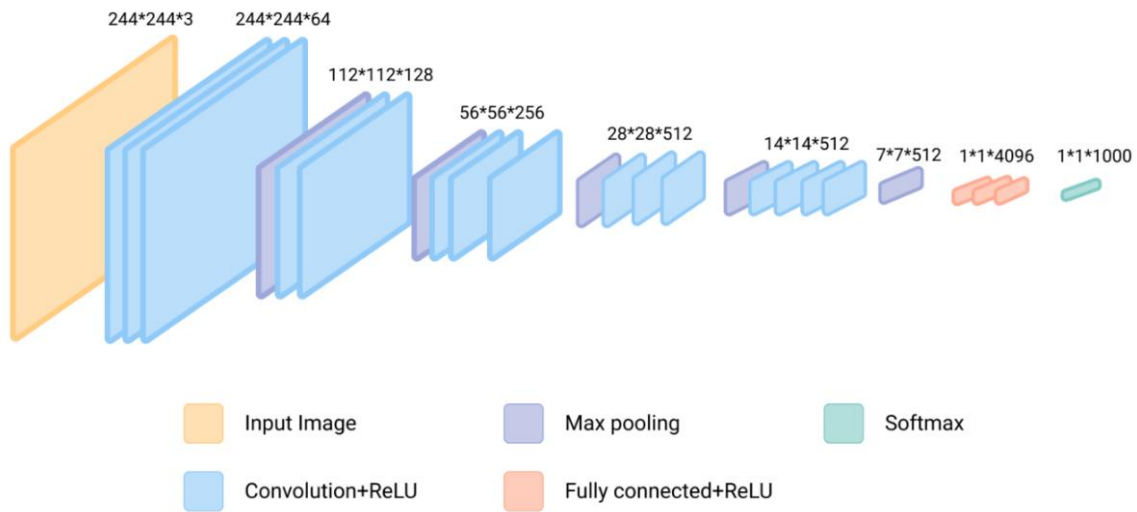
Figure 4: The high level architecture of VGG-19 model (Jian Xiao *et al.*, 2020)

Resnet-50

The ResNet-50 model, illustrated in Figure 5, is a deep residual network that consists of 50 layers with a significant depth (Kaiming *et al.*, 2016). By maintaining the same number of filters for the same feature map size, the model reduces the time complexity associated with training deep networks. ResNet-50 is an extension of ResNet-34 and builds upon its architecture to further enhance the model's performance.
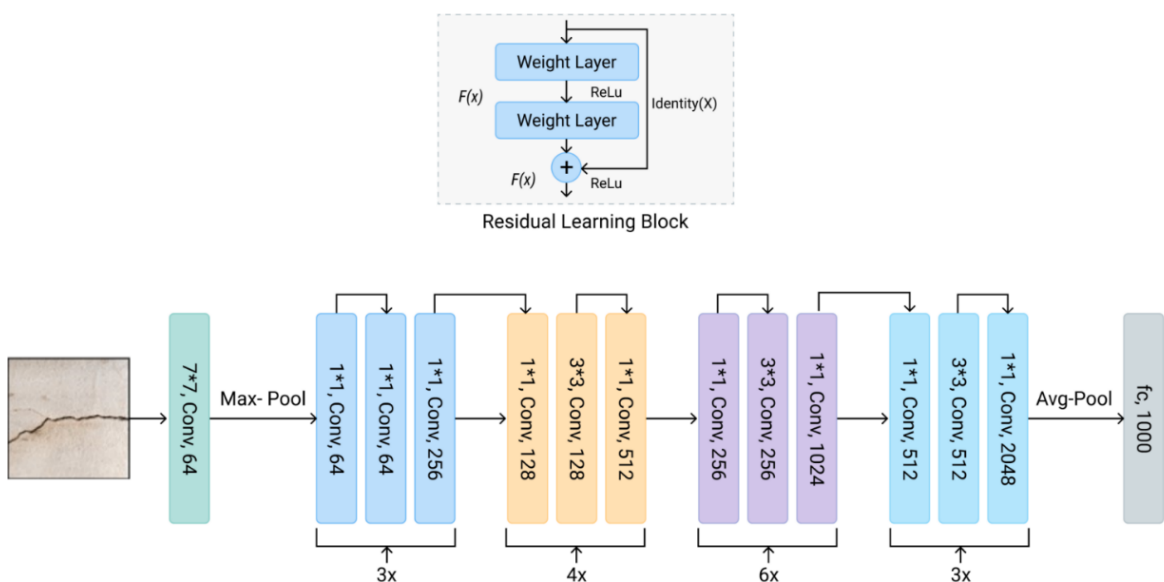
Figure 5: The high level architecture of ResNet-50 model (Ali *et al.*, 2021)

RESULTS AND DISCUSSION

Results of manual classification of Sinhalese inscriptions

Palaeography of Sinhalese inscriptions

The Sinhala characters originated from the Brahmi characters, with their evolution beginning around 1 BC (Thennakoon, 1957). Over time, the shapes of the Sinhala letters began to diverge from those of the Brahmi characters, becoming more circular or rounded. Most of the inscriptions in Sinhalese were written from left to right, although some were written from right to left on rare occasions. During the 8th century, Sinhala characters were influenced by Pallava characters (Thennakoon, 1957).

Some of the Sinhala characters, such as අ, ද, ක, ග, ව, ජ, ඩ, න, බ, ය, ර, ල, ව, භ, and ඦ, were derived from Brahmi letters, while others such as ඉ, ඔ, බ, ජ, ඥ, ට, ඵ, හ, ෂ, and ඝ were derived from Pallava letters. By the 16th century, the Sinhala letters had become more rounded, as they appear today. However, the evolution of these characters came to an end due to the advent of printing technology.

Pictorial symbols

A number of inscriptions contain pictorial symbols that are not Sinhala characters. These symbols may appear at the beginning or end of a line of Sinhala characters, or above or below them. In some inscriptions known as 'Aththani' inscriptions, which were created when donating to temples and hospitals, symbols such as a dog, crow, and monk's fan were common. These symbols served to emphasize that anyone who misused public property would be reborn as a dog or crow in their next life. In inscriptions from the 15th century onwards, common symbols include Bo leaves and Dharmachakra.

Phonology of Sinhalese inscriptions

The inscriptions denote details of pronunciation and phonetic modifications. Spoken Sinhala consists of 40 segmental phonemes, comprising 14 vowels and 26 consonants, which includes a unique set of 4 prenasalized voiced stops. In contrast, the modern Sinhala character set comprises 20 vowels and 40 consonants. However, for this research, these phonemes were not deeply considered.

Morphology of Sinhalese inscriptions

The Sinhalese language of the past typically ended in a vowel, and it was rare to find pronominal forms in the written scripts of that time. Nouns were composed of a base word and an ending, which could be simple, derived, or complex. Sinhalese inscriptions included a set of morphophonemic rules known as 'Sandi'.

Categorization of Sinhalese inscriptions

At present, there is no standard method for categorizing Sinhalese inscriptions into distinct historical eras. Various arguments exist within the academic community, and researchers have developed different classifications for their individual studies. However, due to the historical nature of the inscriptions, it is not always practical to pinpoint their precise time period. Nonetheless, experts in the field of archaeology have introduced several classifications that have greatly advanced our understanding of these important historical artifacts.

Lankage categorized the inscriptions into five eras as follows (Lankage, 1996).
- 1st era -: 3 Century BC - 1 Century BC
- 2nd era -: 1 Century AD - 3 Century AD
- 3rd era -: 4 Century AD - 5 Century AD
- 4th era -: 6 Century AD - 7 Century AD
- 5th era -: 8 Century AD - 10 Century AD

Another categorization based on the palaeography of inscriptions was revealed in Salapathalamaluwa (Mudiyanse, 2020).

- 1st era -: 2 Century BC - 1 Century BC
- 2nd era -: 1 Century AD - 3 Century AD
- 3rd era -: 3 Century AD - 5 Century AD
- 4th era -: 5 Century AD - 8 Century AD
- 5th era -: 8 Century AD - 10 Century AD
- 6th era -: 10 Century AD - 12 Century AD

Thennakoon mentioned eight eras in the book "Parani Lankawa ha Shilalipi," which considered inscriptions up to Kandy era as follows (Thennakoon, 1957).

- 1st era -: 3 Century BC - 1 Century AD
- 2nd era -: 1 Century AD - 5 Century AD
- 3rd era -: 5 Century AD - 8 Century AD
- 4th era -: 8 Century AD - 11 Century AD
- 5th era -: 11 Century AD - 13 Century AD
- 6th era -: 13 Century AD - 15 Century AD
- 7th era -: 15 Century AD - 16 Century AD
- 8th era -: 16 Century AD - 19 Century AD

Karunarathne discussed seven eras in the book 'Sinhala Shila Lekhana,' which considered inscriptions up to the year 1815 (Karunarathne, 1956).

- 1st era -: 300 BC - 1 BC
- 2nd era -: 1 AD - 300 AD
- 3rd era -: 300 AD - 800 AD
- 4th era -: 800 AD - 1000 AD
- 5th era -: 1000 AD - 1200 AD
- 6th era -: 1200 AD - 1415 AD
- 7th era -: 1415 AD - 1815 AD

Fernando defined two eras based on palaeography data as follows (Deraniyagala, 1992).

- Brahmi era -: 3 Century BC - 7 Century AD
- Sinhala era -: 7 Century AD - 15 Century AD

However, based on the evolution of Sinhala characters, inscriptions are categorized commonly into five eras for documentation and academic purposes, as follows.

- Early Brahmi -: 3 Century BC - 1 Century AD
- Late Brahmi -: 2 Century AD - 4 Century AD
- Transitional Brahmi -: 5 Century AD - 7 Century AD
- Medieval Sinhala -: 8 Century AD - 14 Century AD
- Modern Sinhala -: 15 Century AD - Present

The categorization outlined above was duly considered during the process of computational classification in this research.

Results of classification models

The classification models were implemented using the Tesla K80 GPU processor, which boasts a RAM size of 12.6 GB. Our dataset consisted of 475 images, which were divided into training and validation sets at ratios of 85% and 15%, respectively. During the training phase, we utilized the categorical cross entropy function as the loss function, as it is optimal for multi-class classification tasks. We trained the CNN models (including Inception-v3, VGG-19, and ResNet-50) by varying parameters such as filter size and the number of layers for each model. Additionally, we employed transfer learning techniques. Our batch size was set at 32 and we trained each model for 100 epochs. Finally, we evaluated the classification models using accuracy.

CNN model trained from the scratch

The model achieved accuracies of 92.01% and 74.12% for the training and validation datasets, respectively.
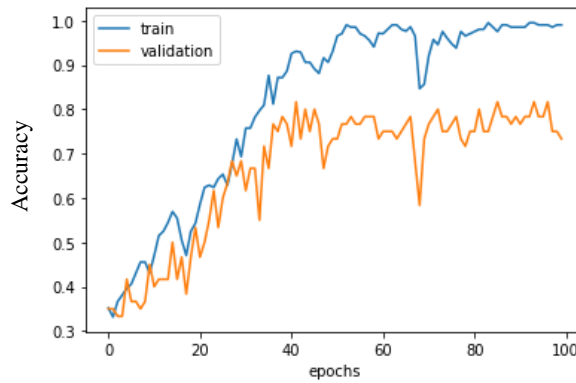
Figure 6: Training and validation accuracies of CNN model

Inception-v3

The model obtained accuracies of 93.25% and 87.21% for the training and validation datasets, respectively.
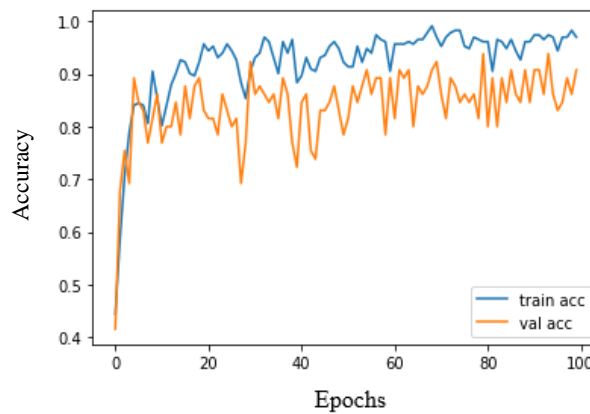
Figure 7: Training and validation accuracies of Inception-v3

VGG-19

The model achieved accuracies of 91.01% and 58.33% for the training and validation datasets, respectively.
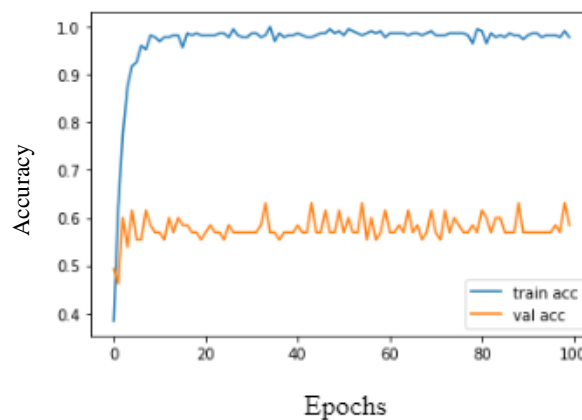
Figure 8: Training and validation accuracies of VGG-19

Resnet-50

The model achieved 78% and 58.74% accuracies for training and validation datasets respectively.
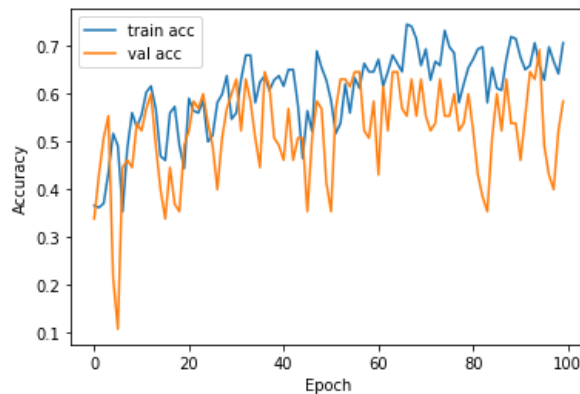
Figure 9: Training and validation accuracies of ResNet-50

Models - Comparison and analysis

Table 2: Results of classification models

Model	Evaluation parameter	Score
CNN model trained from scratch	Training accuracy	92.01%
	Validation accuracy	74.12%
Inception-V3	Training accuracy	93.25%
	Validation accuracy	87.21%
VGG-19	Training accuracy	91.01%
	Validation accuracy	58.33%
ResNet-50	Training accuracy	78.00%
	Validation accuracy	58.74%

Cross-validation was employed to validate the effectiveness of the models, using K-fold cross-validation. The dataset was initially shuffled and divided into K groups. For each group, the following steps were followed: the group was held out, the remaining data was used as the training dataset, a model was trained on the training dataset, and the model was evaluated on the validation dataset.

Table 3: Models performances with 10-fold cross validation

Iteration	CNN model trained from scratch	Inception-V3	VGG-19	ResNet-50
Iteration 1	70.01%	85.27%	55.75%	57.42%
Iteration 2	71.30%	86.21%	58.10%	60.10%
Iteration 3	71.21%	87.01%	57.51%	59.30%
Iteration 4	70.03%	84.99%	58.01%	64.20%
Iteration 5	71.01%	87.21%	56.62%	56.59%
Iteration 6	70.12%	85.66%	56.61%	58.32%
Iteration 7	70.33%	85.38%	58.02%	57.99%
Iteration 8	72.54%	85.68%	57.45%	57.85%
Iteration 9	70.31%	84.69%	58.11%	57.99%
Iteration 10	69.81%	87.31%	58.25%	57.99%
Average	70.66%	85.94%	57.44%	58.77%
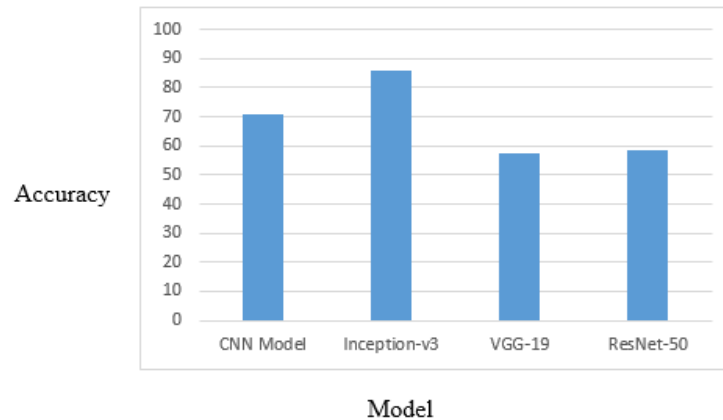
Figure 10: Models' average accuracy score comparison with 10-fold cross validation

This study was conducted in four main steps: data collection, manual classification of Sinhalese inscriptions, computational classification of Sinhalese inscriptions, and analysis of the results. The computational classification process relied on the manual classification carried out previously and was carried out subsequently. The accuracy of the manual classification was verified by collaborating with experts in archaeology.

To document and study Sinhala character inscriptions, paleographical and morphological data have been used to categorize them into five eras: Early Brahmi, Late Brahmi, Transitional Brahmi, Medieval Sinhala, and Modern Sinhala. This classification system was taken into account for the computational classification in this research, which covered twelve districts in Sri Lanka based on the density of inscriptions. Four models were tested for classifying Sinhalese inscriptions, with the first model using only convolutional neural networks and not being a pre-trained model, while the other models utilized transfer learning techniques. Out of these models, the Inception-v3 model achieved the highest accuracy.

Only a few studies have been conducted to identify specific characters in Sinhalese inscriptions within the Sri Lankan context, and there is currently a lack of computational approaches for classifying Sinhalese inscriptions from different eras. However, the application of four deep learning models has shown promising results in the classification of Sinhalese inscriptions.

CONCLUSION

To date, no significant computational study has been conducted to classify Sinhalese inscriptions from different eras, highlighting a gap in the field of computational archaeology. This study aims to address this issue by utilizing a dataset consisting of 475 images from 62 Sinhalese inscriptions, with data augmentation techniques employed to increase the number and variation of the samples. The findings indicate that the Inception-v3 model can accurately identify the period of Sinhalese inscriptions, achieving an 85.94% accuracy level on the validation dataset. To improve the robustness of the model, data augmentation methods can be further utilized. Moreover, the results of the study suggest that deep learning models utilizing transfer learning techniques outperform other models on this dataset.

Future Work

The authors aim to explore the use of alternative machine learning techniques for the classification of Sinhalese inscriptions and analyze their performance. Additionally, a system will be proposed to translate Sinhalese inscriptions into the English language.

Acknowledgments

REFERENCES

Ali L., Alanjir F., Jassmi H.A. & Gochooko M. (2021). Performance evaluation of deep CNN-based crack detection and localization techniques for concrete structures. *Sensors* **21**(5): 1688.
DOI: https://doi.org/10.3390/s21051688

Assael Y., Sommerschield T. & Prag J. (2019). Restoring ancient text using deep learning: a case study on Greek epigraphy. *Proceedings of the 2019 Conference on Empirical Methods in Natural Language Processing,* 3-7 November. Hong Kong, China, pp. 6368–6375.
DOI: https://doi.org/10.18653/v1/D19-1668

Bandara P.B.A.D.W. (2014). Archaeological study of Sri Lankan Brahmi inscriptions by using digital image analysis. *PhD Thesis*, Ibaraki University, Japan.

Bandara D., Warnajith N., Minato A. & Ozawa S. (2012). Creation of precise alphabet fonts of early Brahmi script from photographic data of ancient Sri Lankan inscriptions. *Canadian Journal on Artificial Intelligence, Machine Learning and Pattern Recognition* **3**(3): 33–39.

Deraniyagala S. (1992). *The Prehistory of Sri Lanka*. Department of Archaeology, Colombo, Sri Lanka.

Heenkenda S. & Fernando T.G.I. (2020). Approaches used to recognise and decipher ancient inscriptions: A review. *Vidyodaya Journal of Science* **23**(2): 42–55.

Hettiarchchi K. & Dayananda S. (2018). *Rajagala Sellipi*. Department of Archeology, Colombo, Sri Lanka.

Kaiming H., Xiangyu Z., Ren S. & Sun J. (2016). Deep residual learning for image recognition. *Proceedings of the IEEE conference on computer vision and pattern recognition*, 27-30 June. IEEE, Las Vegas, USA, pp. 770–778,
DOI: https://doi.org/10.1109/CVPR.2016.90.

Karunarathne K.G.N.D., Liyanage K.V., Ruwanmini D.A.S., Dias G.K.A. & Nandasara S.T. (2017). Recognising ancient Sinhala inscription characters using neural network technologies. *International Journal of Scientific Engineering and Applied Sciences* **3**(1): 37–47.

Karunarathne S. (1956). *Sinhala Shila Lekhana*. Department of Archeology of Sri Lanka, Colombo, Sri Lanka.

Lankage J. (1996). *Sinhala Warna Malawe Vikashanaya*. Godage Publishers, Colombo, Sri Lanka.

Mudiyanse N. (2020). *Sinhala Akuruwala Ithihasaya*, Colombo, Sri Lanka.

Peiris T.M.T.H. (2010). Recognition of Inscriptions in Ancient Sri Lanka. *MSc Thesis,* University of Moratuwa, Sri Lanka.

Rustam F., Siddique M.A. & Siddique H.R. (2021). Wireless Capsule Endoscopy Bleeding Images Classification using CNN Based Model. *IEEE Access* **9**: 33675–33688.
DOI: https://doi.org/10.1109/ACCESS.2021.3061592

Ruwanmini D.A.S., Liyanage K.V., Karunarathne K.G.N.D., Dias G.K.A. & Nandasara S.T. (2016). An architecture for an inscription recognition system for Sinhala epigraphy. *International Journal of Research-Granthaalayah* **4**(12): 48–64.
DOI: https://doi.org/ 10.29121/granthaalayah.v4.i12.2016.2392

Szegedy C., Liu W. & Jia W. (2015). Going deeper with convolutions. *Proceedings* of *IEEE Conference on Computer Vision and Pattern Recognition* (CVPR), 07-12 June. Boston,USA, pp. 1–9.
DOI: https://doi.org/10.1109/CVPR.2015.7298594

Thennakoon W. (1957). *Parani Lankawa ha Shilalipi*. MD Gunasena Publishers, Colombo, Sri Lanka.

Wijesekara N. (1990). *Inscriptions,* volume II. Department of Archaeology, Colombo, Sri Lanka.

Withanachchi C. (2013). *Ampara District*. Department of Archeology, Colombo, Sri Lanka.

Xiao J., Wang J., Cao S. & Li B. (2020). Application of a novel and improved VGG-19 network in the detection of workers wearing masks. *Journal of Physics Conference Series* **1518**: 012041.
DOI: https://doi.org/10.1088/1742-6596/1518/1/012041

RESEARCH ARTICLE

Environmental Horticulture

Beyond aesthetics: Integration of textural groups of tropical ornamental shrubs into urban planting designs

K Yakandawala[1*], A Bandara[1], D Yakandawala[2] and R Abeynayake[3]

[1] *Department of Horticulture and Landscape Gardening, Faculty of Agriculture and Plantation Management, Wayamba University of Sri Lanka, Makandura, Gonawila 60170, Sri Lanka.*

[2] *Department of Botany, Faculty of Science, University of Peradeniya, Peradeniya, Sri Lanka.*

[3] *Department of Agribusiness Management, Faculty of Agriculture and Plantation Management, Wayamba University of Sri Lanka, Makandura, Gonawila 60170, Sri Lanka.*

Abstract: Shrubs are popularly incorporated to establish green infrastructure in urban spaces. We argue that the functions provided by shrubs could be further enhanced by giving due consideration to their leaf morphological characters. Therefore, our objective was to recognise how the different morphological characters of leaves, listed as contributing to determining the plant texture in literature, would collectively contribute to recognizing textural groups of plants, and further, to define each of these groups into either coarse, medium, or fine textural categories using ornamental shrubs. We investigated the quantitative and qualitative leaf morphology of 30 tropical ornamental shrubs in the Peradeniya area. According to our analysis, leaf area, petiole length, and internodal distance have significantly contributed to the separation of shrubs into three textural groups; fine, medium and coarse, and were considered as preliminary characters that determine the texture. Leaf hair related characters *viz.*, hair densities on upper and lower surfaces, and the length of hairs on both surfaces, together with qualitative morphological characters, *viz.*, leaf margins, leaf arrangement, and prominent venation were identified as secondary characters that contributed to defining textural groups. Shrubs with coarse texture possess significantly larger leaves, longer petioles and internodal distances compared to fine textured group. Our recommendation is to consider plant textural groups as a criterion in the selection of plants for planting designs during the establishment of green infrastructure in urban spaces, enabling the obtaining of benefits beyond aesthetics, which include other functional, health and environmental benefits, to improve the quality of life of city dwellers under the context of limited urban green spaces.

Keywords: Green infrastructure, leaf morphology, leaf texture, morphometric analysis, ornamental shrubs, urban space.

INTRODUCTION

Urban spaces occupy a small area (~0.5%) of the Earth's total land surface (Schneider *et al*., 2009). Ironically, 55% of the current world population occupies this space (UN, 2019). This indicates a disproportionate relationship between urbanization and urban land cover. Urbanization is considered a major drive of land cover change worldwide (Grimm *et al*., 2008) and is characterized by expanding built-up areas and population growth in cities (Ren, 2015). As a result, it has led to many environmental issues associated with the reduction of green spaces that could directly have an impact on city dwellers (Seto *et al*., 2012). Consequently, the importance of the wise use of the available urban spaces is a topic of concern.

Moreover, urban vegetation plays a vital role as a major component of green infrastructure (GI) in light of urbanisation. Naumann *et al.* (2011) defined GI as a human-made (or human influenced) infrastructure designed and installed to ease environmental pressure. The multifunctional nature of GI is well-documented and these functions are broadly categorized as economic, ecological and sociocultural (Hansen & Pauleit, 2014). Further, aesthetic value considered under the socio-cultural benefits is a widely perceived component, appreciated and highly valued by city dwellers (Nia & Olugbenga, 2020).

* Corresponding author (kapilay@wyb.ac.lk; https://orcid.org/0000-0001-5304-4603)

Urban GI covers a range of landscape types of varying complexity and morphology such as parks, urban forests, roof and vertical greening, and residential gardens (Cameron *et al.*, 2012). Ornamental plants, a major component of urban vegetation, play an important role in green infrastructure (GI) in urban landscapes (Natuhara, 2018). They could be categorized under ground covers, herbs, shrubs, trees, and climbers, growing under terrestrial or aquatic habitats. Among them, shrubs are defined as woody plants which produce multiple branches derived from nodes near the base of the plant (Cameroon, 2016). They are popular in anthropogenic landscapes, specifically due to their tolerance to pruning, fast growth rate, variation in form, the striking nature of their leaves with a range of sizes, shapes, and colours contributing to their overall appearance, and attractive flowers and fruits (Jacobson, 1990; The Royal Horticultural Society, 2013; Cameroon, 2016). Further, during management practices, the tolerance to pruning and clipping and ease of propagation by stem cuttings also contribute to their popularity (Dirr, 2009). As a result, shrubs are widely used globally in urban spaces for decorative and other functions by including them in establishing GI such as hedges, borders, beds, and specimen plants (Kendal *et al.*, 2008). Adding to that, the height of ornamental shrubs is comparable to the human dimension, compared to trees and could, therefore, be appreciated at the human-eye level (Jacobsen, 1990). Therefore, the rationale for selecting shrubs in this study was to add aesthetic and functional value to their present use. The aesthetic attributes of shrubs which include leaf and flower, their colour and size, shape and texture, and form have been widely used in landscape designs from ancient times (Laurie, 1975). The designs in Roman and Persian times, as well as Mediaeval and Renaissance cultures, to the Victorian era and up to the present time, have led to global appreciation of the colour of flowers (Tobey, 1973; Farahani *et al.*, 2016). Particularly from Roman gardens onwards, skilful management practices of shrubs leading to formal hedges and topiaries had further added aesthetics to the design (Laurie, 1975).

With respect to the Sri Lankan context, garden flora was initially elaborated by Macmillan in 1935 in his famous book 'Tropical Gardening and Planting' (Macmillan, 2012). It explained the popular gardening plants (exotics), their management techniques and their applications. Later, the functions of urban plants were discussed in the Guide to Urban Planting in Sri Lanka (Ekanayake, 1982). Though some studies were conducted on popularizing native plants in landscaping (Yakandawala *et al.*, 2013; De Mel and Yakandawala, 2016), these plants are not readily available in the market as opposed to exotic plants despite their functional value (Ranasinghe *et al.*, 2019).

The benefits of plants are closely related to their external appearance (phenotype) or morphology. Plant morphology has undergone fundamental, conceptual, theoretical, and philosophical changes in recent decades (Sattler & Rutishauser 1997). These changes have redirected the course of research in plant morphology and other fields where they are relevant. Apart from these, plant morphology plays a fundamental role in planting design. Hence, Dobrilovič (2006) highlighted the importance of consideration of morphological characteristics of plants as a criterion for selecting plants in planting designs. The visual properties or morphology of plants is a critical parameter for consumers looking to purchase ornamental plants for immediate aesthetic effect (Schreiner *et al.*, 2013; Ferrante *et al.*, 2015). Besides, designers are also concerned about the visual properties of plants. Plant texture is an important visual element in creating plant associations (Joardar, 1998). In his famous book on 'Planting Design', Florence Bell Robinson (1940) describes plant texture as the surface quality of all parts of plants. According to Beaulieu (2019), texture most often reflects observations about how a plant part looks in relation to neighbouring plants. Texture is not something people consciously think about; however, we recognize it subconsciously in plant associations (Anderson, 2014). The texture can be viewed from various distances in landscapes, ultimately affecting the viewer's perception (Robinson, 1940). Robinson (2016), further elaborating on the distance relating to plant texture, states that when a plant is observed from a closer distance, *i.e.*, less than about 2 m (where the details are easy to perceive), the leaves' surface nature contributes to the texture, while from moderate distance (about 2–20 m), petiole length, size and shape of leaves and twigs contribute to the plant's visual texture. However, from a far distance, the visual effect of individual twigs and leaves will be lost and the features of the canopy will contribute. At this distance, in addition, the size arrangement of foliage clusters or branches contributes to the determination of texture, due to the 3-D arrangement of the leaves and twigs. When the distance is further increased, the spacing between plants will contribute to the texture of plant associations. In the present study, we concentrate on the plant texture from a close to moderate distance where leaves play an important role. Leaves show tremendous morphological diversity, and these variations affect the overall texture of the plant. At macroscopic and microscopic levels, plant morphology can contribute to the textural groups (Wijesinghe & Yakandawala, 2013). Texts that describe and illustrate planting design categorize texture as fine,

medium and coarse (Joardar, 1998; Scarfone, 2007). The effect of different textural groups on visual perception and functions in planting designs is well recognized (Joardar, 1998; Robinson, 2016; Mendez, 2019).

Understanding the texture and placement of plants according to the textural groups is crucial to maintain the balance of the garden. Further, mixing plants of different textures is also important to highlight the opposing textural groups (Beaulieu, 2019). Plant texture is an area that has been poorly researched considering its applications in planting designs. Nevertheless, there have been a few research projects carried out on the role of plant texture in pollution control (Wijesinghe & Yakandawala, 2009; 2013). Accordingly, apart from aesthetics, plants with a coarse texture could reduce particulate air pollutants in urban areas (Pallawala *et al.*, 2013).

The popular textbooks (Hackett, 1979; Scarfone, 2007) and extension documents (Hansen, 2019; Lannotti, 2019) in landscape design describe plant texture and its applications in planting designs in detail. Further, they elaborate on this visual property with examples from temperate countries where plants are categorized into textural groups based on how a plant part, particularly leaves, looks relative to similar parts of another plant. According to Joardar (1998), plants are often selected based on expert empirical knowledge in a setting rather than predetermined explicit criteria. In view of filling the above gap, a broader scientific scope backed by a statistical analysis could categorise plants into textural groups with scientific proof. Therefore, in the present research, we addressed the question: Can combinations of leaf morphological characters of shrubs be used to validate textural categories scientifically? Consequently, it is anticipated that the application of the available knowledge in the establishment of GI in urban spaces could enhance city dwellers' quality of life. In this backdrop, this study aimed at recognising how the combination of different vegetative morphological characters that determine the plant texture would contribute to recognising textural categories of popularly used tropical shrubs. We hypothesised that the diversity in morphological characters of leaves and twigs results in different textural categories in shrubs. We have investigated the external leaf morphology of 30 tropical ornamental shrubs used in urban landscaping in Sri Lanka to recognise different textural groups. Our results, which deviated from our expectations, can be applied in the selection of shrubs with different textural groups to obtain not only aesthetics but also other functional and social (manipulating space, focalisation), environmental (reduction of particulate matter pollution, noise amelioration, human thermal comfort), and health benefits (reducing respiratory diseases and stress).

MATERIALS AND METHODS

Location of material collection

Twigs from 24 commonly used ornamental shrub species were collected from the Royal Botanical Gardens, Peradeniya, Sri Lanka, and twigs from four native and two endemic shrub species were collected from a nearby residential garden (2 km apart) for the experiments during the period May to August 2017 (Table 1). The study area receives >1400 mm of average annual rainfall, and average temperatures range from approximately 23.5 ℃ to 26.5 ℃.

Collection of material

Seven individual plants were randomly selected to represent each shrub species, and three mature twigs approximately 15 cm in length at 1.5 – 2.5 m height were selected from each individual for recording characters. All collected twigs were treated separately with a different acronym (Table 1). Thereby, altogether 21 branches were collected from each species, tagged and stored in separate polybags and transported immediately to the Horticulture laboratory of the Wayamba University of Sri Lanka.

Table 1: Shrubs used in the study for collecting leaf morphological characters with their respective family and acronym

Botanical name	Family	Acronym	*Conservation status
Allamanda cathartica	Apocynaceae	AC	Exotic
Acalypha hispida	Euphorbiaceae	AH	Exotic
Acalypha inferno	Euphorbiaceae	AI	Exotic
Acalypha siamensis	Euphorbiaceae	AS	Exotic
Acalypha wilkesiana 'Tricolor'	Euphorbiaceae	AW	Exotic
Barleria lupulina	Acanthaceae	BL	Exotic
Barleria prionitis	Acanthaceae	BPR	Locally common
Brunfelsia pauciflora	Solanaceae	BP	Exotic
Cestrum nocturnum	Solanaceae	CN	Exotic
Excoecaria bicolor	Euphorbiaceae	EB	Exotic
Graptophyllum pictum	Acanthaceae	GP	Exotic
Hamelia patens	Rubiaceae	HP	Exotic
Helicteres isora	Malvaceae	HI	Locally common
Hibiscus rosa-sinensis	Malvaceae	HR	Exotic
Ixora coccinea	Rubiaceae	IC	Locally common
Megaskepasma erythrochlamys	Acanthaceae	ME	Exotic
Memecylon umbellatum	Melastomataceae	MU	Locally common
Murraya paniculata	Rutaceae	MP	Locally common
Odontonema strictum	Acanthaceae	OS	Exotic
Osbeckia octandra	Melastomataceae	OO	Locally common
Pseuderanthemum atropurpureum	Acanthaceae	PAT	Exotic
Plumbago auriculata	Plumbaginaceae	PAU	Exotic
Polyscias balfouriana 'Marginata'	Araliaceae	PB	Exotic
Pseuderanthemum graciflorum	Acanthaceae	PG	Exotic
Pentas lanceolata	Rubiaceae	PL	Exotic
Phyllanthus myrtifolius	Phyllanthaceae	PM	Vulnerable
Pseuderanthemum reticulatum	Acanthaceae	PR	Exotic
Syzygium campanulatum	Myrtaceae	SC	Exotic
Sanchezia nobilis	Acanthaceae	SN	Exotic
Thunbergia erecta	Acanthaceae	TE	Exotic

* Source: The National Red List (2020)

Measurement of quantitative morphological characters

Seven quantitative morphological characters were measured in each twig. Internodal length (the lowermost two nodes and averaged in cm) and petiolar length (the lowermost two leaves and averaged in cm) were measured using a meter ruler. The density of leaf hairs (number of hairs under the magnification ×40, dissecting microscope Model-Labomed, USA) and hair length (average of three hairs using light microscope Model-Labomed fitted with eyepiece graticule Model-Reichert) if present in the upper and lower surface of the leaf were measured. Leaf area was measured using a portable leaf area meter (CID Bio Science Model-CI 202).

Measurement of qualitative morphological characters

Five qualitative morphological characters were also measured in each twig. The leaf margin (entire or non-entire), leaf arrangement (opposite, opposite decussate and whorled, or other), nature of leaf surface (smooth or rough), prominent venation (presence or absence), and hairs in petiole (presence or absence) were recorded by visual observations. The characters related to the hairs on leaves and petioles were studied under the dissecting microscope (Model-Labomed).

Statistical analysis

Data from 630 twigs of 210 individuals belonging to 30 species were collected during the study. These morphological characters included both quantitative and qualitative data. All the qualitative data were coded as binary variables. The Kaiser-Meyer-Olkin (KMO) test (Kaiser, 1970) was applied to check the sampling adequacy

for the multivariate analysis, while the Pearson correlation coefficient was employed to ensure that the multivariate analysis was not distorted (Rohlf, 2009). Then the quantitative morphological characters and qualitative binary variables were subjected to principal component analysis (PCA). The quantitative variables were represented by their mean values and standardized by subtracting the mean and dividing by the standard deviation to equalize the weights in the construction of the PCA axes. This analysis makes it possible to identify the most suitable variables to group the species (Iezzoni & Pritts, 1991). Then the scree plot based PCA was used to determine the number of PCs retained in the PCA (Eigen value greater than 1) (Kaiser, 1960). Then the Biplot-based representation of the PCA was performed for grouping the species considering the associated characteristics. Cluster analysis of all individuals was done to test the integrity of the PCA grouping. Hierarchical cluster analysis was used to group the species with similar morphological characters. Dendrograms using Ward's linkage method based on Gower distance coefficients (Gower, 1971), were produced to assess the similarity between the species. The correlation coefficient (r) was estimated to measure the distortion between the original matrix and the dendrogram (Sneath & Sokal, 1973; Sebola & Balkwill, 2009). To identify the significant difference among clusters identified by the PCA and cluster analysis, based on quantitative variables, one-way analysis of variance (ANOVA) was carried out with Tukey's HSD mean separation procedure at 95% confidence level. All analyses were performed in Minitab 19 (State College, PA: Minitab, Inc., USA).

RESULTS AND DISCUSSION

Morphometric analysis for textural groups

Principal component analysis based grouping.

Principal component analysis is a powerful approach that allows a better understanding of the structure of the entire group of shrubs (Zimisuhara *et al.*, 2015). The KMO test gave a value of 0.68, indicating an adequate sampling for PCA. All 12 variables were retained for the PCA and cluster analysis. The Cophenetic correlation yielded a value of 82 in the PCA, indicating a high Gower distance between species in bi-dimensional and multidimensional space. The first four PCs whose Eigenvalues were greater than one of the PCA accounted for 73.8% of the cumulative variance, and the individual contribution of the PCs is 26.6%, 18.7%, 16.6% and 10%, respectively (Table 2). As the plants employed in the study are from the outdoor environment, it is difficult to expect to capture a higher variation from PCs, where both PC1 and PC2 components explain 47% of the variation. A score plot drawn using PC1 and PC2 factor scores showed a clear grouping pattern among shrub species in the factor plane (Figure 1). The score plot for the first two PCs shows the separation of the three clusters for the 30 species with minimal overlap.

Cluster analysis based grouping

The dendrogram resulting from the cluster analysis identified three distinct clusters for the 30 shrub species, corroborating the PCA clustering (Figure 2). The first cluster showed an early separation at an approximate distance of 5,823.60, including 16 shrub species. The second and third clusters separated at an approximate distance of 1,941.20, encompassing 10 and four shrub species, respectively.

Table 2: Eigen values and variance explained by the four significant principal components

Values	PC 1	PC 2	PC 3	PC 4
Eigen value	3.4267	1.9925	2.2423	1.1986
Proportion of variance	0.286	0.187	0.166	0.100
Cumulative proportion (%)	0.286	0.472	0.638	0.738
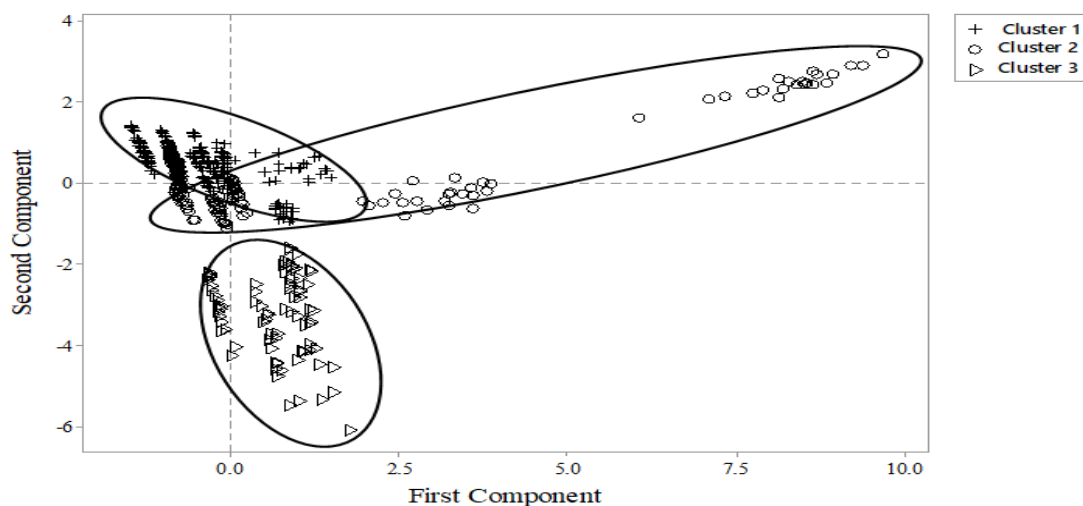
Figure 1: Score plot of first two PCs of the PCA, showing contribution of the quantitative morphological characters. Different symbols represent members of the three clusters (+ = cluster I; o = cluster II; and Δ = cluster III).
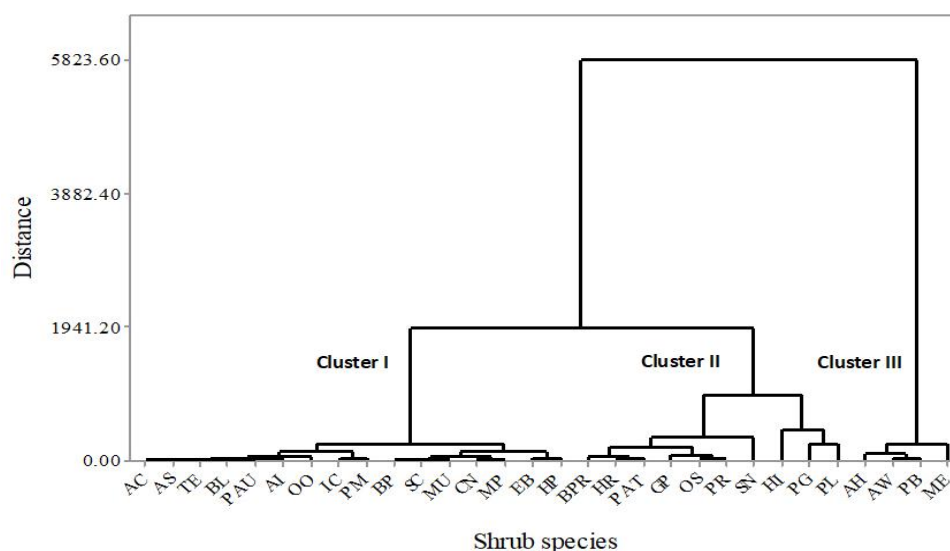
Figure 2: Dendrogram showing the relationship of shrub species based on cluster analysis where species separated into three main clusters.

Contribution of morphological characters for grouping

According to the PCA loadings (Table 3), the characters that contributed to the division of species along the PC1 were leaf lower surface hair density, hair length of upper surface, and lower surface hair length. Along the PC2, internodal distance, total leaf area and prominent venation contributed to the separation. The loading plot for the first two PCs further explained each variable's contribution (Figure 3).

Table 3: PCA loading for the first four highest accounted principal components

Variable	PC1	PC2	PC3	PC4
Internodal distance	0.033	-0.411	-0.287	0.201
Petiole length	0.095	-0.372	0.455	-0.175
Leaf upper (adaxial) surface hair density	0.342	-0.046	-0.275	-0.130
Leaf lower (abaxial) surface hair density	0.506	0.088	-0.123	0.140
Hair length of upper surface	0.478	0.157	0.036	0.217
Hair length of lower surface	0.484	0.144	0.033	0.206
Total leaf area	0.057	-0.527	0.294	0.057
Leaf margin	0.202	-0.067	0.505	0.125
Leaf arrangement	-0.003	0.346	0.460	-0.055
Leaf surface	0.177	-0.038	-0.194	-0.630
Prominent venation	-0.079	0.465	0.150	-0.232
Presence of hair on petiole	0.269	-0.134	0.066	-0.575

The one-way analysis of variance with Tukey mean comparison was carried out to determine the behaviour of quantitative variables on clusters obtained from PCA and cluster analysis. It indicates significant differences in mean values for each variable among the three clusters (Table 4).
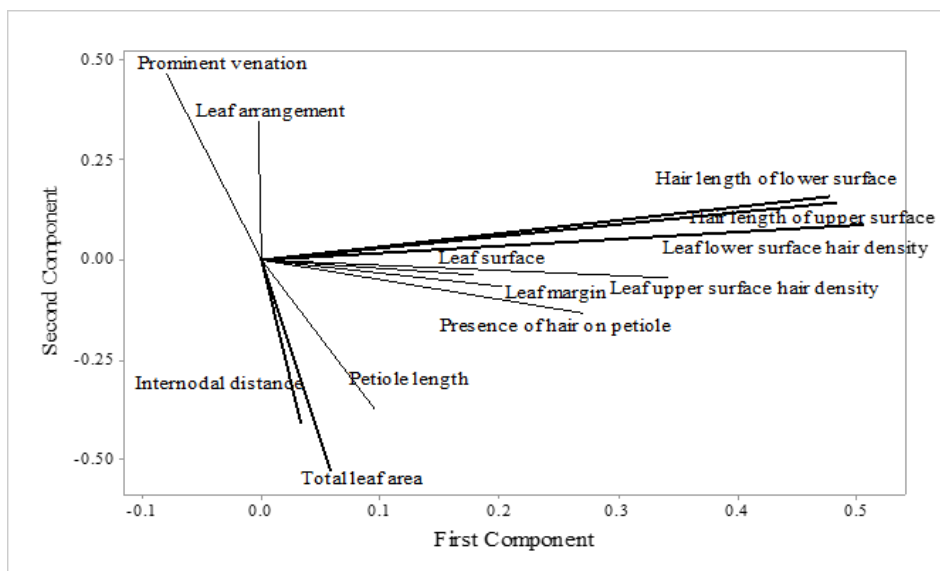
Figure 3: Loading plot (Biplot) of the first two PCs

The analysis indicates that internodal distance, petiole length, and total leaf area are significantly different among the three clusters, while leaf upper surface hair density, leaf lower surface hair density, hair length of upper surface, and hair length of lower surface contributed to the separation of cluster II from clusters I and III. The interval plot for the variables; total leaf area, petiole length, and internodal distance, which contribute significantly to discriminate the three clusters identified by the PCA and cluster analysis, are given in Figures 4a, b and c.

Table 4:   Comparison of each variable among clusters using Tukey Mean separation

Morphological character	Cluster 1	Cluster 2	Cluster 3
Total leaf area	85.62[c]	307.9[b]	1133.5[a]
Petiole length	0.59[c]	0.9328[b]	5.217[a]
Internodal distance	2.47[c]	3.889[a]	3.393[b]
Leaf upper surface hair density	8.13[b]	32.9[a]	4.881[b]
Leaf lower surface hair density	5.66[b]	90.2[a]	13.71[b]
Hair length of upper surface	0.049[b]	1.145[a]	0.3800[b]
Hair length of lower surface	0.26[b]	0.746[a]	0.05652[b]

* Means that do not share a letter are significantly different
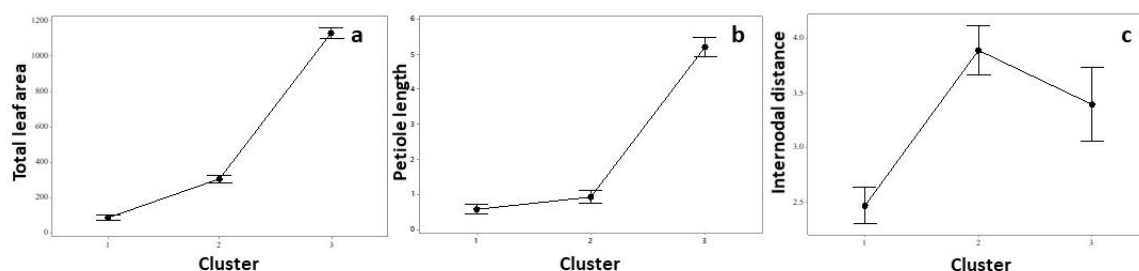
Figure 4:   The mean values of a) total leaf area, b) petiole length and c) internodal distance as a function of three different clusters. Error bars depict 95% confidence intervals associated with each of the group means.

Interval plots for the variables leaf upper surface hair density, leaf lower surface hair density, hair length of upper surface, and hair length of lower surface, which significantly discriminate cluster I and cluster III from cluster II identified by the PCA and cluster analysis, are presented in the Figures 5a to 5d.
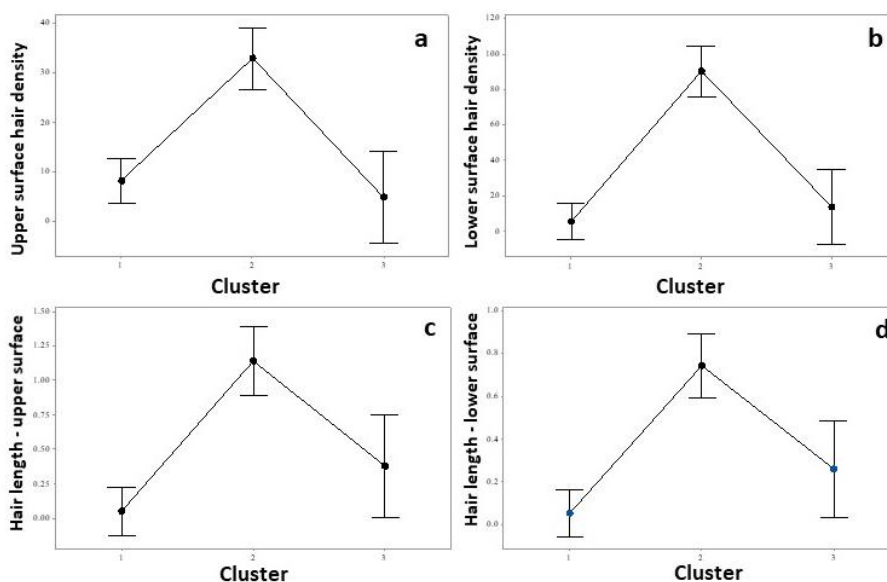
Figure 5:   The mean values of leaf hair characters a) upper surface hair density, b) lower surface hair density, c) hair length of the upper surface, and d) hair length of the lower surface as a function of three different clusters. Error bars depict 95% confidence intervals associated with each of the group means.

Landscape professionals tend to utilize plants in designing based on their experience and recommendations. However, the selection of plants based on scientific evidence would result in an improved outcome. In the present study, we have performed a morphometric analysis to categorize shrubs into different textural groups and define the characters that contribute to these groupings. Subsequently, we argue that plant species should be selected by also considering the texture in addition to their ecological and aesthetical features, which in turn are suitable to perform specific functions in urban spaces. The present study groups 30 tropical ornamental shrubs into three textural groups (Table 5).

Authors describing plant texture recognize the three textural groups as coarse, medium and fine (Blake, 1999; Scarfone, 2007). Accordingly, large leaves, leaflets or needles, broad leaf blades, deeply sinus margins, longer petioles, sparse branching (long internodes), pubescence surfaces, and rough surfaces, which cast deeper shadows contributed to coarse textures. In contrast, fine textured plants have small leaves, leaflets or needles, narrow leaf blades, entire margins, short petioles, dense branching, glossy surfaces and overall smooth surfaces that cast little or no shadows. The medium textured plants are considered as possessing the intermediate characters of both these groups (Steed, 1990; Blake, 1999; Robinson, 2016; Hansen, 2019).

Table 5:   Shrubs belonging to fine, medium and coarse textural groups

Textural group	Shrub species
Fine texture	*Acalypha inferno, Acalypha siamensis, Allamanda cathartica, Barleria lupulina Brunfelsia pauciflora, Cestrum nocturnum, Excoecaria bicolor, Hamelia patens Ixora coccinea, Memecylon umbellatum, Murraya paniculate, Osbeckia octandra Phyllanthus myrtifolius, Plumbago auriculata, Syzygium campanulatum, Thunbergia erecta*
Medium texture	*Barleria prionitis, Graptophyllum pictum, Helicteres isora, Hibiscus rosa-sinensis, Odontonema strictum, Pseuderanthemum atropurpureum, Pseuderanthemum reticulatum, Pentas lanceolata, Sanchezia nobilis, Pseuderanthemum graciflorum*
Coarse texture	*Acalypha hispida, Acalypha wilkesiana* 'Tricolor' *Megaskepasma erythrochlamys, Polyscias balfouriana* 'Marginata'

Corroborating their grouping, the leaf area, petiole length and internodal distance significantly contributed to the separation of the three different textural groups (Table 4). Accordingly, cluster I, encompassing the majority of shrubs, could be categorized as fine textured, and cluster III could be categorized as coarse textured while cluster II was categorized as medium textured (Figure 2). Our results indicate that the shrubs with coarse texture possess significantly large leaves, longer petioles, and longer internodal distances than fine textured groups. These morphological characters give a somewhat lax / loose appearance to the shrubs. On the other hand, the fine textured group gives a dense visual appearance. The medium textured group possessed an intermediate of the above characters compared to the two other groups. However, this group has significantly high internodal distances and this deviation is due to the exceptionally long mean internodal distances (8.514 ± 0.271) recorded in a single shrub *Sanchezia nobilis* (results not given). However, the character 'pubescence surfaces' used to describe plants with coarse texture and 'smooth surfaces' in defining fine texture (Scarfone, 2007; Robinson, 2016), did not contribute to this separation, where the medium texture group (cluster II) exhibited significantly higher hair densities on upper and lower surfaces, together with longer hairs. The term 'pubescence' defining leaf surface nature is a general term for separating a glabrous or shiny surface from a rough surface that possesses hairs or trichomes. According to our findings, the presence of hairs is not a strong character to define textural groups as the shrubs that were included in all three groups possessed hairs to some extent, while the medium textured group exhibited a significantly high amount of hair related characters, contributing to higher leaf hair densities on lower and upper surfaces, together with longer hairs. Of the sixteen shrub species that are included in the fine texture group, three species, *viz.*, *A. inferno*, *O. octandra,* and *H. patens,* exhibited hair related characters (results are not given). Similarly, the leaf margin, a qualitative character used to define textural groups (Robinson, 2016), has not contributed to defining textural groups during the analyses. With regard to leaves with non-entire margins, such as serrate and dentate leaves, even though they contribute to increasing the surface areas of a leaf (leaf size), this character cannot be considered a decisive feature in defining textural groups.

Based on our results, we propose that leaf area, petiole length, and internodal distance are the non-overlapping morphological characters that contribute to the separation of the textural groups. Hence, these can be considered as primary characters. In contrast, hair related characters together with qualitative morphological characters such as leaf margins, leaf arrangement, and prominent venation contribute as secondary characters in defining textural groups. The latter two characters are additional features identified as contributing to defining textural groups during the present study. Plants with opposite, opposite-decussate, or whorled leaf arrangements contribute to a dense canopy, and hence these would contribute to a fine texture, while alternate and spiral arrangements would contribute towards an open canopy resulting in a coarse texture. Further, leaves with prominent venation also contribute to a coarse texture as this gives a rough nature and increases the surface area. In addition to the characters accepted as contributing to textural groups, the optical characteristics of the leaf surface, such as leaf cuticle and architecture of the leaf epidermal cells, could also play a role as these contribute to light reflectance. Thin cuticles reflect limited light while thick cuticles reflect more light (Mulroy, 1979; Pfündel et al., 2006). The shape of epidermal cells contributes to light reflectance, whereas curvature of the outer epiclinal cell wall reduces reflectance (Karabourniotis et al., 2021). According to Xie (2013), when the light bounces back into the viewer's eyes, it enables the viewer to perceive the image as being somewhere it does not actually exist. Hence, the light reflectance could produce eye-catching, striking effects on the plant where the respective plant texture could be highlighted.

The defined textural groups identified have many practical applications in establishing GI in urban spaces, where correct identification of textural groups of shrubs followed by the implementation at the appropriate location would provide not only aesthetic benefits but also many other benefits. The fine textured shrubs have a tight and controlled overall form (Scarfone, 2007; Robinson, 2016) due to its smaller leaves, shorter internodal distances and shorter petioles. Hence, these shrubs are used to establish formal hedges in urban spaces where a sense of order is preferred. Fine textured shrubs such as *A. siamensis, A. inferno, I. coccinea, P. myrtifolius, E. bicolor, H. patens, B. lupulina,* and *S. campanulatum* are popularly used in tropical anthropogenic landscapes to establish formal hedges. According to Robinson (2016), fine-textured species, when tightly clipped, are expressed with the greatest precision. Hence, shrubs such as *A. siamensis, A. inferno, I. coccinea,* and *P. myrtifolius* are popularly used to create topiary in geometrical/formal planting designs in the tropics. Specifically, shrubs used to establish formal hedges and topiary should possess small leaves (dense canopy) as regular clipping is practiced during maintenance. If large leaved shrubs (coarse-textured) are used during clipping, the remaining leftover parts of the leaves in the formal hedges and topiary will give an overall unsightly appearance. Further, it would be difficult to maintain a desirable shape with shrubs with larger leaves and a loose canopy. In establishing informal hedges, where flower and fruit formation is not restricted by regular clipping, any textural group could be incorporated. According to Brun and Dinius (2015), the management practice adopted in maintaining informal hedges is selective pruning, using thinning to maintain the desired height and width. In the tropics, coarse textured shrubs which possess larger leaves such as *P. balfouriana* and *A. wilkesiana 'Tricolor'* and medium textured shrubs which possess medium size leaves such as *G. pictum* and *P. reticulatum* are popularly used in the establishment of informal hedges.

Another application of shrubs in an urban context is their ability to manipulate the apparent size of a space. Scarfone (2007) and Hansen (2010) described that incorporating fine textured shrubs in planting designs tends to make a small space seem larger. With a high proportion of fine-textured plants, it is possible to increase the sense of spaciousness within an enclosure. This effect will add satisfaction and value to the urban dwellers where space could be a limiting factor. In contrast, the incorporation of coarse textured shrubs has the reverse effect. The details of planting design affect the psychological well-being of individuals and the subsequent effect on their social behaviour (Jacobsen, 1990). In extreme applications, when used inappropriately, coarse textured plants can create negative outdoors. According to Robinson (2016), when shrubs with coarse textured foliage are used in confined urban spaces, the advancing effect of the coarse foliage creates a space that feels smaller, causing a claustrophobic effect (fear of confined spaces) for the users. Fine textured plants are easy to look at, and they do not demand the viewers' attention (Scarfone, 2007). Hence, plant associations with fine textured shrubs could be promoted in areas designated for relaxation in public parks and residential gardens, contributing to stress reduction and resulting ultimately in human well-being. In particular, according to Jacobsen (1990), people with visual impairments appreciate coarse vs smooth textured leaves. The coarse texture is dominant over fine texture, and therefore the eyes of the viewers are attracted and held by the coarse textured plants for a longer period (Hansen,

2019). Hence, coarse textured plants such as *M. erythrochlamys* could be incorporated as specimen plants in planting designs to focus the eye, which would help divert attention from less interesting features.

To break the monotony of plant associations, different textural groups can be combined. This can be practised when designing plant borders. According to Hansen (2019), to bridge the gap between the coarse and fine textured foliage, medium textured shrubs could be incorporated. To increase the sense of depth in planting composition, coarse textured shrubs could be placed in the foreground and fine textured shrubs could be placed in the background of a design (Hansen & Alvarez, 2019). Lannotti (2019) suggests that when combining different textural groups in plant associations, as a thumb of rule, a perfect balance can usually be achieved by blending about 1/3 fine texture with 2/3 coarse texture.

Apart from the aesthetics, different textural groups in planting designs could be used to achieve health and environmental benefits by combating air pollution. The interception ability of dust/particulate matter present in the air is positively correlated with the internodal distance, petiole length, leaf area, leaf orientation, margin, folding, arrangement, prominent venation, presence of hairs in leaves; in particular leaf hair density, hair type and length (Varshney & Mitra, 1993; Yunus *et al.*, 1995; Hegazy, 1996; Chaphekar, 2000; Wijesinghe & Yakandawala 2009; Das & Prasad, 2012). Specifically, characters, which contribute to increasing the surface area, can contribute in a positive manner (Leonard *et al.*, 2016). Shrubs with coarse and medium textured plants possess a majority of these favourable morphological characters, positively contributing to the interception of dust /particulate matter present in the air.

Noise has pervasive auditory (psychological) and non-auditory (hypertension, cardiovascular diseases etc.) effects on human beings (Basner *et al.*, 2014; Lim *et al.*, 2018). Green infrastructure can provide varying levels of noise mitigation, and the introduction of buffers with evergreen trees and shrubs has been recommended (Bentrup, 2008). The effectiveness of a noise barrier in a given area has been related to the structure, size, and density of the vegetation (Fang & Ling, 2005; Van Renterghem *et al.*, 2012). According to Capotorti *et al.* (2016), large leaves are more effective in noise attenuation. Thus, shrubs with a coarse texture can contribute to noise attenuation more than smooth textured shrubs. According to studies conducted by Leuzinger *et al.* (2010) and Nicotra *et al.* (2011), species with large leaf lamina often have a high stomatal density and more open stomatal pores, which allow greater latent heat loss when water is available and consequently contribute to the reduction of urban heat island effect. Hence, as coarse textured shrubs possess larger leaves, they are capable of increasing human thermal comfort.

Compared to temperate countries, in the tropics, the texture of shrubs does not change with the seasons as the majority are evergreen. However, plant physiognomy could change depending on the geography, which could influence the texture. Nevertheless, garden plants are subjected to agronomic practices (irrigation, manuring). Therefore, these plants receive favourable conditions irrespective of geography. Hence we could expect a minimum impact on texture. On the other hand, when plants are introduced from their natural environment to man-made urban structures such as roof gardens and planters, plants are subjected to extreme microclimates such as heat stress, drought and soil conditions (Dvorak & Bousselot, 2021). Consequently, plants develop different morphological, anatomical, and physiological adaptations of the leaves, stems and roots in order to survive in these environments. Particularly high temperatures and droughts can diminish the leaf expansion rate and reduce leaf sizes (Petra *et al.*, 2020). These could indirectly influence the texture. Future studies are recommended on the investigation of the effects of physiognomy and man-made urban structures on the visual quality of shrubs.

Understanding the morphological features of shrubs and categorizing them into textural groups could optimize the species selection process of landscape practitioners. The correct plant selection for the right place could guarantee the delivery of shrubs' multiple functions when incorporating them into GI. Finally, city dwellers, the end-users, could enjoy the aesthetic benefits of shrubs while reaping the other benefits.

CONCLUSION

Most shrubs incorporated into urban GI could fulfil the intended functions. However, we argue that giving due consideration to their morphological characters and categorizing them into textural groups systematically, and practical application in GI in urban areas could maximize the benefits. We conclude that the leaf area, petiolar

length and internodal distance are the primary morphological characters that contribute to the separation of the textural groups, while hair related characters together with qualitative morphological characters such as leaf margins, leaf arrangement and prominent venation are secondary characters that contribute to defining textural groups. It is important to bear in mind that the morphological characters of plants are named and categorized by humans for our convenience. Hence, defining strict categories contributing to textural groups would always have outliers. Although our study was focused on tropical shrubs, this concept could be applied to any part of the world.

Acknowledgements

REFERENCES

Anderson J. (2018). *Plant Texture in the Garden*. Available at *https://www.arboretumfoundation.org/wp-content/uploads/2018/12/anderson_texture-in-garden.pdf*, Accessed 29 January 2021.

Basner M., Babisch W., Davis A., Brink M., Clark C., Janssen S. & Stansfeld S. (2013). Auditory and non-auditory effects of noise on health. *Lancet* **383**(9925): 1325–1332.
DOI: https//:doi: 10.1016/S0140-6736(13)61613-X

Beaulieu D. (2019). *Plant Texture: What It Means and How to Add It to a Garden*. Available at *https://www.thespruce.com/plant-texture-meaning-application-2131117*, Accessed 29 September 2021.

Bentrup G. (2008). *Conservation Buffers - Design Guidelines for Buffers, Corridors, and Greenways* (SRS–109). Forest Service, US Department of Agriculture, Southern Research Station, Asheville, USA.
DOI: https://doi.org/10.2737/SRS-GTR-109

Blake J. (1999). *An Introduction to Landscape Design and Construction*, pp 34 – 35. Grower Publishing Ltd., Hampshire, UK..

Blanusa T., Garratt M., Cathcart-James M., Hunt L. & Cameron R.W.F. (2019). Urban hedges: A review of plant species and cultivars for ecosystem service delivery in north-west Europe. *Urban Forestry and Urban Greening* **44**(2019): 12639.
DOI: https://doi.org/10.1016/j.ufug.2019.126391.

Brun C.A. & Dinius P. (2015). *Selecting plants for screens and hedges* (EM089E). In: *Washington State University Extension*. Washington State University, USA.

Cameroon R.W.F. (2016). Landscape trees, shrubs and woody climbing plants. In: *Environmental Horticulture: Science and Management of Green Landscapes* (eds. R.W.F. Cameroon & D.J. Hitchmough), pp. 121–155. CABI, Boston, USA.
DOI: https://doi.org/10.1079/9781780641386.0121

Cameron R.W.F., Blanuša T., Taylor J.E., Salisbury A., Halstead A.J., Henricot B. & Thompson K. (2012). The domestic garden: its contribution to urban green infrastructure. *Urban Forestry and Urban Greening*, **11**(2):129–137.
DOI: https://doi.org/10.1016/j.ufug.2012.01.002.

Capotorti G., Del Vico E., Anzellotti I. & Celesti-Grapow L. (2016). Combining the conservation of biodiversity with the provision of ecosystem services in urban green infrastructure planning: critical features arising from a case study in the metropolitan area of Rome. *Sustainability* **9**(1): 10.
DOI: https://doi.org/10.3390/su9010010

Chaphekar S.B. (2000). Green belts for industrial areas. In *Environmental Stress: Indication, Mitigation and Eco Conservation*. (eds. M. Yunus, N. Singh & J.L. de Kok), pp. 431–443. Kluwer Academic Publishers, Amsterdam, Netherlands.
DOI: https://doi.org/10.1007/978-94-015-9532-2_38

Das S. & Prasad P. (2012). Particulate matter capturing ability of some plant species: implication for phytoremediation of particulate pollution around rourkela steel plant, Rourkela, India. *Nature Environment and Pollution Technology* **11**(4): 657–665.

De Mel L.M.S. & Yakandawala K. (2016). Breaking Seed Dormancy in a Forest Plant: *Grewia damine* Gaertn. *Journal of Environmental Professionals Sri Lanka*. **5**(1): 41–52.
DOI: http://doi.org/10.4038/jepsl.v5i1.7867

Dirr M.A. (2009). *Manual of Woody Landscape Plants*: *Their Identification, Ornamental Characteristics, Culture, Propagation and Uses*. Stipes Publishing L.L.C. Illinois, USA.

Dobrilovič M. (2006). Morphological characteristics of plants as a criterion for selecting plants in landscape design. *Agronomski Glasnik*: *Glasilo Hrvatskog Agronomskog Društva* **68** (3): 161–180.

Dobson M. & Ryan J. (2000). Trees in focus. *Practical Care and Mangement- Arboricultural Practice Notes no 06*. Arboricultural Advisory And Information Service, Farnham,UK.

Dvorak B. & Bousselot J. (2021). Theoretical Development of Ecoregional Green Roofs. In: *Ecoregional Green Roofs. Cities and Nature* (eds. B. Dvorak), PP 41–79. Springer, Switzerland.
DOI: https://doi.org/10.1007/978-3-030-58395-8

Eknayake D.T. (1982). *Guide to Urban Planting in Sri Lanka.* Urban Development Authority, Colombo, Sri Lanka.

Fang C.F. & Ling D.L. (2005). Guidance for noise reduction provided by tree belts. *Landscape and Urban Planning* **71**(1): 29–34.
DOI: https://doi.10.1016/j.landurbplan.2004.01.005

Farahani L.M., Motamed B. & Jamei E. (2016). Persian gardens: meanings, symbolism, and design. *Landscape Online* **46**:1–19.
DOI: http://doi.org/10.3097/LO.201646

Ferrante A., Trivellini A., Scuderi D., Romano D. & Vernieri P. (2015). Post-production physiology and handling of ornamental potted plants. *Postharvest Biology and Technology* **100**: 99–108.
DOI: https://doi.org /10.1016/j.postharvbio.2014.09.005

Gower J.C. (1971). General coefficient of similarity and some of its properties. *Biometrics* **27**: 857–874.
DOI: https://doi.org/10.2307/2528823

Grimm N.B., Faeth S.H., Golubiewski N.E., Redman C.L., Wu J., Bai X. & Briggs J.M. (2008). Global change and the ecology of cities. *Science* **319**(5864): 756–760.
DOI: https://doi.10.1126/science.1150195

Hackett B. (1979). *Planting Design*. McGraw-Hill Companies, New York, USA.

Hansen G. (2019). *Basic Principles of Landscape Design* (CIR536). Environmental Horticulture Department, University of Florida, USA. Available at *https://edis.ifas.ufl.edu/publication/mg086,* Accessed 2 January 2020.

Hansen G. & Alvarez E. (2019). *Landscape Design: Aesthetic Characteristics of Plants* (ENH1172). Environmental Horticulture Department, University of Florida, USA. Available at *https://edis.ifas.ufl.edu/pdffiles/EP/EP43300.pdf,* Accessed 2 September 2020.

Hansen R. & Pauleit S. (2014). From multifunctionality to multiple ecosystem services? a conceptual framework for multifunctionality in green infrastructure planning for urban areas. *Ambio* **43**: 516–529.
DOI: https://doi.org/10.1007/s13280-014-0510-2

Hegazy K. (1996). Effect of cement dust pollution on the vegetation and seed bank species diversity in the eastern desert of Egypt. *Environmental Conservation* **23**(3): 249–258.
DOI: https://doi.org/10.1017/S0376892900038868.

Iezzoni A.F. & Pritts M.P. (1991). Applications of principal component analysis to horticultural research. *HortScience* **26**(4): 334–338.
DOI: https://doi.org/10.21273/HORTSCI.26.4.334

Jacobsen P. (1990). Shrubs and ground cover. In: *Landscape Design with plants*. (ed. B. Clouston,), pp. 40–74. Heinemamn, Portsmouth, USA.
DDOI: https://doi.org/10.1016/B978-0-434-90234-7.50010-0

Joardar S.D. (1998). Classification of landscape plants for environmental design uses. *Journal of Architectural and Planning Research* **15**(2): 109–132.

Kaiser H.F. (1960). The application of electronic computers to factor analysis. *Educational and Psychological Measurement* **20** (1): 141–151.
DOI: https://doi.org/10.1177/001316446002000116

Kaiser H.F. (1970). A second-generation little jiffy. *Psychometrika* **35:** 401–415
DOI: https://doi.org/10.1007/BF02291817

Karabourniotis G., Liakopoulos G., Bresta P & Nikolopoulos D. (2021). The optical properties of leaf structural elements and their contribution to photosynthetic performance and photoprotection. *Plants-Basel* **10**(7): 1455.
DOI: https://doi.org/10.3390/plants10071455

Kendal D., Williams K. & Armstrong L. (2008). Preference for and performance of some Australian native plants grown as hedges. *Urban Forestry and Urban Greening* **7**(2): 93–106.
DOI: https://doi.org/10.1016/j.ufug.2008.02.002

Lannotti M. (2019). *Garden Design with Plant Texture*. Available at *https://www.thespruce.com/garden-design-with-plant-texture-4056275,* Accessed 29 April 2021.

Laurie M. (1975). *An Introduction to Landscape Architecture,* pp 214. Elsevier Publishers, New York. USA.

Leonard R.J., McArthur C. & Hochuli D.F. (2016). Particulate matter deposition on roadside plants and the importance of leaf trait combinations. *Urban Forestry and Urban Greening* **20**: 249–253.
DOI: https://doi.org/10.1016/j.ufug.2016.09.008

Leuzinger S., Vogt R. & Korner C. (2010). Tree surface temperature in an urban environment. *Agricultural and Forest Meteorology* **150**(01): 56–62.
DOI: https://doi: 10.1016/j.agrformet.2009.08.006

Lim J., Kweon K., Kim H.W., Cho S.W., Park J. & Sim C.S. (2005). Negative impact of noise and noise sensitivity on mental health in childhood. *Noise and Health* **20**(96): 199–211.
DOI: https://doi: 10.4103/nah.NAH_9_18

Macmillan H.F. (2012). *Tropical Gardening and Planting,* pp. 634. Vijitha Yapa Publications, Colombo, Sri Lanka

Mendez S. (2019). *Plant Texture in Garden Design. Garden Artistics*. Available at *https://gardenartistics.com/plant-texture-in-garden-design/,* Accessed 29 January 2022.

Metre V. & Ghorpade J. (2013). An overview of the research on texture based plant leaf classification. *International Journal of Computer Science and Network* (IJCSN) **2**(3). Available at https://arxiv.org/ftp/arxiv/papers/1306/1306.4345.pdf

Mulroy T.W. (1979). Spectral properties of heavily glaucous and nonglaucous leaves of a succulent rosette-plant. *Oecologia* **38**:349–357.
    DOI: https://doi.org/10.1007/BF00345193.

Natuhara Y. (2018). Green infrastructure: innovative use of indigenous ecosystems and knowledge. *Landscape and Ecological Engineering* **14**: 187–192.
    DOI: https://doi.org/10.1007/s11355-018-0357-y

Naumann S., McKenna D., Kaphengst T., Pieterse M. & Rayment M. (2011). *Design, Implementation and Cost Elements of Green Infrastructure Projects; Final Report.* Ecologic Institute and GHK Consulting, Overland Park, KS, USA. Available at *https://www.ecologic.eu/11382,* Accessed 4 January 2022.

Nia H.A. & Olugbenga F. (2020). A quest on the role of aesthetics in enhancing functionality of urban planning. *Civil Engineering and Architecture* **8**(5): 873– 879.
    DOI: https://doi.org/10.13189/cea.2020.080514.

Nicotra A.B., Leigh A., Boyce C.K., Jones C.S., Niklas K.J., Royer D.L. & Tsukaya H. (2011). The evolution and functional significance of leaf shape in the angiosperms. *Functional Plant Biology* **38**: 535–552.
    DOI: https://doi.org/10.1071/fp11057.

Pallawala P.A.P.M., Wijesinghe S.A.E.C. & Yakandawala K. (2013). Potential tree species as a source of air filters to capture particulate matter of the atmosphere. *Journal of Food and Agriculture* **6**(1-2): 45–53.
    DOI: http://doi.org/10.4038/jfa.v6i1-2.5187

Petra S.A., Georgescu M.I., Manescu C.R., Toma F., Badea M.L., Dobrescu E. & Popa V.I. (2020). Leaves anatomical and physiological adaptations of Vinca major 'Variegata' and Hedera helix L. to specific roof garden conditions. *Notulae Botanicae Horti Agrobotanici Cluj-Napoca* **48**(1):318–328.
    DOI: http://doi.10.15835/nbha48111784

Pfündel E.E., Agati G. & Cerovic Z.G. (2006). *Optical properties of plant surfaces*. In: *Biology of the Plant Cuticle* (eds. M. Riederer & C. Müller) pp. 216–249. Blackwell, Oxford, UK.
    DOI: https://doi.org/10.1002/9780470988718.ch6

Ranasinghe L.M.M., Yakandawala K. & Abeynayake N.R. (2019). Awareness and demand for native ornamental plants in the nursery industry of Sri Lanka: A case study from Diyatha flower market. *Proceedings of the 24th International Forestry and Environment Symposium,* 11-12 October. Department of Forestry and Environmental Science, University of Sri Jayewardenepura. pp. 5.

Ren G. (2015). Urbanization as a major driver of urban climate change. *Collection of Advances in Climate Change Research*, volume 6. Available at https://www.scipedia.com/public/Ren_2015a, Accessed 30 April 2020.

Robinson F.B. (1940). *Planting Design. Champaign,* 2nd Edition. McGraw-Hill Book Inc. New York, USA.

Robinson N. (2016). *The Planting Design Handbook,* 3rd edition, pp 103–104. Ashgate Publishing Limited, Gower House, UK.
    DOI: https://doi.org/10.4324/9781315554648

Rohlf F.J. (2009). *NTSYSpc Numerical Taxonomy and Multivariate Analysis System Version 2.2. Exeter Software.* Setauket, New York, USA.

Sattler R. & Rutishauser R. (1997). The fundamental relevance of morphology and morphogenesis to plant research. *Annals of Botany* **80**(5): 571–582.
    DOI: https://doi.org/10.1006/anbo.1997.0474

Scarfone S.C. (2007). *Professional Planting Design*: *An Architectural and Horticultural Approach for Creating Mixed Bed Plantings*, pp. 82–85. John Wiley & Sons, New York, USA.

Schneider A., Friedl M.A. & Potere D. (2009). A new map of global urban extent from MODIS satellite data. *Environmental Research Letters* **4**(4): 1–11.
    DOI: https://doi:10.1088/1748-9326/4/4/044003.

Schreiner M., Korn M., Stenger M., Holzgreve L. & Altmann M. (2013). Current understanding and use of quality characteristics of horticulture products. *Scientia Horticulturae* **163:** 63–69.
    DOI: https://doi.org/10.1016/j.scienta.2013.09.027

Sebola R.J. & Balkwill K. (2009). Numerical phenetic analysis of *Olinia rochetiana* sensu lato (Oliniaceae). *Kew Bulletin* **64** (1): 95–121.
    DOI: https://doi.: 10.1007/s12225-008-9095-x.

Seto K.C., Güneralp B. & Hutyra L.R. (2012). Global forecasts of urban expansion to 2030 and direct impacts on biodiversity and carbon pools. *Proceedings of the National Academy of Sciences* **109**(40): 16083–16088.
    DOI: https://doi.org/10.1073/pnas.1211658109

Sneath P.H. & Sokal R.R. (1973). *Numerical Taxonomy: The Principles and Practice of Numerical Classification*. W.H. Freeman & Co, San Francisco, USA.

Steed H. (1990). Planting in tropical lowland areas. In: *Landscape Design With Plants,* (ed. B.Clouston), 2nd Edition, pp.235–275. Heinemann, Portsmouth, USA.
    DOI: https://doi.org/10.1016/B978-0-434-90234-7.50020-3

Ministry of Environment (2020). T*he National Red List 2020 - Conservation Status of the Flora of Sri Lanka.* Biodiversity Secretariat, Ministry of Environment, Battaramulla, Sri Lanka.

The Royal Horticultural Society (2013). *RHS Handbook: Pruning and Training.* Octopus Publishing Group, London, UK.

Tobey G.B. (1973). *A History of Landscape Architecture: The Relationship of People to Environment.* Elsevier Publishing Company, USA.

United Nations (2019). *World Urbanization Prospects*: *The 2018 Revision*. Department of Economic and Social Affairs, United Nations. New York, USA. Available at https://population.un.org/wup/Publications/Files/WUP2018-Report.pdf. Accessed on 6 May 2020.

Van Renterghem T., Botteldooren D. & Verheyen K. (2012). Road traffic noise shielding by vegetation belts of limited depth. *Journal of Sound and Vibration* **331**(10): 2404–2425.
DOI: https://doi.org/10.1016/j.jsv.2012.01.006

Varshney C.K. & Mitra I. (1993). Importance of hedges in improving urban air quality. *Urban Forestry and Urban Greening* **25**(1–2): 85–93.
DOI: https://doi.org/10.1016/0169-2046 (93)90124-V

Wijesinghe S.A.E.C. & Yakandawala K. (2009). Particulate matter interception ability of some selected shrubs used in urban landscaping. *Proceedings of the 9ᵗʰ Agricultural Research Symposium*. Wayamba University of Sri Lanka, Kuliyapitiya, Sri Lanka. pp 363–367.

Wijesinghe S.A.E.C. & Yakandawala K. (2013). Urban Trees: A Contributor for Reduction of Particulate Pollution in Cities. *Proceedings of the 2ⁿᵈ Sri Lankan Roundtable on Sustainable Consumption and Production*. National Cleaner Production Centre, Sri Lanka. pp 284–293.

Xie F. (2013). Spatial phenomenon of reflection effect in landscape design. *Master of Landscape Architecture thesis*, Graduate School of The Ohio State University, Columbus, USA.

Yakandawala K., Weerasinghe M.D.C.P. & Wijesinghe S.A.E.C. (2013). *Osbeckia octandra*: A potential shrub for urban environment. *Acta Horticulturae* **999**: 301–306.
DOI: https://doi.org/10.17660/ActaHortic.2013.999.43

Yunus M., Dwivedi A.K., Kulshreshtha K. & Ahmad K.J. (1985). Dust loadings on some common plants near Lucknow city. *Environmental Pollution Series B, Chemical and Physical* **9**(1): 71–80.
DOI: https://doi:10.1016/0143-148X(85)90040-0.

Zimisuhara B., Valdiani A., Shaharuddin N.A., Qamaruzzaman F. & Maziah M. (2015). Structure and principal components analysis reveal an intervarietal fusion in Malaysian Mistletoe Fig (*Ficus deltoidea* Jack) populations. *International Journal of Molecular Science* **16**: 14369–14394.
DOI: https://doi: 10.3390/ijms160714369.

RESEARCH ARTICLE

Statistical Quality Control

Error detection through modified phase II process monitoring under different classical estimators

R Jabeen[1*] and A Zaka[2]

[1] *Department of Statistics, COMSATS University Islamabad, Lahore Campus, Lahore, Pakistan.*
[2] *Department of Statistics, Government Graduate College of Science, Wahdat Road, Lahore, Pakistan.*

Abstract: In real life, the distribution of the errors during any life testing of products or process does not meet the assumption of normality. Statistical process control (SPC) is defined as the use of statistical techniques to control a process or production method. SPC tools and procedures can help to monitor process behaviour, discover problems in internal systems, and find solutions for production issues. To identify and remove the variation in different reliability processes and to monitor the reliability of machines where the number of errors follows skewed distributions, we develop control charts to keep the process in control. For such situations, we have modified the existing control charts such as Shewhart control chart, exponentially weighted moving average (EWMA), hybrid exponentially weighted moving average (HEWMA) and extended exponentially weighted moving average (EEWMA) control charts. The current study introduced classical estimator based modified control charts for phase-II monitoring by assuming that the errors occur during the process follow skewed distribution called Beta Lehmann 2 Power function distribution (BL2PFD). The proposal for these control charts is based on the percentile estimator. We have compared all these control charts using Monte Carlo simulation studies and real-life applications to compare the proposed control charts. This study shows that an EEWMA control chart based on PE performs better than Shewhart, EWMA and HEWMA control charts, when the underlying distribution of the errors in process monitoring follows BL2PFD. These findings can be useful for researchers and practitioners in dealing with production errors and optimizing the output.

Keywords: Beta Lehmann 2 Power function distribution, exponentially weighted moving average, extended exponentially weighted moving averages, extended hybrid exponentially weighted moving averages, hybrid exponentially weighted moving average, percentile estimator.

INTRODUCTION

The Beta Lehmann 2 Power function distribution was generated by Zaka *et al.* (2020) is used in many real-life applications such as reliability and medical studies. It is a skewed distribution with the following probability density function.

$$f(x) = \frac{\left(1-\left(1-\left(\frac{x}{\beta}\right)^{\gamma}\right)^{\alpha}\right)^{a-1}\left(\left(1-\left(\frac{x}{\beta}\right)^{\gamma}\right)^{\alpha}\right)^{b-1}\alpha\left(1-\left(\frac{x}{\beta}\right)^{\gamma}\right)^{\alpha-1}\frac{\gamma x^{\gamma-1}}{\beta^{\gamma}}}{B(a,b)} \ , \ \ 0 < x < \beta \ .$$

where γ, α, a and b are the shape, scale and tuning parameters.

The shape of the pdf of BL2PFD is approximately Normal for different values of the parameters.

---

[*] Corresponding author (drriffatjabeen@cuilahore.edu.pk; https://orcid.org/0000-0003-1461-0611)
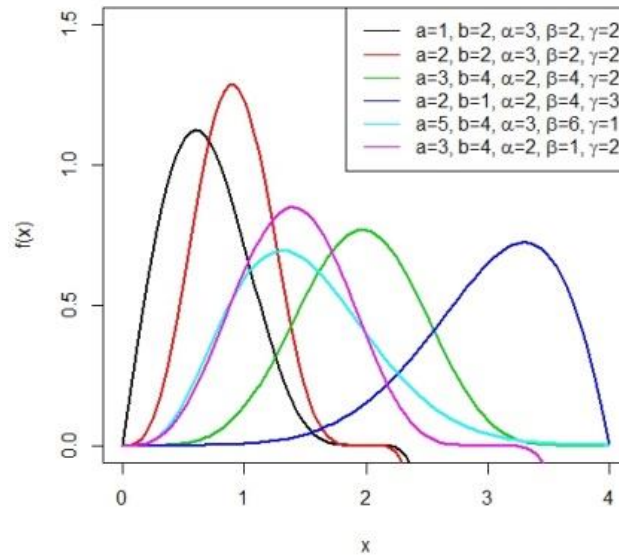
Figure 1: Shape of pdf for BL2PFD

The above plots show that the Beta Lehmann 2 power function distribution is sometimes negatively skewed. To control the variation in process for which the underlying distribution of process follows Beta Lehmann 2 power function distribution is discussed in this paper. We have proposed some modifications to the existing Shewhart, EWMA, HEWMA and EEWMA and compared the performance.

Prior studies related to the control charts are mostly followed the normality assumption. The readers can study Shamma and Shamma (1992), Haq (2013) and Naveed *et al.* (2018). But what can organizations do if the normality assumption fails in the practical life. There are very few studies available in the literature that highlighted this issue, including Qiu and Li (2011), Noorossana *et al.*, (2016), Zhang *et al.* (2017), Lin *et al.*, (2017), Erto *et al.* (2018), Li *et al.* (2018), Liang *et al.*, (2019). Further, Zaka *et al.* (2021a; 2021b), Jabeen *et al.* (2022, 2023) proposed some modified control charts for monitoring the shape parameter of Power function distribution (PFD), Reflected Power function distribution (RPFD) and Weighted Power function distribution (WPFD). As the many production processes are not necessarily follow the normality assumption, therefore, the aim of the study is to introduce the modified control charts, i.e. Shewhart, EWMA, HEWMA and EEWMA and assume that the distribution of underlying process follows a BL2PFD. Further, the proposed control charts are based on the different estimators of the shape parameter of BL2PFD.

This paper is about the use of the shape parameter to control the shape of the process when the distribution of process is BL2PFD. We use Percentile estimator (PE) discussed by Zaka *et al.* (2020) to propose the monitoring statistics under BL2PFD. We propose Monte Carlo simulation to estimate the shape parameter of the BL2PFD and the plotting statistics. It is observed that the proposed EEWMA control chart of the PE detects smaller shifts quicker than the HEWMA control charts.

MATERIALS AND METHODS

The BL2PFD introduced by Zaka *et al.* (2020) is used extensively to study the behavior of different phenomena in real life situations such as to test the life time of the subject of interest in medical and engineering sciences. The probability density function and cumulative density function are given as

$$f(x) = \frac{\left(1-\left(1-\left(\frac{x}{\beta}\right)^\gamma\right)^\alpha\right)^{a-1}\left(\left(1-\left(\frac{x}{\beta}\right)^\gamma\right)^\alpha\right)^{b-1}\alpha\left(1-\left(\frac{x}{\beta}\right)^\gamma\right)^{\alpha-1}\frac{\gamma x^{\gamma-1}}{\beta^\gamma}}{B(a,b)} \ , \ \ 0 < x < \beta \ . \qquad \ldots(1)$$

and

$$F(x) = \frac{B_{\left\{1-\left\{1-\left(\frac{x}{\beta}\right)^\gamma\right\}^\alpha\right\}}(a,b)}{B(a,b)} \qquad \ldots(2),$$

respectively.

Zaka *et al*. (2020) further illustrated the estimates of the shape and scale parameter. In the current study, we will use the shape parameter to provide its application in quality and reliability engineering. The estimate for shape parameter using method of common percentiles is given as

$$\hat{\gamma}_{PE} = \frac{\ln\left(\frac{1-(1-H)^{1/\alpha}}{1-(1-L)^{1/\alpha}}\right)}{\ln\left(\frac{P_H}{P_L}\right)} \qquad \ldots(3),$$

where H= maximum percentile, L= minimum percentile and P = Percentile point.

Monitoring for the process following Beta Lehmann-2 Power function distribution.

We will discuss the monitoring for the shape parameter of the Beta Lehmann-2 Power function distribution using the following methods.

Modification of Shewhart control chart for shape parameter of Beta Lehmann-2 Power function distribution

In the following section, we have constructed a modified Shewhart control chart using PE for the shape parameter of a process following Zaka *et al.* (2021a; 2021b). The control limits are given as

$$LCL_{\hat{\gamma}_{PE}} = E(\hat{\gamma}_{PE}) - K * \sqrt{var(\hat{\gamma}_{PE})} \qquad \ldots(4)$$

$$CL_{\hat{\gamma}_{PE}} = E(\hat{\gamma}_{PE}) \qquad \ldots(5)$$

$$UCL_{\hat{\gamma}_{PE}} = E(\hat{\gamma}_{PE}) - K * \sqrt{var(\hat{\gamma}_{PE})}. \qquad \ldots(6)$$

Modified EWMA control chart to monitor the shape parameter of BL2PFD

Following Zaka *et al*. (2021a; 2021b), the control limits of the modified EWMA are given as,

$$LCL_{EWPE_t} = E(\hat{\gamma}_{PE}) - K * \sqrt{var(\hat{\gamma}_{PE}) * \frac{\lambda}{(2-\lambda)}} \qquad \ldots(7)$$

$$CL_{EWPE_t} = E(\hat{\gamma}_{PE}) \qquad \ldots(8)$$

$$UCL_{EWPE_t} = E(\hat{\gamma}_{PE}) + K * \sqrt{var(\hat{\gamma}_{PE}) * \frac{\lambda}{(2-\lambda)}} \qquad \ldots(9)$$

Modified HEWMA control chart to monitor the shape parameter of BL2PFD.

Following Zaka *et al*. (2021), Jabeen *et al*. (2021) and using Zaka *et al*. (2020), we get the following control limits of modified HEWMA.

$$LCL_{HEWPE_t} = E(\hat{\gamma}_{PE}) - K * \frac{\lambda_1\lambda_2}{(\lambda_1-\lambda_2)}\sqrt{\left(\sum_{i=1}^2 \frac{(1-\lambda_i)^2(1-(1-\lambda_i)^{2t})}{1-(1-\lambda_i)^2} - \frac{2(1-\lambda_1)(1-\lambda_2)\{1-(1-\lambda_1)^t(1-\lambda_2)^t\}}{1-(1-\lambda_1)(1-\lambda_2)}\right)var(\hat{\gamma}_{PE})}$$
$$\ldots(10)$$

$$CL_{HEWPE_t} = E(\hat{\gamma}_{PE}) \qquad \qquad \ldots(11)$$

$$UCL_{HEWPE_t} = E(\hat{\gamma}_{PE}) + K * \frac{\lambda_1\lambda_2}{(\lambda_1-\lambda_2)} \sqrt{\left(\sum_{i=1}^{2} \frac{(1-\lambda_i)^2(1-(1-\lambda_i)^{2t})}{1-(1-\lambda_i)^2} - \frac{2(1-\lambda_1)(1-\lambda_2)\{1-(1-\lambda_1)^t(1-\lambda_2)^t\}}{1-(1-\lambda_1)(1-\lambda_2)}\right) var(\hat{\gamma}_{PE})} \quad \ldots(12)$$

Modified extended EWMA control charts for monitoring the shape parameter of BL2PFD

The EEWMA statistic using PE of the shape parameter of the RPFD was given by Zaka *et al*. (2021a; 2021b), we follow Zaka *et al*. (2021a; 2021b) and using Zaka *et al*. (2020), the control limits are given as

$$UCL_{EEWPE_t} = E(\hat{\gamma}_{PE}) + K\sqrt{V_{PE}\left\{(\lambda_1^2 + \lambda_2^2)\left(\frac{1-(1-\lambda_1+\lambda_2)^{2t}}{1-(1-\lambda_1+\lambda_2)^2}\right) - 2a\lambda_1\lambda_2\left(\frac{1-(1-\lambda_1+\lambda_2)^{2t-2}}{1-(1-\lambda_1+\lambda_2)^2}\right)\right\}} \qquad \ldots(13)$$

$$CL_{EEWPE_t} = E(\hat{\gamma}_{PE}) \qquad \qquad \ldots(14)$$

$$LCL_{EEWPE_t} = E(\hat{\gamma}_{PE}) - K\sqrt{V_{PE}\left\{(\lambda_1^2 + \lambda_2^2)\left(\frac{1-(1-\lambda_1+\lambda_2)^{2t}}{1-(1-\lambda_1+\lambda_2)^2}\right) - 2a\lambda_1\lambda_2\left(\frac{1-(1-\lambda_1+\lambda_2)^{2t-2}}{1-(1-\lambda_1+\lambda_2)^2}\right)\right\}} \qquad \ldots(15)$$

RESULTS AND DISCUSSION

The following steps for simulation study assuming BL2 PFD as process distribution is executed.

Step 1: We generate a random sample of size n=100 from BL2PFD taking the $(\beta, \gamma) = (1.5, 2.5)$ and calculate the PE for the shape parameter from BL2PFD.

Step 2: We take 5000 repetitions of step 1 and compute $E(\hat{\gamma}_{PE})$ and $V(\hat{\gamma}_{PE})$. Compute the control limits to construct the proposed EWMA, HEWMA and EEWMA control limits using the statistics mention in equations (4) to (15).

Step 3: Compute ARL value for in control process and fix it at 500 by searching the suitable value of K.

Step 4: Now we take the shift of 0.05 in process parameter (γ). We calculate ARL and plot them against the shifted process. We observe the process and if it is in-control then we go to step 1. Otherwise, we record the Run Length and repeat the same process for 5000 times.

Table 1: Shewhart control chart based on PE for BL2PFD

Estimation method					Shift				
		0	0.01	0.03	0.120	0.180	0.60	1.00	1.5
	ARL	500.112	419.257	315.537	120.781	67.769	4.435	1.531	1.244
	SDRL	494.452	400.9711	323.4627	123.102	62.744	3.888	0.9294	0.210
	P10	51.0	44.9	33.9	14.9	7.90	1	1	1
PE	P25	145	111.0	94.0	39.0	20	2	1	1
	P50	348	262.5	216.0	81.5	52	3	1	1
	P75	699	535.5	422.5	161.0	97.25	6	2	1
	P90	1179.5	919.4	752.0	277.1	151.2	10	3	1

Table 2: EWMA control chart based on PE for BL2PFD

Estimation method					Shift				
		0	0.01	0.03	0.120	0.180	0.60	1.00	1.5
	ARL	500.748	290.138	183.057	60.016	30.803	2.036	1.03	1
	SDRL	478.0	336.079	170.97	21.079	9.248	1.223	0.662	0.3776
PE	P10	64.0	48.00	32.00	12	2	1	1	1
L=4.20	P25	162.0	110.00	62.75	37	11	2	1	1
$\lambda = 0.10$	P50	368.0	264.00	165.00	46	28	2.3	1	1
	P75	677.0	493.25	247.00	64	32	4	1	1
	P90	1107.1	786.30	410.6	90	39	5	2	1

	ARL	500.137	330.241	203.07	80.6	50.03	2.12	1.07	1
	SDRL	492.2264	422.12	328.01	85.615	58.602	2.015	0.674	0.269
	P10	54.90	51.00	34.90	10.0	8.0	1	1	1
PE	P25	141.00	118.75	92.75	25	19	2	1	1
L=4.20	P50	341.00	302.5	225.00	61	46	3	1.03	1
$\lambda = 0.20$	P75	726.75	623	427.25	118	86	4	2	1
	P90	1211.20	1019.5	736.10	195.1	135.1	6	2	1
	ARL	500.663	370.1	198.07	92.01	60.03	2.32	1.13	1
	SDRL	484.7689	432.3127	319.7975	104.374	51.22	2.71	0.753	0.248
PE	P10	55.90	51.9	38.0	11.9	6.00	1	1	1
L=4.15	P25	141.75	127.0	95.0	30	17	2	1	1
$\lambda = 0.30$	P50	341.50	312.5	231.0	75	42	3	1	1
	P75	707.50	627.0	459.0	147	76.25	5	2	1
	P90	1184.10	1023.4	752.2	235	115.2	7	2	1
	ARL	500.112	392.257	250.537	105.781	63.769	3	1.2	1
	SDRL	494.452	400.9711	323.4627	123.102	62.744	3.888	0.9294	0.210
PE	P10	51.0	44.9	33.9	14.9	7.90	1	1	1
L=4.175	P25	145	111.0	94.0	39.0	20	2	1	1
$\lambda = 0.75$	P50	348	262.5	216.0	81.5	52	3	1.1	1
	P75	699	535.5	422.5	161.0	97.25	6	2	1
	P90	1179.5	919.4	752.0	277.1	151.2	10	3	1

Table 3: HEWMA control chart based on PE for BL2PFD

Estimation Methods					Shift				
		0	0.01	0.03	0.120	0.180	0.60	1.00	1.5
PE	ARL	500.748	205.13	123.07	20.01	5.803	1.03	1	1
L=4.065	SDRL	478.0	336.079	170.97	21.079	9.248	1.223	0.662	0.3776
$\lambda_1 = 0.20$,	P10	64.0	48.00	32.00	12	2	1	1	1
$\lambda_2 = 0.10$	P25	162.0	110.00	62.75	17	3	1	1	1
	P50	368.0	254.00	125.00	26	6	1.01	1	1
	P75	677.0	493.25	247.00	41	22	3	1	1
	P90	1107.1	786.30	410.6	59	31	5	1.02	1
	ARL	500.137	220.138	144.05	40.016	20.03	1.152	1	1
	SDRL	492.2264	422.12	328.01	85.615	58.602	2.015	0.674	0.269
PE	P10	54.90	51.00	34.90	10.0	8.0	1	1	1
L=3.82	P25	141.00	118.75	92.75	25	19	1.08	1	1
$\lambda_1 = 0.20$,	P50	341.00	230.5	162.01	51	32	1.1	1	1
$\lambda_2 = 0.60$	P75	726.75	623	427.25	118	86	3	1	1
	P90	1211.20	1019.5	736.10	195.1	135.1	5	1.07	1
	ARL	500.663	260.13	168.07	51.01	27.20	1.372	1	1
	SDRL	484.7689	432.3127	319.7975	104.374	51.22	2.71	0.753	0.248
PE	P10	55.90	51.9	38.0	11.9	6.00	1	1	1
L=3.885	P25	141.75	127.0	95.0	30	17	2	1	1
$\lambda_1 = 0.20$,	P50	341.50	252.5	161.0	48	21.2	1.2	1	1
$\lambda_2 = 0.75$	P75	707.50	627.0	459.0	147	76.25	4	1	1
	P90	1184.10	1023.4	752.2	235	115.2	7	1.02	1
	ARL	500.748	215.12	133.03	25.01	6.203	1.046	1	1
	SDRL	922.781	638.93	298.782	28.718	12.675	1.3705	0.6443	0.478
	P10	55.90	50.1	38.0	11.9	2	1	1	1
PE	P25	140.5	128.01	95.0	28	4.1	1.01	1	1
L=4.065	P50	345.01	212.5	130.0	38	5.8	1.03	1	1
$\lambda_1 = 0.30$,	P75	654.5	415	226.25	36	17	3	1	1
$\lambda_2 = 0.10$	P90	1785.8	1039.5	574.5	61.1	27	6	1.001	1

		500.137	226.2	154.057	47.016	24.203	1.252	1	1
	ARL	500.137	226.2	154.057	47.016	24.203	1.252	1	1
	SDRL	491.464	373.008	234.365	37.25	15.797	1.2435	0.593	0.253
PE	P10	58.00	45.90	27.00	8.0	5	1	1	1
L=3.82	P25	152.5	113.75	71	15	8	1	1	1
$\lambda_1 = 0.30,$	P50	365.5	221.50	141	41	19	1.1	1	1
$\lambda_2 = 0.60$	P75	694.75	528.50	337.25	56	26	3	1	1
	P90	1137.10	869.10	543.30	92.1	39	4	1.1	1
	ARL	500.663	270.1	178	61.01	32.03	1.472	1.02	1
	SDRL	476.8266	365.166	239.856	39.8348	16.93	1.289	0.5901	0.243
PE	P10	56.90	50.0	27.00	9.0	5.0	1	1	1
L=3.885	P25	150.0	115	72	16	9	1	1	1
$\lambda_1 = 0.30,$	P50	368.0	260.5	162	51.5	30.1	1.5	1	1
$\lambda_2 = 0.75$	P75	695.75	544.0	334.25	58	27	3	1.08	1
	P90	1130.0	887.5	572.30	97.1	42.1	4	1.1	1

Table 4: ARL$_S$ for PE Based EEWMA control charts.

		Shift							
		0	0.01	0.03	0.120	0.180	0.60	1.0	1.5
	ARL	500.836	114.863	73.211	11.464	1.067	1.003	1.001	1
PE	SDRL	492.8587	9.447194	1.4527	0.5558	0.2501	0.0547	0.0316	0
$\lambda_1 = 0.20,$	P10	56.80	25	20	4	1	1	1	1
$\lambda_2 = 0.10$	P25	153.75	88	31	7	1	1	1	1
L= 7.25	P50	358.50	113	65	10.3	1.03	1	1.0001	1
	P75	707.00	189	99	42	1.1	1.08	1.0012	1
	P90	1124.10	270	200	82	1.8	1.3	1.01	1
	ARL	500.748	132.614	83.661	15.453	1.259	1.1	1	1
PE	SDRL	496.0317	34.778	2.1005	0.5693	0.2357	0.04469	0.0316	0
$\lambda_1 = 0.20,$	P10	53.90	6.0	11	1	1	1	1	1
$\lambda_2 = 0.60$	P25	146.75	11.0	21	5	1.1	1.08	1	1
L=7.59	P50	337.50	125.0	76	14	1.19	1.17	1	1
	P75	708.75	152.0	95	29	1.8	1.7	1	1
	P90	1156.20	198.1	181	62	2.1	1.5	1.05	1
	ARL	500.222	166.909	101.239	17.526	1.377	1.2	1.02	1
PE	SDRL	495.0974	45.73822	2.846	0.6047	0.26672	0.07056	1.001	0
$\lambda_1 = 0.20,$	P10	60.0	16	11	4	1	1	1	1
$\lambda_2 = 0.75,$	P25	147.0	114	102	9	1.1	1.1	1	1
L=7.66	P50	337.5	164	114	16	1.3	1.17	1.01	1
	P75	711.0	196	175	22	2.1	2	1.7	1
	P90	1217.7	207	188	42	2.12	2.01	1.8	1
	ARL	500.836	138.863	94.211	14.464	1.167	1.1	1.002	1
PE	SDRL	515.024	17.76437	1.6695	0.5572	0.2241	0.0446	0.0316	0
$\lambda_1 = 0.30,$	P10	46.00	35	21	1	1	1	1	1
$\lambda_2 = 0.10$	P25	142.00	109	89	6	1.09	1.08	1.001	1
L=7.00	P50	332.00	136	93	13	1.13	1.1	1.002	1
	P75	712.25	192	164	29	2.1	2	1.1	1
	P90	1160.10	246	206	62	5	4	1.2	1
	ARL	500.748	142.614	98.661	17.453	1.3	1.2	1.01	1
PE	SDRL	486.214	66.673	4.607	0.7368	0.3281	0.0772	0.03162	0
$\lambda_1 = 0.30,$	P10	64.9	29.0	25	3	1	1	1	1
$\lambda_2 = 0.60$	P25	154.0	82.0	71	9	1.1	1.06	1.002	1
L=7.35	P50	343.5	133.0	120	16	1.2	1.1	1.01	1
	P75	688.0	201.0	188	40	3	2	1.9	1
	P90	1174.4	260.1	240	99	7	5	4	1
	ARL	500.222	178.909	106.239	20.26	1.577	1.3	1.1	1.03
PE	SDRL	490.6586	86.438	7.653	0.9214	0.3561	0.08341	0.0316	0
$\lambda_1 = 0.30,$	P10	63.9	111.00	22	3	1.1	1	1	1
$\lambda_2 = 0.75$	P25	155.0	169.00	78	9	1.2	1.2	1.08	1.02
L=7.44	P50	346.0	266.00	102	18	1.4	1.28	1.1	1.03
	P75	693.0	292.25	211	32	2	2	2	2
	P90	1178.7	306.00	298.10	63	4	3.9	3.5	3.2

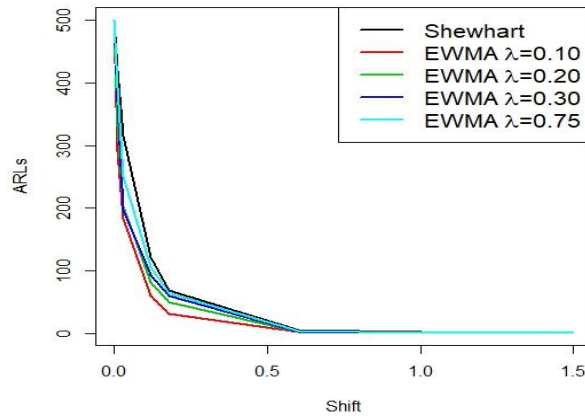**Figure 2:** ARLs for the shape parameter of BL2PFD under
Shewhart and EWMA control charts

Figure 3: ARLs for the shape parameter of BL2PFD under EWMA
(λ=0.10), HEWMA and EEWMA control charts at
λ_1=0.20, λ_2=0.10
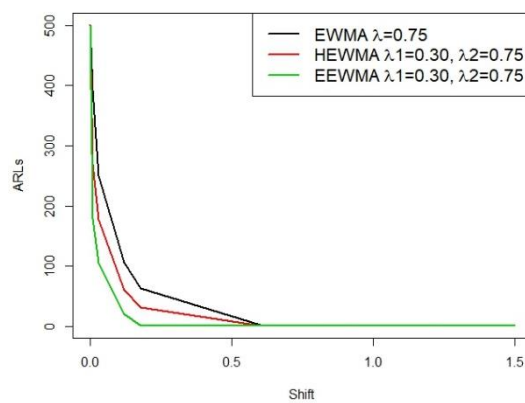
Figure 4: ARLs for the shape parameter of BL2PFD under EWMA
(λ=0.75), HEWMA and EEWMA control charts at
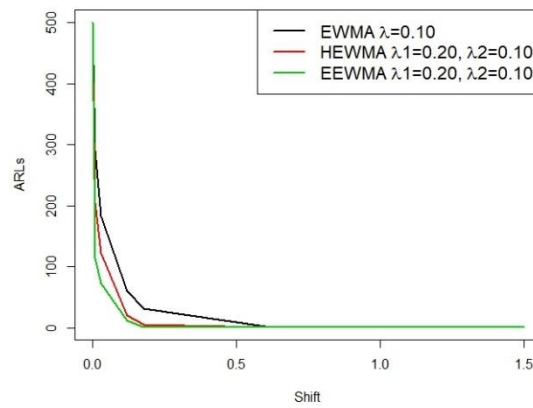λ_1=0.20, λ_2=0.75
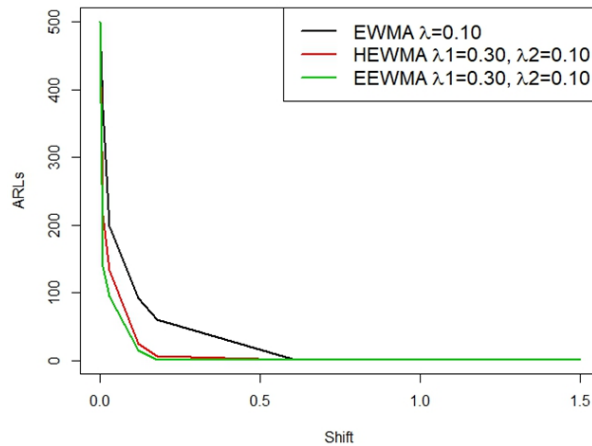
Figure 5: ARLs for the shape parameter of BL2PFD under EWMA (λ=0.10), HEWMA and EEWMA control charts at λ_1=0.30, λ_2=0.10
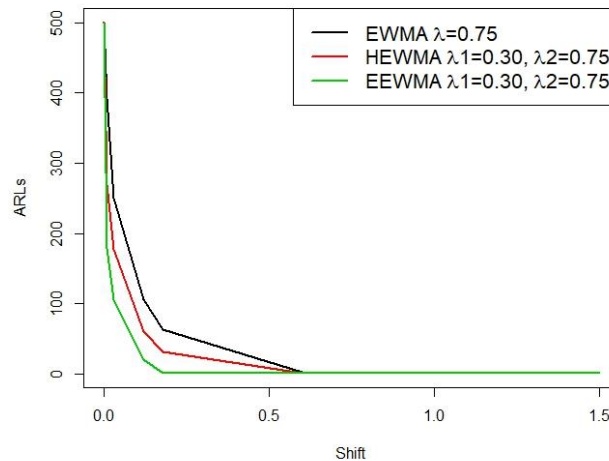
Figure 6: ARLs for the shape parameter of BL2PFD under EWMA (λ=0.75), HEWMA and EEWMA control charts at λ_1=0.30, λ_2=0.75

We observe from Tables 1-4 and Figures 2-6, that EEWMA control chart under PE ($\lambda_1 = 0.20, \lambda_2 = 0.10$) performs better as compared to Shewhart, EWMA and HEWMA control charts under PE. We take a shift of 0.01 in the shape parameter of BL2PFD and see that Shewhart control chart under PE provide ARL_1=419.257, EWMA control chart under PE ($\lambda = 0.60$) gives ARL_1=290.138, HEWMA control chart under PE ($\lambda_1 = 0.20, \lambda_2 = 0.10$) gives ARL_1=205.13 and EEWMA control chart under PE gives ARL_1=114.863. So, we see that a control chart under EEWMA is better than Shewhart, EWMA and HEWMA control charts under PE. We take different shifts and observe the same behavior. We observe that the ARL_1 approaches to 1 more efficiently when we use EEWMA control chart under PE as compared to the other control charts under PE.

We also observe from that EEWMA control chart (for all λ_1 and λ_2) performs better as compared to Shewhart, EWMA and HEWMA control charts under PE by giving less ARL_1 value which means an early detection of any shift in the process.

Table 5: Simulated data

| HEWMA | | | EEWMA | | |
| $\lambda_1 = 0.20$, $\lambda_2 = 0.10$, L= 4.065 | | | $\lambda_1 = 0.20$, $\lambda_2 = 0.10$, L= 7.25 | | |
$HEWPE_t$	LCL	UCL	$EEWPE_t$	LCL	UCL
2.003035	2.001297	2.038704	1.999922	2.001297	2.038704
2.015575	1.984710	2.055290	2.009740	1.984710	2.055290
2.035488	1.969518	2.070482	2.013428	1.969518	2.070482
2.037292	1.956267	2.083733	2.009999	1.956267	2.083733
2.032129	1.945017	2.094983	2.007248	1.945017	2.094983
2.030353	1.935621	2.104379	2.013095	1.935621	2.104379
2.034773	1.927854	2.112146	2.020617	1.927854	2.112146
2.033791	1.921479	2.118521	2.022756	1.921479	2.118521
2.032368	1.916270	2.123730	2.026333	1.916270	2.123730
2.034350	1.912028	2.127972	2.024896	1.912028	2.127972
2.037700	1.908582	2.131418	2.019637	1.908582	2.131418
2.044160	1.905786	2.134214	2.011215	1.905786	2.134214
2.043985	1.903520	2.136480	1.995523	1.903520	2.136480
2.043668	1.901684	2.138316	1.992991	1.901684	2.138316
2.053700	1.900198	2.139802	1.987555	1.900198	2.139802
2.058514	1.898995	2.141005	1.988376	1.898995	2.141005
2.052912	1.898022	2.141978	1.981422	1.898022	2.141978
2.055571	1.897234	2.142766	1.983265	1.897234	2.142766
2.048172	1.896597	2.143403	1.983712	1.896597	2.143403
2.046945	1.896081	2.143919	1.989081	1.896081	2.143919
2.040349	1.895664	2.144336	1.990513	1.895664	2.144336
2.031455	1.895326	2.144674	2.008520	1.895326	2.144674
2.025016	1.895052	2.144948	2.006625	1.895052	2.144948
2.014828	1.894831	2.145169	2.010102	1.894831	2.145169
2.004909	1.894652	2.145348	2.017664	1.894652	2.145348
2.010919	2.001297	2.038704	2.027329	1.894507	2.145493
2.025538	1.984710	2.055290	2.048474	1.894389	2.145611
2.038631	1.969518	2.070482	2.063326	1.894294	2.145706
2.045303	1.956267	2.083733	2.070312	1.894217	2.145783
2.054403	1.945017	2.094983	2.077926	1.894155	2.145845
2.078672	1.935621	2.104379	2.094428	1.894104	2.145896
2.089144	1.927854	2.112146	2.111844	1.894063	2.145937
2.087476	1.921479	2.118521	2.122475	1.894030	2.145970
2.075752	1.916270	2.123730	2.134089	1.894003	2.145997
2.073981	1.912028	2.127972	2.139766	1.893981	2.146019
2.073262	1.908582	2.131418	2.140586	1.893964	2.146036
2.073125	1.905786	2.134214	2.137590	1.893949	2.146051
2.078779	1.903520	2.136480	2.125775	1.893938	2.146062
2.078492	1.901684	2.138316	2.128186	1.893929	2.146071
2.072080	1.900198	2.139802	2.126809	1.893921	2.146079
2.056733	1.898995	2.141005	2.131641	1.893915	2.146085
2.039243	1.898022	2.141978	2.127647	1.893910	2.146090
2.026515	1.897234	2.142766	2.132809	1.893906	2.146094
2.030019	1.896597	2.143403	2.136058	1.893903	2.146097
2.028108	1.896081	2.143919	2.144269	1.893900	2.146100
2.024789	1.895664	2.144336	2.147808	1.893898	2.146102
2.020850	1.895326	2.144674	2.169608	1.893896	2.146104
2.018151	1.895052	2.144948	2.169412	1.893895	2.146105
2.013678	1.894831	2.145169	2.174811	1.893894	2.146106
2.021826	1.894652	2.145348	2.184422	1.893893	2.146107
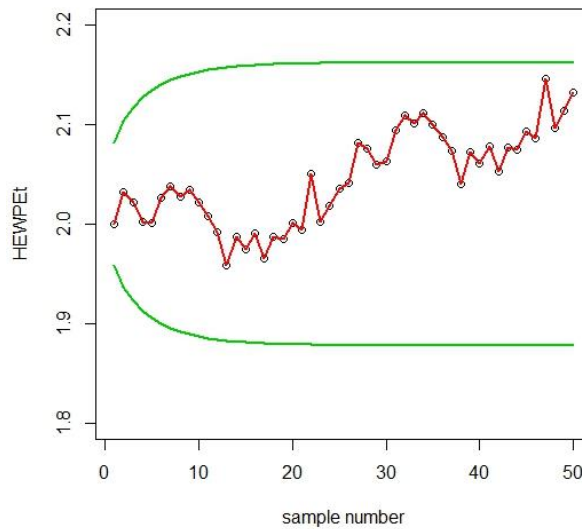
Figure 7:   Simulated data of the proposed HEWMA control chart under PE.
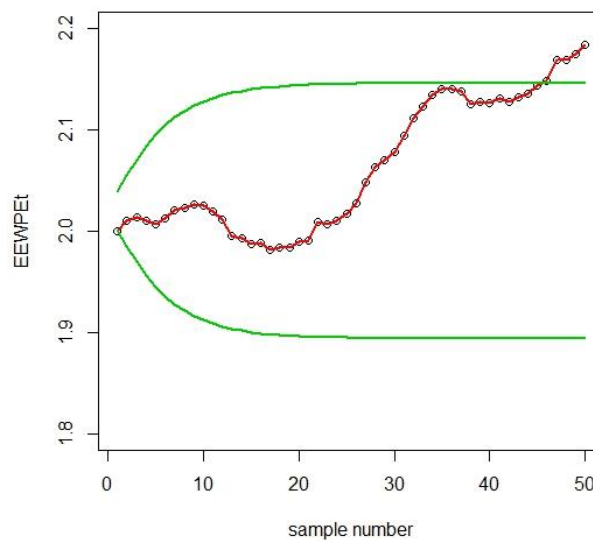
Figure 8:   Simulated data of the proposed EEWMA control chart under PE.

Real life applications

Data set 1

The first set of data is taken from Montgomery (2012) about the automobile ring piston diameter size. Each sample or subgroup consists of five piston rings. We object to controlling the flow width of the resist in the process by using proposed control charts.

We compare HEWMA and EEWMA and from Figure 9 and Figure 10, we observe that EEWMA performs better than HEWMA. This indicates that EEWMA under PE provides more applicable to detect any shift in the process early when the underlying process is based on BL2PFD.
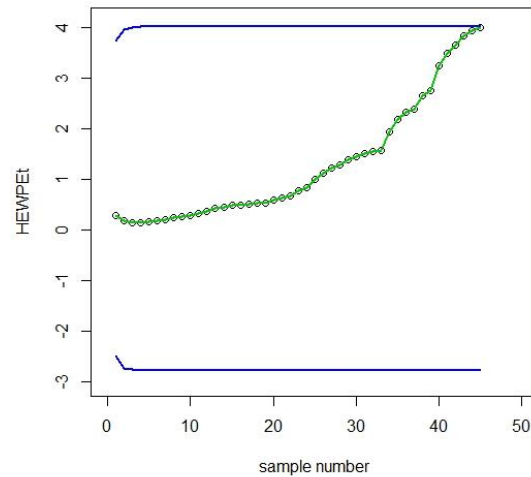
Figure 9:   Automobile engine piston rings data of the HEWMA control chart under PE
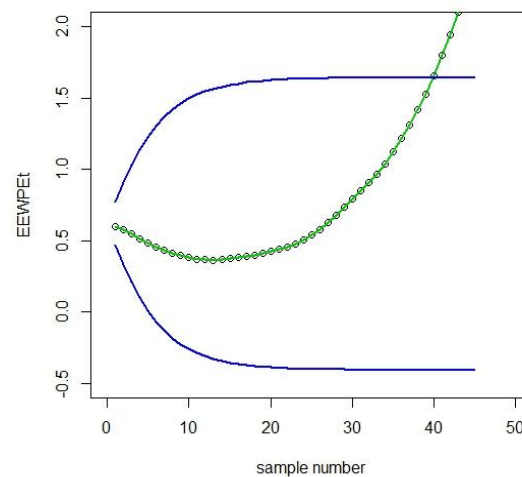
Figure 10:   Automobile engine piston rings data of the EEWMA control chart under PE

Data set 2

We use the data of fracture toughness which was used by Arifa *et al*. (2017). The data are:

0.025,   0.089,   0.089,   0.250,   0.311,   0.345,   0.476,   0.565,   0.567,   0.656,   0.674,
0.675,   0.675,   0.769,   0.837,   0.839,   0.842,   0.864,   0.885,   0.911,   0.912,   0.983,
1.048,   1.059,   1.077,   1.173,   1.257,   1.277,   1.299,   1.321,   1.350,   1.355,   1.459,
1.488,   1.572,   1.573,   1.708,   1.726,   1.746,   1.763,   1.774,   1.827,   1.837,   1.850,
1.880,   1.887,   1.881, 1.931, 1.955, 2.004, 2.040, 2.090, 2.109, 2.133, 2.21, 2.246, 2.287, 2.323, 2.347, 2.351,
2.495, 2.526, 2.991, 3.025, 3.267, 3.404, 3.484, 3.743, 3.745, 3.914, 4.8073, 5.400, 5.443, 5.529, 6.554, 9.09..

We construct HEWMA and EEWMA control charts for the above data. For example, in Figure 11 and Figure 12, we observe that EEWMA is better to be used than HEWMA when the distribution of process is based on BL2PFD.
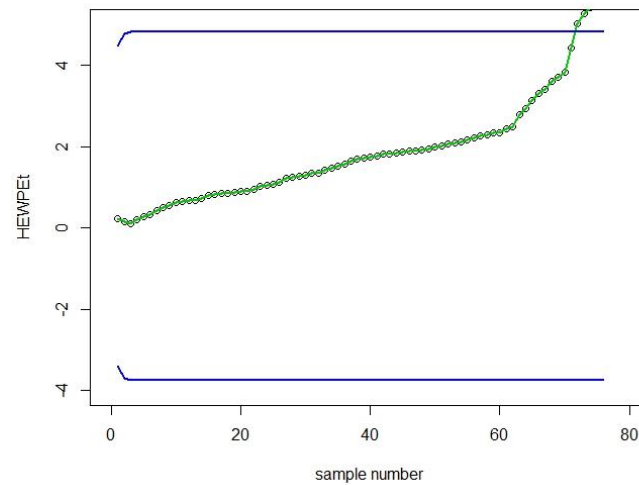
Figure 11:   Fracture toughness data of the HEWMA control chart under PE
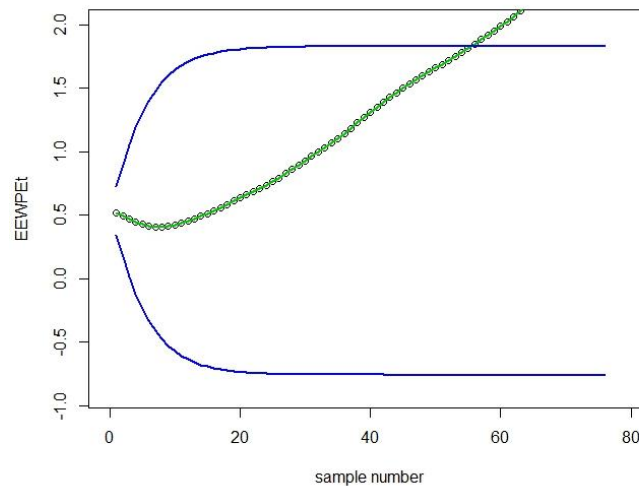
Figure 12:   Fracture toughness data of the EEWMA control chart under PE

CONCLUSION

In this research paper, some modifications to existing control charts to monitor the shape parameter of BL2PFD are proposed, these modified control charts are named as modified Shewhart control chart, modified EWMA control chart, modified HEWMA control chart, modified extended EWMA control chart. The shape parameter of BL2 PFD is estimated through percentile estimator. The study of the proposed control charts for the processes using BL2 PFD as baseline distribution are done through simulation study and real-life applications.

We showed the application of BL2PFD in the field of reliability and engineering sciences using the proposed control charts. We conclude that among our proposed charts, EEWMA performs better than other control charts when the distribution of underlying process is BL2PFD.

Data Availability: The data used to support the findings of this study are included in the article.

REFERENCES

Arifa S., Yab M.Z. & Ali A. (2017). The modified Burr III G family of distributions. *Journal of Data Science* **15**: 41–60.
   DOI: https://doi.org/10.6339/JDS.201701_15(1).0003

Erto P., Pallotta G., Palumbo B. & Mastrangelo C.M. (2018). The performance of semi empirical Bayesian control charts for monitoring Weibull data. *Quality Technology and Quantitative Management* **15**(01): 69–86.
   DOI: https://doi.org/10.1080/16843703.2017.1304036

Haq A. (2013). A new hybrid exponentially weighted moving average control chart for monitoring process mean. *Quality and Reliability Engineering International* **29**: 1015–1025.
   DOI: https://doi.org/10.1002/qre.1453

Jabeen R. & Zaka A. (2021). The modified control charts for monitoring the shape parameter of weighted power function distribution under classical estimator**.** *Quality and Reliability Engineering International* **37**(08): 3417–3430.
   DOI: https://doi.org/10.1002/qre.2925

Jabeen R., Akhtar A. & Zaka A. (2023). Modified calibrated control charts for monitoring the population mean under stratified sampling. *Quality and Reliability Engineering International* **39**(01): 143–163.
   DOI: https://doi.org/10.1002/qre.3225

Jabeen R., Zaka A. & Khan K.I. (2022). Classical estimator based modified control charts for phase-II monitoring in real life. *Quality and Reliability Engineering International* **28**(5): 2862–2880.
   DOI: https://doi.org/10.1002/qre.3112

Li Z., Xie M. & Zhou M. (2018). Rank-based EWMA procedure for sequentially detecting changes of process location and variability. *Quality Technology and Quantitative Management* **15**(03): 354–373.
   DOI: https://doi.org/10.1080/16843703.2016.1208941

Liang W., Xiang D., Pu X., Li Y. & Jin L. (2019). A robust multivariate sign control chart for detecting shifts in covariance matrix under the elliptical directions distributions. *Quality Technology and Quantitative Management* **16**(01): 113–127.
   DOI: https://doi.org/10.1080/16843703.2017.1372852

Lin Y.C., Chou C.Y. & Chen C.H. (2017). Robustness of the EWMA median control chart to non- normality. *International Journal of Industrial and Systems Engineering* **25**(1): 35–58.
   DOI: https://doi.org/10.1504/IJISE.2017.10000683

Montgomery D.C. (2012). *Introduction to Statistical Quality Control*, 7th edition. John Wiley and Sons, New York, USA.

Naveed M., Azam M., Khan N. & Aslam M. (2018). Design of a control chart using extended EWMA statistic. *Technologies* **6**(108): 2–15.
   DOI: https://doi.org/10.3390/technologies6040108

Noorossana R., Fathizadan S. & Nayebpour M.R. (2016). EWMA control chart performance with estimated parameters under non-normality. *Quality Technology and Quantitative Management* **32**(05): 1638–1654.
   DOI: https://doi.org/10.1002/qre.1896

Qiu P. & Li Z. (2011). Distribution-free monitoring of univariate processes. *Statistics and Probability Letters* **81**(12): 1833–1840.
   DOI: https://doi.org/10.1016/j.spl.2011.07.004

Shamma S.E. & Shamma A.K. (1992). Development and evaluation of control charts using double exponentially weighted moving averages. *International Journal of Quality and Reliability Management* **9**(06): 18–25.
   DOI: https://doi.org/10.1108/02656719210018570

Zaka A., Akhter A.S. & Jabeen R. (2020). Beta Lehmann-2 power function distribution with application to bladder cancer susceptibility and failure times of air-conditioned system. *Indian Journal of Science and Technology* **13**(23): 2371–2386.
   DOI: https://doi.org/10.17485/IJST/v13i23.178

Zaka A., Akhter A.S., Jabeen R. & Sanaullah A. (2021a). Control charts for the shape parameter of reflected power function distribution under classical estimators**.** *Quality and reliability engineering international* **37**(06): 2458–2477**.**
   DOI: https://doi.org/10.1002/qre.2866

Zaka A., Akhter A.S., Jabeen R. & Sanaullah A. (2021b). Control charts for the shape parameter of power function distribution under different classical estimators**.** *Computer Modeling in Engineering and Sciences* **127**(03): 1201–1223**.**
   DOI: https://doi.org/10.32604/cmes.2021.014477

Zhang J., Li E. & Li Z. (2017). A Cramér-von Mises test-based distributionfree control chart for joint monitoring of location and scale. *Computers and Industrial Engineering* **110**: 484–497.
   DOI: https://doi.org/10.1016/j.cie.2017.06.027

RESEARCH ARTICLE

Agronomy and Plant Nutrition

Distribution of phosphorus and potassium in selected rice cultivated soils and their accumulation in rice grains under farmer-managed field conditions in Sri Lanka

LDB Suriyagoda[*], NASA Neththasinghe, EDCT Chandrasekara, EMS Ekanayake, DMSB Dissanayaka, M Ariyarathne and B Marambe
Department of Crop Science, Faculty of Agriculture, University of Peradeniya, Peradeniya, Sri Lanka.

Abstract: Rice (*Oryza sativa* L.) is the staple food in Sri Lanka and phosphorus (P) and potassium (K) are major nutrients for the rice plant. However, the variation of P and K contents (mg kg^{-1}) in rice soils and rice grains as affected by agro-climatic zones (ACZs), water source used (*i.e.*, major irrigation, minor irrigation and rain-fed) and cropping systems adopted (*i.e.*, fallow, vegetable, perennials, other field crops) by Sri Lankan farmers are not well elucidated, and are thus investigated in the present study. A total of 200 rice soil and 230 rice grain samples across the country were collected from farmer fields, representing different ACZs, water sources used, and cropping systems adopted using a stratified random sampling approach. The total and available P and K contents in rice soil, and the P and K contents in rice grains were determined. The plant-available P contents in soil were similar among ACZs, water sources, and rice-based cropping systems. Exchangeable K content was higher in rice fields where vegetables were cultivated in the previous season. Grain P and K contents were similar among the water sources used and rice-based cropping systems. Grain P contents was the lowest in the Low country Wet zone. Soil available-P and total-P contents ($r = 0.29$, $p < 0.0001$), and grain P and K contents were positively correlated ($r = 0.51$, $p < 0.0001$). The knowledge generated in the present study is important in P and K nutrient management in rice cultivation in the country.

Keywords: Agro-climatic zones, cropping systems, irrigation methods, P and K contents, rice soils and grains.

INTRODUCTION

Rice (*Oryza sativa* L.) is the staple food crop for about half of the world's population (Priya *et al*., 2019). In addition, rice is a vital source of minerals and vitamins. About 40% of total calorie intake and 45% of total protein requirement of a Sri Lankan adult is fulfilled by rice (Liyanaarachchi *et al*., 2020). Moreover, more than 1.8 million farm families in Sri Lanka rely on the cultivation of rice as their livelihood and therefore, rice has become the most important cereal crop in the country (Hettiarachchi *et al*., 2016). In Sri Lanka, rice is grown under a wide range of environments in different elevations, soil types, and hydrological regimes (FAO, 2000).

Phosphorus (P) and potassium (K) are two major essential mineral elements required by plants and thus determine the growth and yield of crops (Moe *et al*., 2019; Ma *et al*., 2020). Application of P and K containing fertilizers and manures is recommended to increase the grain yield of rice by ensuring soil fertility (Ma *et al*., 2020; Suriyagoda, 2022). In rice, P fertilizer-use efficiency for the production of above-ground biomass is approximately 25% (Vinod & Heuer, 2012; Suriyagoda, 2022). Malpractices in nutrient management have led to deficiencies and toxicities of nutrients for crop growth, thereby negatively affecting the crop productivity (Masni & Wasil 2019; Moe *et al*., 2019). Moreover, improper fertilization has been a serious issue in agricultural fields contributing to the degradation of soil, eutrophication of water bodies, pollution of groundwater and emission of toxic gases (Ju *et al*., 2009; Ye *et al.,* 2015; Sirisena & Suriyagoda, 2018).

[*] Corresponding author (lalith.suriyagoda@agri.pdn.ac.lk; https://orcid.org/0000-0002-5253-2717)

When considering elevation, areas located below 300 m, between 300-900 m and above 900 m of sea level in Sri Lanka are identified as Low-, Mid-, and Up-Country regions, respectively (Punyawardane, 2008). Based on the rainfall pattern, areas receiving mean annual rainfall less than 1750 mm and having a relatively dry period from June to September are considered as the Dry zone. The areas receiving a mean annual rainfall greater than 2500 mm and without any dry period throughout the year are considered as the Wet zone, while the Intermediate zone has characteristics in between with respect to the amount and distribution of annual rainfall. Considering both mean annual rainfall and elevation, Sri Lanka is divided into seven agro-climatic zones (ACZs). Out of those, five ACZs are considered as main rice growing zones in the country, *i.e.*, Low country Dry zone (DL), Low country Intermediate zone (IL), Up country Intermediate zone (IU), Mid country Intermediate zone (IM) and Low country Wet zone (WL) (DOA, 2021). Phosphorus and K fertility of rice cultivated soils in these ACZs would vary due to the differences in soil forming parent materials, climate, and agronomic practices adopted. Therefore, it is important to understand the variability of soil P and K contents (mg kg^{-1}) among ACZs and their relationships to grain accumulation.

Based on the major water source used, rice cultivation in Sri Lanka is devided into three categories, namely major irrigation, minor irrigation and rainfed (Navarathna *et al.,* 2021). Reservoirs in major irrigation schemes have more than 80 ha of command area (irrigated land) while the minor irrigation schemes are comprised less than 80 ha of command area (Imbulana *et al.,* 2006). Rice cultivation in DL and IL of Sri Lanka largely depends on the well-distributed cascade irrigation network covering both major and minor irrigation schemes. Rice cultivation in other regions largely depends on rainfall. This variation in water source may contribute to spatial variation of P and K availability in rice soils and their accumulation in rice grains.

Rice cultivation in Sri Lanka is generally practised in two seasons, *i.e.*, *Yala* (minor season; March-September) and *Maha* (main season; October-February in the following year). In order to obtain the best returns from resources used such as land and water, economically valuable non-rice crops are cultivated in rotation with rice, mainly in the water-limited *Yala* season (Dimantha, 1987; Panabokke, 1989). Considering this, rice-based cropping systems can be recognised either as rice-rice, rice-fallow, rice-other field crops (OFC) or rice-vegetables cropping systems (Bandara *et al.*, 2003). However, the impacts of crop rotation in rice-based cropping systems on soil P and K availability and rice grain P and K status are not known. Therefore, the objectives of the present study were to determine the, (i) total and plant-available P and K contents in selected rice soils, (ii) P and K contents in rice grains, and (iii) relationships between soil and grain P and K contents as affected by the ACZ, water source used, and rice-based cropping systems adopted in rice lands.

MATERIALS AND METHODS

A total of 200 soil samples and 230 rice grain samples collected from farmer fields were used for the study. These samples were collected from five ACZs (except Up and Mid Country Wet zones), three major water sources used for rice cultivation (*i.e.*, major irrigation, minor irrigation and rain-fed), and four major rice-based cropping systems (*i.e.*, rice-rice, rice-vegetable, rice-other field crops and rice-fallow) adopted. A structured and pre-tested questionnaire was used to collect the information on the major water source used, and rice-based cropping system adopted. The number of soil and grain samples used for the analysis of P and K contents from different ACZs, rice-based cropping systems, and water sources is summarized in Tables 1 and 2.

Table 1: Number of soil samples used for the analysis of total and available P and K contents in rice soils

Agro-climatic zone	No.	Rice-based cropping system adopted	No.	Major water source used	No.
Dry zone Low country	128	Rice-Rice	113	Major irrigation	89
Intermediate zone Low country	28	Rice-Fallow	40	Minor irrigation	55
Intermediate zone Mid country	13	Rice-OFC	11	Rain-fed	38
Intermediate zone Upcountry	12	Rice-Vegetable	13		
Wet zone Low country	19				
Total	200		177		182

Table 2: Number of rice grain samples used for the analysis of total and available P and K contents in rice grains.

Agro-climatic zone	No.	Rice-based cropping system adopted	No.	Major water source used	No.
Dry zone Low country	138	Rice-Rice	113	Major irrigation	89
Intermediate zone Low country	33	Rice-Fallow	40	Minor irrigation	55
Intermediate zone Mid country	18	Rice-OFC	11	Rain-fed	38
Intermediate zone Upcountry	17	Rice-Vegetable	13		
Wet zone Low country	24				
Total	230		177		182

One soil sample was a composite of four to six samples collected from a rice track (*Yaya*) considering field level soil heterogeneity. Each sample was collected from top 0-15 cm soil layer using a soil auger. For grain collection, the same rice fields used to collect soil samples were considered. In addition, 30 rice fields selected randomly from other locations were also used. Twenty-five panicles were collected from the selected *Yaya* to represent the mainly cultivated rice variety of that *Yaya*. Soil and grain samples were collected using a stratified random sampling approach as described in Kadupitiya *et al.* (2021) before (*i.e.*, September and October, 2019) and at the end of the *Maha* 2019/20 season (*i.e.*, February and March, 2020), respectively.

Soil samples were air dried, gravel and plant parts were removed, the samples were homogenized, and then sieved using a 2 mm sieve. The samples were stored at room temperature, in a dry and dark room until used for analysis. The total K content of soil was determined using the Niton XL5 XRF analyzer (Thermo Fisher, USA). An air dried, ground soil sample was filled into a plastic ring and sealed with a polythene membrane. The packed ring was placed in the safety box of the X-ray shutter. Data of total soil-K content was recorded through a laptop installed with a Niton Connect ZRF analyzer (Thermo Fisher, USA) and expressed as mg K kg^{-1} soil. For exchangeable soil K determination, about 2.5 g of dried, ground soil samples were treated with 50 mL of 1 M NH_4OAc solution. The pH of the sample was buffered at 7 and shaken for 2 h using an orbital shaker at room temperature. Then, the solution was filtered using Whatman® filter papers (No. 40; D = 110 mm). The exchangeable K content of soil was measured using a flame photometer at 766.5 nm wavelength and expressed as mg K kg^{-1} soil.

For the determination of soil total P, two grams of soil was measured into a 250 mL Erlenmeyer flask. About 25 mL of 70% $HClO_4$ was added and the mixture allowed to digest at 80-120 °C until the dark color of the organic matter disappeared. After cooling, the digested samples were transferred into 250 mL volumetric flasks and the volume adjusted to the mark with distilled water. Samples were homogenized and the solid particles allowed to settle down. Then, 2 mL from the sample was pipetted out in to a test tube and mixed with 2 mL of colour development reagent and 6 mL of distilled water (Van Ranst *et al.*, 1999). After 10 min of standing, the optical density was measured using a spectrophotometer (A & E, AE-S70-2U, England) at 430 nm and the P concentration expressed as mg P kg^{-1} soil. The colour development reagent was prepared by combining two solutions. One solution was made by dissolving 25 g of ammonium molybdate (Fisher Scientific, UK) in 400 mL of hot distilled water. In order to prepare other solution, 1.25 g of ammonium metavanadate (Fisher Scientific, UK) was dissolved in 300 mL of hot distilled water. After that, about 250 mL of concentrated HNO_3 was added. The two solutions were mixed in 1 L volumetric flask and the volume adjusted to 1 L (Van Ranst *et al.*, 1999).

The available P content in soil samples was determined using the Olsen method (Olsen, 1954). Dried, homogenized, and sieved soil samples of 2.5 g were measured into clean and dry conical flask of 250 mL. Then soil samples were treated with 50 mL of 0.5 M sodium bicarbonate ($NaHCO_3$) and allowed to shake for one hr on an orbital shaker at room temperature. Then the solution was filtered using Whatman® filter papers (No. 40; D = 110 mm). Next, 5 mL of the extract and 5 mL of colour developing reagent were pipetted out into a 25 mL volumetric flask, volume up to 25 mL using distilled water and mixed. The solution was kept for 20 min for colour development. The available P content was determined using a spectrophotometer at 880 nm and expressed as mg P kg^{-1} soil (Van Ranst *et al.*, 1999).

The colour developing reagent was prepared by adding 0.739 g of ascorbic acid to 140 mL of mixed reagent. The mixed reagent was made by mixing two solutions. The first solution was prepared by dissolving 12 g of ammonium molybdate (Fisher Scientific, UK) in 250 mL distilled water. To prepare the second reagent, 0.29 g of antimony potassium tartrate (Fisher Scientific, UK) was dissolved 1 L of 5 M sulfuric acid. The two solutions were dissolved together and made up to 2 L with distilled water (Van Ranst *et al.*, 1999).

The phosphorus standard graph was prepared as described in Van Ranst *et al.* (1999). Here, 0, 0.5. 1.0, 1.5, 2.0 and 2.5 mL of 5 mg P L^{-1} of standard solution were separately pipetted out into different labelled conical flasks. Then 5 mL of 0.5 M $NaHCO_3$ solution and 5 mL of mixed reagent were added and mixed. Distilled water was added to each flask to reach the 25 mL level and the solutions allowed to stand for 15 min for colour development. Absorbance levels for the known available P contents (*i.e.*, 0, 0.1, 0.2, 0.3, 0.4, and 0.5) were determined using a spectrophotometer at 880 nm and calibration graph was drawn by plotting absorbance value and available P content. The available P content of a sample was determined using the following calculation:

Available soil P content (mg kg^{-1}) = (X × 25 × 50) / 5 × W (Van Ranst *et al.*, 1999)

where X is the graph reading and W is the weight of the soil sample.

For the determination of grain P and K contents (mg kg^{-1}), one gram of de-husked grain sample was burnt in a muffle furnace for 2 h until converted to ash. The temperature was set to 200 °C in the 1st hour and 450 °C in the 2nd hour. After cooling the sample, 5 mL of 6 M nitric acid was added into the crucible and thoroughly mixed by using a glass rod. Then, the sample was put into a 100 mL beaker, and the crucible and glass rod were washed with 1% nitric acid and placed in the beaker. The sample was then boiled for about 15 min, and 5 mL of 3 M nitric acid were added during boiling. Thereafter, the sample was kept outside for cooling. The beaker solution was filtered into a 50 mL volumetric flask and the volume adjusted to 50 mL using distilled water. The grain P content in the solution was measured using a spectrophotometer at 430 nm wavelength and expressed as mg P g^{-1} grains. Two mL of the previous solution was pipetted out into a test tube. Six milliliters of distilled water and 2 mL of nitro-vanadomolybdate was added and mixed properly. The grain K content in the solution was measured by using a flame photometer (Jenway, Sussex, England) at 766.5 nm wave length and expressed as mg kg^{-1} grains.

Data were statistically analysed using SAS 9.1 software. Element contents in soil and grain samples collected from different sources (*i.e.*, ACZ, water sources and cropping systems) were analysed using analysis of variance (Proc GLM) and mean separation was done through Duncan's New Multiple Range Test (DNMRT). Strengths of the relationships between elements (paired comparisons) were determined using Pearson's linear correlation coefficient (*r*). Statistical significances were expressed at α = 0.05.

RESULTS AND DISCUSSION

P and K contents in rice soils

The available P content in rice soil samples ranged between 5.4 and 220.1 mg kg^{-1} with a mean content of 22.1 mg kg^{-1} (Figure 1). The critical soil available P content causing P deficiency symptoms in Sri Lankan rice is generally considered as 10 mg kg^{-1} (Sims, 2000). It has also been reported that the critical available P content would vary from 10 to 40 mg kg^{-1} based on the geographical region, crop type, and soil type, including soil structure, pH, soil depth, and organic matter content (Bai *et al.*, 2013). When considering the soil pH, critical available P content recorded for acidic soil is 5 mg kg^{-1} and it is more than 25 mg kg^{-1} in calcareous soils (Dobermann & Fairhurst 2000).

Over 70% of rice soil samples recorded available P contents less than 30 mg kg^{-1} and 23% of soil samples had available P contents less than 10 mg kg^{-1}. Total P content of rice soil samples ranged between 24 and 4,929 mg kg^{-1} (Figure 1). According to Sirisena and Suriyagoda (2018), the mean available P content of continuously rice-cultivated soils in Sri Lanka was around 13 mg kg^{-1}, and 44% of rice growing soils in the country recorded an available P contents less than 10 mg kg^{-1}. Farmers have applied P fertilizers as a routine practice without considering the 2013 fertilizer recommendation in the Department of Agriculture. This might have caused an

increase in the mean available P content in selected rice tracts in the present study compared to that reported by Sirisena and Suriyagoda (2018).

The mean exchangeable K content in rice soil was 257.8 mg kg^{-1}, and it ranged from 26.4 to 1,372.8 mg kg^{-1} (Figure 1). The total K content in rice soil samples was in the range of 316 - 31,153 mg kg^{-1} (Figure 1). Bandara *et al*. (2003) reported that soil critical exchangeable K content for rice is 78 mg kg^{-1}. According to the Department of Agriculture recommendation, the optimum exchangeable K content for rice cultivation in Sri Lanka is considered as 80 – 160 mg kg^{-1} (Rathnayake *et al*., 2015). However, according to Dobermann and Fairhurst (2000), soil exchangeable K contents less than 60 mg kg^{-1}, between 60 mg kg^{-1} and 175 mg kg^{-1}, more than 175 mg kg^{-1} are considered as deficient, optimal, and excess exchangeable K contents for rice, respectively. Accordingly, out of the total samples used in the present study, 4.0%, 39.5% and 56.5% of soil samples had exchangeable K contents less than 60 mg kg^{-1}, between 60 and 175 mg kg^{-1} and greater than 175 mg kg^{-1} contents, respectively. However, the critical exchangeable K content may vary from 40 to 156 mg kg^{-1} depending on soil texture, clay mineralogy, rainfall variation, and K inputs, especially from the natural resources (Bandara *et al*., 2003; Rathnayake *et al*., 2015).
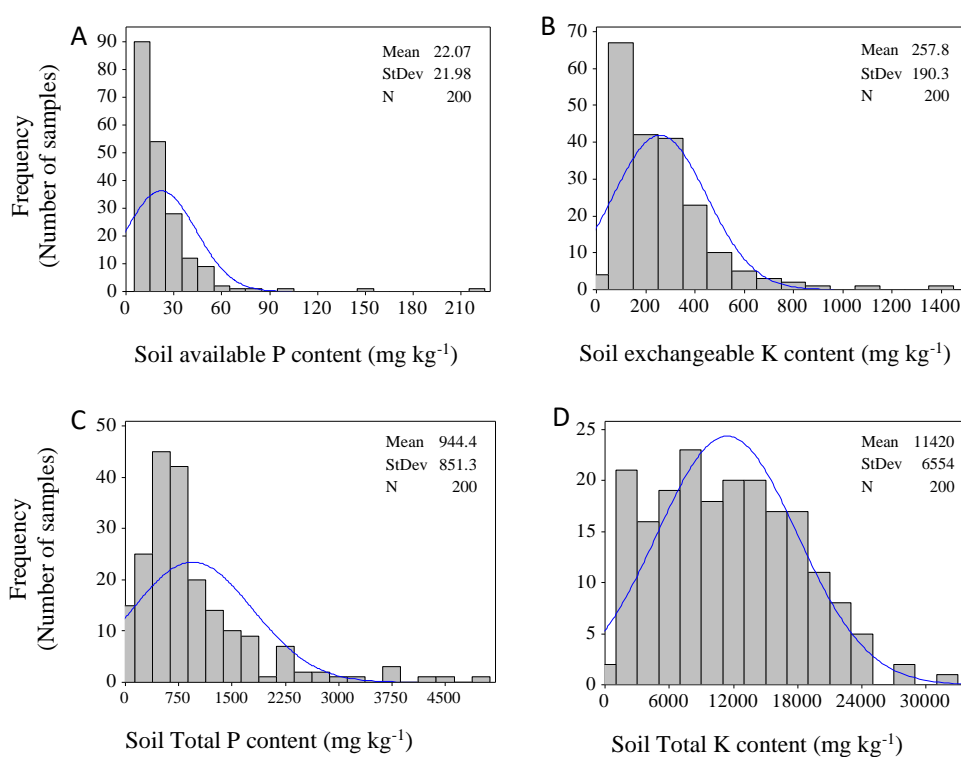
Figure 1: Distribution of (A) available phosphorus (P); (B) exchangeable potassium (K); (C) total P and (D) total K content of the rice soil samples collected from Sri Lanka.
Note: blue line in each sub-figure indicates the fitted frequency distribution, N = Sample Size

The total and available P content in soil samples were similar among ACZs (p > 0.05) (Table 3). However, the total soil K content was the lowest in WL and exchangeable K content was the highest in IM (p < 0.05) (Table 3).

The comparatively higher exchangeable K content observed in IM could be due to the presence of Immature Brown Loam (IBL) soil in this region (Bandara *et al*., 2003; Wickramasinghe *et al*., 2003). The amount of K taken up and tissue K content in rice were the highest when grown in IBL soil due to the higher initial exchangeable K content and the higher negative K balance in IBL soil (Mapa, 1992; Bandara *et al*., 2003; Wickramasinghe *et al*., 2003). Rezania (1993) reported that almost 50% of the rice growing soils in WL have exchangeable K content less than 58 mg kg^{-1}, which is lower than that reported in the present study. However, consistent with the present study, Rubasinghe *et al*. (2021) also observed similar exchangeable K content in WZ and DZ soils. In the WZ, K

could be lost due to leaching as a result of higher mean annual rainfall than in DZ and IMZ (Wickramasinghe *et al.*, 2003).

Table 3: Phosphorus (P) and potassium (K) contents (mg kg^{-1}) in samples from rice cultivated soils collected from different agro-climatic zones.

Element	Agro-climatic zone				
	DL	IL	WL	IM	IU
Total P	934 ± 75[a]	879 ± 110[a]	920 ± 192[a]	1,705 ± 139[a]	1,046 ± 243[a]
Total K	12,270 ± 534[a]	11,402 ± 1,144[ab]	3,317 ± 421[b]	10,739 ± 399[ab]	15,488 ± 740[a]
Available P	24 ± 2[a]	19 ± 2[a]	15 ± 2[a]	27 ± 2[a]	26 ± 5[a]
Exchangeable K	265 ± 17[b]	224 ± 30[b]	230 ± 26[b]	603 ± 57[a]	166 ± 43[b]

Note: means followed by the same letter within a row are not significantly different at α = 0.05. Values represent the mean ± SE (DL = Dry zone Low country, IL = Intermediate zone Low country, WL = Wet zone Low country, IM = Intermediate zone Mid country, IU = Intermediate zone Upcountry)

The total P, total K, and available P contents in soils from different rice-based cropping systems were similar (p > 0.05) (Table 4). However, the exchangeable K contents in soils collected from the rice-vegetable cropping system was higher than those of other rice-based cropping systems (p < 0.05). Vegetables demand a frequent and steady supply of nutrients due to the presence of a shallow root system and fast growth rate (Suriyagoda *et al.*, 2012; Upekshani *et al.*, 2018). Therefore, frequent application of inorganic fertilizers in combination with organic manures such as cattle and poultry manure, during the period of vegetable cultivation in the rice-vegetable cropping system is essential (Maraikar *et al.*, 1997; Wickramasinghe *et al.*, 2003; Sirisena and Suriyagoda, 2018; Suriyagoda *et al.*, 2022). It is also reported that the fertilizer use in upcountry vegetable cultivating systems was higher than the recommended rates (Upekshani *et al.*, 2018; Suriyagoda *et al.*, 2022), e.g., 30% to 50% of the upcountry vegetable farmers have applied more than the recommended rate of muriate of potash for K when cultivating carrot, leeks, and cabbage in Nuwara Eliya and tomato, snake gourd, and bitter gourd in the Marassana area (Upekshani *et al.*, 2018). In general, the organic fertilizer application rates for vegetable cultivation in this region varied from 10 to 15 t ha^{-1} yr^{-1} of poultry manure and 20 to 30 t ha^{-1} yr^{-1} of cattle manure (Suriyagoda *et al.*, 2012). Vegetables such as pole bean take up low amounts of K whereas cabbage acquires a high amount of K, indicating that soil K content is also influenced by the type of vegetable cultivated in the cropping system (Maraikar *et al.*, 1997). Overall results suggest that the higher rates and frequencies of K fertilizer application have contributed to an increase in exchangeable K content in rice-vegetable cropping systems than other rice-based cropping systems tested in the study.

The available P content reported in rice-vegetable cropping systems was around 26 mg P kg^{-1} soil (Table 4). In contrast, Sirisena and Suriyagoda (2018) reported an available P content of 85 mg P kg^{-1} in rice-vegetable cropping systems. Comparatively lower available soil P content observed in the present study in comparison to the previous report would be due to the reduced rate in the recommendation of P fertilizers, P fixation in soil, removal of P with the harvest of vegetable crops, leaching and runoff. Phosphorus removal through harvesting of rice may also contribute to the decline in soil P availability. For example, 20 kg of P is removed with the harvest of 6 t ha^{-1} of rice grains (Sirisena & Suriyagoda, 2018). Moreover, unlike K, most of the P taken up by rice plants is stored in rice grains; thereby a considerable amount of P is removed from soil with the harvest of rice grains (Somaweera *et al.*, 2017).

Table 4: Phosphorus (P) and potassium (K) contents in soil samples collected from different rice-based cropping systems.

Element	Rice-based cropping systems			
	Rice-rice	Rice-fallow	Rice-vegetables*	Rice-other field crops
Total P (mg g^{-1})	0.9 ± 0.09[a]	1.1 ± 0.19[a]	1.7 ± 0.14[a]	1.5 ± 0.2[a]
Total K (mg g^{-1})	11.0 ± 0.86[a]	10.1 ± 1.2[a]	10.7 ± 0.40[a]	13.4 ± 1.99[a]
Available P (mg kg^{-1})	18.2 ± 1.5[a]	29.4 ± 8.4[a]	26.9 ± 2.2[a]	25.6 ± 4.4[a]
Exchangeable K (mg kg^{-1})	203.1 ± 13.1[b]	274.6 ± 27.7[b]	603.4 ± 56.5[a]	337.5 ± 80.8[b]

Note: means followed by the same letter within a row are not significantly different at α = 0.05. Values represent the mean ± SE

* values presented in this column are similar to that in IM column of Table 3 as rice-vegetable farmers were found only in IM

The total P and K content in soil samples collected from rain-fed fields were lower than the soil samples collected from major and minor irrigated fields (p < 0.05) (Table 5). However, the available P and exchangeable K content in soils were similar among major water sources used for rice cultivation (p > 0.05) (Table 5). The wet zone receives higher total annual rainfall than DZ and IZ (DOA, 2021), which could cause a higher loss of nutrients from soil through leaching and runoff (Wickramasinghe 1991; Kumaragamage & Indraratne, 2011; Rubasinghe *et al.,* 2021). Moreover, rivers originating from Up country WZ carry nutrients to lowlands in the DZ where rice is extensively cultivated (Kumaragamage & Indraratne, 2011). Therefore, the irrigation water distributed through both major and minor irrigation schemes have become a major source of K supply for rice cultivation in the DZ and IZ (Kulasinghe *et al.,* 2020). Irrigation water contributes 43-57% of the recommended amount of nutrients in major and minor irrigation schemes (Wickramasinghe, 1991). Moreover, K content in surface waters in the DZ of Sri Lanka was 2-8 mg L^{-1}, which is higher than the permissible level (2 mg L^{-1}) of the World Health Organization (Wijesundara *et al.*, 2012). Therefore, the heterogeneous nature of the supply of irrigation water has an influence on the variability of soil total K content in Sri Lankan rice fields. Irrigation water is not considered as a source of P as it contains negligible amounts of P for rice cultivation (Buresh *et al.* 2010; Somaweera *et al.,* 2017). Therefore, accumulation of runoff-K in rivers and tanks has resulted in a higher K content in rice fields in the DZ and IZ of Sri Lanka. Soils in DZ have originated from basic cation-rich parent materials with less weathering capacity, due to the low rainfall (Indraratne, 2020). In addition, compared to WZ, DZ and IZ have high temperature and high evaporation (Kumaragamage & Kendaragama, 2010). These conditions have created high base saturation in DZ and IZ soils, recording high K content (Kumaragamage and Kendaragama, 2010; Wickramasinghe 2010). In contrast, Ultisols is the model soil of WZ and potassium feldspars are the primary mineral found in Ultisols (Indraratne, 2020). The highly weathered nature of Ultisols resulting from high rainfall may have leached K out from potassium feldspars and transported it to DZ and IZ soils through rivers (Kumaragamage & Indraratne, 2011).

Table 5: Phosphorus (P) and potassium (K) contents in soil samples receiving water from different sources for rice cultivation.

Element	Major water sources		
	Major irrigation	Minor irrigation	Rain-fed
Total P (mg g^{-1})	1.1 ± 0.11^a	1.1 ± 0.14^a	0.68 ± 0.09^b
Total K (mg g^{-1})	13.5 ± 0.85^a	11.5 ± 1.05^a	6.9 ± 1.05^b
Available P (mg kg^{-1})	27.7 ± 5.4^a	20.5 ± 2.0^a	16.7 ± 2.2^a
Exchangeable K (mg kg^{-1})	252.4 ± 30.5^a	256.3 ± 26.2^a	238.0 ± 27.6^a

Note: means followed by the same letter within a row are not significantly different at α = 0.05. Values represent the mean ± SE

P and K content in rice grains

The grain P content was in the range of 0.10 - 1.76 mg g^{-1} with a mean of 1.17 mg g^{-1} while grain K content was in the range of 1.61 - 4.65 mg g^{-1} with a mean of 2.81 mg g^{-1} (Figure 2). The results of the present study further revealed that 20% of selected grain samples had P content less than 1 mg g^{-1}. When over 50 recommended rice varieties were tested under experimental field conditions at the Rice Research and Development Institute at Batalagoda in Sri Lanka, the grain P and K contents were in the ranges of 1.5 - 2.9 mg P g^{-1} and 1.6 - 2.1 mg Kg^{-1}, respectively (Kekulandara *et al.*, 2019). The difference of grain P content observed between the present study and previous studies indicates that the accumulation of grain P in actual farmer field conditions is less than that observed under experimental field conditions at research stations. Moreover, a wide range of rice varieties was included in the present study; e.g., At308, At362, Bg300, Bg357, Bg358, Bg359, Bg360, Bg367, Bg379/2, Bg403, Bw367, Ld365 and Ld368. However, the differences in grain P content observed between studies may not be due to the differences of varieties tested, but may be due to the difference in soil fertility between farmer field conditions and experimental fields at research stations.
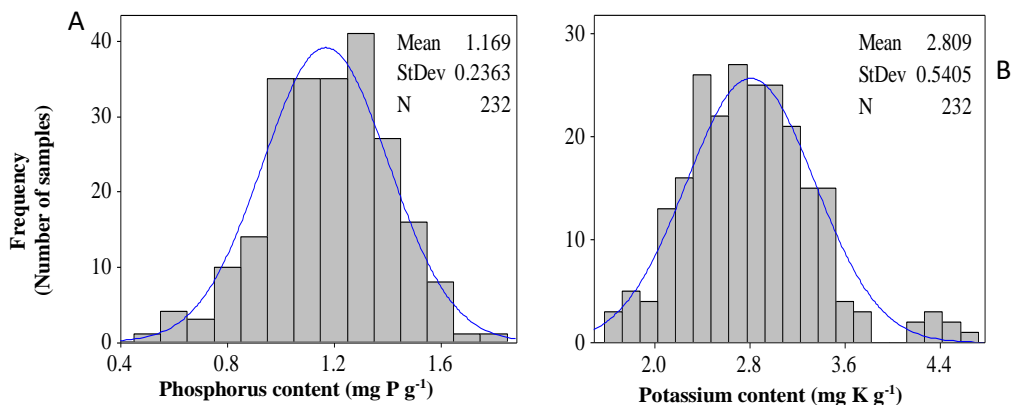
Figure 2: Distribution of (A) phosphorus (P) and (B) potassium (K) content of rice grain samples collected from rice fields in Sri Lanka.
Note: the blue line in each sub-figure indicates the fitted frequency distribution

Grain K content was similar among different ACZs ($p > 0.05$) (Table 6). However, grain P content was the lowest in WL ($p < 0.05$) which could be due to the lower P availability in WZ soils as a result of higher rainfall, lower soil pH and higher P fixation than other ACZs (Wickramasinghe, 1991; Ahn *et al*., 2010; Sirisena and Suriyagoda, 2018).

Table 6: Phosphorus (P) and potassium (K) contents (mg g^{-1}) in rice grain samples collected from different agro-climatic zones.

	Agro-climatic zone				
Elements	DL	IL	WL	IM	IU
P	1.30 ± 0.03[ab]	1.20 ± 0.06[bc]	0.90 ± 0.05[c]	1.30 ± 0.10[ab]	1.60 ± 0.01[a]
K	2.90 ± 0.08[a]	2.70 ± 0.11[a]	2.70 ± 0.20[a]	2.30 ± 0.54[a]	3.20 ± 0.26[a]

Note: means followed by the same letter within a row are not significantly different at α = 0.05. Values represent the mean ± SE

(DL=Dry zone Low country, IL=Intermediate zone Low country, WL=Wet zone Low country, IM=Intermediate zone Mid country, IU=Intermediate zone Upcountry)

Nutrient accumulation in rice grains is affected by many factors such as climate, soil, crop management including fertilizer application, water management, and crop rotation (Johnson *et al.,* 2021; Suriyagoda, 2022). Therefore, environment and management practices largely affect the accumulation of nutrients in rice grains (Du *et al*., 2013; Huang *et al*., 2016; Johnson *et al*., 2021; Suriyagoda, 2022). However, as observed in the present study, grain P and K content were similar ($p > 0.05$) among major water sources used for rice cultivation and rice-based cropping systems tested (Tables 7 and 8). Therefore, different water sources and rice-based cropping systems tested in the present study did not significantly contribute to P and K content of rice grains under the tested conditions.

Table 7: Phosphorus (P) and potassium (K) contents (mg g^{-1}) in rice grain samples collected from different rice-based cropping systems

	Rice-based cropping systems			
Elements	Rice-rice	Rice-fallow	Rice-vegetables	Rice-other field crops
P	1.30 ± 0.03[ab]	1.20 ± 0.06[bc]	0.90 ± 0.05[c]	1.30 ± 0.10[ab]
K	2.90 ± 0.08[a]	2.70 ± 0.11[a]	2.70 ± 0.20[a]	2.30 ± 0.54[a]

Note: means followed by the same letter within a row are not significantly different at α = 0.05. Values represent the mean ± SE

Table 8: Phosphorus (P) and potassium (K) contents (mg g^{-1}) in rice grain samples collected from the areas receiving water from different sources for rice cultivation

| Elements | Major water source | | |
	Major irrigation	Minor irrigation	Rain-fed
P	1.20 ± 0.02[a]	1.20 ± 0.03[a]	1.20 ± 0.04[a]
K	2.70 ± 0.05[a]	2.80 ± 0.07[a]	2.90 ± 0.11[a]

Note: means followed by the same letter within a row are not significantly different at α = 0.05. Values represent the mean ± SE

Strengths of the relationships between soil and grain P and K contents

There were positive correlations between soil available P and soil total P contents, and grain P and grain K contents (Table 9). These results revealed that the soils with higher total P content make more P available for plant uptake. According to Lee *et al*. (2004), the available P fraction is correlated with total soil P due to the long-term P fertilizer application. Moreover, the significant correlation observed between grain K and P contents would be due to the presence of P in the form of K-Mg salt in phytic acid (Pinson *et al*., 2014). Irrespective of the weak soil P and K relationships, the strong grain P and K relationship also reveal that the rice plant has the ability to take up P and K selectively to optimize the growth and grain P and K nutrition.

Table 9: Correlations between the soil and grain phosphorus (P) and potassium (K) contents.

	Soil total P	Soil exchangeable K	Soil total K	Grain K	Grain P
Soil available P	0.2911	0.0986	0.2046	0.1426	0.1176
	<0.0001	0.1649	0.0037	0.1776	0.2669
Soil total P		0.2271	0.1437	0.0452	−0.0498
		0.0012	0.0423	0.6705	0.6393
Soil exchangeable K			−0.0274	−0.0628	0.1661
			0.7006	0.5542	0.1156
Soil total K				−0.0017	0.2193
				0.9869	0.0368
Grain K					0.5141
					<0.0001

Note: upper and lower values in each pair represent the correlation coefficient and the corresponding probability (P) level, respectively.

CONCLUSION

Soil available and total P and K contents are adequate for rice cultivation in most of the rice fields in the country. Rice lands used for vegetable-rice rotation recorded significantly higher soil exchangeable K content than other rice-based cropping systems. Rice grain P and K contents were similar among different water sources used for rice cultivation and rice-based cropping systems adopted. Grain P contents was lower in WL than that in other ACZs. There was a positive correlation between grain P and K contents. The results of the present study provide important information for sustainable soil P and K management in selected rice-based cropping systems using different water sources.

Acknowledgment

REFERENCES

Ahn D.J., Won J.G., Rico C.M. & Lee S.C. (2010). Influence of variety, location, growing year, and storage on the total phosphorus, phytate-phosphorus, and phytate-phosphorus to total phosphorus ratio in rice. *Journal of Agricultural and Food Chemistry* **58**: 3008−3011.
   DOI: https://doi.org/10.1021/jf1001167

Bai Z., Li H., Yang X., Zhou B., Shi X., Wang B. & Zhang F. (2013). The critical soil P levels for crop yield, soil fertility and environmental safety in different soil types. *Plant and Soil* **372**: 27−37.

Bandara W.M.J., Wickramasinghe W.M.A.D.B. & Sirisena D.N. (2003). Potassium fertilization of paddy in Sri Lanka. In: *Importance of Potash Fertilizers for Sustainable Production of Plantation and Food Crops in Sri Lanka* (Eds. V.V. Nossov & J.D.H. Wijewardena). pp. 143−160. International Potash Institute, Horgen, Switzerland.

Buresh R.J., Pampolino M.F. & Witt C. (2010). Field-specific potassium and phosphorus balances and fertilizer requirements for irrigated rice-based cropping systems. *Plant and Soil* **335**: 35−64.
   DOI: https://doi.org/10.1007/s11104-010-0441-z

Dimantha S. (1987). *Irrigation Management for Crop Diversification in Sri Lanka*, pp. 135−150. International Water Management Institute, Colombo, Sri Lanka.

DOA (Department of Agriculture) (2021). *Rice Research and Development Institute Bathalagoda (RRDI).* Available at *https://doa.gov.lk/rrdi_climate/*, Accessed 31 January 2022.

Dobermann A. & Fairhurst T. (2000) *Rice Nutrient Disorders and Nutrient Management*, 1st edition, pp. 203. Potash and Phosphate Institute (PPI), Canada, International Rice Research Institute (IRRI), Laguna, Philippines.

Du J., Zeng D., Wang B., Qian Q., Zheng S. & Ling H.Q. (2013). Environmental effects on mineral accumulation in rice grains and identification of ecological specific QTLs. *Environmental Geochemistry and Health* **35**: 161−170.
   DOI: https://doi.org/10.1007/s10653-012-9473-z

FAO (Food and Agriculture organization) 2020. *Crop Diversification In Sri Lanka.* Available at *https://www.fao.org/3/x6906e/x6906e0b.htm*, Accessed 31 Januay 2022.

Hettiarachchi H.A.P.W., Ribeira S.P., Prasantha B.D.R. & Wickramasinghe H.A.M. (2016). Diversity of physical and cooking quality characters of selected traditional and improved rice varieties in Sri Lanka. *Sri Lankan Journal of Biology* **1**: 15−26.

Huang Y., Tong C., Xu F., Chen Y., Zhang C. & Bao J. (2016). Variation in mineral elements in grains of 20 brown rice accessions in two environments. *Food Chemistry* **192**: 873−878.
   DOI: https://doi.org/10.1016/j.foodchem.2015.07.087

Imbulana L. (2006). Water allocation between agriculture and hydropower: A case study of Kalthota irrigation scheme, Sri Lanka. In: *Integrated Water Resources Management: Global Theory, Emerging Practice and Local Needs* (Eds. P.P. Mollinga, A. Dixit & K. Athukorala), pp. 219−248. Sage Publications, New Delhi, India.

Indraratne S.P. (2020). Soil Mineralogy. In: *The Soils of Sri Lanka* (Ed. R. Mapa), pp.35−48. Springer Cham, Switzerland.
   DOI: https://doi.org/10.1007/978-3-030-44144-9_4

Johnson J.M., Silva A., Senthilkumar K., Shepherd K.D. & Saito K. (2021). Application of infrared spectroscopy for estimation of concentrations of macro-and micronutrients in rice in sub-Saharan Africa. *Field Crops Research* **270**: 108222.
   DOI: https://doi.org/10.1016/j.fcr.2021.108222

Ju X.T., Xing G.X., Chen X.P., Zhang S.L., Zhang L.J., Liu X.J., Cui Z.L., Yin B., Christie P., Zhu Z.L. & Zhang F.S. (2009). Reducing environmental risk by improving N management in intensive Chinese agricultural systems. *Journal of Agricultural Sciences* **106**(9): 3041−3046.
   DOI: https://doi.org/10.1073/pnas.0813417106

Kadupitiya H.K., Madushan R.N., Rathnayake U.K., Thilakasiri R., Dissanayaka S.B., Ariyaratne M. & Suriyagoda L. (2021). Use of smartphones for rapid location tracking in mega scale soil sampling. *Open Journal of Applied Sciences* **11**: 239−253.
   DOI: https://doi.org/10.4236/ojapps.2021.113017

Kekulandara D.S., Sirisena D.N., Bandaranayake P.C.G., Samarasinghe G., Wissuwa M. & Suriyagoda L.D.B. (2019). Variation in grain yield, and nitrogen, phosphorus and potassium nutrition of irrigated rice cultivars grown at fertile and low-fertile soils. *Plant and Soil* **434**: 107−123.
   DOI: https://doi.org/10.1007/s11104-018-3663-0

Kulasinghe H.P.G.T.N., Dharmakeerthi R.S., Sirisena D.N. & Rathnayake W.M.U.K. (2020). Exploring the yield response of paddy (*Oryza sativa* L.) under varying levels of soil nitrogen, phosphorus and potassium. *Tropical Agricultural Research* **31**: 1−12.

Kumaragamage D. & Indraratne S.P. (2011). Systematic approach to diagnosing fertility problems in soils of Sri Lanka. *Communications in Soil Science and Plant Analysis* **42**: 2699−2715.
   DOI: https://doi.org/10.1080/00103624.2011.622818

Kumaragamage D. & Kendaragama K. M. A. (2010). Risk and limitations of dry zone soils. *Soils of the Dry Zone of Sri Lanka* (Eds. R.B. Mapa, S. Somasiri & A.R. Dassanayake), pp. 239−258. Soil Science Society of Sri Lanka, Peradeniya, Sri Lanka.

Lee C.H., Park C.Y., Do Park K., Jeon W.T. & Kim P.J. (2004). Long-term effects of fertilization on the forms and availability of soil phosphorus in rice rice. *Chemosphere* **56**: 299−304.
   DOI: https://doi.org/10.1016/j.chemosphere.2004.02.027

Liyanaarachchi G.V.V., Mahanama K.R.R., Somasiri H.P.P.S., Punyasiri P.A.N. & Kottawa-Arachchi J.D. (2020). Total and free amino acid contents of popular rice varieties (*Oryza sativa* L.) consumed in the capital city of Sri Lanka. *Journal of the National Science Foundation of Sri Lanka* **48**: 199−211.

DOI: http://dx.doi.org/10.4038/jnsfsr.v48i2.9565

Ma L., Duan T. & Hu J. (2020). Application of a universal soil extractant for determining the available NPK: A case study of crop planting zones in central China. *Science of the Total Environment* **704**: 135253.
DOI: https://doi.org/10.1016/j.scitotenv.2019.135253

Mapa R.B. (1992). Clay mineralogy of six Sri Lankan soils. *Journal of Geology Society of Sri Lanka* **4**: 45−47.

Maraikar S., Wijewardena J.D.H. & Amarasiri S.L. (1997). Improving productivity of vegetable cultivation in ultisols of Sri Lanka. *Proceeding of the International Conference on Managing Soil Fertility for Intensive Vegetable Production Systems in Asia*. World Vegetable Centre, Tainan, Taiwan, pp. 270−282.

Masni Z. & Wasli M.E. (2019). Yield performance and nutrient uptake of red rice variety (MRM 16) at different NPK fertilizer rates. *International Journal of Agronomy* **2019**.
DOI: https://doi.org/10.1155/2019/5134358

Moe K., Htwe A.Z., Thu T.T.P., Kajihara Y. & Yamakawa T. (2019). Effects on NPK status, growth, dry matter and yield of rice (*Oryza sativa* L.) by organic fertilizers applied in field condition. *Agriculture* **9**: 109.
DOI: https://doi.org/10.3390/agriculture9050109

Navarathna C., Pathiratne S., de Silva D.S.M., Rinklebe J., Mohan D. & Mlsna T. (2021). Intrusion of heavy metals/metalloids into rice (*Oryza sativa* L.) in relation to their status in two different agricultural management systems in Sri Lanka. *Groundwater for Sustainable Development* **14**: 100619.
DOI: https://doi.org/10.1016/j.gsd.2021.100619

Olsen S.R., Cole C.V., Watanabe F.S. & Dean L.A. (1954): *Estimation of Available Phosphorus in Soils by Extraction with Sodium Bicarbonate*, 1st edition, pp. 19. Department of Agriculture, Washington D.C., USA.

Panabokke C.R. (1989): *Irrigation Management for Crop Diversification in Sri Lanka: A Synthesis of Current Research.* International Irrigation Management Institute, Colombo, Sri Lanka. Available at *https://pdf.usaid.gov/pdf_docs/pnabf279.pdf*

Pinson S.R., Tarpley L., Yan W., Yeater K., Lahner B., Yakubova E. & Salt D.E. (2014). Worldwide genetic diversity for mineral element concentrations in rice grain. *Crop Science* **55**: 294−311.
DOI: https://doi.org/10.2135/cropsci2013.10.0656

Priya T.R., Nelson A.R.L.E., Ravichandran K. & Antony U. (2019). Nutritional and functional properties of coloured rice varieties of South India: A review. *Journal of Ethnic Foods* **6**: 1−11.
DOI: https://doi.org/10.1186/s42779-019-0017-3

Punyawardane B.V.R. (2008). *Evolution of Climatic Zones in Sri Lanka, Agro-climatological Zones and Rainfall Pattern in Sri Lanka.* pp. 44−113. Department of Agriculture, Peradeniya, Sri Lanka.

Rathnayake W.M.U.K., De Silva R.P. & Dayawansa N.D.K. (2015). Variability of some important soil chemical properties of rainfed low land paddy fields and its effect on land suitability for rice cultivation. *Tropical Agricultural Research* **26**: 506−516.
DOI: http://doi.org/10.4038/tar.v26i3.8113

Rezania M. (1993). Preliminary investigations on nutrient management of subsidiary field crop cultivation in Sri Lanka. Food and Agriculture Organization. Rome, Italy.

Rubasinghe R., Gunatilake S. & Chandrajith R. (2021). Climatic control of major and trace elements in rice soils from wet and dry regions of Sri Lanka. *Environmental Challenges* **5**: 100361.
DOI: https://doi.org/10.1016/j.envc.2021.100361

Sims J.T. (2000): Soil test phosphorus: Olsen P. (2000). In: *Methods of Phosphorus Analysis For Soils, Sediments, Residuals, And Waters* (Pierzynski G.M. Eds), pp. 20-21. North Carolina State University, Raleigh, USA.

Sirisena D. & Suriyagoda L.D. (2018). Toward sustainable phosphorus management in Sri Lankan rice and vegetable-based cropping systems: A review. *Agriculture and Natural Resources* **52**: 9−15.
DOI: https://doi.org/10.1016/j.anres.2018.03.004

Somaweera K.A.T.N., Sirisena D.N., De Costa W.A.J.M. & Suriyagoda L.D.B. (2017). Age-related morphological and physiological responses of irrigated rice to declined soil phosphorus and potassium availability. *Paddy and Water Environment* **15**: 499–511.
DOI: https://doi.org/10.1007/s11104-018-3663-0

Suriyagoda L.D.B. (2022). Rice production in nutrient-limited soils: Strategies for improving crop productivity and land sustainability. *Journal of the National Science Foundation of Sri Lanka* **50**: 521–539.
DOI: https://jnsfsl.sljol.info/articles/abstract/10.4038/jnsfsr.v50i3.10601/

Suriyagoda L.D.B., Dissanayake O., Kodithuwakku V., Maduwanthi I., Dissanayaka N. & Chandrajith R. (2022). Accumulation of essential mineral and toxic trace elements in crops and soils of vegetable cropping systems in central highlands of Sri Lanka. *The Journal of Agricultural Science* **160**(1-2): 86−97.
DOI: https://doi.org/10.1017/S0021859622000156

Suriyagoda L.D.B., Ranil R.H.G., Dissanayaka D.M.S.B. & Weerakkody W.A.P. (2012). The sustainability of intensive vegetable farming systems in Sri Lanka. International Society of Horticultural Science. *Chronica Horticulturae* **52**:14−17.

Upekshani H.A.N., Dharmakeerthi R.S., Weerasinghe P. & Dandeniya W.S., (2018): Fertilizer usage and land productivity in intensively cultivated vegetable farming systems in Sri Lanka: an analysis based on a questionnaire survey. *Tropical Agricultural Research* **30**: 44−55.
DOI: http://doi.org/10.4038/tar.v30i1.8277

Van Ranst E., Verloo M., Demeyer A. & Pauwels J.M. (1999). *Manual for the Soil Chemistry and Fertility Laboratory-Analytical Methods for Soils and Plants, Equipment, and Management of Consumables*, 1st edition, pp. 243. Ghent, Belgium.

Vinod K.K. & Heuer S. (2012). Approaches towards nitrogen- and phosphorus-efficient rice. *AoB Plants* **2012**: 28.
DOI: https://doi.org/10.1093/aobpla/pls028

Wickramasinghe L.A. (1991): Soil constraints on sustainable plant production in Sri Lanka. *Japan International Research Center for Agricultural Sciences* **24**: 12−29. Available at https://www.jircas.go.jp/sites/default/files/publication/tars/tars24-_12-29.pdf

Wickramasinghe W.M.A.D.B. 2010. Management of dry zone soils. *Soils of the Dry Zone of Sri Lanka* (eds. R.B. Mapa, S. Somasiri & A. R. Dassanayake), pp. 259−266. Soil Science Society of Sri Lanka. Peradeniya, Sri Lanka.

Wickramasinghe W.M.A.D.B., Dasanayake A.R. & Sirisena D.N. (2003): Potassium status of rice growing soils in Sri Lanka. In: *Importance of Potash Fertilizers for Sustainable Production of Plantation and Food Crops in Sri Lanka* (Eds. V.V. Nossov & J.D.H. Wijewardena), pp. 35−41. International Potash Institute, Horgen, Switzerland.
DOI: https://doi.org/10.1007/978-981-15-3673-1_10

Wijesundara W.M.G.D., Nandasena K.A. & Jayakody A.N. (2012). Spatial and temporal changes in nitrogen, phosphorus and potassium concentration in water in the thirappane tank cascade in dry zone of Sri Lanka. *Journal of Environmental Professionals Sri Lanka* **1**: 70−81.
DOI: https://dx.doi.org/10.4038/jepsl.v1i1.5143/galley/4109/download/

Ye Y.S., Liang X.Q., Li L., Yuan J. & Zhu S. (2015): Effects of different water and nitrogen managements on phosphorus loss via runoff and leaching from paddy fields in Taihu L. Taihu Lake basin. *Acta Scientiac Circumstantiac* **35**(4): 1125–1135

RESEARCH ARTICLE

Molecular Phylogeny

Rediscovery, identity, and conservation strategies of a critically endangered endemic plant, *Hedyotis quinquinervia* Thwaites (Rubiaceae) in Sri Lanka

A Gunarathne[1], HDRVL Harasgama[1], T Wijewickrama[2], AS Attanayake[2], RN Attanayake[1] and RMCS Ratnayake[1*]

[1] *Department of Plant and Molecular Biology, Faculty of Science, University of Kelaniya, Kelaniya, Sri Lanka.*
[2] *Royal Botanic Gardens, Peradeniya, Sri Lanka.*

Abstract: Sri Lanka, a biodiversity hotspot in Asia, records 30 *Hedyotis* species of which 25 species and a variety are endemic. Among these 25 species, seven *Hedyotis* species were categorized as critically endangered (CR), and 13 as endangered (EN). During our field survey in 2014, an extremely attractive plant belonging to the genus *Hedyotis* was discovered from Mount Thotupola, Sri Lanka. The plant was tentatively identified as *H. quinquinervia*. For accurate species identification, morphological characters were compared with voucher specimens, and identification keys were also used. In addition, DNA barcoding using the sequence of the internal transcribed spacer region of the nuclear ribosomal DNA (rDNA-ITS) region was performed, followed by molecular phylogenetic analysis. A simple method to remove a thick cuticle layer on the leaves was employed to obtain a sufficient amount of DNA suitable for Polymerase Chain Reaction. A comparison with its protologue and type specimen along with molecular phylogenetic analysis confirmed that the unidentified plant was *H. quinquinervia* Thwaites. The National Red List of Sri Lanka (2020) had revised *H. quinquinervia* as a CR species upon the rediscovery confirmed after the lapse of a century. Habitat characteristics, *ex situ* and *in situ* conservation measures for *H. quinquinervia,* and general conservation strategies applicable to threatened heterostylous plants are also discussed.

Keywords: Critically endangered, *Hedyotis quinquinervia,* internal transcribed spacer (ITS), Rubiaceae.

INTRODUCTION

The genus *Hedyotis* L. is one of the largest genera in the family Rubiaceae, also known as the coffee family. Five hundred to 600 species belonging to the genus *Hedyotis* are found in tropical and subtropical zones (Wikström *et al.*, 2013). Ridsdale (1998) has described 28 *Hedyotis* species found in Sri Lanka. Among them, the lesser-known endemic species *H. quinquinervia* was first described in 1859 from Mount Pedro, the tallest mountain in Sri Lanka, by Thwaites. The last available record of *H. quinquinervia* in Sri Lanka was the specimen collected and deposited in the National Herbarium, Peradeniya, Sri Lanka (PDA) by A. M. de Silva in 1906 from Mount Pedro, where four other previously collected specimens have been deposited as well. According to global red list categories and criteria (version 9) and the categories adapted at the national level (MOE, 2012), critically endangered, possibly extinct [CR(PE)] is defined as a species with no distribution records in the past 60 years. In the surveys conducted for the past 107 years, no *H. quinquinervia* plants have been found in the previously recorded location, Mount Pedro, or elsewhere. Hence, the National red list of Sri Lanka 2012 recognized *H. quinquinervia* as a critically endangered, possibly extinct [CR(PE)] species (MOE, 2012). However, based on the abstract publication of Harasgama *et al.* (2014) reporting the rediscovery of the plant in 2014, the status of CR(PE) was changed to CR in 2020 (MOE, 2020).

Species belonging to the genus *Hedyotis* show extensive variation in morphology and are often confused with the genus *Oldenlandia* (Guo *et al.*, 2013). Morphological identification of species at times could be challenging due to the morphological plasticity and overlapping characteristics of the members. Therefore, for a controversial genus like *Hedyotis*, species identity based on molecular phylogenetic relationships is more suitable (Guo *et al.*,

---

[*] Corresponding author (ratna@kln.ac.lk; https://orcid.org/0000-0002-2794-0153)

2013). A species identification method based on molecular characters, especially DNA barcoding is not affected by the age, environmental conditions, or handling and processing of the material (Kazi *et al*., 2013). However, DNA extraction from certain plant species presents great challenges at times due to the presence of various secondary metabolites and polysaccharides (Katterman & Shattuck, 1983). During DNA extraction from CR(PE) plant materials, extra care should be taken to use a minimal amount of plant materials. Therefore, molecular-based identification poses unexpected challenges at times especially when there is no or limited access to liquid N_2.

Heterostyly is a complex floral polymorphism controlled by its genetics and, is associated with self-incompatibility mechanisms (Barrett & Cruzen, 1994). Self-compatibility is rare among distylous Rubiaceae taxa (Mahadura & Saunders, 2021). Several species of the genus *Hedyotis* are heterostylous, such as *H. quinquinervia, H. brachiata* (Raju & Radhakrishna, 2018), *H. sithiravaraiensis*, *H. uncinella* (Muruganandam *et al*., 2018) and *H. caerulea* (Ornduff, 1980). *Hedyotis pulcherrima* is also a distylous species with heteromorphic self-incompatibility (Liu *et al*., 2021). Self-incompatible plant species in biodiversity hotspots of the world suffer from pollen limitation than the regions with lower biodiversity and therefore, subsequent population decline is evident. Hence, maintaining an adequate population for the long-term survival of the species is a must.

The present study was aimed at confirming the identity of *H. quinquinervia* rediscovered using morphological and molecular data and implementation of *in situ* and *ex situ* conservation strategies for this CR species. Such rediscoveries and accurate species identification have a tremendous impact on species conservation, especially on oceanic islands where geographic barriers hindered free pollen flow.

MATERIALS AND METHODS

Study area

The study site was Mount Thotupola, the third highest mountain (2,357 m) of Sri Lanka, located within the Horton Plains National Park, Central Province, Sri Lanka (summit, 6° 49.982' N - 80° 49.211' E and the bottom, 6° 50.121' N - 80° 48.634' E). Horton Plains is a gently undulating highland plateau at the southern end of the central mountain massif of the country. The weather of the sampling site is usually dominated by persistent cloud cover and strong winds, sometimes gale-force, during the southwest monsoon. The mean annual temperature is about 13 °C during the driest period of the year and night temperature drops below 5 °C. The mean total rainfall is about 2540 mm/annum (Premathilake & Risberg, 2003). The geological structure of this region is made up of highly crystalline, non-fossiliferous rocks of the Precambrian age, belonging to the Highland Series. Soil is characterized as a thick, black, organic layer at the surface, as indicated by Saroja and Gunatilake (2013). The bedrock consists of high-grade metamorphic rocks of charnockitic gneiss, quart feldspathic gneiss, hornblende biotite gneiss, quartzite, khondalite, and garnet biotite gneiss.

Vegetation sampling for the floristic structure of the study site

A sampling permit was obtained from the Department of Wildlife Conservation, Sri Lanka. To determine the floristic composition and plant species abundance on Mount Thotupola, a stratified random plot sampling method, as described by Abeywickrama (2014), was carried out in 2014. Overstorey vegetation was studied by using randomly selected 10 m × 10 m plots (Wright *et al*., 1997). To study understorey vegetation, two randomly selected 1 m × 1 m subplots were demarcated within each overstorey plot. Due to the extreme heterogeneity of the terrain, and dense scrub-type vegetation dominated by small bamboo, small square plot demarcation was relatively convenient. In transect selection for sampling plots, the direction of slope, physiognomy of the forest, and altitude were considered. Few plots were demarcated on the northern slope of the mountain, due to the steepness of the slope and the presence of a dense bamboo layer (Figure 1).
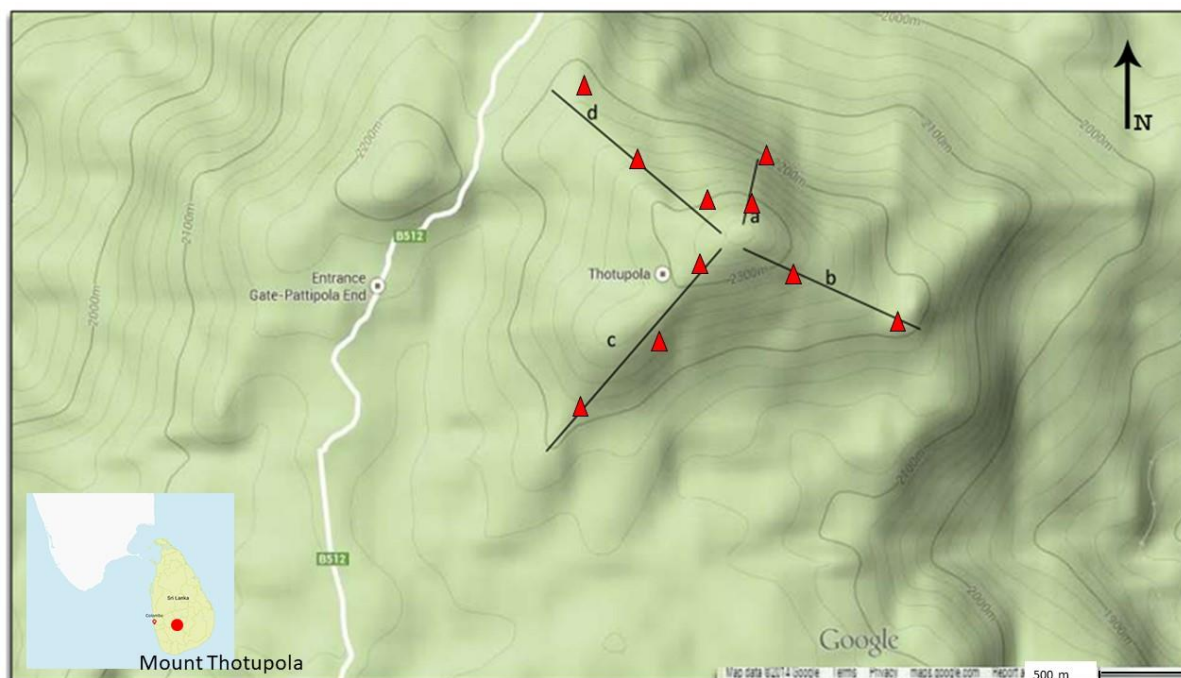
Figure 1: Distribution of overstorey and understory plots of the sampling sites in Mount Thotupola. (a) Northern slope; (b) Eastern slope; (c) Southern slope; (d) Western slope.

Field sampling covered three altitudinal ranges: lower elevation (2200 m – 2270 m), middle elevation (2270 m – 2340 m), and higher elevation (above 2340 m). The number of plots used for each elevation level is shown in Table 1. Data collection was done by both absolute (density, girth measurements, and basal area) and non-absolute (frequency) measures (Kent & Coker, 1996). Following Ratnayake *et al*. (1996) and Wright (1999), plants with girth at breast height (GBH) values ≥ 10 cm, and height > 1 m were considered as overstorey vegetation while plants below those limits were considered as understory vegetation. From each plant enumerated in each elevation level, specimens were collected and identified using identification keys and descriptions and comparison with the specimens deposited in the PDA.

Table 1: Number of over-story and understory plots sampled at each elevation level on Mount Thotupola.

Elevation (m)	No. of overstory plots	No. of understory plots
Lower (2200 - 2270)	15	30
Middle (2270 - 2340)	10	20
Higher (above 2340)	6	12
Total	31	62

Morphological identification of selected *Hedyotis* species

Among plant species found at mid-elevation, an extremely attractive plant of the genus *Hedyotis* was subjected to detailed morphological characterization following the protologue, keys, and information provided in the Revised Handbook to the Flora of Ceylon (Ridsdale, 1998). Specimens were compared with the type specimen and other specimens available at the National Herbarium, Peradeniya (PDA). Key morphological characters such as the presence of stipules and their morphology, position of the inflorescences, leaf arrangement, and leaf characteristics were examined. Herbarium specimens were prepared and deposited at the PDA (Figure 2).

Figure 2: Herbarium specimen of *Hedyotis quinquinervia* plant (Reproduced with the permission of the Director General of the Department of National Botanic Gardens, Sri Lanka). Magnification 1 x 0.5

DNA barcoding and molecular phylogeny

DNA barcoding work was done in 2019. The uprooted plant was established in the Hakgala Botanic Garden (described under conservation) and leaves were used for DNA extraction. Young leaves (n = 5) from the specimen were collected in a plastic zip-lock bag and transported to the University of Kelaniya for further studies. Leaves were surface sterilized by washing with tap water and dipping in 70% ethanol for 10 s, followed by three serial washings in sterilized distilled water. The excess water was removed using tissue papers. Leaf samples with cuticles were initially used, but it did not work well, so cuticle removal was attempted. Half of the samples were subjected to cuticle removal and the other half was used with the cuticle. Cuticle removal was done by placing a piece of clear tape on the adaxial surface of the leaf and quickly removing it so that the epidermis with the cuticle was separated from the leaf. Cuticle removal was confirmed by observing it under the microscope. Samples, with or without the cuticle, were stored at -80 °C and in silica gel at room temperature (25 °C). DNA extraction was performed using three protocols, Inglis *et al*. (2018), Guo *et al*. (2011), and modified Doyle & Doyle (1987), with varying β–mercaptoethanol concentrations, with a minimal amount of plant materials. Due to the limited amount

of material available from the desired specimen, optimization of DNA extraction was conducted with another commonly found species of the genus, *H. auricularia* L. which was recently synonymized to *Exallage auricularia* (L.) Bremek. Samples of *H. auricularia* stored in silica gel and at -80 °C were used for DNA extraction using the above three methods. The quality of DNA was determined using spectroscopic methods. Genomic DNA was subjected to polymerase chain reaction (PCR) amplification of the internal transcribed spacer (*ITS*) *region* of the nuclear *ribosomal DNA* (rDNA) using either the primer pairs, ITS1/4 (Hadi *et al.*, 2016) or P17 and 26S-82R (Popp & Oxelman, 2001). P17 and 26S-82R primers (Popp & Oxelman 2001) were specific for the ITS region of the genus *Hedyotis* (Table 2). Once the protocol was optimized, leaves of *H. quinquinervia* were used to extract DNA, which was subjected to PCR.

Table 2: Primer name, sequence, and reference used in PCR amplification of selected *Hedyotis* sp.

No.	Primer Name	Primer Sequence (5' – 3')	Reference
1	ITS 1	AGGAGAAGTCGTAACAAGGT	Hadi *et al.* (2016)
2	ITS 4	TCCTCCGCTTATTGATATGC	
3	P17	CTACCGATTGAATGGTCCGGTGAA	Popp & Oxelman (2001)
4	26S-82R	CCCGGTTCGCTCGCCGTTACTA	

The PCR reaction mixture consisted of 1X buffer, 4 mM MgCl$_2$, 0.2 mM dNTPs, 0.4 µM forward and reverse primers, and 0.25 U/µL of GoTaq® DNA polymerase (Promega, USA). The PCR reaction regime was carried out as initial denaturation for 5 min at 94 °C followed by 40 cycles of denaturation for 30 s at 94 °C followed by annealing at 55 °C for 30 s, or as described in Popp & Oxelman (2001), 1 min extension at 72 °C and final extension of 10 min at 72 °C. Amplicons were separated in 1% agarose gel using agarose gel electrophoresis (Bio-Rad, USA). Successfully amplified PCR products were subjected to Sanger bidirectional dideoxy chain termination reaction at Gen-Tech., Colombo. Sequences were manually edited using Bioedit (version 7.2.5) and compared with the authenticated or vouched for sequences available in the GenBank using the BLASTn search tool. Good sequences were deposited in the GenBank and accession numbers were obtained.

Molecular phylogenetic analysis was performed using MEGA ver. 6 software (Kumar *et al.*, 2018) to determine the phylogenetic relatedness of putatively identified *H. quinquinervia* with the other *Hedyotis* spp. available in the GenBank using ITS sequence data. Twenty-two sequences of *Hedyotis* sp. mentioned in Guo *et al.* (2011) were obtained from the NCBI database and used in the phylogenetic analyses (Table 3). *Paraknoxia parviflora* (Stapf ex Verdc.) Verdc. ex Bremek. was selected as the outgroup according to Wikström *et al.* (2013). Sequences were aligned using ClustalW (Thompson *et al.*, 1994) and the maximum likelihood method based on the Kimura-2 parameter model (Kimura, 1980) was performed as implemented in MEGA. Branch lengths were measured in the number of substitutions per site and the tree was drawn to scale. Every position that contained missing data and/or gaps were eliminated.

In situ and *ex situ* conservation of *Hedyotis quinquinervia*

In situ conservation of *H. quinquinervia* has been ensured as the location is situated within a conserved montane forest, Mount Thotupola located within Horton Plains, Sri Lanka. Officers of the Wildlife Conservation and Forest Departments of Sri Lanka, university academia, and policy decision-making bodies have been made aware of the discovery (Harasgama *et al.*, 2014). As *ex situ* conservation measures, a few individual specimens of *H. quinquinervia* were carefully root balled by trained staff of the Botanical garden, immediately transported, and transplanted in the Botanical Gardens, Hakgala, Sri Lanka in 2014, where similar climatic and weather conditions prevailed (tropical wet montane forests). The plant has been established and maintained following general plant establishment and maintenance procedures by the Hakgala Botanical Garden, Sri Lanka. In 2019, leaves from the established plant were used for molecular work described earlier. Common conservation strategies for critically endangered heterostylous plant species were also suggested.

RESULTS AND DISCUSSION

Floristic structure of the study site

Plant heights of Mount Thotupola were variable depending on the elevation of the sampling site. The maximum plant height recorded in the lower elevation was about 12 m, while the minimum height was about 1.5 m in the higher elevation. Most of the species at lower elevations had a height of 2 - 8 m. Clearly indistinguishable, two different strata were arbitrarily identified as canopy and sub-canopy. The canopy height was about 6 - 12 m in height and mostly dominated by plant species such as *Michelia nilagirica* (Zenker) Figlar, *Calophyllum walkeri* Wight, *Litsea ovalifolia* (Wight) Trimen, *Vaccinium symplocifolium* (D.Don ex G.Don) Alston, *Actinodaphne ambigua* Hook. f. and *Symplocos* spp. The sub-canopy layer was mostly dominated by the species such as *Rhododendron arboreum* Sm., *Syzygium* spp., *Hedyotis* spp., *Rhodomyrtus tomentosa* var. *parviflora* (Alston) A.J. Scott. Hook. f., *Lasianthus gardneri* (Thwaites) Hook. f. and *Osbeckia* spp.

The middle elevation was occupied by a fairly open area dominated by pigmy forests, a preliminary version of tropical upper montane forests. The vegetation at this elevation was only 1 – 5 m in height. Species such as *Elaeocarpus montanus* Thwaites, *Vaccinium symplocifolium* (D.Don ex G.Don) Alston, and *Litsea ovalifolia* (Wight) Trimen were the dominant plants, and species like *Ochlandra stridula* Thwaites, *Psychotria gardneri* Hook. f., and *Lycianthes bigeminata* (Nees) Bitter were the dominant shrubs.

The vegetation at a higher elevation was only 1 – 5 m in height, the same as at the middle elevation. The tree layer was composed of species such as *Symplocos bractealis* Thwaites and *Symplocos cochinchinensis* (Lour.) S. Moore. The shrub layer was mainly dominated by *Rhodomyrtus tomentosa* var. *parviflora* (Alston) A.J. Scott. Hook. f. and *Psychotria gardneri* var. *gardneri* (Thwaites) Hook. f. An extremely attractive plant belonging to the genus *Hedyotis* was found in the open, marshy, or wet grasslands on rocky substrates of small valleys on mountain slopes. Seasonal or non-seasonal streams associated with these valleys maintain a small seepage on the rocky substrate providing semi-aquatic conditions. Accordingly, herbaceous species, *Eriocaulon* spp. and *Neanotis nummularia* (Arn.) W.H. Lewis which prefer semi-aquatic conditions, were commonly found in the habitat. In addition, some herb or shrub species such as *Strobilanthes calycina* Nees, *Knoxia platycarpa* var. *hirsuta* (Arn.) Thwaites, *Hedyotis ceylanica* N. Wikstr. & Neupane, *Anaphalis subdecurrens* Gamble, *Emilia speeseae* Fosberg, *Osbeckia parvifolia* Arn., *Chrysopogon nodulibarbis* (Hochst. ex Steud.) Henrard, *Impatiens leptopoda* Arn., are also commonly inhabited in this herb-dominated vegetation.

Table 3: Gene sequences used in phylogenetic analyses (species, GenBank accession number, and reference).

Species	GenBank accession number	Reference
Hedyotis assimilis Tutcher	JF699903.1	Guo *et al.* (2011)
Hedyotis auricularia L.	JF699904.1	Guo *et al.* (2011)
Hedyotis biflora (L.) Lam.	JF699908.1	Guo *et al.* (2011)
Hedyotis bodinieri H. Lév.	JF699909.1	Guo *et al.* (2011)
Hedyotis cantoniensis F.C. How ex W.C. Ko	JF699912.1	Guo *et al.* (2011)
Hedyotis diffusa Hance	JF699933.1	Guo *et al.* (2011)
Hedyotis mellii Tutcher	JF699936.1	Guo *et al.* (2011)
Hedyotis ovatifolia Cav.	JF699940.1	Guo *et al.* (2011)
Hedyotis pulcherrima Dunn	JF699946.1	Guo *et al.* (2011)
Hedyotis quinquinervia Thwaites	AM939458.1	Karehed *et al.* (2008)
Hedyotis shenzhenensis Tao Chen	JF699951.1	Guo *et al.* (2011)
Hedyotis tenuipes Hemsl.	JF699960.1	Guo *et al.* (2011)
Hedyotis trichoclada Merr. & L.M. Perry	HE657714.1	Wikström *et al.* (2013)
Hedyotis trimenii Seb & Ratna Dutta	HE657716.1	Wikström *et al.* (2013)
Hedyotis uncinella Hook. & Arn.	JF699964.1	Guo *et al.* (2011)
Hedyotis verticillata Blume	JF699969.1	Guo *et al.* (2011)
Hedyotis yangchunensis W.C. Ko & Zhang	JF699972.1	Guo *et al.* (2011)
Paraknoxia parviflora (Stapf ex Verdc.) Verdc. ex Bremek.	AM267020.1	Kårehed and Bremer (2007)

Morphological identification of *Hedyotis* species

Among plant species identified in the mid-elevation of the forest, which was an open grass and rocky marsh area, an extremely attractive plant specimen (Figure 3) belonging to the genus *Hedyotis* was collected, subjected to further studies, and identified as *H. quinquinervia*. The plant is a perennial woody shrub with a height of 0.5-1 m and leaves oppositely and compactly arranged. The leaves are small (1-1.5 cm), curled, waxy, and glabrous on both surfaces. They are simple and ovate-orbicular or broadly obovate-shaped with two to three pairs of lateral nerves with five nerves appearing at the base. Leaves have entire margins and the apex is acute (Figure 3b and 3d). *Hedyotis quinquinervia* was not found at the higher and lower elevations of the forest.

Morphology of flower in relation to pollination

The flowers are arranged as terminal inflorescences with a short (0.5-1 cm) axis, which stands out prominently above the foliage (Figure 3a). The corolla is white and funnel-shaped (2 mm long). Pubescent hairs arranged as a ring are found at the throat of the corolla tube. Small, actinomorphic, bisexual sub-sessile, four-petaled flowers are heterostylous. Due to its heterostylous nature, natural self-pollination would not happen. The style of the flower is 1 - 3 mm or 4.6 mm long. Filaments of the stamens were short in pin-flowers (0.3 - 0.5 mm) and long in thrum-flowers (1-2 mm). Hence both pin and thrum floral morphs were evident. Filaments were shorter than the style favouring cross-pollination. The stigma is bi-lobed. The ovary is bi-locular. The fruits are brownish, ellipsoid small (2 - 3 × 1.5 - 2 mm) capsules with four to six brownish seeds per placenta.

Figure 3:   Rediscovered *Hedyotis quinquinervia* plant from Mount Thotupola, Sri Lanka. (a) Terminal inflorescence with each floret having four white petals; (b) and (d) Compactly arranged, curved leaves on a woody shrub; (c) Brownish ellipsoidal capsules arranged in fruit.

Conspicuous terminal inflorescence above the foliage with white flowers facilitates the attraction of pollinators as a visual cue. To prevent the entrance of floral larcenists a ring of pubescent hairs at the throat of the corolla tube is important. Heterostyly enhances the possibility of cross-pollination to increase genetic variations within a population. Heterostyly promotes outbreeding (Barrett, 1992; Barrett & Shore, 2008). The bi-lobed stigma of *H. quinquinervia* may facilitate efficient pollen attachment. Accordingly, the pollination syndrome would be

entomophilous with the help of small insects. Most of the heterostylous flowers are pollinated by insects, particularly bees, flies, moths, butterflies, and beetles (Ganders, 1979), bombyliid flies (Ornduff, 1980), and *Apis cerana*, the Asian honeybee (Mahadura, 2020). Several findings indicated that *Hedyotis* species are mainly meiophilous and pollinated by small bees (Mahadura & Saunders, 2021) as reported for *H. shenzhenensis* Tao Chen (syn. *H. shiuyingiae*), *H. acutangula* Champ. ex Benth., *H. loganioides* Benth. (also syn. *H. bodinieri* H. Lév.), and *H. vachellii* Hook. & Arn. species. Another dehiscence and stigmatic receptivity in the morning also coincide with the timing of bee foraging.

DNA barcoding and molecular phylogeny

In a recent floristic survey conducted at Mount Thotupola, *H. quinquinervia* was rediscovered. The plant was identified using morphological catalogues, comparison with authentic specimens deposited in the National Herbarium, Peradeniya, Sri Lanka (PDA), following taxonomic keys, and DNA barcoding. A field study by Prabhukumar *et al*. (2018) confirmed the identity and rediscovery of *Hedyotis beddomei* Hook. f. from the Western Ghats, India, only with morphological comparison. However, in the present study, we confirmed the identity of the species with the currently most accepted DNA technology too. Except for the limited availability of plant materials, the biggest challenge in this study was to isolate DNA without liquid N_2. DNA isolation was successful by the modified Doyle & Doyle (1987) procedure and PCR was successful with the DNA isolated. The removal of the cuticle from the leaves was critical, and the novel modified method could be applied to other plant species with a thick cuticle layer.

After several attempts and modifications of DNA extraction methods, high-quality DNA of *H. quinquinervia* was isolated by the modified method described in Doyle & Doyle (1987). The modifications were: removal of the leaf cuticle layer by the clear tape method, followed by storage at -80 ℃. In addition, the reduction of β-mercaptoethanol from 4% to 2%, and using 0.2 g of leaf material was found to be effective in obtaining a relatively high-quality DNA. OD value at 260/280 nm was 1.69 whereas all the other methods yielded below 1.4. The simple method of cuticle removal was successful, and it was evident when the stained clear tapes were observed using a light microscope. All the samples stored in silica gel gave very poor-quality DNA and were not suitable for PCR. Good ITS sequences were obtained from the above sample in both directions. The rDNA-ITS sequence was deposited at the GenBank under accession number MT373691. BLASTn analysis showed our sample was 99% similar to the sequence of the *H. quinquinervia* (AM939458.1) deposited by Karehed *et al*. (2008), from a voucher specimen that was also from Sri Lanka. The sequences have been available since 2008, from the DNA that was extracted most likely from an old herbarium specimen.

Guo *et al*. (2011) reported that in the genus *Hedyotis*, the success rate of PCR amplification of the ITS region was the greatest, whereas all the other barcoding regions (*matK, trnH–psbA, petD, rbcL* of plastid DNA) yielded the lowest amplification. Therefore, only the ITS region of *H. quinquinervia* was used in the phylogenetic analyses. The evolutionary history was inferred using the Maximum Likelihood method and Kimura 2-parameter model. The tree with the highest log likelihood (-1893.67) is shown (Figure 4). The percentage of trees in which the associated taxa clustered together is shown next to the branches. Initial tree(s) for the heuristic search were obtained automatically by applying Neighbor-Join and BioNJ algorithms to a matrix of pairwise distances estimated using the maximum composite likelihood (MCL) approach, and then selecting the topology with superior log likelihood value. The tree is drawn to scale, with branch lengths measured in the number of substitutions per site. This analysis involved 25 sequences. There was a total of 321 positions in the final dataset. Evolutionary analyses were conducted in MEGA X.

The *H. quinquinervia* sequence (MT373691) was clustered with the *H. quinquinervia* (AM939458.1) DNA barcode (Karehed *et al*. 2008) obtained from a Sri Lankan voucher specimen (Figure 3). In addition, the ML approach, NJ and maximum parsimony analyses produced the same tree topology and hence are not included. For a complete picture of the evolutionary history of our sample, a multigene approach should be applied (Guo *et al*., 2011; Wikström *et al*., 2013). However, this study was able to clarify the phylogenetic placement of *H. quinquinervia* from Sri Lanka in the genus *Hedyotis* (Salmaki *et al*., 2019).
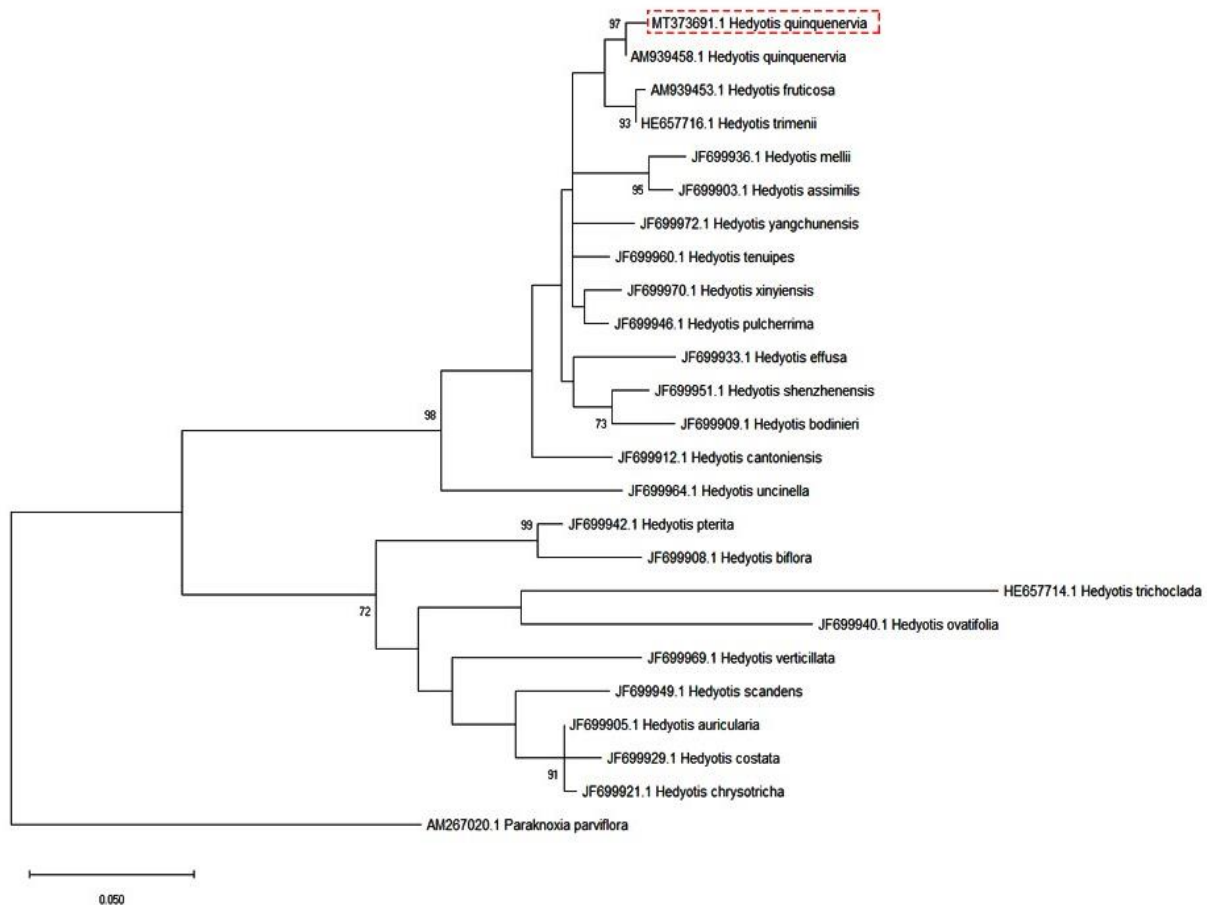
Figure 4: Phylogenetic relationships of *Hedyotis quinquinervia* with selected *Hedyotis* sp. The tree was constructed using maximum-likelihood method. The tree is drawn to scale (branch lengths proportional to evolutionary distances) and has been rooted with *Paraknoxia parviflora* (AM267020.1). Bootstrap support values are shown above branches (values > 70 are shown). Sample of the current study is in a box with a dotted line.

In-situ and *ex-situ* conservation of *Hedyotis quinquinervia*

According to the National Red List of Sri Lanka 2012, *H. quinquinervia* was a critically endangered, possibly extinct [CR(PE)] species (MOE, 2012). After the abstract publication of the same study, the status had been revised to critically endangered (CR) in 2020 (MOE, 2020). The discovery of *H. quinquinervia* at Mount Thotupola is important because it had not been found during recent floristic surveys conducted on Mount Pedro where the species had been reported more than 100 years ago (Attanayake, unpublished data). Therefore, at present, the plant is found only on Mount Thotupola. Mount Thotupola, in Horton Plains, is a conserved forest under the Department of Wildlife Conservation, which is the responsible institute for the *in situ* conservation of the species on Mount Thotupola. Due to the limited number of individuals found on Mount Thotupola, only a single plant was removed for *ex situ* conservation keeping more individuals intact in the forest for natural seedling establishment.

As per the *ex situ* conservation measures, one individual of *H. quinquinervia* was successfully transplanted to the Hakgala Botanic Garden, Sri Lanka (6.9266° N, 80.8215° E). However, as no studies are available on the reproductive biology of the species, its breeding system is not yet defined. Experimental pollination revealed that both pin and thrum flowers of *Oldenlandia salzmannii* (DC.) Benth. & Hook.f. ex B.D.Jacks. (syn. *Hedyotis salzmannii* (DC.) Steud.) are self-compatible. Karunarathne *et al.* (2005) found that three other *Hedyotis* species, *Oldenlandia corymbosa* L. (syn. *Hedyotis corymbosa* (L.) Lam.)*, Hedyotis fruticosa* L., and *Hedyotis trimenii* Deb & Ratna Dutta, are pollinated by a diverse array of hymenopterans. Based on the floral phenology, there is a high probability that *H. quinquinervia* is also entomophilous. If that is the case, the low abundance of individuals in the original site limits the probabilities of cross-pollination. That might have been one of the reasons for its

rarity and its being categorized as critically endangered (CR). Under such circumstances, the possibility of colonization by a single plant is uncertain under *ex situ* conservation, since the fecundity of the next generations after self-pollination is uncertain due to its heterostyly and the presence of two floral morphs. Therefore, the future addition of other floral morphs for *ex situ* conservation would facilitate cross-pollination and can be used in the expansion of the populations. Therefore, detailed studies of the reproductive biology and pollination biology of *H. quinquinervia* is essential. Evidence proposes that pollen limitation for reproduction is severe in plants in biodiversity hotspots than those in less diverse areas, mainly due to the response of self-incompatible species (Alonso *et al*., 2010). The given IUCN category of CR is also due to the self-incompatibility of heterostylous species in which only pin flowers can fertilize thrum flowers, and vice versa. That prevents further expansion by selfing. Most of the Rubiaceae individual plants can only have pin flowers or thrum flowers, but not both and therefore, one heterostylous rubiaceous plant in the Hakgala botanical garden is not sufficient to address *ex situ* conservation fully. Therefore, addition of a minimum of two heterostylous individuals, one pin and one thrum, are essential for effective *ex situ* conservation. According to the replanting of the plant successfully *ex situ*, future addition of another floral morph will complete the *ex situ* conservation attempt. However, the available plant can be used for attempts of vegetative propagation experiments like layering and tissue culture. There is a potential to use a derived mechanism like pre-anthesis cleistogamy which ensures reproductive assurance of a single individual conserved *ex situ,* despite potential mate and pollinator limitations for *H. quinquinervia,* as it was successfully used for *H. bodinieri* in Hong Kong by Mahadura (2020). Mahadura & Saunders (2021) found that the breakdown of self-incompatibility facilitates interspecific hybridization in *Hedyotis*. With the advancement of technology, even with a single plant, colonization may be possible.

The genus *Hedyotis* has 30 species in Sri Lanka and out of that, 25 species and a variety are endemic to the island (MOE, 2020). Seven of them are critically endangered (CR), 13 are endangered (EN), 1 each vulnerable (VU) and near threatened (NT) while only 2 are of least concern (LC) (MOE, 2020). The rediscovery of this CR species is of great interest from the conservation point of view because Sri Lanka is extraordinarily rich in biodiversity with 3087 indigenous plant species of which 863 are endemic (MOE, 2020). However, the plant is, at present, restricted to the area of Mount Thotupola. Even in the past, *H. quinquinervia* was only recorded from the natural montane forest in the central highland of Sri Lanka. For the conservation of threatened species protection of the whole ecosystem is essential. Species in biodiversity hotspots may thus be more at risk due to limited reproduction success and subsequent population decline (Alonso *et al*., 2010). Watanabe & Sugawara (2015) stated that in some oceanic islands, a shift from heterostyly to other sexual systems may occur and that contributes to the rarity of heterostyly and the difficulty in colonization of heterostylous species on oceanic islands.

The current state of its low abundance might be due to several facts, such as anthropogenic activities, global warming, alien invasive species, plant diseases, and wildfires. Rapidly spreading alien invasive species such as *Ageratina riparia* (Regel) R.M. King & H. Rob., *Ageratina adenophora* (Spreng.) R.M. King & H. Rob., *Aristea ecklonii* Baker, *Austroeupatorium* spp., and *Pennisetum* Rich. spp. (Ranwala *et al*., 2012) are a threat to the native flora, including *H. quinquinervia*. Additionally, grasslands are more prone to fire than tree vegetation. Therefore, the implementation of appropriate conservation measures is essential, not only for the protection of *H. quinquinervia* but also to conserve other endemic and native flora and fauna in the area. In distylous plants, the supergene controls a diallelic sporophytic self-incompatibility system according to Ganders (1979). This could be another reason for the resulting lack of pollen for cross-fertilization leading to the decline of the population of *H. quinquinervia*.

Grass species *Cenchrus clandestinus* (Hochst. ex Chiov.) Morrone (syn. *Pennisetum clandestinum* Hochst. ex Chiov.) and *Cenchrus geniculatus* Thunb. (syn. *P. glabarum* Steud.) in the Horton Plains National Park have been reported to be infected by the fungus *Laetisaria fuciformis* (McAlpine) Burds. causing the red thread disease (Adikaram *et al*., 2001). Such diseases might also pose a threat to the natural habitat of *H. quinquinervia*. In addition, it has been reported that a high level of Pb in soils on the slopes leads to forest die-back in the montane forests (Fernando *et al*., 2009). In addition to the global climatic changes and other reasons discussed above, wildfires might have affected the disappearance of the species. It is recommended to establish wildfire protection procedures, such as maintaining a fire belt, removing combustible materials, and frequent monitoring. As Ashton & Zhu (2020) suggested possible catastrophic restrictions on forests, and the reproduction, dispersal, and survival of species should be predicted and appropriate conservation strategies should be implemented.

CONCLUSION

During a field survey in 2014, a tentative morphology-based identification of *H. quinquinervia* was done, and it was recognized that the plant is CR(PE). The finding of this study led to the revision of the status to CR in 2020. By 2019, both *in situ* and *ex situ* conservation strategies were addressed for the species. DNA extraction was also attempted in 2019 using the conserved plant from Hakgala Botanic gardens. This extremely attractive plant was accurately identified as *H. quinquinervia* using a DNA barcoding approach. An efficient DNA extraction protocol for *H. quinquinervia* and possibly for both *Hedyotis* and *Oldenlandia* genera was developed by removing the thick cuticle, which facilitated efficient DNA extraction and PCR amplification. Pre-treatment of leaves by storing at -80 °C prior to DNA extraction was more suitable for the leaf samples than silica gel drying. This method is suitable for resource-limited settings of developing countries with no regular access to liquid N_2. The floral trials of *H. quinquinervia* are indicative of entomophilous pollination syndrome. The presence of heterostylous flowers suggests a requirement of cross-pollination between individuals. These facts need to be considered when taking conservation measures for the species.

Acknowledgement

REFERENCES

Alonso C., Vamosi J.C., Knight T.M. & Steets J.A. (2010). Is reproduction of endemic plant species particularly pollen limited in biodiversity hotspots? *Oikos* **119**: 1192–1200.
DOI: https://doi.org/10.1111/j.1600-0706.2009.18026.x

Ashton P. & Zhu H. (2020). The tropical-subtropical evergreen forest transition in East Asia: an exploration. *Plant Diversity* **42**: 255–280.
DOI: https://doi.org/10.1016/j.pld.2020.04.001

Barrett S.C.H. (1992). Heterostylous genetic polymorphisms: model systems for evolutionary analysis. In: *Evolution and Function of Heterostyly* (ed. S.C.H. Barrett), pp. 1–29. Springer, New York, USA.
DOI: https://doi.org/10.1007/978-3-642-86656-2_1

Barrett S.C.H. & Cruzan M.B. (1994). Incompatibility in heterostylous plants. In: *Genetic Control of Self-incompatibility and Reproductive Development in Flowering Plants* (eds. E.G. Williams, A.E. Clarke & R.B. Knox), pp. 189-219. Springer, Dordrecht, Netherlands.
DOI: https://doi.org/10.1007/978-94-017-1669-7_10

Barrett S.C.H. & Shore J.S. (2008). New insights on heterostyly: comparative biology, ecology, and genetics. In : *Self-incompatibility in Flowering Plants – Evolution, Diversity, and mechanisms* (Ed. V.E. Franklin-Tong), pp. 3–32. Springer, Berlin, Germany.
DOI: https://doi.org/10.1007/978-3-540-68486-2_1

Doyle J.J. & Doyle J.L.A. (1987). Rapid DNA isolation procedure for small quantities of fresh leaf tissue. *Phytochemical Bulletin* **19**: 11–15.

Fernando G.W.A.R., Ranasinghe P., Wimalasena M.D.N.R. & Ekanayake S.P. (2009). Dieback in tropical montane forests of Sri Lanka: anthropogenic or natural phenomenon? *Journal of the Geological Society of Sri Lanka* **13**: 27–52.

Ganders F. (1979). The biology of heterostyly. *New Zealand Journal of Botany* **17**(4): 607–635.
DOI: https://doi.org/10.1080/0028825X.1979.10432574

Guo X., Simmons M., But P., Shaw P. & Wang R. (2011). Application of DNA barcodes in *Hedyotis* L. (Spermacoceae, Rubiaceae). *Journal of Systematics and Evolution* **49**(3): 203–212.
DOI: https://doi.org/10.1111/j.1759-6831.2011.00130.x

Guo X., Wang R., Simmons M., But P. & Yu J. (2013). Phylogeny of the Asian Hedyotis–Oldenlandia complex (Spermacoceae, Rubiaceae): Evidence for high levels of polyphyly and the parallel evolution of diplophragmous capsules. *Molecular Phylogenetics and Evolution* **67**(1): 110–122.
DOI: https://doi.org/10.1016/j.ympev.2013.01.006

Hadi S., Santana H., Brunale P., Gomes T., Oliveira M., Matthiensen A., Oliveira M., Silva F. & Brasil B. (2016). DNA barcoding green microalgae isolated from Neotropical Inland Waters. *PLOS ONE* **11**(2).
DOI: https://doi.org/10.1371/journal.pone.0149284

Harasgama H.D.R.V.L., Wijewickrama T., Ratnayake R.M.C.S. & Attanayake A. (2014). Rediscovery of *Hedyotis quinquinervia* Thwaites (Rubiaceae): a critically endangered shrub from Horton Plains, Sri Lanka. *Proceedings of the 19ᵗʰ International Forestry and Environment Symposium,* 24- 25 October. University of Sri Jayewardenpura, Sri Lanka, pp. 24.

Inglis P., Pappas M., Resende L. & Grattapaglia D. (2018). Fast and inexpensive protocols for consistent extraction of high-quality DNA and RNA from challenging plant and fungal samples for high-throughput SNP genotyping and sequencing applications. *PLOS ONE* **13**(10): e0206085.
DOI: https://doi.org/10.1371/journal.pone.0206085

Kårehed J. & Bremer B. (2007). The systematics of Knoxieae (Rubiaceae)-molecular data and their taxonomic consequences. *Taxon* **56**(4): 1051–1076.
DOI: https://doi.org/10.2307/25065904

Karehed J., Groeninckx I., Dessein S., Motley T. & Bremer B. (2008). The phylogenetic utility of chloroplast and nuclear DNA markers and the phylogeny of the Rubiaceae tribe Spermacoceae. *Molecular Phylogenetics and Evolution* **49**(3): 843–866.
DOI: https://doi.org/10.1016/j.ympev.2008.09.025

Karunarathne I., Edirisinghe J. & Gunatilleke C.V.S. (2005). Floral relationships of bees in selected areas of Sri Lanka. *Ceylon Journal of Science* **34**: 27–45.

Katterman F.R.H. & Shattuck V.I. (1983). An effective method of DNA isolation from the mature leaves of *Gossypium* species that contain large amounts of phenolic terpenoids and tannins. *Preparative Biochemistry and Biotechnology* **13**: 347–359.
DOI: https://doi.org/10.1080/00327488308068177

Kazi T., Hussain N., Bremner P., Slater A. & Howard C. (2013). The application of a DNA-based identification technique to over-the-counter herbal medicines. *Fitoterapia* **87**: 27–30.
DOI: https://doi.org/10.1016/j.fitote.2013.03.001

Kent M. & Coker P. (1996). *Vegetation Description and Analysis: A Practical Approach*, pp. 363. John Wiley, New York, USA.

Kumar S., Stecher G., Li M., Knyaz C. & Tamura K. (2018). MEGA X: Molecular evolutionary genetics analysis across computing platforms. *Molecular Biology and Evolution* **35(6)**: 1547–1549.
DOI: https://doi.org/10.1093/molbev/msy096

Liu X., Wu X. & Zhang D. (2021). Distyly and heteromorphic self-incompatibility of *Hedyotis pulcherrima* (Rubiaceae). *Biodiversity Science* **20**(3): 337–347.
DOI: https://doi.org/10.3724/SP.J.1003.2012.11243

Mahadura A.D. (2020). Mating systems in sympatric *Hedyotis* species (Rubiaceae) in Hong Kong: the breakdown of distyly and its impact on hybridization and self-fertilization. *M. Phil thesis*, University of Hong Kong, China.

Mahadura A.D. & Saunders R.M.K. (2021). Correlation of self- and interspecific incompatibility among sympatric *Hedyotis* species (Rubiaceae) and consequences for hybridization. *Journal of Systematics and Evolution*: **60**: 998–101.

MOE (2012). *The National Red List 2012 of Sri Lanka- Conservation Status of the Fauna and Flora,* pp. 324. Ministry of Environment, Colombo, Sri Lanka.

MOE (2020). *The National Red List 2020- Conservation Status of the Flora of Sri Lanka*, pp. 153. Ministry of Environment, Colombo, Sri Lanka.

Muruganandam S., Devanathan K., Ravikumar S. & Narasimhan D. (2020). *Hedyotis sithiravaraiensis* (Rubiaceae): a new species from Southern India. *Journal of Asia-Pacific Biodiversity* **13**(4): 749–754.
DOI: https://doi.org/10.1016/j.japb.2020.08.003

Ornduff R. (1980). Heterostyly, population composition, and pollen flow in *Hedyotis caerulea*. *American Journal of Botany* **67**(1): 95–103.
DOI: https://doi.org/10.1002/j.1537-2197.1980.tb07627.x

Prabhukumar K., Jagadeesan R., Aiswarya P., Sunil C., Thomas V., Prasad K. & Balachandran I. (2018). On the identity and rediscovery of *Hedyotis beddomei* Hook. f. (Rubiaceae): a lesser known endemic species of Western Ghats, India. *Phytotaxa* **375**(3): 229–234.
DOI: https://doi.org/10.11646/phytotaxa.375.3.5

Popp M. & Oxelman B. (2001). Inferring the history of the polyploid *Silene aegaea* (Caryophyllaceae) using plastid and homoeologous nuclear DNA sequences. *Molecular Phylogenetics and Evolution* **20**(3): 474–481.
DOI: https://doi.org/10.1006/mpev.2001.0977

Premathilake R. & Risberg J. (2003). Late quaternary climate history of the Horton Plains, central Sri Lanka. *Quaternary Science Reviews* **22**(14): 1525–1541.
DOI: https://doi.org/10.1016/S0277-3791(03)00128-8

Raju A.J.S. & Radhakrishna J. (2018). Pollination ecology of the annual herb, *Hedyotis brachiata* (Rubiaceae). *Annali di Botanica* **8**: 9–16.

Ranwala S., Marambe B., Wijesundara D. & Silva P. (2012). Post-entry risk assessment of invasive alien flora of Sri Lanka - present status, gap analysis, and the most troublesome alien invaders. *Pakistan Journal of Weed Science* **18**: 863–871.

Ratnayake R.M.W., Jayasekara L.R. & Solanaarachchi S.M. (1996). A quantitative study of overstory vegetation of an upper montane rain forest. *The Sri Lanka forester* **22**(3,4): 43–49.

Ridsdale C.E. (1998). Hedyotis. In: *A revised handbook to the flora of Ceylon- volume 12* (Ed. M.D. Dassanayake) pp. 238–268. A.A. Balkema, Rotterdam, Netherlands.

Salmaki Y. & Müller J. (2019). Rediscovery of the enigmatic *Scutellaria xylorrhiza* (Scutellarioideae; Lamiaceae) - a rare endemic species from Iran. *Phytotaxa* **394**(4): 267–275.
    DOI: https://doi.org/10.11646/phytotaxa.394.4.4

Saroja K.G.N. & Gunatilake J. (2013). Compilation of detailed geological map and soil geochemical maps for Horton Plains National Park. *Proceedings of 29ᵗʰ Technical Sessions of Geological Society of Sri Lanka.* Colombo, Sri Lanka, pp. 79–82.

Thompson J., Higgins D. & Gibson T. (1994). CLUSTAL W: improving the sensitivity of progressive multiple sequence alignment through sequence weighting, position-specific gap penalties and weight matrix choice. *Nucleic Acids Research* **22**(22): 4673–4680.
    DOI: https://doi.org/10.1093/nar/22.22.4673

Thwaites G.H.K. (1859). *Enumeratio Plantarum Zeylaniae.* William Pamplin, Soho Square, London, UK.

Watanabe K. & Sugawara T. (2015). Is heterostyly rare on oceanic islands? *Annals of Botany* **7**: 1–16.
    DOI: https://doi.org/10.1093/aobpla/plv087

Wikström N., Neupane S., Kårehed J. & Motley T.J. (2013). Phylogeny of *Hedyotis* L. (Rubiaceae: Spermacoceae): redefining a complex Asian Pacific assemblage. *Taxon* **62**(2): 357–374.

Wright S.J. (1999). Plant diversity in tropical forests. In: *Handbook of Functional Plant Ecology* (Eds F.I. Pugnaire & F. Valladares), pp. 449–472. Dekker, New York, USA.
    DOI: https://doi.org/10.12705/622.2

RESEARCH ARTICLE

Environmental Toxicology

Single and combined effect of fluoride and hardness of drinking water on nephrotoxicity: *in-vivo* study using Wistar rats as an animal model

KT Dilrukshi[1,2], DH Beneragama[3], TS Suresh[4], JKP Wanigasuriya[5] and PM Manage[1,2*]

[1] *Centre for Water Quality and Algae Research, Department of Zoology, Faculty of Applied Sciences, University of Sri Jayewardenepura, Gangodawila, Nugegoda, 10250, Sri Lanka.*

[2] *Faculty of Graduate Studies, University of Sri Jayewardenepura, Gangodawila, Nugegoda, Sri Lanka.*

[3] *Department of Pathology, Faculty of Medical Sciences, University of Sri Jayewardenepura, Gangodawila, Nugegoda, Sri Lanka.*

[4] *Department of Biochemistry, Faculty of Medical Sciences, University of Sri Jayewardenepura, Gangodawila, Nugegoda, Sri Lanka.*

[5] *Centre for Kidney Research, Department of Medicine, Faculty of Medical sciences, University of Sri Jayewardenepura, Gangodawila, Nugegoda, Sri Lanka.*

Abstract: Drinking water in areas with a high prevalence of chronic kidney disease of unknown aetiology (CKDu) in Sri Lanka, is known to have high concentrations of fluoride and hardness. The present study evaluated the individual and combined effects of water hardness and fluoride on potential nephrotoxicity, using Wistar rats as an animal model. Thirty-five Wistar rats were randomly assigned into five groups (n=7). Test groups F, H, RL, and RH were given de-ionized water containing 1.5 mg/L fluoride, 200 mg/L hardness, 1.5:200 mg/L fluoride: hardness, and 5:800 mg/L fluoride: hardness respectively, while control group C was given de-ionized water. Body weight and daily water consumption were measured. Serum creatinine, urine creatinine, and urinary biomarker KIM-1 were analyzed. Histopathological changes in the kidneys were observed. There were no significant differences in body weights ($p > 0.05$) while daily water consumption was reduced significantly in the test groups RL and RH ($p < 0.05$). A significant increment in serum creatinine in the RL and RH groups ($p < 0.05$), and a significant reduction in urine creatinine in the F, H, RL and RH groups ($p < 0.05$), were recorded compared to the control. However, the highest magnitude of the effect on serum creatinine and urine creatinine was recorded in the RL group. Significant increment in KIM-1 levels were recorded in the RH group ($p < 0.05$) while the RH group indicated a more rapid increment from the 28th day. When considering histopathology, renal tubular changes were observed in the test groups. The individual and combined effects of water hardness and fluoride may contribute to the aetiology of CKDu in Sri Lanka.

Keywords: CKDu, combined effect, fluoride, hardness, *in-vivo*, nephrotoxic effect.

INTRODUCTION

Chronic kidney disease (CKD) is a significant public health concern. It is the 12th major cause of death and the 17th leading cause of disability worldwide (Veerappan & Abraham, 2013). Though conventional CKD is caused by traditional risk factors such as diabetes, hypertension, and high cholesterol, chronic kidney disease of unknown aetiology (CKDu) appears to be a new form of CKD as it is not associated with the conventional risk factors listed above (Gifford *et al.*, 2017). The prevalence of CKDu has been on the rise in Sri Lanka for the past two decades. First reported in the North Central Province of Sri Lanka, the disease later spread to North Western, Uva, Eastern, and Northern Provinces (Athuraliya *et al.*, 2011; Wanigasuriya, 2014). CKDu remains concentrated in the country's dry zone regions (Wanigasuriya, 2014).

Considering the discrete geographical locations, risk factors for CKDu, and clustering of cases, CKDu was postulated to be an environmental disease (Wanigasuriya *et al.*, 2007). It was hypothesized that CKDu in Sri Lanka is partially attributed to groundwater, which is the primary source of drinking water in CKDu endemic districts. Drinking water in areas with a high prevalence of CKDu is known to have a high concentration of fluoride and hardness. Further, heavy metals, cyanotoxins, pesticides, and fertilizers are under investigation as potential risk factors.

The fluoride anion has the smallest radius and atomic weight of all the halogens, which facilitates entry into cells, easily. Fluorine toxicity may be exacerbated in soft tissues since they lack the buffer factors found in bones, where apatite is considered to be the factor that neutralizes fluoride ions (Birkner *et al*., 2006). Furthermore, kidneys, which are responsible for efficient fluoride excretion, play an important role in fluoride regulation (Cárdenas-González *et al*., 2013). The recommended value for the concentration of fluoride in drinking water by the World Health Organization is 1.5 mg/L while, the Sri Lanka Standard Institute (SLSI) guidelines recommend a 1 mg/L value for the concentration of fluoride in drinking water (WHO, 1993; SLS 614: 2013).

Water with a high concentration of calcium and magnesium ions, is generally indicated as hard water. Other dissolved metals, such as aluminum, barium, strontium, iron, zinc, and manganese, can cause hardness in the form of divalent or multivalent cations. Even though hard water has no known adverse health impacts, it could significantly supplement total calcium and magnesium intake (Galan *et al*., 2002). Health implications of intake of hard water are primarily attributable to its salts, mainly calcium and magnesium. More than 75% of kidney stones are calcium salts, which frequently appear as calcium oxalate and less commonly as calcium phosphate (Sengupta, 2013).

Existing evidences suggest that the combination of fluoride and hardness in ground water may contribute to the aetiology of CKDu in Sri Lanka. This hypothesis is due to the overlap of geographical distribution of fluoride and hardness in ground water and the CKDu prevalent regions in Sri Lanka. The areas with high CKDu prevalence such as Anuradhapura (18.9%) and Polonnaruwa (13.9%), (Kafle *et al*., 2019) have recorded high concentrations of both fluoride (Anuradhapura >2 mg/L, Polonnaruwa > 1 mg/L) (Chandrajith *et al*., 2011) and hardness (Anuradhapura 241-300 mg/L, Polonnaruwa 181-240 mg/L) (Indika *et al*., 2022). The wet zone areas are identified as CKDu non- prevalent areas and they have recorded low concentrations of both fluoride and hardness (Chandrajith *et al*., 2011). Although, Ampara district has been highlighted as an area with high fluoride concentrations (1.0 -1.5 mg/L), the level of hardness of water as well as the CKDu prevalence was recognized in minute levels (Ranasinghe *et al*., 2019). Furthermore, Jaffna and Mannar districts have recorded high hardness values while the concentration of fluoride in the ground water (<0.5 mg/L) and the CKDu prevalence was very low (Chandrajith *et al*. 2011; Ranasinghe *et al*., 2019).

According to the studies so far, the multifactorial effect of water chemistry, emphasizing fluoride and hardness, is considered substantial. Based on the findings mentioned above, the present study seeks to evaluate the *in-vivo* single and combined effects of fluoride and hardness in drinking water utilizing Wistar rats model as an animal model.

MATERIALS AND METHODS

Ethics approval

The Ethics Review Committee of the Institute of Biology, Sri Lanka (ERCIOBSL 194062019) granted ethical permission for the experimental procedure. The animal experimental procedures were carried out in accordance with their guidelines on housing, husbandary, animal care, and monitoring, as well as the guidelines laid down by European Community Directive 86/609/EEC were followed during the experiment.

The experiments employed *Rattus norvegicus*, Wistar strain (origin: CLEA, Japan) bred at the Animal Centre in Medical Research Institute (MRI), Sri Lanka, under microbiologically controlled conditions. Thirty-five (35) male Wistar rats, aged eight weeks and weighing 150-250 g, were recruited for the study. The rats were allowed to acclimatize to the animal house settings for 8-10 days. The Animal House conditions maintained during the study period were; 12:12 hour light-dark cycle, temperature of 25-26°C, and humidity of 40–70%. Furthermore, standard rat cages of $1500 \, cm^2 \times 24 \, cm$ were used, with autoclaved wooden shavings as bedding material and two animals were housed in each rat cage. A standard pellet diet for the Wistar rats was prepared with locally available food ingredients. Considering the CKDu prevalence among the human population, recorded evidence showed high incidents in males (Ruwanpathirana *et al*., 2019; Pett *et al*., 2022). Therefore, considering previous literature, male animals were recruited for the current experiment (Ruwanpathirana *et al*., 2019; Pett *et al*., 2022).

Chemicals

Sodium fluoride (NaF) with ≥ 99 % purity, Calcium carbonate (CaCO$_3$) with ≥ 99 % purity, and Magnesium chloride (MgCl$_2$) with ≥ 98 % purity, were purchased from Sigma Aldrich, USA and these were dissolved in de-ionized water to prepare the fluoride and hard water samples which were given to rats.

Design of the experiment

The experiment utilized de-ionized water and laboratory-made water samples to evaluate the individual and combined effects of water hardness and fluoride on the kidneys of rats. A water sample with a fluoride concentration of 1.5 mg/L was used to test the effect of fluoride, while a water sample with a hardness concentration of 200 mg/L was used to test the effect of water hardness. Two mixtures having fluoride: hardness concentration combinations of 1.5:200 and 5.0:800 mg/L, were used to detect the combined effect of fluoride and hardness. The ratio between Ca^{2+} to Mg^{2+} used to prepare drinking water with 200 mg/L and 800 mg/L total hardness was 4:1, according to the recommendations of the Organization for Economic Cooperation and Development (OECD, 1992) and the ratio was associated with the Ca^{2+} and Mg^{2+} content in drinking water sources in CKDu prevalent areas. The treated concentrations were selected considering the average concentration distributions of fluoride and hardness in CKDu prevalent areas as well as the recommended concentration levels specified by WHO and SLSI for drinking water.

After ten days of acclimatization, 35 rats were divided into five groups, each with seven rats (C, F, H, RL, and RH). Before treatment, the weights of the rats were recorded and used as baseline body weights. The control group (C) received de-ionized water daily. Group F received 1.5 mg/L of NaF dissolved in de-ionized water daily, while group H received 200 mg/L of CaCO$_3$ and MgCl$_2$ dissolved in de-ionized water daily. Group RL received NaF, CaCO$_3$, and MgCl$_2$ dissolved in de-ionized water at fluoride: hardness concentrations of 1.5:200 mg/L daily, whereas group RH received NaF, CaCO$_3$, and MgCl$_2$ dissolved in de-ionized water at fluoride: hardness concentrations of 5.0:800 mg/L daily. Water samples were given to all of the groups for a duration of 90 days and each individual rat was allowed access to water from the respective water samples ad libitum.

Sample size calculation

Sample size per group = 2 SD^2 (Z$_{α/2}$ +Z$_β$)^2/d^2 (Charan & Kantharia, 2013).
SD - Standard deviation from previous study by Thammitiyagodage *et al*., 2017
Z$_{α/2}$ = Z$_{0.05/2}$ = Z$_{0.025}$ = 1.96 (From Z table) at type 1 error of 5%
Z$_β$ = Z$_{0.20}$ = 0.842 (From Z table) at 80% power
d = effect size = difference between mean value
Hence,
Sample size   = 2 SD^2 (1.96 + 0.842)^2 / d^2
              = 2 (10.37)^2 (1.96 + 0.842)^2/17^2
              = 5.84 ~ 6
Expected attrition or death of animals: 10%
For 10% attrition (6/0.9 = 6.7) **~ 7**

Bodyweight gain, absolute weight, and relative organ weights

During the experiment, the body weights of each group of rats were recorded twice a week. The final body weight of each rat was measured on the day of sacrifice, and the bodyweight gain was calculated by subtracting the final body weight from the initial body weight. The absolute and relative organ weights were determined.

$$Relative\ organ\ weight = \frac{Fresh\ organ\ weight\ (g)}{Body\ weight\ (g)} \times 100$$

Sample collection

Blood: Blood was drawn from the lateral tail vein (Lee & Goosens, 2015) of rats that had been anesthetized using CO_2 anaesthesia and placed in a rat holder. At days 0, 7, 14, 28, 42, 60, and 90, blood samples were drawn with 27 gauge needles and 1 mL syringers. After performing cardiac punctures on the animals, the final blood samples were taken. After centrifugation at 5000 rpm for 5 min, the serum was separated from the blood and kept at –20 °C until it was used for serum biochemistry analysis.

Urine: Each rat was placed in a metabolic cage for 24 h to collect urine at days 0, 7, 14, 28, 42, 60, and 90 which were stored at -80 °C until the analysis was completed.

Urine analysis and serum biochemistry

The levels of creatinine in the urine of each rat were measured using commercially available creatinine - Jaffe multifunctional reagents (DiaSys Diagnostic Systems, Germany). KIM-1 was tested as a urinary biomarker to diagnose acute kidney damage using the urine samples collected. The expression of KIM-1 was evaluated using an ELISA kit from Elab Science, USA (Catalog Number: E-EL-R3019). Quality assurance and quality control measures were followed to assure the precision of the serum biochemistry and urine tests. Sampling procedure, sampling plan, transportation, storage, and sample analysis were well planned prior to the study and quality control samples were maintained. Furthermore, calibration curves, and check lists were prepared and measurements on two different instruments were obtained for accurate readings.

Histopathology

After 90 days, the rats were euthanized using CO_2 anaesthesia and final blood samples were taken after sacrificing the animals by performing cardiac punctures. Each rat was dissected, the kidneys removed, and the removed kidneys were weighed on a digital scale. Each kidney was bi-valved, and both cut surfaces were examined for colour changes, necrosis, or fibrosis. Kidney tissues were fixed in 10% formalin for 24-48 h and then dehydrated in a series of ethanol concentrations and cleared by using xylene. The tissues were then paraffin-embedded. Hematoxylin and Eosin stains were used to stain kidney tissues and the slides were examined under a light microscope. The significant levels of renal histological lesions were graded using scoring classification defined by Toblli *et al.*, (2019) and the lesions were classified as mild, moderate, and severe. All histopathological studies were conducted at the Department of Pathology, Faculty of Medical Sciences, University of Sri Jayewardenepura, Sri Lanka.

The animals were disposed of according to the guidelines of the Animal House of the Faculty of Medical Sciences, University of Sri Jayewardenepura, and were buried at a designated location.

Statistical analysis

The data are presented as means and standard deviations. One-way analysis of variance (ANOVA) was used to detect the levels of statistical significance between groups with a $p < 0.05$ limit. Furthermore, Tukey's test was used to compare means of different treatment groups. The Minitab 14 statistical software package for Windows was used for statistical calculations.

RESULTS AND DISCUSSION

The present study explored the individual and combined effects of fluoride and hardness as a novel hypothesis on CKDu aetiology. There is a geographic correlation of high CKDu prevalence regions and drinking water with high concentrations of both fluoride and hardness suggesting a combined effect of fluoride and hardness on nephrotoxicity (Water Resources Board, Sri Lanka 2016; Dissanayake & Chandrajith, 2017). Chandrajith *et al.*, (2011) argued that the cytotoxicity effect of fluoride appears to be the effect of Na^+ and Ca^{2+} ratio of the ingested water on the F^- metabolism. Acute tubular injury with elevated serum creatinine was observed in rats fed with hard water with high fluoride content, and the changes were minimized by administration of distilled water (Perera *et al.*, 2020).

In this study, the weight gain of the animals, which is a toxicological indicator, was assessed. The body weights of rats in all the groups increased gradually during the experiment, with no significant differences (p>0.05) in weight gain between the treated groups compared with the control group (Figure 1). The body weights gradually increased until the 12th week, after which they remained at the same level.
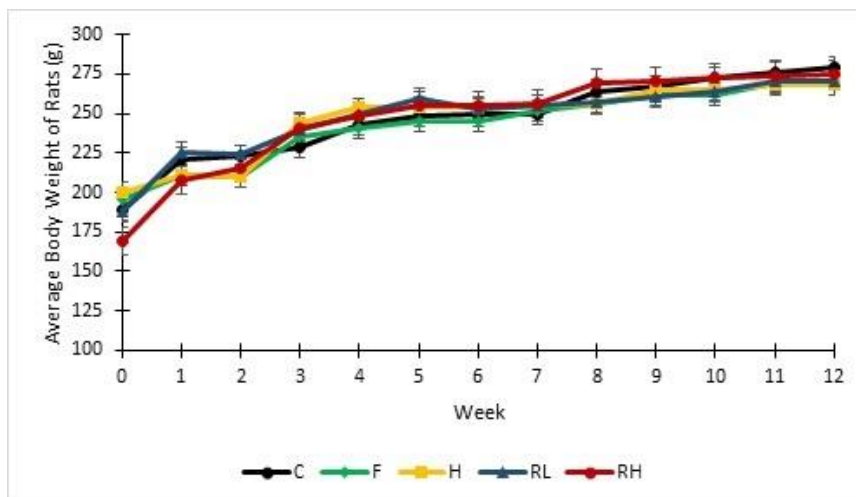

Figure 1: Variation in body weight of rats treated with de-ionized water and test water ad-libitum for 90 days. Data are presented as mean ± SD. (N=7). C- control, F- group for 1.5 mg/L fluoride alone, H - group for 200 mg/L hardness alone, RL - group for fluoride: hardness concentration of 1.5:200 mg/L, RH - group for fluoride: hardness concentration of 5:800 mg/L

Previous studies have shown that a reduction in organ weight was associated with chemically‑ induced organ damage. To assess the effect of fluoride and hardness on the kidneys, the relative organ weights of the kidneys (organ weight to body weight ratio) was measured. Compared to the control group, the absolute and relative weight of both right and left kidneys in the RL and RH groups were marginally higher at the end of the experiment however, it is not statistically significant (p>0.05) (Table. 1).

Table 1: Absolute and relative weight of kidneys of rats treated with de-ionized water and test water ad-libitum for 90 days.

	Right kidney		Left kidney	
	Absolute weight	Relative weight	Absolute weight	Relative weight
C	0.68 ± 0.04	0.24 ± 0.01	0.68 ± 0.02	0.24±0.01
F	0.69 ± 0.04	0.26 ± 0.02	0.68 ± 0.05	0.25±0.03
H	0.66 ± 0.06	0.23 ± 0.01	0.65 ± 0.04	0.23±0.01
RL	0.70 ± 0.02	0.25 ± 0.01	0.70 ± 0.03	0.25±0.01
RH	0.74 ± 0.03	0.26 ± 0.01	0.76 ± 0.02	0.27±0.01

Data are presented as mean ± SD. (N=7). (C- control, F - group for 1.5 mg/L fluoride alone, H - group for 200 mg/L hardness alone, RL - group for fluoride: hardness concentration of 1.5:200 mg/L, RH - group for fluoride: hardness concentration of 5:800 mg/L)

Toxicological studies done in animals have shown that decrease in weight gain precedes organ damage and the development of other clinical signs (Chapman *et al*., 2013). In the current study, there was no significant difference in body weight gain between the test groups and the control group, indicating that fluoride and hardness had no effect on weight gain in rats during the 90-day experiment. Previous studies have shown that chemical toxicity was associated with changes in body weight gain and the organ weight in experimental animals (Manage *et al*., 2009; Lazic *et al*., 2020). A decrease in kidney weight has been linked to renal toxicity, chronic progressive nephropathy, and tubular hypertrophy (Hard *et al*., 2013). The results of this study showed a slight increase in the

relative weights of both right and left kidneys in the test groups F, RL, and RH, as well as a slight decrease in the H group, suggesting that there was no significant effect on the kidneys of rats in the treated groups compared to the control group. Furthermore, compared to the control group, the difference in body weight gain, absolute weight, and relative weight of kidneys was not statistically significant ($p > 0.05$). Perera *et al*., (2020) found no significant differences in the relative weight of kidneys in the treated group compared to the control group after treating test water samples collected from Mihintale with high concentrations of hardness and fluoride and normal samples collected from Kandy. A study done by Wasana *et al*., (2017) using ICR female mice to evaluate the synergistic effects of the heavy metals arsenic, aluminium, hardness, and fluoride in water on kidneys, showed a weight loss in all the treatment groups while a weight gain was observed in the control group.

Rats were routinely examined for behavioral changes such as salivation, cannibalism, lethargy. However, no significant behavioral changes were noticed in any group of rats throughout the experimental period. The Tukey's pairwise comparisons indicate that the differences in the daily water consumption of the rat groups F and H were not significantly different from the control ($p > 0.05$) while the RL and RH groups were significantly different ($p < 0.05$). According to the results of the present study, water consumption in test groups were lower than the control group and the RL and RH groups indicated a prominent reduction in the daily water consumption during the experiment (Figure 2). According to the findings of the study conducted by Wasana *et al*., (2017) to examine the synergistic effect of heavy metals, fluoride, and hardness, no significant differences in the volume of water consumed by mice in the test and control groups were observed. However, a study done by Siglin *et al*., (2000) evaluated the subchronic toxicity of environmental contaminant perchlorate in Sprague-Dawley rats and revealed occasional significant reductions in consumption of water by rats over 90 days.
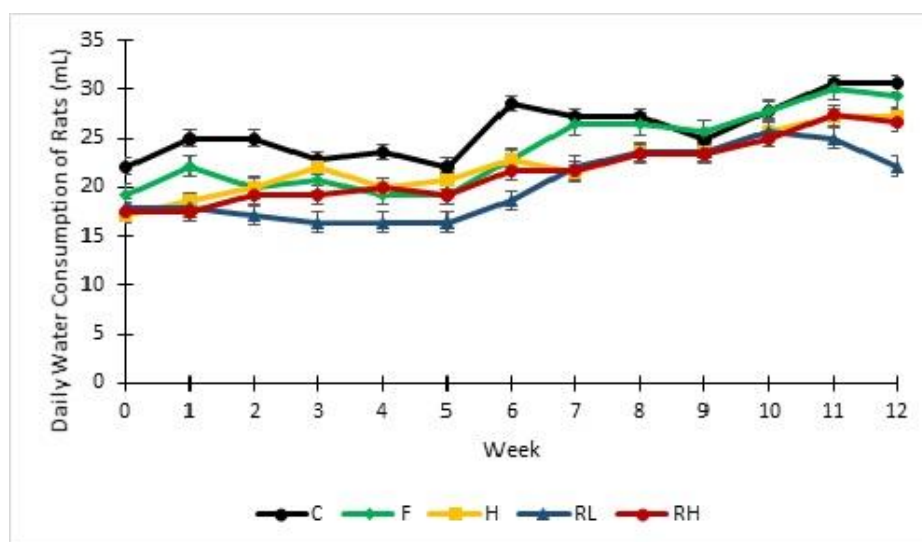

Figure 2: Variation in daily water consumption of rats treated with de-ionized water and test water ad-libitum for 90 days. Data are presented as mean ± SD (N=7). C- Control, F - group for 1.5 mg/L fluoride alone, H - group for 200 mg/L hardness alone, RL - group for fluoride: hardness concentration of 1.5:200 mg/L, RH - group for fluoride: hardness concentration of 5:800 mg/L

In this study, serum creatinine was used as a marker of renal function in rats. The Tukey's pairwise comparisons indicate that the differences in the increment of the serum creatinine level of the rat groups F and H were not significantly different from the control ($p > 0.05$) while the RL and RH groups were significantly different ($p < 0.05$). The magnitude of the increment in serum creatinine levels in group F, H, RL and RH were 64.65%, 59.60%, 85.49% and 80.56% respectively at the end of the experiment. According to the results, the serum creatinine levels increased notably in RL and RH than the F and H groups in the present study (Figure 3).
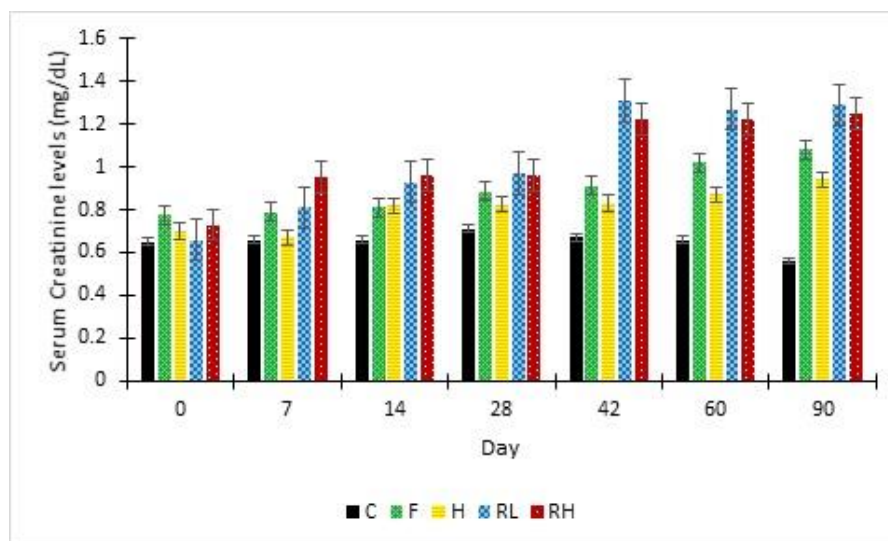
Figure 3: Variation in serum creatinine levels of rats treated with de-ionized water and test water ad-libitum for 90 days. Data are presented as mean ± SD (N=7). C- control, F - group for 1.5 mg/L fluoride alone, H - group for 200 mg/L hardness alone, RL - group for fluoride: hardness concentration of 1.5:200 mg/L, RH - group for fluoride: hardness concentration of 5:800 mg/L

Creatinine is a waste product formed when creatine phosphate is broken down in muscle tissue and excreted in urine after limited tubular reabsorption (Brisco *et al*., 2016). The accumulation of creatinine in the blood can occur due to renal dysfunction, and elevated serum creatinine level is a marker of renal impairment (Al Salhen & Mahmoud, 2016). The results of this study indicate an increment in serum creatinine levels in all the treated groups compared to the control group, suggesting renal dysfunction in the test groups. However, the RL and RH groups had a greater elevation in serum creatinine than the F and H groups, and the rise in the RL and RH groups occurred earlier than in the F and H groups, showing that the RL and RH groups had more severe renal damage. This finding is similar to that of Perera *et al*., (2020) who examined the nephrotoxic effects of water hardness combined with high fluoride levels. When test groups were given water samples collected from Mihintale, which had a fluoride level of 1.66 mg/L and hardness of 364 mg/L, serum creatinine levels were considerably higher than the control group treated with water samples collected from the Kandy region with a fluoride level of 0.2 mg/L and hardness of 84 mg/L, which were within the standard limits recommended by the WHO. In addition, Thammitiyagodage *et al*., (2020) obtained similar results in their study. They observed significantly higher serum creatinine levels in rats who were administered test water samples with high fluoride and calcium concentrations collected from a high CKDu prevalent location in the North Central Province, Sri Lanka.

The level of urine creatinine was evaluated in this experiment to determine the degree of renal injury in rats. The Tukey's pairwise comparisons indicate that the differences in the reduction of the urine creatinine level of the test groups F, H, RL and RH groups were significantly different from the control group (p<0.05). The magnitude of the reduction in urine creatinine levels in group F, H, RL and RH were 74.62%, 71.35%, 80.21% and 78.22% respectively at the 90th day of the experiment. Though, there was significant difference in all test groups compared to the control group the highest magnitude of the reduction in urine creatinine was recorded in the RL group indicating prominent effect at the end of the study (Figure 4).
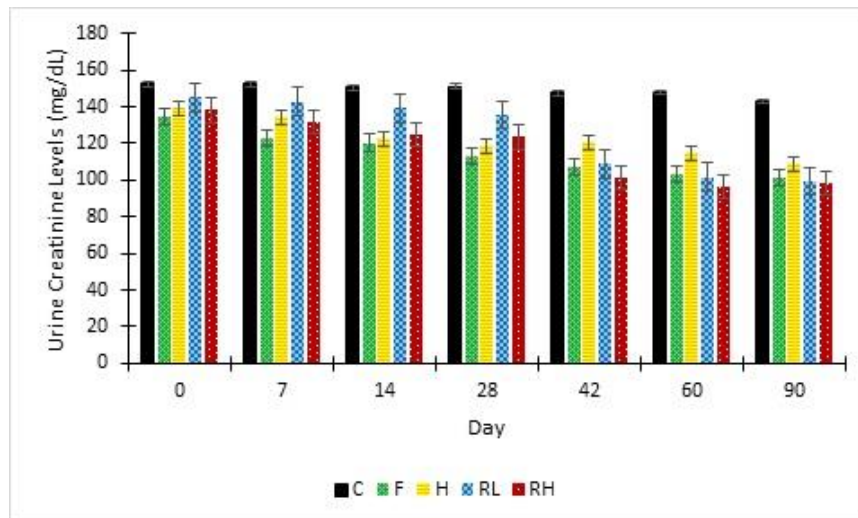
Figure 4: Variation in urine creatinine levels of rats treated with de-ionized water and test water ad-libitum for 90 days. Data are presented as mean ± SD (N=7). C- control, F - group for 1.5 mg/L fluoride alone, H - group for 200 mg/L hardness alone, RL - group for fluoride: hardness concentration of 1.5:200 mg/L, RH - group for fluoride: hardness concentration of 5:800 mg/L

In contrast, decreased urine creatinine levels have been linked to renal impairment (Di Micco *et al.*, 2013). According to the results of the present study, all the treated groups reported decreased urine creatinine levels compared to the control group, with the RL and RH groups demonstrating a more significant reduction than the F and H groups. The relationship between urine creatinine and renal survival in CKD patients were studied by Di Micco *et al.*, (2013), and similar results were found, suggesting a decline in urine creatinine excretion in CKD patients. Furthermore, reduction in urine creatinine excretion rate were observed in the study done by Tynkevich *et al.*, (2014) with 1072 men and 537 women CKD patients.
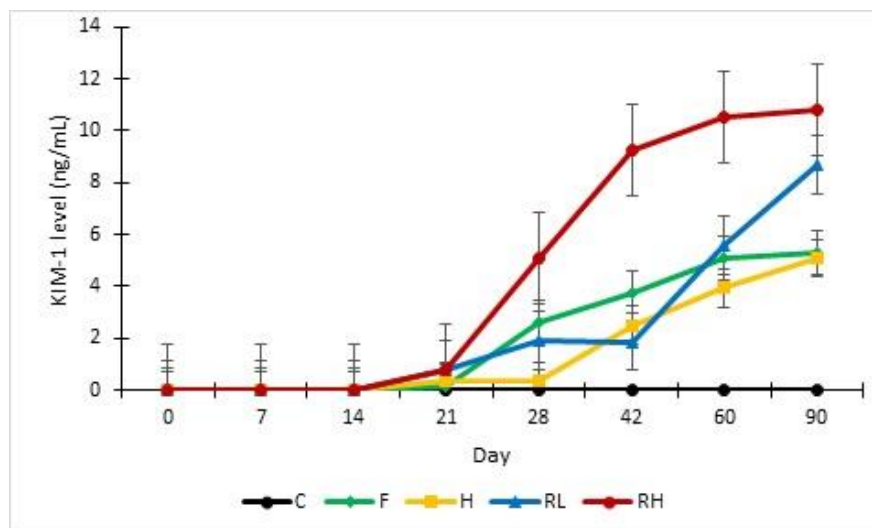

Figure 5: Variation in KIM-1 levels of rats treated with de-ionized water and test water ad-libitum for 90 days. Data are presented as mean ± SD (N=7). C- control, F - group for 1.5 mg/L fluoride alone, H - group for 200 mg/L hardness alone, RL - group for fluoride: hardness concentration of 1.5:200 mg/L, RH - group for fluoride: hardness concentration of 5:800 mg/L

Kidney injury molecule-1(KIM-1) was measured in this experiment as a marker of renal tubular injury in rats. Elevated KIM-1 levels were recorded in all the test groups from the 21st day of the experiment, while the control

group remained at the baseline. The Tukey's pairwise comparisons indicate that the differences in the increment of the KIM-1 level of the rat groups F, H and RL were not significantly different from the control ($p > 0.05$) while the RH group was significantly different ($p < 0.05$). According to the results, RH group indicated a more rapid increment in KIM-1 level at the end of the study indicating a renal damage (Figure 5).

Renal KIM-1 levels increase rapidly when there is an acute renal injury, whereas healthy renal tissues do not express KIM-1 (Wu *et al.*, 2018). KIM-1 levels are recognized as a sensitive indicator of renal impairment and it is mostly expressed in inflammatory epithelial cells in the proximal renal tubule (Song *et al.*, 2019). The extracellular fragment of KIM-1 is released into the urine after the renal tubular cell damage and mitogen activated protein kinase signaling pathway controls the shedding of KIM-1 (Zhang *et al.*, 2007). Therefore, KIM-1 levels are recognized as a sensitive indicator of renal impairment and can be used as a biomarker for early detection of renal damage (Cárdenas-González *et al.*, 2013; Song *et al.*, 2019). KIM-1 levels were greater in all of the treated groups than in the control group, with the RH group showing a rapid increase, suggesting early kidney injury. Early renal injury was described by Cárdenas-González *et al.*, (2013) after exposure to environmental fluoride concentrations, as evidenced from the elevated KIM-1 levels. Moreover, research using urine samples from adults and children showed that KIM-1 levels were associated with CKD patients (Carter *et al.*, 2016).

The sections of the renal tissues in the rats belonging to the treated groups showed features of mild renal tubular damage, while sections of the kidneys of the control group had normal histology. The histological alterations were observed in renal tubules in the treated groups F, H, RL, and RH, with the RL and RH groups showing the foremost alterations (Table 2 and Figures 6 to 9).

Table 2: Histopathological evaluations in kidney lesions in rats treated with de-ionized water and test water ad-libitum for 90 days.

Group	Histological features	Control	F	H	RL	RH
Cortex-Tubules	Intraluminal protein	Absent (0)	Mild (1)	Mild (1)	Mild (1)	Mild (1)
	Epithelial alterations- swelling	Absent (0)	Mild (1)	Mild (1)	Mild (1)	Mild (1)
	Nuclear Pyknosis	Absent (0)	Mild (1)	Absent (1)	Mild (1)	Mild (1)
	Vascular Dilatation	Absent (0)	Absent (0)	Absent (0)	Mild (1)	Mild (1)
	Tubular Necrosis	Absent (0)	Absent (0)	Absent (0)	Mild (1)	Absent (0)
	Vascular Congestion	Absent (0)	Absent (0)	Absent (0)	Absent (0)	Mild (1)
Cortex Glomeruli	Mesangium	Normal (0)	Normal (0)	Normal (0)	Normal (0)	Normal (0)
	Glomerular tuft	Normal (0)	Normal (0)	Normal (0)	Normal (0)	Normal (0)
	Bowman's space	Normal (0)	Normal (0)	Normal (0)	Normal (0)	Normal (0)
	Fibrosis	Normal (0)	Normal (0)	Normal (0)	Normal (0)	Normal (0)
Outer medulla	Epithelial alteration- swelling	Absent (0)	Absent (0)	Absent (0)	Absent (0)	Absent (0)
	Intraluminal protein	Absent (0)	Absent (0)	Absent (0)	Absent (0)	Absent (0)
Inner medulla	Intraluminal protein	Absent (0)	Absent (0)	Absent (0)	Absent (0)	Absent (0)
Interstitium	Inflammation	Normal (0)	Normal (0)	Normal (0)	Normal (0)	Normal (0)
	Fibrosis	Normal (0)	Normal (0)	Normal (0)	Normal (0)	Normal (0)

C- control, F - group for 1.5 mg/L fluoride alone, H - group for 200 mg/L hardness alone, RL - group for fluoride: hardness concentrations of 1.5:200 mg/L, RH - group for fluoride: hardness concentrations of 5:800 mg/L (N=7); (0) – normal, (1) – mild, (2) – moderate, (3) - severe
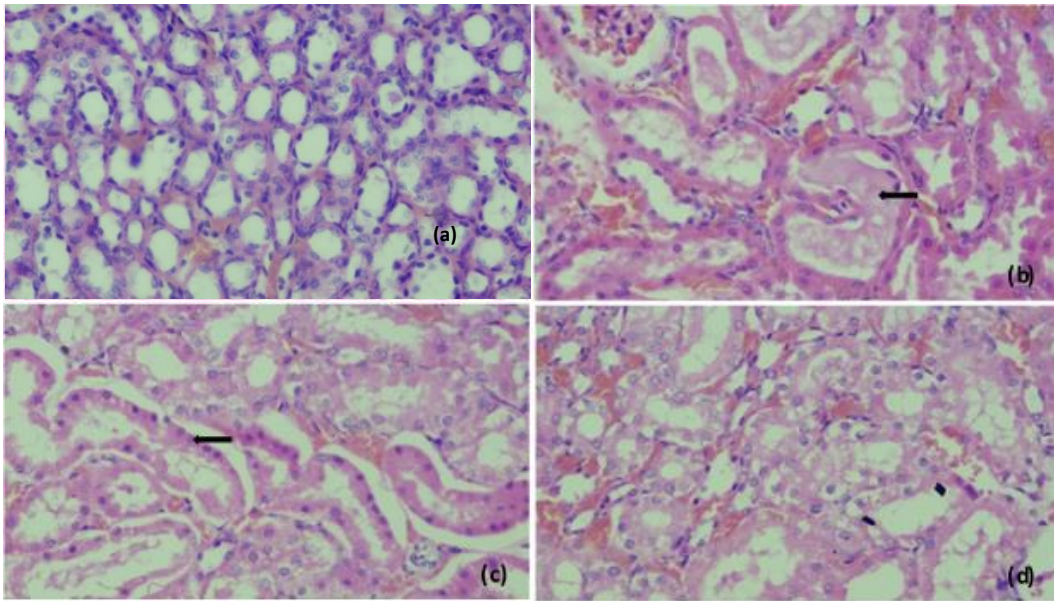
Figure 6: Histopathological evaluations of kidney tissues in 1.5 mg/L fluoride alone group (F) under H & E stain
a) control (x400), b) Arrow- intraluminal proteins (x400), c) Arrow- cytoplasmic eosinophilia and nuclear pyknosis (x400), d) cellular swelling (x400)
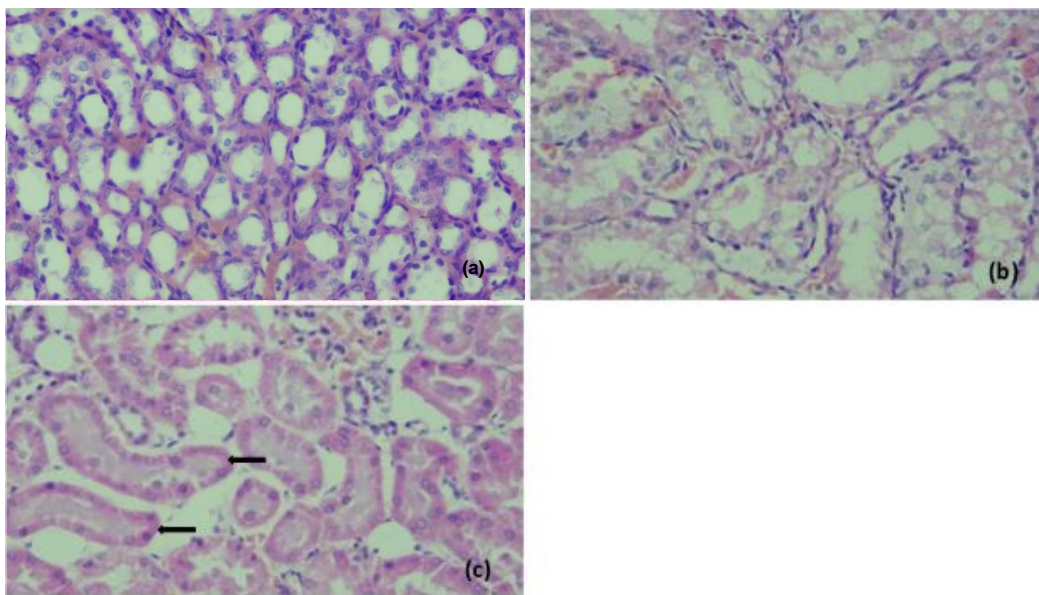

Figure 7: Histopathological evaluations of kidney tissues in 200 mg/L hardness alone group (H) under H & E stain
a) control (x400) b) cellular swelling (x400), c) Arrow- cytoplasmic eosinophilia (x400)
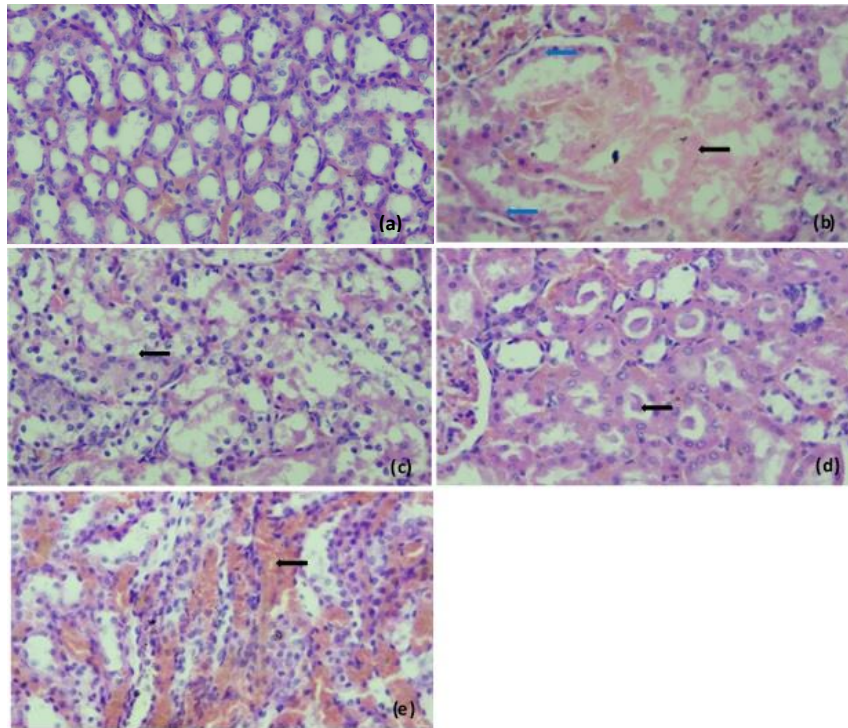
Figure 8: Histopathological evaluations of kidney tissues in 1.5 mg/L fluoride: 200 mg/L hardness concentration group (RL) under H & E stain a) control (x400) b) Arrow (Black) - tubular necrosis (x400), Arrows (Blue) - surrounding tubules with cytoplasmic eosinophilia and nuclear pyknosis c) Arrow- cellular swelling (x400), d) Arrow- intraluminal protein (x400), e) Arrow- vascular dilatation (x400)
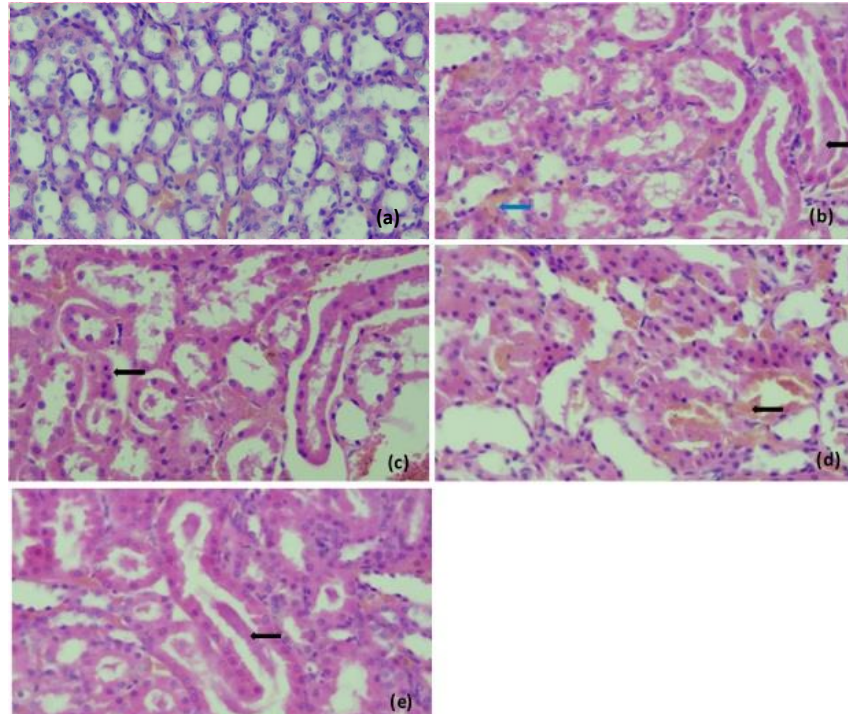

Figure 9: Histopathological evaluations of kidney tissues in 5 mg/L fluoride: 800 mg/L hardness concentration group (RH) under H & E stain a) control (x400), b) Arrow (Black)- intraluminal protein (x400), Arrow (Blue) - vascular dilatation (x400), c) Arrow- nuclear pyknosis (x400), d) Arrow- vascular dilatation (x400), e) Arrow- intraluminal protein (x400)

Histopathological alterations were observed in the renal tubules. Glomeruli lesions such as global glomerular sclerosis, focal glomerular sclerosis, and glomerular enlargement were not observed in the rat renal tissues in the present experiment. Furthermore, interstitial inflammation and the presence of plasma cells, which are representative of interstitial nephritis were also not observed in the interstitium of the kidney tissues in the present study. However, tubular lesions such as the presence of intraluminal proteins, vascular dilatation, cellular swelling, cytoplasmic eosinophilia, nuclear pyknosis, and focal tubular necrosis were observed as histopathological changes in the kidney tubules in the treated groups (F, H, RL, and RH) compared to the control group (Figures 6 to 9).

Similarly, the findings of the histopathology in the study done by Thammitiyagodage *et al*., (2020) discovered a significantly high index of renal tubular lesions including tubular degeneration and regeneration in the kidneys of the rats that were treated with water collected from the North Central province, which have recorded high hardness and fluoride concentrations compared to the rats treated with water collected from Colombo. The study done by Perera *et al*., (2020) revealed that there were several histopathological changes in the kidneys, of rats belonging to the groups which were given Mihintale water samples that had fluoride level of 1.66 mg/L and hardness of 364 mg/L. The observed histopathological changes can be listed as loss of brush border, epithelial degeneration in renal tubules. However, the control group treated with distilled water was not exhibited such morphological changes in renal tissues of rats in their study (Perera *et al*., 2020).

CONCLUSION

The combined effect of fluoride and hardness in drinking water observed in the combination groups (RL and RH) of rats may contribute to more severe impairment of kidneys than the effects of either fluoride or hardness alone (F and H groups of rats). Even though fluoride has nephrotoxic effects, its combined action with hardness may more prominent. The results of the current study indicate that the high fluoride and hardness concentration in drinking water may be a significant contributory factor to the aetiology of CKDu in Sri Lanka. It is recommended to conduct further testing with more exposure combinations of fluoride and hardness in an animal model to confirm a possible synergistic effect.

Conflict of interest

All the authors state that there is no competing financial interests or personal relationships that may influence the research work reported here.

Acknowledgements

REFERENCES

Al Salhen K.S. & Mahmoud A.Y. (2016). Determinants of abnormal kidney function tests in diabetes patient type 2 in Libya. *International Journal of Scientific Study* **4**(6): 99–103.

Athuraliya N.T., Abeysekera T.D., Amerasinghe P.H., Kumarasiri R., Bandara P., Karunaratne U., Milton A.H. & Jones A.L. (2011). Uncertain etiologies of proteinuric-chronic kidney disease in rural Sri Lanka. *Kidney International* **80**(11): 1212–1221.
DOI: https://doi.org/10.1038/ki.2011.258

Beauchamp R.O., Andjelkovich D.A., Kligerman A.D., Morgan K.T., Heck H.D.A. & Feron V.J. (1985). A critical review of the literature on acrolein toxicity. *CRC Critical Reviews in Toxicology* **14**(4): 309–380.
DOI: https://doi.org/10.3109/10408448509037461

Birkner E., Grucka-Mamczar E., Żwirska-Korczala K., Zalejska-Fiolka J., Stawiarska-Pięta B., Kasperczyk S. & Kasperczyk A. (2006). Influence of sodium fluoride and caffeine on the kidney function and free-radical processes in that organ in adult rats. *Biological Trace Element Research* **109**(1): 35–47.
DOI: https://doi.org/10.1385/BTER:109:1:035

Brisco M.A., Zile M.R., Hanberg J.S., Wilson F.P., Parikh C.R., Coca S.G., Tang W.W. & Testani J.M. (2016). Relevance of changes in serum creatinine during a heart failure trial of decongestive strategies: insights from the DOSE trial. *Journal of Cardiac Failure* **22**(10): 753–760.
  DOI: https://doi.org/10.1016/j.cardfail.2016.06.423

Cárdenas-González M.C., Del Razo L.M., Barrera-Chimal J., Jacobo-Estrada T., López-Bayghen E., Bobadilla N.A. & Barbier O. (2013). Proximal renal tubular injury in rats sub-chronically exposed to low fluoride concentrations. *Toxicology and Applied Pharmacology* **272**(3): 888–894.
  DOI: https://doi.org/10.1016/j.taap.2013.07.026

Carter J.L., Parker C.T., Stevens P.E., Eaglestone G., Knight S., Farmer C.K. & Lamb E.J. (2016). Biological variation of plasma and urinary markers of acute kidney injury in patients with CKD. *Clinical Chemistry* **62**: 876–883.
  DOI: https://doi.org/10.1373/clinchem.2015.250993

Chandrajith R., Dissanayake C.B., Ariyarathna T., Herath M.J.M.K. & Padmasiri J.P. (2011). Dose dependent Na and Ca in fluoride rich drinking water - another major cause of chronic renal failure in tropical arid regions. *Science of the Total Environment* **409**: 671–675.
  DOI: https://doi.org/10.1016/j.scitotenv.2010.10.046

Chapman *et al.* (11 authors) (2013). A global pharmaceutical company initiative: An evidence-based approach to define the upper limit of body weight loss in short term toxicity studies. *Regulatory Toxicology and Pharmacology* **67**(1): 27–38.
  DOI: https://doi.org/10.1016/j.yrtph.2013.04.003

Di Micco L., Quinn R.R., Ronksley P.E., Bellizzi V., Lewin A.M., Cianciaruso B. & Ravani P. (2013). Urine creatinine excretion and clinical outcomes in CKD. *Clinical Journal of the American Society of Nephrology* **8**(11): 1877–1883.
  DOI: https://doi.org/10.2215/CJN.01350213

Dissanayake C.B. & Chandrajith R. (2017). Groundwater fluoride as a geochemical marker in the etiology of chronic kidney disease of unknown origin in Sri Lanka. *Ceylon Journal of Science* **46**(2): 3–12.
  DOI: https://doi.org/10.4038/cjs.v46i2.7425

Galan P., Arnaud M.J., Czernichow S., Delabroise A.M., Preziosi P. & Bertrais S. (2002). Contribution of mineral waters to dietary calcium and magnesium intake in a French adult population. *Journal of the American Dietetic Association* **102**: 1658–1662.
  DOI: https://doi.org/10.1016/S0002-8223(02)90353-6

Gifford F.J., Gifford R.M., Eddleston M. & Dhaun N. (2017). Endemic nephropathy around the world. *Kidney International reports* **2**(2): 282–292.
  DOI: https://doi.org/10.1016/j.ekir.2016.11.003

Hard G.C., Banton M.I., Bretzlaff R.S., Dekant W., Fowles J.R., Mallett A.K., McGregor D.B., Roberts K.M., Sielken Jr R.L., Valdez-Flores C. & Cohen S.M. (2013). Consideration of rat chronic progressive nephropathy in regulatory evaluations for carcinogenicity. *Toxicological Sciences* **132**(2): 268–275.
  DOI: https://doi.org/10.1093/toxsci/kfs305

Hewa M.S.W., Gamage D.R.K.P., Panduka De S.G., Palika S.F. & Jayasundara B. (2017). WHO water quality standards Vs synergic effect(s) of fluoride, heavy metals and hardness in drinking water on kidney tissues. *Scientific Reports* **201**(7): 42516.
  DOI: https://doi.org/10.1038/srep42516

Indika S., Wei Y., Cooray T., Ritigala T., Jinadasa K.B.S.N., Weragoda S.K. & Weerasooriya R. (2022). Groundwater-based drinking water supply in Sri Lanka: Status and perspectives. *Water* **14**(9): 1428.

Kafle K., Balasubramanya S. & Horbulyk T. (2019). Prevalence of chronic kidney disease in Sri Lanka: A profile of affected districts reliant on ground water. *Science of the Total Environment* **694**: 133767.
  DOI: https://doi.org/10.1016/j.scitotenv.2019.133767

Lazic S.E., Semenova E. & Williams D.P. (2020). Determining organ weight toxicity with Bayesian causal models: Improving on the analysis of relative organ weights. *Scientific Reports* **10**(1): 1–12.
  DOI: https://doi.org/10.1038/s41598-020-63465-y

Lee G. & Goosens K.A. (2015). Sampling blood from the lateral tail vein of the rat. *JoVE; Journal of Visualized Experiments* 99: e52766.
  DOI: https://doi.org/10.3791/52766

Manage P.M., Yasawardena S.G. & Wedage W.S. (2009). Hepatotoxic effects of *Microcystis aeruginosa* (PCC 7820) on Wister Rats. *Vidyodaya Journal of Humanities and Social Sciences* Golden Jubilee Issue: 53–68.

OECD (1992). OECD guidelines for the testing of chemicals. Effects on biotic systems test no 203: acute toxicity for fish. Organization for Economic Cooperation and Development. Paris, France.

Perera T., Ranasinghe S., Alles N. & Waduge R. (2020). Experimental rat model for acute tubular injury induced by high water hardness and high water fluoride: efficacy of primary preventive intervention by distilled water administration. *BMC Nephrology* **21**(1): 103.
  DOI: https://doi.org/10.1186/s12882-020-01763-3

Pett J., Mohamed F., Knight J., Linhart C., Osborne N.J. & Taylor R. (2022). Two decades of chronic kidney disease of unknown aetiology (CKDu) research: Existing evidence and persistent gaps from epidemiological studies in Sri Lanka. *Nephrology* **27**(3): 238–247.

DOI: https://doi.org/10.1111/nep.13989

Ranasinghe N., Kruger E. & Tennan M. (2019). Spatial distribution of groundwater fluoride levels and population at risk for dental caries and dental fluorosis in Sri Lanka. *International Dental Journal* **69**: 295–302.
DOI: https://doi.org/10.1111/idj.12476

Ruwanpathirana T., Senanayake S., Gunawardana N., Munasinghe A., Ginige S., Gamage D., Amarasekara J., Lokuketagoda B., Chulasiri P., Amunugama S. & Palihawadana P., (2019). Prevalence and risk factors for impaired kidney function in the district of Anuradhapura, Sri Lanka: a cross-sectional population-representative survey in those at risk of chronic kidney disease of unknown aetiology. *BMC Public Health* **19**(1): 1–11.
DOI: https://doi.org/10.1186/s12889-019-7117-2

Sengupta P. (2013). Potential health impacts of hard water. *International Journal of Preventive Medicine* **4**(8): 866–875.

Siglin J.C., Mattie D.R., Dodd D.E., Hildebrandt P.K. & Baker W.H. (2000). A 90-day drinking water toxicity study in rats of the environmental contaminant ammonium perchlorate. *Toxicological Sciences*, **57**(1): 61–74.
DOI: https://doi.org/10.1093/toxsci/57.1.61.

Song J., Yu J., Prayogo G.W., Cao W., Wu Y., Jia Z. & Zhang A. (2019). Understanding kidney injury molecule 1: a novel immune factor in kidney pathophysiology. *American Journal of Translational Research* **11**(3): 1219-1229.

SLS (2013). SLS 614, *UDC 663.6 Specification for Potable Water (First Revision)* Sri Lanka Standards Institution, Colombo, Sri Lanka.

Thammitiyagodage M.G., de Silva N.R. & Rathnayake C. (2020). Biochemical and histopathological changes in Wistar rats after consumption of boiled and un-boiled water from high and low disease prevalent areas for chronic kidney disease of unknown etiology (CKDu) in north Central Province (NCP) and its comparison with low disease prevalent Colombo, Sri Lanka. *BMC Nephrology* **21**(1): 38.
DOI: https://doi.org/10.1186/s12882-020-1693-3

Toblli J.F., Ferder I., Angerosa M. & Inserra F. (1999). Effects of amlodipine on tubulointerstitial lesions in normotensive Hyperoxaluric rats. *Hypertension* **34**: 854–858.
DOI: https://doi.org/10.1161/01.HYP.34.4.854

Tynkevich E *et al.* (11 authors) (2014). Decrease in urinary creatinine excretion in early stage chronic kidney disease. *PloS One* **9**(11): e111949.
DOI: https://doi.org/10.1371/journal.pone.0111949

Veerappan I. & Abraham G. (2013). Chronic kidney disease: current status, challenges and management in India. *Ch* 130: 593-597.

Wanigasuriya K. (2014). Update on uncertain etiology of chronic kidney disease in Sri Lanka's North-Central dry zone, *MEDICC Review* **16**(2): 61–65.
DOI: https://doi.org/10.37757/MR2014.V16.N2.10

Wanigasuriya K.P., Peiris-John R.J., Wickremasinghe R. & Hittarage A. (2007). Chronic renal failure in North Central Province of Sri Lanka: an environmentally induced disease. *Transactions of the Royal Society of Tropical Medicine and Hygiene* **101**(10): 1013–1017.
DOI: https://doi.org/10.1016/j.trstmh.2007.05.006

Water Resources Board (2016). *Annual report*. Water Resources Board, Sri Jayawardenepura Kotte, Sri Lanka.

WHO. Guidelines for drinking water quality (1993). Vol 1 Recommendations. 2nd; Geneva: World Health Organization.

Wu M *et al.*, (13 authors) (2018). Celastrol aggravates LPS-induced inflammation and injuries of liver and kidney in mice. *American Journal of Translational Research* **10**(7): 2078–2086.

Zhang Z., Humphreys B.D. & Bonventre J.V. (2007). Shedding of the urinary biomarker kidney injury molecule-1 (KIM-1) is regulated by MAP kinases and juxtamembrane region. *Journal of the American Society of Nephrology* **18**(10): 2704–2714.
DOI: https://doi.org/10.1681/ASN.2007030325

RESEARCH ARTICLE

Agriculture

Submergence tolerance and tolerance mechanism: A study on traditional and improved rice genotypes at the seedling stage under complete submergence stress in Sri Lanka

HAPA Shyamalee and AL Ranawake[*]

Department of Agricultural Biology, Faculty of Agriculture, University of Ruhuna, Mapalana, Kamburupitiya, Sri Lanka.

Abstract: Submergence-tolerant genotypes in rice are essential for flood-prone lands, and recent studies have focused on dissecting tolerance mechanisms considering morphological and physiological changes in the plants upon submergence. Thirty improved rice varieties and sixty-two traditional rice accessions were screened for submergence tolerance under complete 9-day and 14-day submergence stress at the two-week-old seedling stage. The submergence tolerance level of each rice genotype was evaluated according to IRRI guidelines based on survival rates. Accordingly, rice genotypes were categorized into four groups: tolerant, moderately tolerant, moderately susceptible, and highly susceptible. Two Mawee accessions (3704, 3618) were submergence tolerant at 14-day submergence stress. The traditional rice accessions Ratawee3466, Mawee (8552, 4145), and Heenati4935 and improved rice varieties Bw400 were moderately submergence tolerant at 14-day submergence stress. Survival rates of the rice genotypes, their initial plant height, and shoot elongation at 9-day and 14-day submergence stress showed that seedling elongation (escape strategy) or reduction of elongation compared to control plants (quiescence strategy) under submergence stress cannot be used as phenotypic markers for selecting rice genotypes for submergence tolerance in rice. Further, the escape strategy or the quiescence strategy was not unique to the genotype, and the survival strategy of some rice genotypes changed with prolonged submergence stress. The escape strategy tended to be an SOS (Save Our Souls) strategy under prolonged submergence stress from 9 days to 14 days. No correlations between initial plant height and survival rate or survival rate and the height gain or reduction at 9-day and 14-day submergence stress showed that the submergence tolerance mechanism in rice was genotype-specific. The submergence-tolerant and moderately tolerant rice genotypes could be further investigated in future studies.

Keywords: Improved rice varieties, seedling stage, Sri Lanka traditional rice accessions, submergence tolerance.

INTRODUCTION

According to current trajectories, the world population will become 10 billion by 2056 (Persaud *et al.,* 2018), and rice consumption will be 360 million tons in 2050 (Timmer *et al.,* 2010). In the global climate change scenario, floods have increased by 65% in the last 25 years (FOASTAT, 2022). The total rice cultivation area in the world is 164.19 million hectares, and 20 million hectares of the land are located in flood plains in Asia (Manikmas, 2008; Redfern *et al.,* 2012; Singh *et al.,* 2016). Around 90% of global rice production is from eleven countries in Asia, and 45% of the rice cultivating lands in Asia are rain-fed (Rai, 1999).

The annual economic loss in rice production by flood in the world is recorded as one billion US dollars (Manikmas, 2008) and threatens global food security. Food security has three facets: malnutrition, lack of materials, and socio-cultural deprivation (Hendriks, 2015). Disappearance of traditional accessions and knowledge has been identified as a socio-cultural impact of food insecurity (Saint Ville *et al.,* 2019). The species that evolved in diverse natural habitats acquire numerous tolerances since they have adapted to local conditions. Hence, traditional rice accessions are a treasure for buffering the rice gene pool for food security. Submergence-tolerant traditional rice accessions are still cultivated in India (Ram *et al.,* 2002) and cultivating such traditional accessions ensures a local food supply in marginal environments (Pretty & Hine, 2000). However, naturally

---

evolved submergence-tolerant rice accessions have been replaced in the irrigated commercial rice cultivation system.

Sri Lankan traditional rice accessions have been identified as a source of many abiotic and biotic stress tolerances, and submergence tolerance has been assessed at the seedling stage (Ranawake & Hewage, 2014) and post-germination stage (Ranawake *at el.,* 2010). Further, indigenous rice genotypes have been screened for submergence tolerance in different studies (Goswami *et al.,* 2017; Kumar *et al.,* 2017).

Submergence occurs in two different conditions: partial submergence and complete submergence. Under partial submergence conditions, a part of the plant is covered by water, initiating metabolic changes inside the plant (Nishiuchi *et al.,* 2012). Under complete submergence conditions, the entire plant including the leaf tip is covered by water, and the ability of a rice plant to survive 10–14 days of complete submergence and renew its growth when the water subsides is defined as complete submergence tolerance (Catling, 1992). Generally, lowland rice species cannot tolerate submergence stress for more than two weeks (Mittal *et al.,* 2022).

There are two different survival strategies in rice under submergence stress: escape strategy and quiescence strategy. Deepwater rice varieties follow escape strategy to bring the canopy above the water level faster. Ethylene elongates shoots in rice under submergence stress (Jackson, 2008), and ethylene promotes carbohydrate metabolism and adventitious root formation (Fukao & Bailey-Serres, 2008). The ethylene production rate in completely submerged rice coleoptiles has coincided with the coleoptile elongation rate under submergence stress (Kato-Noguchi, 2001). Some rice varieties reported elongating of shoots up to 25 cm/day under submergence stress (Vergara *et al.,* 2014). Two genes, *SK1* and *SK2,* assist rice plants in elongating their internodes during submergence (Nishiuchi *et al.,* 2012). The aerenchyma develops in the leaves, stems, and roots, facilitating internal aeration from shoot to root (Winkel *et al.,* 2013). The aerenchyma consists of air-filled space and helps to survive under submergence conditions. The aerenchyma is present in plants even under well-drained conditions and improves further when the soil becomes waterlogged (Zhang *et al.,* 2015).

The wetland rice type follows the quiescence strategy that limits plant elongation under submergence stress, to survive by conserving carbohydrate reservoirs. The submergence-tolerant QTL located on chromosome number 9 in rice is named *SUB1* (Bailey-Serres *et al* 2010; dos Santos *et al.,* 2017; Kuanar *et al.,* 2019). The *SUB1* locus is responsible for submergence tolerance and for post submergence adaptability by regaining photosynthesis (Nurrahma *et al.,* 2022), and it is a polygenic locus that encodes a few ethylene-responsive factor (ERF) DNA-binding proteins (Afrin *et al.,* 2018). The *SUB1* locus has been introgressed into high-yielding varieties through marker assisted selection (Ray *et al.,* 2022). The Sri Lankan traditional rice accessions, *Goda Heenati, Kurkaruppan,* and *Thavalu,* also possess *SUB1* (Panda *et al.,* 2021).

The *SUB1* QTL contains three ERF genes; *SUB1A, SUB1B*, and *SUB1C. SUB1A* has two alleles, namely *SUB1A-1* and *SUB1A-2,* that differ due to a single nucleotide polymorphism (Xu *et al.,* 2006). The *ERF66* and *ERF67* genes that are targeted by *SUB1A-1* downstream are directly responsible for submergence tolerance in rice (Lin *et al.,* 2019). *SUB1* regains photosynthesis (Nurrahma *et al.,* 2022) and reduces shoot elongation under flooding (Sarkar *et al.,* 2014). Contrary to this, the rice variety *FR13A* exhibited slower shoot elongation and additional biomass accumulation to recover better than a rice variety with the *SUB1* gene under submergence stress (Singh *et al.,* 2014). *FR13A* carries both *SUB1A* and *SK* genes (Oe *et al.,* 2022) and a similar result has been reported by Samanta *et al.* (2022). In principle, this proves the coexistence of escape strategy and quiescence strategy in some of the rice genotypes. Coexistence of both mechanisms in rice cultivars have also been reported in Amazon wild rice species *O. grandiglumis,* by exhibiting quiescence strategy at the seedling stage and escape strategy at the vegetative stage (Okishio *et al.,* 2014). Hence, individual rice genotypes must be studied for submergence tolerance and its mechanism.

Screening rice cultivars by imposing submergence stress at different growth stages has been practised in many studies; post-germination (Ranawake *et al.,* 2010), seedling emergence stage (Su *et al.,* 2022), seedling stage (Hussain, 2018), vegetative stage (Yi *et al.,* 2014), and reproductive stage (Ray *et al.,* 2017). The intensity of the submergence stress has been changed by applying submergence stress for different durations; six days (Devender Reddy & Mittra, 1985), seven days and 14 days (Saika *et al.,* 2021) 9 and 12 days (Saidur Rahman, 2018), five days, ten days, and 14 days (Ranawake *et al.,* 2014), over two weeks (Das *et al.,* 2009) and 14 days and 20 days

(Sarkar & Bhattacharjee, 2011) However, these studies have focused on evaluating rice genotypes under submergence stress while providing less attention to distinguishing the underlying mechanisms of shoot growth in different rice genotypes under submergence stress.

Submergence tolerance in rice cultivars can be evaluated by using biochemical markers after imposing submergence stress. Two identified biochemical markers for submergence tolerance (Sayani *et al.,* 2017) are *Adh1* (Rahman *et al.,* 2001) and *pdc1* (Quimio *et al.,* 2000). Screening by imposing submergence stress on farmer fields (Mishra *et al.,* 1996; Das *et al.,* 2009; Sarkar *et al.,* 2009), artificial tanks (Hansen *et al.,* 1986; Das *et al.,* 2009; Goswami *et al.,* 2017), and laboratory conditions (Kumar *et al.,* 2017; Sayani *et al.,* 2017) has been reported with promising results.

In the present study, thirty improved rice varieties, including four submergence tolerant check varieties, and sixty-two traditional rice accessions were screened for complete submergence tolerance at the two-week-old seedling stage to explore submergence tolerant levels and the mode of the tolerance mechanism under submergence stress.

MATERIALS AND METHODS

The study was carried out at the Faculty of Agriculture, University of Ruhuna, Mapalana, Kamburupitiya, Sri Lanka (Latitude 6.06105° or 6° 3' 40" North, Longitude 80.56586° or 80° 33' 57" East). Twenty-six (26) improved rice varieties and sixty-two (62) traditional rice accessions, along with four submergence tolerant check varieties, *IRRISub1*, *IRRI64*, *Swarnasub1*, and *Sambamasuri,* were included in the study. Traditional rice accessions and improved rice varieties (referred to as rice genotype hereafter) were collected from Plant Genetic Resources Centre, Gannoruwa, Sri Lanka.

Method of screening traditional rice accessions and improved rice varieties for submergence tolerance at the seedling stage

Dormancy broken and surface sterilized seeds were kept in an incubator at 35 °C under dark conditions with enough water for 7 ds for germination. The experiment was carried out following a randomized complete block design (RCBD) with 4 replicates, and 10 seedlings were used for each replicate. Uniformly germinated seedlings were planted in trays filled with homogenized soil. Two-week-old seedlings were subjected to 9-day, and 14-day complete submergence stresses separately. The control experiment was maintained without submergence stress. After the complete submergence period, plants were kept for recovery under de-submerged conditions for 2 wks. Green plant height was measured in submerged and control seedlings just before the submergence stress, and after the submergence stress (Supplementary Figure 1). The survival rate was scored after a 2-week recovery period.

$$\text{Survival rate} = \frac{\text{Number of surviving plants after recovery}}{\text{Number of plants before submergence}} \times 100$$

Submergence tolerance was calculated as survival rate. Survival rates were categorized into four groups based on the IRRI standard evaluation system (Table 1).

Table 1: Standard submergence scoring criteria (IRRI 1996).

Submergence scale	Survival rate	Category
1	100% survival (check variety)	Tolerant
3	95-99% survival	Tolerant
5	75-94% survival	Moderately tolerant
7	50-74% survival	Moderately susceptible
9	0-49% survival	Highly susceptible

The effect of submergence stress on seedling elongation was measured as height reduction or height gain during the submergence stress, as shown in the equation below.

| Height gain or reduction of the submerged seedlings (cm) | = | (Average seedling height after the submergence) | _ | (Average seedling height before the submergence) |

The height gain of the control plants was calculated by considering the same time duration of the submerged plants.

| Height gain of the height control seedlings (cm) | = | (Average seedling height on the date of de-submergence of submerged seedlings) | _ | (Average seedling at two weeks) |

Data analysis

Eighty seedlings of four replicates were evaluated in the submergence experiment. Genotypes were categorized into submergence tolerant levels according to survival percentage: Tolerant (95% - 100%), moderately tolerant (75% - 94%), moderately susceptible (50% - 74%), and highly susceptible (0% - 49%). The height gain of the submerged seedlings and control seedlings were calculated, and Duncan's multiple range test was performed to test for significant differences among height gain values of genotypes. In addition, correlation analysis was performed to see the relationship between the evaluated parameters. Data were analyzed using SAS statistical software (SAS Institute Inc., 2000).

RESULTS AND DISCUSSION

Submergence tolerance level in tested rice genotypes at 9-day and 14-day submergence stress

Traditional rice accessions: *Heenati3707, Kaluheenati4991, Mawee4145, Ratawee365,* and *Rathuheenati4992,* three improved rice varieties, namely *At306, At354, Ld371,* and check varieties*, IRRIsub1*, *IRRI64,* and *Swarnasub1* scored 100% survival rate at the 9-day submergence stress. Another check variety, *Sambamasuri,* and improved rice varieties *Bg251, At402, Bw372, Bw400*, and *Bw453* were moderately tolerant together with some traditional accessions, namely, four *Heenati* accessions (*6402, 4935, 4618, 3936*), two *Pokkali* accessions (*3573, 3562*), *Dikwee2203, Kaluwee3876, Kaluheenati7802, Kuruwee3465, Mawee5531*, and *Murungakyan3489*. Eight (8) improved varieties and 15 traditional accessions were moderately susceptible to submergence under 9-day submergence stress with a 50 - 74 % survival rate (Table 2).

Table 2: Submergence tolerance levels of rice genotypes at 9-day complete submergence stress at the seedling stage

Type	Tolerant	Moderately tolerant	Moderately susceptible	Highly susceptible
Improved rice varieties	At354, At306 Ld371, IRRIsub1 IRRI64 Swarnasub1	Bg251, At402 Bw372, Bw400 Bw453, Sambamasuri	Bg250, Bg352, Bg369 Bg359, Ld368, At401, Bg455, At308	Bg300, Bg35 Bg300, Bg350, Bg94-1, At307At353, At362, At353, At362, At405, Bw367 Ld408, At358 Ld408, At358
Traditional rice accessions	Heenati3707 Kaluheenati4991 Mawee4145 Mawee5384 Ratawee3655 Rathuheenati4992 Mawee3704 Mawee3618	Dikwee2203 Heenati6402 Heenati4935 Heenati4618 Heenati3936 Kaluwee3876 Kaluheenati7802 Kuruwee3465 Mawee5531 Murungakayan3489 Pokkali3573 Pokkali3562	Dahanala3304 Kalubalawee5479 Kaluheenati5191 Kaluheenati4621 Kuruwee3898 Mawee8552 Murungakayan3809 Murungakayan3490 Pokkali3922 Pokkali3567 Ratawee4580 Rathuwee3905 Rathuwee3473 Suduheenati7799 Sudurusamba4362	Dikwee3741, Dikwee3504 Kaluwee3728, Kalubalawee3976 Kuruwee3982, Mawee3683 Mawee8551, Polayal3661 Pokkali3881, Ratawee3466 Ratawee3525, Heenati3998 Dahanala3917, Kaluheenati3471 Kalubalawee5480, Mawee8497 Kuruwee3552, Murungakayan6263 Murungakayan6285, Sudurusamba2202 Murungakayan3921, Murungakayan3492 Murungakayan3495, Rathuheenati5486 Rathuheenati6249, Sudurusamba3671 Suduheenati3932

Tolerant: Survival rate 95-100%, Moderately tolerant: Survival rate 75-94%, Moderately susceptible: Survival rate 50-74%, Highly susceptible: Survival rate 0-49%

All improved submergence tolerant rice varieties (*At354*, *At306*, *Ld371*), which showed submergence tolerance at 9-day submergence stress, became moderately susceptible at 14-day submergence stress. Three improved rice varieties (*Bg251*, *At402*, *Bw372*), moderately tolerant at 9-day submergence stress, were recorded to be moderately susceptible at 14-day submergence stress. Only *Bw400* was stable at the same level of moderate tolerance at both 9-day and 14-day submergence stress (Table 3).

Table 3: Submergence tolerance levels of rice genotypes at 14-day complete submergence stress at the seedling stage

Tolerant	Moderately tolerant	Moderately susceptible	Highly susceptible		
IRRI64	*Bw400*	*Bg251*	*Bg300*	*Ld368*	*At308*
Swarnasub1	*IRRIsub1*	*At306*	*Bg352*	*Bg250*	*At362*
		At354	*Bg369*	*Bg350*	*Bw367*
		At402	*Bg455*	*Bg359*	*Bw453*
		At405	*At353*	*Bg94-1*	*Ld408*
		Bw372	*At358*	*At307*	*Sambamasuri*
		Ld371	*At401*		
Mawee3704	*Heenati4935*	*Kaluheenati4991*	*Kaluwee3876*	*Kalubalawee3976*	*Rathuheenati6249*
Mawee3618	*Mawee8552*	*Kaluheenati4621*	*Mawee5531*	*Kalubalawee5480*	*Rathueenati5486*
	Mawee4145	*Ratawee3655*	*Mawee3683*	*Kaluheenati7802*	*Rathuheenati4992*
	Ratawee3466		*Murungakayan6285*	*Kaluheenati5191*	*Suduheenati7799*
			Murungakayan6263	*Kaluhheenati3471*	*Suduheenati3932*
			Sudurusamba4362	*Kuruwee3982*	*Sudurusamba3671*
			Dahanala3917	*Kuruwee3898*	*Sudurusamba2202*
			Dahanala3304	*Kuruwee3552*	*Pokkali3922*
			Dikwee3741	*Kuruwee3465*	*Pokkali3881*
			Dikwee3504	*Mawee8497*	*Pokkali3573*
			Dikwee2203	*Mawee8551*	*Pokkali3567*
			Heenati6402	*Mawee5384*	*Pokkali3562*
			Heenati4618	*Murungakayan3921*	*Polayal3661*
			Heenati3998	*Murungakayan3809*	*Ratawee4580*
			Heenati3936	*Murungakayan3495*	*Ratawee3525*
			Heenati3707	*Murungakayan3492*	*Rathuwee3905*
			Kaluwee3728	*Murungakayan3490*	*Rathuwee3473*
			Kalubalawee5479	*Murungakayan3489*	

Tolerant: Survival rate 95-100%, Moderately tolerant: Survival rate 75-94%, Moderately susceptible: Survival rate 50-74%, Highly susceptible: Survival rate 0-49%

Rice genotypes in different submergence tolerant groups varied from 9-day to 14-day submergence stress. Out of six submergence tolerant improved rice varieties at 9-day submergence stress, only two were submergence tolerant at 14 days. Further, out of eight submergence tolerant traditional rice accessions at 9-day submergence stress, two were submergence tolerant at 14 days (Tables 2 and 3). Nineteen improved rice varieties and 53 traditional rice accessions were highly susceptible at 14-day submergence stress.

Only *Mawee4145* scored a 100% survival rate at both 9-day and 14-day stress conditions, and one-third of the traditional rice accessions that scored more than a 60% survival rate at the 9-day submergence stress (Table 4) achieved more than a 60% survival rate at the 14-day submergence stress (Table 5). The results prove that traditional rice accessions harbour more submergence-tolerant traits than the improved varieties do. *Kaluheenati4991* and *Ratawee3655*, which scored a 100% survival rate at 9-day submergence stress, had the survival rate reduced to 60% and 70%, respectively, at 14-day submergence stress.

Table 4: The survival rate, shoot elongation, and initial plant height of the best performing rice genotypes at 9-day submergence stress.

Name	SR (%)	G	IPH (cm)	Name	SR (%)	G (cm)	IPH (cm)
Traditional							
Heenati3707	100	1.3	27.4	*Rathuwee4580*	67	1.7	25.1
Kaluheenati4991	100	NE	29	*Sudurusamba4362*	67	3.6	20.5
Mawee4145	100	7.9	23.1	*Kuruwee3898*	62	6.1	12.5
Mawee5384	100	13	28.7	*Kalubalawee5479*	60	5.0	26.4
Ratawee3655	100	3.8	33.5	*Murungakayan3809*	50	5.3	21.1
Rathuheenati4992	100	10.8	25.9	*Murungakayan3490*	50	0.7	34.8
Kaluwee3876	95	NE	28.6	*Pokkali3922*	50	5.5	30.1
Kuruwee3465	89	10	13.2	*Pokkali3567*	50	3.3	25.7
Murungakayan3489	89	6.0	24.7	*Rathuwee3473*	50	4.4	24.8
Pokkali3562	89	NE	40.0	*Suduheenati7799*	50	13.4	30.0
Heenati3936	87	NE	28.3	Improved			
Heenati6402	8	NE	23.9	*At306*	100	2.0	21.3
Heenati4618	83	NE	28.5	*At354*	100	0.5	16.4
Kaluheenati7802	83	7.3	27.0	*Ld371*	100	6.3	12.1
Dikwee2203	80	1.6	29.5	*IRRIsub1*	100	6.5	17.0
Heenati4935	80	NE	31.3	*IRRI64*	100	0.2	21.0
Mawee5531	80	NE	27.5	*Swarnasub1*	100	1.6	11.1
Pokkali3573	80	8.7	20.6	*Bw400*	90	NE	19.5
Kaluheenati4621	71	1.1	23.3	*Sambamasuri*	90	4.0	11.6
Mawee8552	70	2.9	32.1	*Bw372*	80	4.4	14.7
Dahanala3304	67	8.9	21.6	*At402*	77	5.6	12.8
Kaluheenati5191	67	NE	27.4	*Bg251*	75	5.0	15.9
Ratawee3466	67	3.9	21.2	*Bw453*	75	7.3	16.8

SR:Survival rate, G: Height gain during the submergence stress, NE: Not elongated IPH: Initial plant height before submergence

Two *Mawee* accessions (*3704, 4145*) that scored 100% survival rate were better than the tolerant check variety, *IRRISub1* (90%), at 14-day submergence stress. *Ratawee3466*, *Mawee8552*, *Heenati4935*, and *Mawee3618* scored survival rates of 87%, 86%, 75%, and 75%, respectively, at 14-day submergence stress (Table 5). The Sri Lankan traditional rice gene pool is comparatively rich in submergence tolerant traits. Compared to that, none of the rice lines scored a 100% survival rate out of 525 lines in screening for submergence tolerance (Nishanth *et al.,* 2017) and three lines out of fourteen reported a 99% survival rate at 24-day submergence stress at the seedling stage (Sultana *et al.,* 2019).

Submergence tolerance mechanism in tested rice genotypes at 9-day and 14-day submergence stress

Among traditional accessions that scored a 100% survival rate at 9-day submergence stress, only *Kaluheenati4991* showed reduced height compared to the control plants. Other than *Kaluheenati*, all traditional rice accessions that showed 100% survival were elongated compared to the control plants at 9-day submergence stress (Table 4). All the improved rice varieties that scored more than 75% survival rate at 9-day submergence stress elongated under the stressed conditions compared to the control plants, other than *Bw400,* which achieved a 90% survival rate. Interestingly, among improved rice varieties, only the *Bw400* variety remained in the same moderately tolerant (survival rate 75% - 90%) group at both 9-day and 14-day submergence stress (Table 5 and 6).

Table 5: Survival rate, shoot elongation, and initial plant height of the best-performed rice genotypes at 14-day submergence stress.

Name	SR (%)	G (cm)	IPH (cm)
Traditional rice			
Mawee4145	100	NE	32.9
Mawee3704	100	NE	37.3
Ratawee3466	87	2.3	27.2
Mawee8552	88	0.7	34.4
Heenati4935	75	NE	32.3
Mawee3618	75	NE	33.4
Kaluheenati4621	71	4.7	23.5
Ratawee3655	70	NE	37.4
Kaluheenati4991	60	4.3	23.4
Improved rice			
IRRI64	100	NE	22.7
Swarnasub1	100	1.8	12.5
IRRIsub1	90	NE	17.9
Bw400	83	8.0	17.5
At405	71	NE	13.5
Ld371	67	NE	16.3
At306	62	NE	22.6
Bg251	50	3.8	15.3
At354	50	0.6	14.5
At402	50	NE	17.4
Bw372	50	5.0	14.2

SR:Survival rate, G: Height gain during the submergence stress, NE: Not elongated IPH: Initial plant height before submergence

Kaluheenati4991, *Kaluwee3876*, *Pokkali3562*, *Heenati* (*3936, 6402, 4618, 4935*), and *Mawee5531* traditional accessions that showed reduced plant height compared to the control plants at 9-day submergence stress scored more than an 80% survival rate. Among them, only *Kaluheenati4991* scored more than a 60% survival rate at the 14-day submergence stress. *Kaluheenati4991* did not elongate at 9-day submergence, but it elongated at 14-day submergence stress. The only improved rice variety that did not elongate at 9-day submergence stress, *Bw400*, was also elongated at 14-day submergence stress. *Mawee4145* behaved the other way; it elongated at 9-day submergence stress and did not elongate at 14-day submergence stress. The elongation of rice genotypes at 9-day (Table 5) and 14-day (Table 6) submergence stress varied regardless of tolerance level (Table 7).

The improved and traditional rice genotypes were prepared according to the descending order of height gain at 9-day and 14-day submergence stress. Twenty-five of each rice genotype that followed the escape strategy at 9-day (Table 5) and 14-day (Table 6) submergence stress and the quiescence strategy at 9-day and 14-day (Table 7) submergence stress were selected to show the submergence tolerance levels.

In the highest height gain group, rice genotypes that followed the escape strategy at 9-day submergence stress, were in all tolerant (20%), moderately tolerant (28%), moderately susceptible (8%), and highly susceptible (44%) categories (Table 6). However, by 14-day submergence stress, 92% of rice genotypes with the highest height gain were highly susceptible (Table 6). This emphasizes that elongation under submergence stress is a successful strategy for a relatively short (9 days) submergence period to escape the stress. Elongation under prolonged submergence stress (14 days) is the last option or SOS mechanism for the rice seedlings to escape submergence stress. All the genotypes selected for this pathway would not survive in the end. Hence, elongation is not a phenotypic marker for submergence tolerance or susceptibility, at least for the studied materials at 9-day or 14-day submergence stress. A negative correlation between shoot elongation and the survival rate under submergence at the seedling stage has been reported (Setter & Laureles, 1996). But deep water rice stimulates shoot elongation during submergence to reach photosynthetic parts to the water surface. This escape reaction is controlled by an ethylene synthesis (Fukao & Bailey-Serres, 2008). The survival mechanism of deep-water rice

genotypes is to elongate under submergence stress, sometimes up to 25 cm/day (Vergara *et al.,* 2014). The submergence susceptibility under submergence stress in shoot elongation is due to excessive consumption of carbohydrates which leads to plant death (Mackill *et al.,* 2012). This is why a strong negative correlation is observed between survival percentage and plant elongation under submergence stress (Panda & Sarkar, 2013).

Table 6: Tolerance levels of twenty-five rice genotypes that followed escape strategy during 9-day and 14-day submergence stress

| | 9-day | | | | | 14-day | | | |
Name	THG (cm)	CHG (cm)	THG-CHG (cm)	Survival rate (%)	Name	THG (cm)	CHG (cm)	THG-CHG (cm)	Survival rate (%)
Traditional									
Suduheenati7799	13.4 [a]	0.6 [jk]	12	Moderately susceptible	*Pokkali3922*	16.9 [a]	2.1 [ijk]	14.8	Highly susceptible
Mawee5384	13. [ab]	0.8 [jk]	12.2	Tolerant	*Suduheenati3932*	16.1 [ab]	5.8 [f]	10.3	Highly susceptible
Dikwee3504	12.7 [ab]	3.0 [cdefg]	9.7	Highly susceptible	*Kaluheenati3471*	15.5 [b]	3.5 [gh]	12.0	Highly susceptible
Murungakayan3495	11.9 [b]	4.6 [b]	7.3	Highly susceptible	*Murungakayan3489*	11.7 [c]	2.7 [hij]	9.0	Highly susceptible
Kuruwee3982	11.8 [b]	3.3 [bcdef]	8.5	Highly susceptible	*Pokkali3562*	10.7 [d]	4.3 [g]	6.3	Highly susceptible
Mawee3704	10.5 [c]	2.8 [defgh]	7.7	Highly susceptible	*Kaluwee3876*	9.3 [e]	0.8 [k]	8.5	Highly susceptible
Rathuheenati4992	10.2 [cd]	7.8 [a]	2.3	Tolerant	*Sudurusamba2202*	8.1 [fg]	10.7 [bc]	-2.6	Highly susceptible
Kuruwee3465	10 [cde]	1.4 [hijk]	8.6	Moderately tolerant	*Heenati4618*	7.3 [fghi]	3.2 [ghi]	4.1	Highly susceptible
Mawee3618	9.2 [defg]	0.8 [jk]	8.4	Highly susceptible	*Murungakayan6285*	7.1 [ghij]	10.7 [bc]	-3.6	Highly susceptible
Dahanala3304	8.9 [defg]	2.5 [efgh]	6.4	Moderately susceptible	*Dikwee3741*	7.0 [hljk]	3.8 [gh]	3.2	Highly susceptible
Pokkali3573	8.7 [efghi]	0.4 [k]	8.3	Moderately tolerant	*Mawee5384*	6.5 [ijkl]	0.7 [k]	5.8	Highly susceptible
Murungakayan3492	8.1 [fghij]	4.3 [bc]	3.8	Highly susceptible	*Pokkali3573*	6.2 [jklmn]	1.2 [k]	5.0	Highly susceptible
Mawee4145	7.9 [ghijk]	7. 8 [bcde]	0.1	Tolerant	*Polayal3661*	6.0 [klmno]	13.1 [a]	-7.6	Highly susceptible
Rathuheenati5486	7.6 [hijkl]	2.2 [fgi]	5.2	Highly susceptible	*Kuruwee3898*	5.9 [klmno]	12.9 [a]	-6.9	Highly susceptible
Pokkali3881	7.5 [hijkl]	6.9 [a]	0.6	Highly susceptible	*Mawee8497*	5.7 [lmno]	1.8 [jk]	3.9	Highly susceptible
Kaluheenati7802	7.3 [ijklm]	1.4 [ijk]	5.9	Moderately tolerant	*Murungakayan6263*	5.0 [0]	0.8 [k]	4.2	Highly susceptible
Dahanala3917	7.0 [jklm]	1.7 [ghijk]	5.3	Highly susceptible	Improved				
Kuruwee3898	6.1 [m]	6.6 [a]	-0.5	Moderately susceptible	*Bg94-1*	8.3 [f]	10.7 [bc]	-2.44	
Murungakayan3489	6.0 [m]	2.8 [defgh]	3.2	Moderately tolerant	*Bw400*	8.0 [fgh]	4.0 [gh]	3.98	Highly susceptible
Bg94-1	9.5 [cdef]	6.6 [a]	2.9	Highly susceptible	*Bg350*	6.8 [ijkl]	7.0 [e]	-0.27	Highly susceptible
Bw453	7.2 [jklm]	2.0 [fghij]	5.3	Moderately tolerant	*At353*	6.4 [jklm]	1.5 [jk]	4.81	Highly susceptible
Bg350	6.5 [klm]	1.7 [hijk]	4.9	Highly susceptible	*Bg455*	5.9 [lmno]	8.7 [d]	-2.83	Highly susceptible
IRRIsub1	6.5 [klm]	0.6 [jk]	5.9	Tolerant	*Bg250*	5. 8 [lmno]	11.0 [b]	-5.27	Highly susceptible
Ld371	6.3 [m]	4.0 [bcd]	2.2	Tolerant	*Bg352*	5.3 [mno]	11.2 [b]	-5.88	Highly susceptible
Bg251	5.9 [m]	7.0 [a]	-0.8	Moderately tolerant	*Ld408*	5.2 [no]	4.1 [g]	1.11	Highly susceptible
					Bw372	5.0 [m]	9.6 [cd]	-4.57	Highly susceptible

The means of the same letters are not significantly different. THG: Height gain under submergence stress, CHG: Height gain in control plants, Tolerant: Survival rate 95-100%, Moderately tolerant: Survival rate 75-94%, Moderately susceptible: Survival rate 50-74%, Highly susceptible: Survival rate 0-49%

Setter *et al*. (1997) concluded that elongation and survival under submergence stress rarely overlap. Contrary to this theory, Chen *et al.,* (2010) have reported that plant elongation and carbohydrate levels are not significantly correlated in plants undergoing submergence stress. Supporting this, Barik *et al.,* (2020) said that the five most submergence-tolerant rice genotypes performed better than the standard positive control of *FR 13A* and significantly elongated under submergence stress.

Table 7: Tolerant levels of rice genotypes followed the quiescence strategy under 9-day and 14-day complete submergence stress

9-day			14-day		
Name	CHG (cm)	Tolerant level	Name	CHG (cm)	Tolerant level
Heenati4935	3.3 de	Moderately tolerant	*Rathuheenati6249*	1.0 mn	Highly susceptible
Polayal3661	6.0 b	Highly susceptible	*Murungakayan3492*	0.6 n	Highly susceptible
Mawee3683	3.8 cd	Highly susceptible	*Mawee4145*	5.8 fg	Tolerant
Heenati3936	3.2 de	Moderately tolerant	*Murungakayan3490*	8.6 cd	Highly susceptible
Kalubalawee3976	5.5 b	Highly susceptible	*Sudurusamba3671*	7.5 de	Highly susceptible
Ratawee3466	2.7 de	Highly susceptible	*Mawee3618*	1.4 lmn	Moderately tolerant
Kaluheenati3471	5.0 b	Highly susceptible	*Rathuheenati5486*	4.1 nij	Highly susceptible
Pokkali3562	2.5 def	Moderately tolerant	*Kaluheenati7802*	1.2 lmn	Highly susceptible
Kaluwee3876	0.7 h	Moderately tolerant	*Pokkali3881*	16.5 a	Highly susceptible
Sudurusamba3671	4.9 bc	Highly susceptible	*Mawee3704*	3.7 ijk	Tolerant
Heenati6402	3.1 de	Moderately tolerant	*Rathuwee3905*	2.4 klm	Highly susceptible
Kaluheenati4991	1.0 h	Tolerant	*Heenati4935*	3.3 ijk	Moderately tolerant
Heenati4618	1.4 fgh	Moderately tolerant	*Rathuheenati4992*	9.7 bc	Highly susceptible
Mawee5531	3.2 de	Moderately tolerant	*Rathuwee3473*	3.5 ijk	Highly susceptible
Kaluheenati5191	8.9 a	Moderately susceptible	*Ratawee4580*	0.8 mn	Highly susceptible
Murungakayan3490	8.6 a	Moderately susceptible	*Murungakayan3921*	4.8 ghi	Highly susceptible
Heenati3998	3.0 de	Highly susceptible	*Heenati3998*	1.1 lmn	Highly susceptible
Kaluheenati4621	2.4 efg	Moderately susceptible	*Ld368*	3.5 ijk	Highly susceptible
Bg250	4.9 bc	Moderately susceptible	*At405*	6.4 ef	Moderately susceptible
Bg369	1.4 fgh	Moderately susceptible	*At362*	3.1 jk	Highly susceptible
At353	1.1 h	Highly susceptible	*At401*	2.7 klmn	Highly susceptible
At354	1.2 gh	Tolerant	*Ld371*	2.7 jkl	Moderately susceptible
Bw400	3.2 de	Moderately tolerant	*At306*	10.7 b	Moderately susceptible
			At402	2.7 jkl	Moderately susceptible
			IRRI64	5.7 fgh	Tolerant

The means of the same letters are not significantly different. CHG: Height gain of the control plants, susceptible: Tolerant: Survival rate 95-100%, Moderately tolerant: Survival rate 75-94%, Moderately susceptible: Survival rate 50-74%, Highly susceptible: Survival rate 0-49%

In the genotypes, there was no height gain during the submergence stress; rice genotypes that followed the quiescence strategy belonged to all tolerant (12%), moderately tolerant (32%), moderately susceptible (24%), and highly susceptible (32%) categories at the 9-day submergence stress. Altogether, 44% of rice genotypes that followed the quiescence strategy were moderately tolerant or tolerant.

The highly susceptible rice genotypes that followed the quiescence strategy (18.9%) were less than that of rice genotypes that followed the escape strategy (81.08%) at 9-day submergence stress. Similarly, 23.61% followed the quiescence strategy, and 76.38% followed the escape strategy at 14-day submergence stress. These findings emphasize that the quiescence strategy is much more stable than the escape strategy for survival under submergence stress when the submergence condition continues (increased from 18.9% to 23.61%). The quiescence strategy is said to be led by the *SUB1* gene in rice that limits ethylene production for reduce shoot elongation under submergence stress (Sarkar *et al.,* 2014). In a previous study where fourteen rice lines were tested for submergence tolerance, only three lines scored a 99% survival rate under 24-day submergence stress at the seedling stage. They had shown lower elongation rates (Sultana *et al.,* 2019) that derives from *SUB1A*. The Sri Lankan submergence-tolerant traditional rice accession *Godaheenati* and another accession *Vaidehi* have been reported to practise another submergence-tolerant mechanism unrelated to *SUB1* (Jackson & Ram, 2003).

However, *Godaheenati* possesses *SUB1* (Panda *et al.,* 2021). *SUB1* carrying genotypes that exclude the quiescence strategy reveals that *SUB1* alone does not decide the quiescence strategy in rice, or other gene expressions override the *SUB1* activity. The present study's findings propose that limited growth under submergence stress alone is insufficient to develop submergence tolerance in rice seedlings.

Pearson's correlation coefficients were calculated to find possible correlations among initial plant height, survival rate, height gain or reduction under submergence stress at 9-day and 14-day submergence stress. There was no significant correlation between any of the two parameters at 9-day or 14-day submergence stress other than a weak correlation between initial plant height and survival rate in traditional rice accessions at 14-day submergence stress (Table 8). This finding emphasizes that the submergence tolerance mechanism is genotype specific. Further, the correlation analysis reveals that submergence tolerance is not directly governed by elongation or reduction of plant height during submergence stress. Quiescence strategy or escape strategy alone is not capable of tolerating submergence stress. At the same time, correlation analysis indicates that the initial plant height is not a factor in deciding rice seedlings' submergence tolerance level. Submergence tolerance is a complex mechanism that many factors involved in different scales other than quiescence or escape strategy. Submergence tolerance has been identified as a complex mechanism involving balancing carbohydrate utilization for shoot elongation and maintenance and gibberellic acid function that restricts shoot elongation (Setter *et al.,* 1997). Hence, there would not be distinct groups of genotypes in rice that undergo quiescence or escape strategy at all submergence stress conditions at all growth stages.

Table 8: The correlation coefficient of initial plant height, survival rate, height gain and survival rate at 9-day and 14-day complete submergence stress

Genotype	Correlation	9-day		14-day	
		r	α	r	α
Improved varieties	Initial plant height × survival rate	0.127	0.505	0.145	0.445
	Height gain × survival rate	0.133	0.488	0.301	0.106
Traditional accessions	Initial plant height × survival rate	0.142	0.271	0.328**	0.009
	Height gain × survival rate	-0.060	0.644	-0.183	0.156
Improved tolerant	Initial plant height × survival rate	0.173	0.590	0.003	0.997
	Height gain × survival rate	-0.515	0.015	-0.729	0.271
Traditional tolerant	Initial plant height × survival rate	0.061	0.811	0.293	9.573
	Height gain × survival rate	0.370	0.136	-0.271	0.604
Improved moderately susceptible	Initial plant height × survival rate Height gain × survival rate	-0186 0.577	0.659 0.134	0.123 -0.713	0.794 0.072
Traditional moderately susceptible	Initial plant height × survival rate	-0.305	0.269	0.401	0.737
	Height gain × survival rate	-0.333	0.226	-0.334	0.783
Traditional highly susceptible	Initial plant height × survival rate	0.119	0.538	0.071	0.615
	Height gain × survival rate	-0.600	0.756	0.071	0.611
Improved highly susceptible	Initial plant height × survival rate	0.386	0.274	0.071	9.772
	Height gain × survival rate	0.589	0.373	-0.169	0.488

r: Pearson's correlations, α: significant level, Tolerant: Survival rate 75-100%, Moderately susceptible: Survival rate 50-74%, Highly susceptible: Survival rate 0-49%

CONCLUSION

Mawee accessions *3704* and *3618* were submergence tolerant, and *Ratawee3466, Mawee (8552, 4145)* and *Heenati4935* were moderately submergence tolerant. The improved *Bw400* rice variety can be recommended as a moderately tolerant rice variety according to the IRRI-adapted screening technique. Submergence-tolerant rice genotypes in the present study must be evaluated at other growth stages. Promising rice genotypes can be incorporated into future breeding programs to develop submergence-tolerant rice varieties.

The submergence tolerance mechanism in rice is genotype-specific. Further, the same rice genotype adapted different strategies to survive under different periods of submergence stress. Hence, the same submergence-tolerant approach cannot be expected at any submergence stress at any growth stage.

The quiescence strategy is much more stable for prolonged submergence stress. The escape strategy is very common as an SOS strategy under prolonged submergence stress.

Initial plant height, shoot elongation, or reduction of shoot height gain under submergence stress compared to control plants may not be phenotypic markers for selecting rice genotypes for submergence tolerance. However, the survival rate of the rice seedlings after the recovery period followed by the submergence stress is a successful direct method to evaluate the submergence tolerance in rice genotypes. Future studies must examine reliable submergence-tolerant physiological markers for screening rice genotypes.

Acknowledgement

REFERENCES

Afrin W., Nafis M.H., Hossain Muhammed Ali., Islam M.M. & Hossain Md Amir (2018). Responses of rice (*Oryza sativa* L.) genotypes to different levels of submergence. *Comptes Rendus - Biologies* **341**: 85–96.
DOI: https://doi.org/10.1016/j.crvi.2018.01.001

Bailey-Serres J., Fukao T., Ronald P., Ismail A., Heuer S. & Mackill D. (2010). Submergence tolerant rice: SUB1's journey from landrace to modern cultivar. *Rice* **3**: 138–147.
DOI: https://doi.org/10.1007/s12284-010-9048-5

Barik J., Kumar V., Lenka S.K. & Panda D. (2020). Assessment of variation in morpho-physiological traits and genetic diversity in relation to submergence tolerance of five indigenous lowland rice landraces. *Rice Science* **27**: 32–43.
DOI: https://doi.org/10.1016/j.rsci.2019.12.004

Catling D. (1992). Deepwater rice cultures in the Ganges-Brahmaputra Basin. In: *Rice in Deep Water,* pp. 213–244. Palgrave Macmillan, London, UK.
DOI: https://doi.org/10.1007/978-1-349-12309-4_17

Chen X., Pierik R., Peeters A.J.M., Poorter H., Visser E.J.W., Huber H., de Kroon H. & Voesenek L.A.C.J. (2010). Endogenous abscisic acid as a key switch for natural variation in flooding-induced shoot elongation. *Plant Physiology* **154**: 969–977.
DOI: https://doi.org/10.1104/pp.110.162792

Das K.K., Panda D., Sarkar R.K., Reddy J.N. & Ismail A.M. (2009). Submergence tolerance in relation to variable floodwater conditions in rice. *Environmental and Experimental. Botany* **66:** 425–434.
DOI: https://doi.org/10.1016/J.ENVEXPBOT.2009.02.015

Devender Reddy M. & Mittra B.N. (1985). Effects of complete plant submergence on vegetative growth, grain yield and some biochemical changes in rice plants. *Plant and Soil* **87**: 365–374.
DOI: https://doi.org/10.1007/BF02181904

Dos Santos, R.S., da Rosa Farias, D., Pegoraro C., Rombaldi C.V., Fukao T., Wing R.A. & de Oliveira A.C. (2017). Evolutionary analysis of the SUB1 locus across the *Oryza* genomes. *Rice* **10(4)**: 1–5.
DOI: https://doi.org/10.1186/s12284-016-0140-3

FOASTAT (2022). *Production Quantities of Rice, Paddy by Country*. Food and Agriculture Organization. United Nations, Rome, Italy.

Fukao T. & Bailey-Serres J. (2008). Ethylene-A key regulator of submergence responses in rice. *Plant Science* **175**: 43–51.
DOI: https://doi.org/10.1016/j.plantsci.2007.12.002

Goswami S., Kar R.K., Paul A. & Dey, N. (2017). Genetic potentiality of indigenous rice genotypes from Eastern India with reference to submergence tolerance and deepwater traits. *Current Plant Biology* **11-12**: 23–32
DOI: https://doi.org/10.1016/j.cpb.2017.10.002

Hansen M., Busch L., Burkhardt J., Lacy W.B. & Lacy L.R. (1986). Plant Breeding and Biotechnology. *Bioscience* **36**: 29–39.
DOI: https://doi.org/10.2307/1309795

Hendriks S. (2015). The food security continuum: a novel tool for understanding food insecurity as a range of experiences. *Food Security* **7**: 609–619.

Hussain M. (2018). Phenotypic response of rice genotypes under submergence conditions at seedling stage. *Current Investigations in Agriculture and Current Research* **5(4)**: 722–726.
DOI: https://doi.org/10.32474/ciacr.2018.05.000220

IRRI (1996). *Standard Evaluation System for Rice*. IRRI, International Rice Research Institute, Philippine.

Jackson M.B. (2008). Ethylene-promoted elongation: an adaptation to submergence stress. *Annals of Botany* **101**: 229–248.
  DOI: https://doi.org/10.1093/aob/mcm237

Jackson M.B. & Ram P.C. (2003). Physiological and molecular basis of susceptibility and tolerance of rice plants to complete submergence. *Annals of Botany* **91**: 227–241.
  DOI: https://doi.org/10.1093/aob/mcf242

Kato-Noguchi H. (2001). Submergence tolerance and ethanolic fermentation in rice coleoptiles. *Plant Production Science* **4**(1): 62–65.
  DOI: https://doi.org/10.1626/pps.4.62

Kuanar S.R., Molla K.A., Chattopadhyay K., Sarkar R.K. & Mohapatra P.K. (2019). Introgression of Sub1 (SUB1) QTL in mega rice cultivars increases ethylene production to the detriment of grain- filling under stagnant flooding. *Scientific Report* **9**(1): 18657 1–12.
  DOI: https://doi.org/10.1038/s41598-019-54908-2

Kumar S., Dwivedi S.K., Kumar R., Bhakta N., Prakash V., Rao K.K., Kumar R., Yadav S., Choubey A.K. & Mishra J.S. (2017). Screening of different rice germplasm against multiple disease under submergence condition in middle Indo Gangetic plain. *International Journal of Current Microbiology and Applied Sciences* **6**(5): 335–339.
  DOI: https://doi.org/10.20546/ijcmas.2017.605.038

Lin *et al.* (20 authors) (2019). Regulatory cascade involving transcriptional and N-end rule pathways in rice under submergence. *Proceedings of the National Academy of the Sciences USA* **116**: 3300–3309.
  DOI: https://doi.org/10.1073/pnas.1818507116

Mackill D.J., Ismail A.M., Singh U.S., Labios R.V. & Paris T.R. (2012). Development and rapid adoption of submergence-tolerant (Sub1) rice varieties. *Advances in Agronomy* **115**: 299–352.
  DOI: https://doi.org/10.1016/B978-0-12-394276-0.00006-8

Manikmas M.O. (2008). Developing submergence-tolerant rice varieties in Indonesia. *Journal of Sub1 News* **2**: 4–5.

Mishra S.B., Senadhira D. & Manigbas N.L. (1996). Genetics of submergence tolerance in rice (*Oryza sativa* L.). *Field Crop Research* **46**: 177–181.
  DOI: https://doi.org/10.1016/0378-4290 (95)00088-7

Mittal L., Tayyeba S. & Sinha A.K. (2022). Finding a breather for *Oryza sativa*: Understanding hormone signalling pathways involved in rice plants to submergence stress. *Plant Cell and Environment* **45(2)**: 279–295.
  DOI: https://doi.org/10.1111/pce.14250

Nishanth G.K., Dushyanthakumar B.M., Gangaprasad S., Gowda T.H., Nataraju S.P. & Shashidhar H.E. (2017). Screening and genetic variability studies in submergence tolerance rice germplasm lines under flood prone lowlands of hill zone of Karnataka. *International Journal of Current Microbiology and Applied Sciences* **6**: 1254–1260.
  DOI: ttps://doi.org/10.20546/ijcmas.2017.607.152

Nishiuchi S., Yamauchi T., Takahashi H., Kotula L. & Nakazono M. (2012). Mechanisms for coping with submergence and waterlogging in rice. *Rice* **5**: 1–4.
  DOI: https://doi.org /10.1186/1939-8433-5-2

Nurrahma A.H.I., Yabuta S., Junaedi A. & Sakagami J.I. (2022). Different survival strategies involve carbon translocation rather than de novo C assimilation under complete submergence in rice plant. *Photosynthesis Research* **154**(2): 183–193.
  DOI: https://doi.org/10.1007/s11120-022-00959-y

Oe S., Sasayama D., Luo Q., Fukayama H., Hatanaka T. & Azuma T. (2022). Growth responses of seedlings under complete submergence in rice cultivars carrying both the submergence-tolerance gene SUB1A-1 and the floating genes SNORKELs. *Plant Production Science* **25**: 70–77.
  DOI: https://doi.org/10.1080/1343943X.2021.1943465

Okishio T., Sasayama D., Hirano T., Akimoto M., Itoh K. & Azuma T. (2014). Growth promotion and inhibition of the Amazonian wild rice species *Oryza* grandiglumis to survive flooding. *Planta* **240**(3): 459–469.
  DOI: https://doi.org/10.1007/s00425-014-2100-8

Panda D., Barik J. & Sarkar R.K. (2021). Recent advances of genetic resources, genes and genetic approaches for flooding tolerance in rice. *Current Genomics* **22**: 41–58.
  DOI: https://doi.org/10.2174/1389202922666210114104140

Panda D. & Sarkar R.K. (2013). Structural carbohydrates and lignifications associated with submergence tolerance in rice (*Oryza sativa* L.). *Journal of Stress Physiology and Biochemistry* **9**: 299–306.

Persaud A., Bhat P.S., Ventriglio A. & Bhugra D. (2018). Geopolitical determinants of health. *Industrial Psychiatry Journal* **27**: 308.

Pretty J. & Hine R. (2000). The promising spread of sustainable agriculture in Asia. *Natural Resources Forum* **24**(2): 107–121.
  DOI: https://doi.org/10.1111/j.1477-8947.2000.tb00936.x

Quimio *et al.* (11 authors) (2000). Enhancement of submergence tolerance in transgenic rice overproducing pyruvate decarboxylase. *Journal of Plant Physiology* **156**: 516–521.
  DOI: https://doi.org/10.1016/S0176-1617(00)80167-4

Rahman M., Grover A., Peacock W.J., Dennis E.S. & Ellis M.H. (2001). Effects of manipulation of pyruvate decarboxylase and alcohol dehydrogenase levels on the submergence tolerance of rice. *Australian Journal of Plant Physiology* **28**: 1231–1241.

Rai M. (1999). Rice germplasm evaluation and enhancement in India: issues, status, options, and future plan of action. *Proceedings of the International Symposium on Rice Germplasm Evaluation and Enhancement*. Arkansas Agricultural Experiment Station, USA, pp. 83–91.

Ram *et al.* (15 authors) (2002). Submergence tolerance in rainfed lowland rice: physiological basis and prospects for cultivar improvement through marker-aided breeding. *Field Crop Research* **76**(2-3): 131–152.
DOI: https://doi.org/10.1016/S0378-4290(02)00035-7

Ranawake A.L., Dahanayaka N. & Senadhipathy D.D. (2010). Evaluation of level of submergence tolerance in traditional rice cultivars at post germination stage. *Proceedings of the 8th Academic Sessions*. University of Ruhuna, Sri Lanka, pp 233.

Ranawake A.L., Amarasinghe U.G.S. & Senanayake S.G.J.N. (2014). Submergence tolerance of some modern rice cultivars at seedling and vegetative stages. *Journal of Crop and Weed* **10**: 240–247.

Ranawake A.L. & Hewage M.J. (2014). Correlation analysis of drought, salinity and submergence tolerance in some traditional rice cultivars of Sri Lanka. *International Journal of Scientific and Research Publications* **4**(7): 1–5.

Ray B.P., Nath U.K. & Azad A.K. (2022). Genetic analysis of submergence tolerance rice genotypes by intro-gression of sub1 QTL to Indica HYV through breeding populations (F 2) with Marker Assay. *American Journal of Pure and Applied Biosciencec* **4**(1): 10–21.

Ray A., Panda D. & Sarkar R.K. (2017). Can rice cultivar with submergence tolerant quantitative trait locus (SUB1) manage submergence stress better during reproductive stage? *Archives of Agronomy and Soil Science* **63**: 998–1008.
DOI: https://doi.org/10.1080/03650340.2016.1254773

Redfern S.K., Azzu N. & Binamira J.S. (2012). Rice in Southeast Asia: facing risks and vulnerabilities to respond to climate change. *Building Climate Resilience in the Agriculture Sector of Asia and the Pacific* **23**: 1–14.

Saidur Rahman (2018). Effect of submergence durations on yield and yield contributing characters of hybrid and inbred aman rice. *Asian-Australasian Journal of Bioscience and Biotechnology* **3**: 225–230.

Saikia D., Kalita J., Chutia J., Vemireddy L.N.R. & Tanti B. (2021). Dissecting the morpho-physiological and biochemical responses in some traditional rice cultivars under submergence stress. *Vegetos* **34 (1)**: 191–204.

Saint Ville A., Po J.Y.T., Sen A., Bui A. & Melgar-Quiñonez H. (2019). Food security and the Food Insecurity Experience Scale (FIES): ensuring progress by 2030. *Food Security* **11**: 483–491.
DOI: https://doi.org/10.1007/S12571-019-00936-9/TABLES/3

Samanta P., Chakrabarti A. & Dey N. (2022). Study on physiological responses with allelic diversity of Sub1A and SK loci in rice seedlings under complete submergence. *Plant Physiology Reports* **27** (2): 275-281.
DOI: https://doi.org/10.1007/s40502-022-00660-1

Sarkar R.K., Das K.K., Panda D., Reddy J.N., Patnaik S.S.C., Patra B.C. & Singh D.P. (2014). *Submergence Tolerance in Rice: Biophysical Constraints, Physiological Basis and Identification of Donors,* pp. 36. Central Rice Research Institute, Cuttck, India.

Sarkar R.K. & Bhattacharjee B. (2011). Rice genotypes with SUB1 QTL differ in submergence tolerance, elongation ability during submergence and re-generation growth at re-emergence. *Rice* **5**: 1–11
DOI: https://doi.org/10.1007/s12284-011-9065-z

Sarkar R.K., Panda D., Reddy J.N., Patnaik S.S.C., Mackill D.J. & Ismail A.M. (2009). Performance of submergence tolerant rice (*Oryza sativa*) genotypes carrying the Sub1 quantitative trait locus under stressed and non-stressed natural field conditions. *Indian Journal of Agricultural Science*s **79**: 876–883.

SAS Institute Inc. (2000). SAS Online Doc, version 8. Available at *https://www.sfu.ca/sasdoc/sashtml/main.htm.*

Sayani G., Kumar K.R., Anupam P. & Narottam D. (2017). Study of selected biochemical parameters related to submergence tolerance in rice (*Oryza sativa* L.) with special reference to land races and wild species. *Research Journal of Chemistry and Environment* **21**: 29–38.

Setter T.L., Ellis M., Laureles E.V., Ella E.S., Senadhira D., Mishra S.B., Sarkarung S. & Datta S. (1997). Physiology and genetics of submergence tolerance in rice. *Annals of Botany* **79**: 67–77.
DOI: https://doi.org/10.1006/anbo.1996.0304

Setter T.L. & Laureles E.V. 1996. The beneficial effect of reduced elongation growth on submergence tolerance of rice. *Journal of Experimental Botany* **47**: 1551–1559.
DOI: https://doi.org/10.1093/jxb/47.10.1551

Singh R. *et al*., (11 authors) (2016). From QTL to variety-harnessing the benefits of QTLs for drought, flood and salt tolerance in mega rice varieties of India through a multi-institutional network. *Plant Sciences*. **242**: 278–287.

Singh S., Mackill D.J. & Ismail A.M. (2014). Physiological basis of tolerance to complete submergence in rice involves genetic factors in addition to the SUB1 gene. *AOB Plants Journal for plant Science* **6**: 1–20.
DOI: https://doi.org/10.1093/aobpla/plu060

Su X., Wu H., Xiang J., Zhan J., Wang J., Li X., Wei Y., Dai H. & Chen H. (2022). Evaluation of submergence tolerance of different rice genotypes at seedling emergence stage under water direct seeding. *Open Access Library Journal* **09**: 1–15.
DOI: https://doi.org/10.4236/oalib.1108706

Sultana A., Islam M.M., Sultana A. & Khanom M.S.R. (2019). Screening of rice genotypes for submergence stress at seedling stage. *Journal of Agroforestry and Environment* **13**: 1–4.

Timmer C.P., Block S. & Dawe D. (2010). Long-run dynamics of rice consumption, 1960–2050. In: *Rice in the Global Economy: Strategic Research and Policy Issues for Food Security. Resources for the Future* (eds. S. Pandey, D. Byerlee & D. Dawe), pp.139–173. Los Banos, Philippines.

Vergara G.V., Nugraha Y., Esguerra M.Q., Mackill D.J. & Ismail A.M. (2014). Variation in tolerance of rice to long-term stagnant flooding that submerges most of the shoot will aid in breeding tolerant cultivars. *AOB Plants Journal for Plant Sciences* **6**: 1–16.
DOI: https://doi.org/10.1093/aobpla/plu055

Winkel A., Colmer T.D., Ismail A.M. & Pedersen O. (2013). Internal aeration of paddy field rice (*Oryza sativa*) during complete submergence - importance of light and floodwater O_2. *New Phytologist* **197**: 1193–1203.
DOI: https://doi.org/10.1111/nph.12048

Xu K., Xu X., Fukao T., Canlas P., Maghirang-Rodriguez R., Heuer S., Ismail A.M., Bailey-Serres J., Ronald P.C. & Mackill D.J. (2006). Sub1A is an ethylene-response-factor-like gene that confers submergence tolerance to rice. *Nature* **442**: 705–708.
DOI: https://doi.org/10.1038/nature04920

Yi Y., Ella E., Ismail A.M., Woo S. & Lee C. (2014). Screening analysis for submergence tolerance of 6 rice cultivars at vegetative stages. *Proceedings of the 240th Annual Meeting of the Crop Science Society of Japan.* Crop Science Society of Japan, Japan, pp 82.

Zhang Y., Wang Z., Li L., Zhou Q., Xiao Y. & Wei X. (2015). Short-term complete submergence of rice at the tillering stage increases yield. *PLOS One* **10**(5): e0127982.
DOI: https://doi.org/10.1371/journal.pone.0127982

RESEARCH ARTICLE

Microbiology and Molecular Biology

Pulsed-field gel electrophoresis typing and molecular characterization of *Listeria monocytogenes* isolates in raw milk samples from Polonnaruwa District, Sri Lanka

WAS Wijendra[*]**, AGG Kaushalya, KGR Kuruppuarachchi, HBC Harshani, WASI Fonseka and R Ramesh**

Department of Molecular Biology, Medical Research Institute, Colombo 8, Sri Lanka

Abstract: *Listeria monocytogenes* is an important food borne human pathogen associated with severe diseases in humans and animals. Human infection is associated with high mortality rates. Our previous studies done in 2012 on milk and milk products revealed 4b as the dominant serotype followed by 1/2a, 1/2b and 1/2c. Therefore, this study was conducted to determine the sources of contamination and to identify the strain differences (pulsotypes) by pulsed-field gel electrophoresis (PFGE) typing and serotype profiles of *L. monocytogenes* isolates from farm collected raw milk samples from randomly identified locations in Grama Niladhari divisions of the Polonnaruwa district, Sri Lanka. Eighty isolates obtained from raw milk samples were confirmed as *L. monocytogenes* by Polymerase Chain Reaction, belonging to serotypes 4b, 1/2a, 1/2b and 1/2c. The strains were identified by PFGE. PFGE analysis digested with AscI and ApaI enzymes revealed different banding patterns. All the pulsotypes were found to be serotype 4b. The sub typing indicated the diversity of the *Listeria* species. The presence of serotypes 1/2a, 1⁄2b, 1/2c, and 4b in raw milk is a public health concern, as these serotypes are frequently associated with foodborne outbreaks and sporadic cases of human listeriosis. In our study, PFGE analysis allowed discrimination among isolates of the same serogroup. Further PFGE analysis showed heterogeneity among isolates recovered from both same sampling areas and different areas.

Keywords: Polymerase chain reaction, pulsotypes, serogroup, serotypes.

INTRODUCTION

The genus *Listeria* consists of six species including *Listeria monocytogenes, Listeria ivanovii, Listeria seeligeri, Listeria innocua, Listeria welshimeri* and *Listeria grayi* (Sarfraz *et al*., 2017). *L. monocytogenes* is pathogenic for humans and animals whereas *L. ivanovii* is pathogenic to ruminants, and the other species are nonpathogenic (Osman *et al*., 2016). *L. monocytogenes* is a pathogenic bacterial species that can survive under various conditions of refrigeration, freezing, heating, and drying (Jones & D'Orazio, 2013).

Food borne *L. monocytogenes*causes significant outbreaks of Listeriosis in humans, with mortality rates ranging from 9% to 44% (Clark *et al*., 2010). The virulence or the pathogenicity of *L. monocytogenes* appears to be serotype based, with serotypes 1/2a, 1/2c, 1/2b, and 4b being involved in 98% of documented human listeriosis cases (Wiedmann *et al*., 1997; Jacquet *et al*., 2002). Even though thirteen *L. monocytogenes* serotypes have been recognized, only three serotypes (1/2a, 1/2b, and 4b) cause the vast majority of the clinical cases and 4b is the commonest (Tappero *et al*., 1995; Doumith*et al*., 2004).

Listeriosis is one of the most important zoonotic bacterial illnesses with worldwide distribution. The disease has great economic and public health importance. *L. monocytogenes* has been defined as an opportunistic pathogen mainly affecting children, pregnant women, and aged and immune-challenged individuals (Walter *et al*., 2000).

[*] Corresponding author (wijendra@mri.gov.lk; https://orcid.org/0000-0002-1449-5492)

Only three studies have been reported from Sri Lanka to ascertain the presence of *L. monocytogenes* in our dairy merchandise. These studies revealed the percentage of *L. monocytogenes* contaminated milk samples in Sri Lanka is comparatively higher than other countries (Gunasena *et al*., 1995; Jayamanne *et al*., 2001; Wijendra *et al*., 2014). For the first time, Wijendra *et al.* (2014) have reported circulating serotypes (1/2a, 1/2b, and 1/2c) isolated from milk and milk products in Sri Lanka. The serotypes may potentially be useful in tracing *L. monocytogenes* strains involved in disease out-breaks, however, the value of serotyping in epidemiological investigations is somewhat limited due to the unavailability of scientific data on strain differences among the *L. monocytogenes*. Therefore, it is very important to identify strain differences by using sub typing methods for source tracking and epidemiologic investigations of infection caused by *L. monocytogenes*. The PFGE is considered as the 'gold standard' sub typing method for epidemiological studies due to its high discrimination power, robustness, and reproducibility (Martin *et al*., 2006), with limitations such as being time consuming and labour intensive (usually taking 2–3 days), and the high cost of the equipment (Olive & Bean, 1999).

The aim of this study is to identify the strain differences (pulsotypes) by PFGE typing of the isolates from farm collected raw milk samples in the Polonnaruwa district, Sri Lanka. Further PFGE identified strains of the circulating serotypes should sound an alarm to the stakeholders of public health sector in Sri Lanka, to take appropriate control measures in preventing outbreaks. Milk farmers will be made aware of the microbial quality of their products, which will ensure the production and supply of hygienic, quality raw milk to the collection centres.

MATERIALS AND METHODS

Organisms used

Standard cultures of *L. monocytogenes* ATCC 51776 as the positive control and *L. innocua* ATCC 33090 as the negative control were used.

Sample collection and preparation

Sampling was carried out according to the proportional sampling method (MINITAB14 software, 2009). In the Polonnaruwa District there are seven divisional secretariats. Two hundred raw milk samples were collected from 21 collection centres located in each divisional secretariat and brought to the laboratory under cold chain. These samples may or may not be taken from a single cow. As enrichment, 25 mL of raw milk samples were incubated in 225 mL of Listeria enrichment broth (LEB, Oxoid, England) at 37 °C for 24 h. After 24 h of incubation, 500 µL of suspension was subjected to DNA extraction and also poured onto the Listeria selective agar plates (Listeria selective agar, Oxoid, England), and incubated at 37 °C for 24 h.

Bacterial DNA extraction from enriched milk samples

Total DNA extraction was carried out for all the 150 of enriched milk samples using NORGEN milk bacterial DNA extraction kit (NORGEN BIOTEK, Canada).

Isolation of *Listeria*

As enrichment, 25 mL of raw milk samples were incubated in 225 mL of LEB at 37 °C for 24 h. After the incubation, 500 µL of suspension was streaked on the Listeria selective agar plates and incubated at 37 °C for another 24 h (Lovett *et al*., 1987).

DNA Extraction from cultures

Total DNA extraction was carried out from bacterial cultures of all samples using a commercial bacterial DNA extraction kit (QIAamp DNA Mini Kit, QIAGEN).

PFGE typing and molecular characterization of *L. monocytogenes*

L. monocytogenes isolates were confirmed using the polymerase chain reaction (PCR). According to Lieve *et al.* (1995) with modifications, nested PCR detection was performed. To achieve the optimal sensitivity, 1 μL of the first PCR mixture was used as a template in the second PCR. PCRswere done using Thermal cycler 9600 (Perkin–Elmer Corp.).

Serotyping by PCR

Molecular serotyping for all positive samples of *L. monocytogenes* was performed using multiplex PCR method, according to the Doumith *et al.* (2004). *L. monocytogenes* ATCC 51776, serotype 1/2a was used as the control.

PFGE analysis

PFGE analysis was performed according to the Centers for Disease Control and Prevention PulseNet standardized procedure for *L. monocytogenes* with AscI and ApaI as the restriction endonucleases (Pulse Net USA, 2017), as described previously (Acciari *et al.*, 2017). The PFGE typing was carried out in a CHEF-MAPPER apparatus (Bio-Rad Laboratories, Des Plaines, USA). Isolate similarity dendrograms were generated using open-source software Gel J version 2.0. The similarities between the AscI and ApaI macro-restriction profiles (MRPs) were calculated using the Dice coefficient, applying an optimization coefficient and band tolerance of 1.0% for both enzymes. Isolates with a similarity coefficient equal or above 85% were clustered as the same genotype (Heras *et al.*, 2015).

RESULTS AND DISCUSSION

Out of 200 raw milk samples, 150 were enriched. After culturing, only 80 samples tested positive for PCR detection. Among the PCR-positive samples, 42.5% were of serotype 4b, while 30% were serotype 1/2b, 10% were serotype 1/2c, and 11.25% were serotype 1/2a. (Figure 1).

Serotyping was done for all the positive samples among the enriched samples by the multiplex PCR method. Amplified fragment combinations were analyzed to identify the serotypes. Identification by this method could not be completed in some of these samples due to the non-amplifications and the presence of non-specific fragments (Figure 1 and Figure 2).
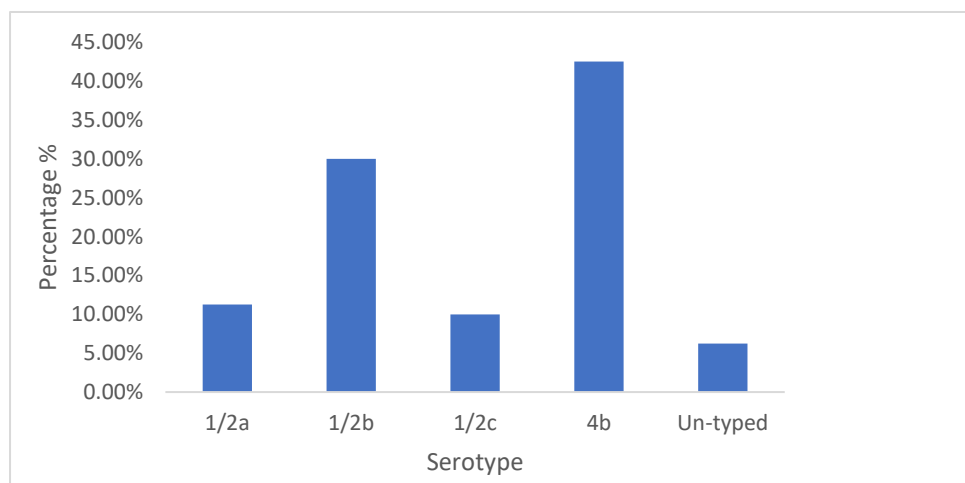

Figure 1: Serotype distributions (%) of *Listeria monocytogenes* in Polonnaruwa District

This study reveals that 53% of the collected raw milk samples were contaminated with *L. monocytogenes*. One major finding is thatthe majority of the isolates found in raw milk samples belong to 1/2b or 4b (Figure 1).

With regard to the distribution of serotype patterns in the areas of the Grama Niladhari divisions (GN divisions), Bakamuna, Madirigiriya, and Sangabodigama had all five serotypes. The areas of Unagalawehera, Nawanagaraya, Nagapokuna, Mahakirimatiyaya, Kaudulla, Kaduruwela, Chandanapokuna, Bisobandaragama and Thuna-Ela showed only a single serotype. Patunugama became a unique area in which no isolates were detected. Apart from that, the isolates from areas Sungawila and Deka-Ela were not typed (Figure 2).
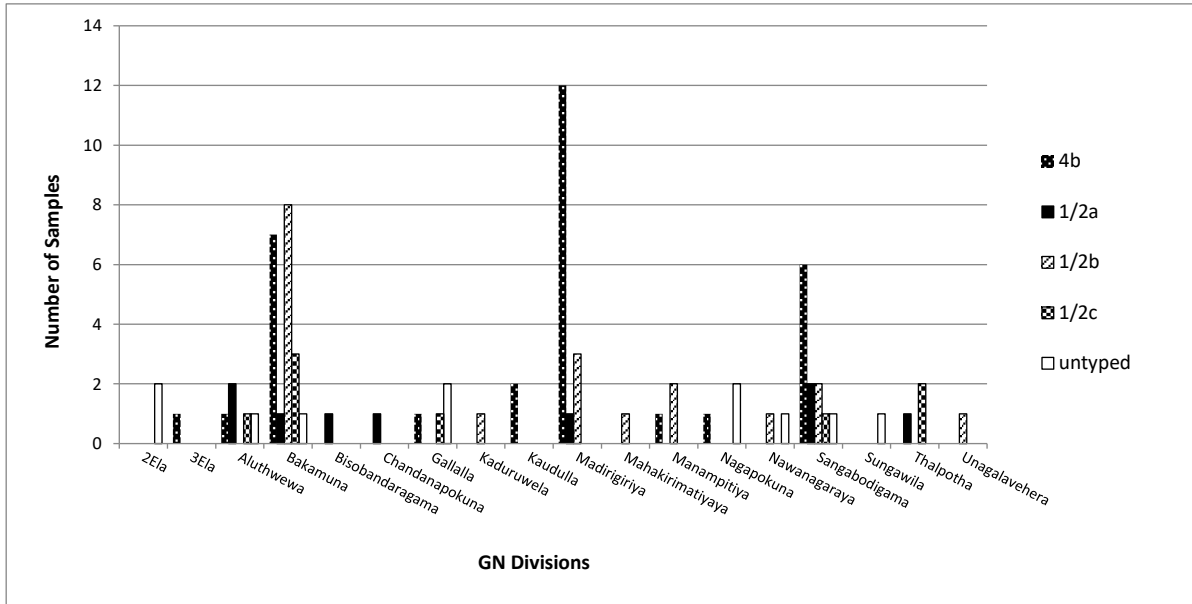
Figure 2: Distribution of serotypes in GN Divisions of Polonnaruwa District

In the PFGE analysis, digestion with AscI and ApaI enzymes revealed different banding patterns (Figure 3a and 3b).

a

b
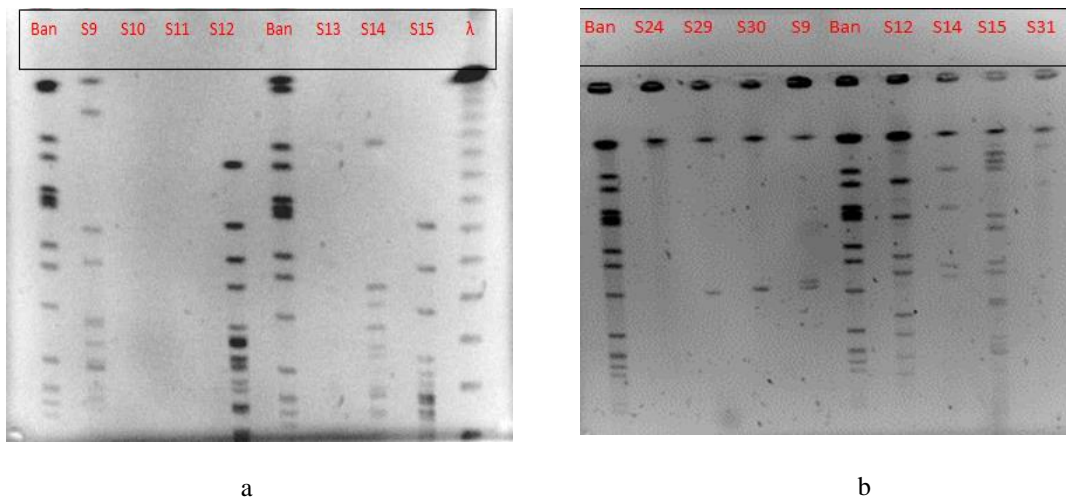
Figure 3: PFGE analysis of Sangabodigama samples a) Digestion with AscI; b) Digestion with ApaI
(S- Sangabodigama samples, Ban-Standard culture λ- Ladder)

Additionally, the results of another twenty-three isolates which were digested only with ApaI, revealed that there are 12 different pulsotypes. The overall PFGE results indicated that 11 out of 33 were serotype 4b isolates, and are part of a single pulsogroup (similarity ≥ 85%).

This study revealed that 53% of the raw milk samples had been contaminated with *L. monocytogenes* which agrees with our previous study (Wijendra *et al*., 2014). High to low percentages of prevalence were reported by Waak *et al*. (2002), Vardar-Unlu *et al*. (1998), Hayes *et al*. (1986), Holko *et al*. (2002), Rahimi *et al*. (2010), and Kells and Gilmour (2004). In comparison to the above studies, we observed a higher prevalence of *Listeria* in raw milk. A higher prevalence of pathogens represents a potential risk to consumers of raw milk and raw milk products.

It is important to note here the seriousness of the health risk in supplying contaminated milk to the dairy industry. Such contaminated milk increases the chances of post pasteurization contamination through biofilms (Husu, 1990).

Despite the high importance of diary-foods listeriosis, only a few studies have been reported to determine the presence of *L. monocytogenes* in our dairy products, and also only four suspected cases of listeriosis have been reported in Sri Lanka (Gunasena*et al*., 1995; Jayamanne*et al*., 2001; Wijendra *et al*., 2014). According to their results, the percentage of *L. monocytogenes* contaminated milk samples in Sri Lanka is much higher compared to developed countries. But the determinations of pathogenicity and the presence of virulence factors of the *L. monocytogenes* isolates present in Sri Lanka needs in-depth research.

One major finding of this study was that the majority of the isolates found in raw milk samples belong to 1/2a, 1/2b, and 4b serotypes, and these serotypes are linked with most of the human listeriosis cases (Jersek *et al*., 1996; Ryser *et al*., 1999; Wojciech *et al*., 2004; Liu, 2006; De Santis *et al*., 2007; O'Connor *et al*., 2010). These results have demonstrated that the molecular method used in this study has a good discriminatory capacity for identifying the serovars.

PFGE analysis revealed that there are strain differences among the serotypes. The data obtained from the study indicated that the molecular comparison of these isolates can be used in epidemiological investigations and even to trace outbreak sources in a case where the products may be implicated.

These results also emphasize the need for implementing programmes which will employ molecular identification of pathogenic strains along with measures that may guide infection control in the food industry (Graves & Swaminathan, 2001; Zdolec*et al*, 2019; Warke *et al*., 2023). There may be geographical and other differences in areas of the GN divisions which contribute variation in the prevalence of *L. monocytogenes.* Since the area under study only covered some areas of the GN divisions in the entire district, further study is warranted.

CONCLUSION

The presence of serotype 1/2a, 1/2b, 1/2c, and 4b in raw milk is of public health concern, as these serotypes are frequently associated with food borne outbreaks and sporadic cases of human listeriosis. PFGE analysis has identified the different strains of isolates belonging to various serotypes.

In this study, PFGE analysis enables us to distinguish between isolates of the same serogroup, as well as isolates retrieved from the same or different sampling areas. Finally, the obtained data indicated that comparison of these isolates can be used in epidemiological investigations and even to trace outbreak sources in a case where the products may be implicated. These results also emphasize the need to implement programmes thatwill employ molecular identification of pathogenic strains in the food industry along with measures that may guide infection control. However, these pathogens represent a potential risk to consumers of raw milk and raw milk products. We suggest that it may be reasonable to give priority to PFGE analysis of serotype 4b isolates from non-human sources, as the information yielded may be of greater value to public health.

Acknowledgements

REFERENCES

Acciari *et al.* (15 authors) (2017). *Listeria monocytogenes* in smoked salmon and other smoked fish at retail in Italy: Frequency of contamination and strain characterization in products from different manufacturers. *Journal of Food Protection* **80**: 271–278.
   DOI: https://doi.org/10.4315/0362-028X.JFP-15-599

Clark C.G., Farber J., Pagotto F., Ciampa N., Dore K., Nadon C., Bernard K. & Ng L.K. (2010). Surveillance for *Listeria monocytogenes* and listeriosis, 1995–2004. *Epidemiology and Infection* **138**: 559–572.
   DOI: https://doi.org/10.1017/S0950268809990914

De Santis E.P.L., Pilo A.L., Cosseddu A.M., Canu N.A., Scarano C. & Marongiu P. (2007). Multiplex PCR for the identification and serotyping of *L. monocytogenes* isolated from sheep cheese–processing plants. *Veterinary Research Communications*. **31**: 359–363.
   DOI: https://doi.org/10.1007/s11259-007-0037-0

Doumith M., Cazalet C., Simoes N., Frangeul L., Jacquet C., Kunst F., Martin P., Cossart P., Glaser P. &Buchrieser C. (2004). New aspects regarding evolution and virulence of *Listeria monocytogenes* revealed by comparative genomics and DNA arrays. *Infection and Immunity* **72**:1072–1083.
   DOI: https://doi.org/10.1128/IAI.72.2.1072-1083.2004

Graves M.L. & Swaminathan B. (2001). Pulse Net standardized protocol for subtyping *Listeria monocytogenes* by macro restriction and pulsed-field gel electrophoresis. *International Journal of Food Microbiology* **65**: 55–62.
   DOI: https://doi.org/10.1016/s0168-1605(00)00501-8

Gunasena D.K., Kodikara C.P., Ganepola K. & Widanapathirana S. (1995). Occurrence of *Listeria monocytogenes* in food in Sri Lanka. *Journal of National Science CouncilSri Lanka* **23**(3): 107– 114.
   DOI: http://dx.doi.org/10.4038/jnsfr.v23i3.5848

Hayes P.S., Feeley J.C., Graves L.M., Ajello G.W. & Fleming D.W. (1986). Isolation of *Listeria monocytogenes* from raw milk. *Applied Environmental Microbioloy* **51:** 438–440.
   DOI: https://doi.org/10.1128/aem.51.2.438-440.1986

Heras J., Dominguez C., Mata E., Pascual V., Lozano C., Torres C. &Zarazaga M. (2015). GelJ-a tool for analyzing DNA fingerprint gel images. *BMC Bioinformatics* **16**: 270.
   DOI: https://doi.org/10.1186/s12859-015-0703-0

Holko I., Urbanova J., Kantikova M., Pastorova K. & Kmet' V. (2002). PCR Detection of *Listeria monocytogenes* in milk and milk products and differentiation of suspect isolates. *Acta Veterinaria Brunensis* **71**: 125–131.
   DOI: https://doi.org/10.2754/avb200271010125

Husu J. (1990). Epidemiological and experimental studies of *Listeria* infections with special reference to faecal excretion in ruminants, contaminations of fresh milk, presence of the silage and growth at low temperatures. *Dissertation*, College of Veterinary Medicine, Helsinki, Finland.

Jacquet C., Gouin E., Jeannel D., Cossart P. & Rocourt J. (2002). Expression of ActA, Ami, InlB, and listeriolysin O in *Listeria monocytogenes* of human and food origin. *Applied Environmental Microbiology* **68**(1): 616–622.
   DOI: https://doi.org/10.1128/AEM.68.2.616-622.2002

Jayamanne V.S. & Samarajeewa U. (2001). Incidence and detection of *Listeria monocytogenes* in milk and milk products of Sri Lanka. *Tropical Agricultural Research* **13**: 42–50

Jersek B., Tcherneva E., Rijpens N. & Herman L. (1996). Repetitive element sequence-based PCR for species and strain discrimination in the genus *Listeria*. *Letters in Applied Microbiology* **23**: 55–60.
   DOI: https://doi.org/10.1111/j.1472-765x.1996.tb00028.x

Jones G.S. & D'Orazio S. (2013). *Listeria monocytogenes*: Cultivation and laboratory maintenance. *Current Protocols in Microbiology* **31**(9B): 2.1–2.7.
   DOI: https://doi.org/10.1002/9780471729259.mc09b02s31

Kells S. & Gilmour A. (2004). Incidence of *Listeria monocytogenes* in two milk processing environments and assessment of *Listeria monocytogenes* blood agar for isolation. *International Journal of Food Microbiology* **91**:167–174.
   DOI: https://doi.org/10.1016/S0168-1605(03)00378-7

Lieve M.H., De Block J.H. &Moermans R.J. (1995). Direct Detection of *Listeria monocytogenes* in 25 Milliliters of Raw Milk by a Two–Step PCR with Nested Primers. *Applied Environmental Microbiology* **61**(2): 817–819.

Liu D. (2006). Identification, subtyping and virulence determination of *Listeria monocytogenes*, an important foodborne pathogen. *Journal of Medical Microbiology* **55**: 645–659.
   DOI: https://doi.org/10.1099/jmm.0.46495-0

Lovett J., Francis D.W. & Hunt J.M. (1987) Listeria in raw milk: Detection, incidence and pathogenicity. *Journal of Food Protection* **50**: 188–192.
DOI: https://doi.org/10.4315/0362-028X-50.3.188

Martin P., Jacquet C., Goulet V., Vaillant V. & De Valk H. Participants in the PulseNet Europe Feasibility Study (2006). Pulsed-field gel electrophoresis of *Listeria monocytogenes*strains: the PulseNet Europe Feasibility Study. *Foodborne Pathogen Disease* **3**: 303–308.
DOI: https://doi.org/10.1089/fpd.2006.3.303

Michael Evans University of Toronto (2009). *MINITAB Manual.* W.H. Freeman and Company, New York, USA.

O'Connor L., O'Leary M., Leonard N., Godinho M., O'Reilly C., Egan J. & O'Mahony R. (2010). The characterization of *Listeria* spp. isolated from food products and the food-processing environment. *Letters in Applied Microbiology* **51**(5): 490–498.
DOI: https://doi.org/10.1111/j.1472-765X.2010. 02928.x

Olive D.M. & Bean P. (1999). Principles and applications of methods for DNA-based typing of microbial organisms. *Journal of Clinical Microbiology* **37**(6): 1661–1669.
DOI: https://doi.org/10.1128/JCM.37.6.1661-1669.1999

Osman K.M., Samir A., Abo-Shama U.H., Mohamed E.H., Orabi A. & Zolnicov T. (2016). Determination of virulence and antibiotic resistance pattern of biofilm producing Listeria species isolated from retail raw milk. *BMC Microbiology* **16**(1): 263.
DOI: https://doi.org/10.1186/s12866-016-0880-7

PulseNet-International (2013). *Standard Operating Procedure for PulseNet PFGE ofListeria monocytogenes.* Available at *http://www.cdc.gov/pulsenet/PDF/listeria-pfge-protocol-508c.pdf,* Accessed 21 November 2019.

Rahimi E., Ameri M. & Momtaz H. (2010). Prevalence and antimicrobial resistance of *Listeria* species isolated from milk and dairy products in Iran. *Food Contro l***21**: 1448–1452.
DOI: https://doi.org/10.1016/j.foodcont.2010.03.014

Ryser T. & Marth E. (1999). *Listeria, Listeriosis and Food Safety*, 2nd edition.. Marcel Dekker Inc., New York, USA.

Sarfraz M., Ashraf Y. & Ashraf S. (2017). A Review: Prevalence and antimicrobial susceptibility profile of listeria species in milkproducts.*Matrix Science Medica* **1**(1): 03–09.
DOI: https://doi.org/10.26480/msm.01.2017.03.09

Tappero *et al.* (29 authors) (1995). Reduction in the incidence of human listeriosis in the United States. Effectiveness of prevention efforts? *Journal of the American Medical Association* **273**:1118–1122.
DOI: https://doi.org/10.1001/jama.1995.03520380054035

Vardar-Unlu G., Candan F., Sokmen A., Daferera D., Polissiou M., Sokmen M., Donmez E. & Tepe B. (2003). Antimicrobial and antioxidant activity of the essential oil and methanol extracts of Thymus pectinatus Fisch. etMey. Var. pectinatus (Lamiaceae). *Journal of Agricultural and Food Chemistry* **51**: 63–67.
DOI: https://doi.org/10.1021/jf025753e

Waak E., Tham W. & Danielsson-Tham M.L. (2002). Prevalence and fingerprinting of *Listeria monocytogenes* strains isolated from raw whole milk in *farm* bulk tanks and in dairy plant receiving tanks. *Applied Environmental Microbiology* **68**: 3366–3370.
DOI: https://doi.org/10.1128/AEM.68.7.3366-3370.2002

Walter F.S. & Acheson D. (2000). Foodborne listeriosis. *Clinical Infectious Diseases*. **31**(3): 770–775.
DOI: https://doi.org/10.1086/314008

Warke S.R., Ingle V.C. & Kurkure N.V. (2023). PFGE analysis of *Listeria monocytogenes* isolates from milk, bovine clinical and bovine environment origin from Nagpur. *The Indian Journal of Veterinary Sciences and Biotechnology* **19**(2): 78–82.
DOI: https://doi.org/10.48165/ijvsbt.19.2.15

Wiedmann M., Bruce J.L., Keating C., Johnson A.E., McDonough P.L. & Batt C.A. (1997). Ribotypes and virulence gene polymorphisms suggest three distinct *Listeria monocytogenes* lineages with differences in pathogenic potential. *Infection and Immunity* **65**: 2707–2716.
DOI: https://doi.org/10.1128 / iai.65.7.2707-2716.1997

Wijendra W.A.S., Kulathunga K.A.C.C. & Ramesh R. (2014). First report of *Listeriamonocytogenes* serotypes detected from milk and milk products in Sri Lanka. *Advances in Animal and Veterinary Sciences* **2**:11–16.
DOI: https://doi.org/10.14737/journal.aavs/2014/2.5s.11.16

Wojciech L., Kowalczyk K., Staroniewicz Z., Kosek K., Molenda J. & Ugorski M. (2004). Genotypic characterisation of *Listeria monocytogenes* isolated from foodstuffs and farm animals in Poland. *Bulletin of the Veterinary Institute in Pulawy* **48**: 427–435.

Zdolec N., Jankuloski D., Kiš M., Hengl B. & Mikulec N. (2019). Detection and pulsed-field gel electrophoresis typing of *Listeria monocytogenes* isolates from milk vending machines in Croatia. *Beverages* **5**(3):46.
DOI: https://doi.org/10.3390/beverages5030046

RESEARCH ARTICLE

Atmospheric Science

Variations of pre-monsoon season related atmospheric parameters over Kakinada region

TR Vishnu[1], KS Kumar[2], SKH Ahammad[2], GNS Kumar[3], N Umakanth[4], MC Rao[5*] and S Krishna[6]

[1] *Department of Electronics and Communication Engineering, Priyadarshini Institute of Technology and Science For Women, Chintalapudi, India.*

[2] *Department of Electronics and Communication Engineering, Koneru Lakshmaiah Education Foundation, Vaddeswaram, India.*

[3] *Department of Mechanical Engineering, R K College of Engineering, Amaravathi, India.*

[4] *Department of Electronics and Communication Engineering, Kallam Haranadhareddy Institute of Technology, Chowdavaram, India.*

[5] *Department of Physics, Andhra Loyola College, Vijayawada, India.*

[6] *Department of Electronics and Communication Engineering, Dhanekula Institute of Engineering and Technology, Vijayawada, India.*

Abstract: Pre-monsoon showers occur before the beginning of the rainy season. From the months of March to May, they take place, and can be anything from little drizzles to powerful thunderstorms. March, April and May are known as the pre-monsoon season (PRMS). The precipitation patterns recorded in PRMS are critical because they have an impact on a wide range of crop-related operations across the country. During PRMS, the maximum temperature (TMAX), minimum temperature (TMIN), soil moisture, relative humidity, latent heat, convective available potential energy (CAPE), and total precipitable water (TPW) were analysed at Kakinada region. These variables were collected using daily ERA5 reanalysis data for the PRMS from 1981 to 2021. Studying the convection-related characteristics over the Kakinada station during the PRMS was our goal. During the study period, the five years with the highest PRMS rainfall were 1990, 1995, 2008, 2010 and 2016 and the five years with the lowest rainfall were 1990, 1995, 2008, 2010 and 2016. In the months leading up to the monsoon, the Kakinada station experiences CAPE values between 1000 and 6000 J/kg, while TPW values are between 25 and 60 mm. The PRMS values for CAPE and TPW both show that the prerequisites for moderate to severe convection activity have been fulfilled. TPW, soil moisture, relative humidity, and CAPE parameters during PRMS were well estimated using the ARMA and ARIMA models.

Keywords: Convection, pre-monsoon, soil moisture, total precipitable water.

INTRODUCTION

PRMS (March-May) in India is a transitional period between the winter and monsoon seasons (Ray *et al.*, 2016). The monsoon season usually begins in advance of the month of June and continues till the end of September across the Indian region (Tyagi *et al.*, 2019). Thunderstorms have become increasingly regular in recent years and they have been accompanied by heavy rain and lightning strikes. Every year, these thunderstorms kill hundreds of people and destroy vast quantities of property. Hundreds of people are being affected by thunderstorm activity in India every year. In 2022, till November, 907 people were dead due to thunderstorm events that occurred over different regions (The Hindu, 2023). A high death rate is observed in West Bengal, Jharkhand, Bihar, Assam, and Odisha states. The common scenario which we observe during these events is a large growing cloud. These systems occur from a small area to larger areas depending on the local instability that triggers the thunderstorm events (single cell or multi-cell) (Bharadwaj *et al.*, 2017).

The instability is caused by the heating of the land surface. This heating makes the air warm and moist. This air collides with the oceanic air mass. Numerous studies have been conducted on the PRMS thunderstorms and other convective events in northern India. In moisture advection phenomena, the southerly winds are absent. This was investigated by Srinivasan (1962) and he found that the Gangetic West Bengal region experiences more

favourable convection conditions for thunderstorm occurrences. In a few occasions, though the favourable situations exists, convection initiation does not takes place in the region of occurrence. Srinivasan *et al.* (1973) discovered that heavy rainfall periods in northern India are linked to horizontal scale westerly trough winds that supply a good moisture content to the PRMS convective zone, despite the fact that the westerly continental airflow contributes limited precipitation.

The convection linked systems over eastern India and Bangladesh are of the squall line type of convection, which causes high winds and precipitation (Rafiuddin *et al.* 2009). The squall line is one of the forms of convective storms that lead to hail storm and tornado activity in eastern parts of India (Bhattacharya & Bhattacharya, 1983). They also determined that storm seasons are usually associated with convection variations that occur due to heating activity that take place in the lower atmospheric pressure levels. There is a lot of lightning during these severe convective storms. Nor'westers that possess high surface wind speeds which are greater than 50 km h^{-1} have high counts of lightning strikes, *i.e.*, 30 per minute on a regular basis (Midya *et al.*, 2021). They also discovered that the lightning strikes keep increasing rapidly before 10–40 minutes of onset of the convective storm. According to Chaudhuri (2008), cumulonimbus and stratocumulus clouds are the most commonly seen clouds over eastern parts of India during the PRMS. According to Nayak and Mandal (2014), energy-helicity index, wind shear parameter derived between 3 and 7 km s^{-1}, and the vorticity generation parameters play a critical role in the assessment of thunderstorm precipitation. Roy (2021) discovered three areas in the Indian subcontinent having maximum thunderstorm occurrences. They identified those areas by analysing long-term patterns in thunderstorm frequency. They also revealed that in the second part of the twentieth century, the frequency of thunderstorm days in eastern and southern India is dropping. But in the recent two decades they were increasing at an abnormal rate, which is due to the effect of global warming. Thunderstorms were most common at night in north-eastern India, whereas they were most common in the evening in eastern India, according to Ray *et al.*, 2016. They also determined that thunderstorms occur often at night in the sub-Himalayan West Bengal and Sikkim regions. However, the Odisha, Bihar, and West Bengal states have suffered more thunderstorm occurrences in the evening times (Ravi *et al.*, 1999; Tyagi *et al.*, 2011). Several studies were conducted to see how well various stability criteria predicted favourable circumstances for convection to form and develop into thunderstorms (Schultz, 1989; Kunz, 2007; Dhawan *et al.*, 2008).

CAPE is a great predictor of convection activity over eastern India, and it's also great for operational forecasting (Roy *et al.*, 2008). This indicator gives information on buoyant energy in the atmosphere as well as wet instability (Neelin, 1997). Numerous studies were published on convection based events during monsoon time.

Kakinada is the state's sixth largest city and the district headquarters of the East Godavari district in Andhra Pradesh, India. On the Bay of Bengal's coast, it is located at 16.93°N latitude and 82.22°E longitude. Kakinada has a tropical, dry climate with hot, humid weather for the majority of the year. With maximum temperatures of 38–42 °C, late May and early June are the warmest months of the year. The coldest month is January with minimum temperatures of 18–20 °C. The southwest monsoon provides the majority of the city's seasonal rainfall; however the northeast monsoon also provides significant rain (from mid-October to mid-December). The city is frequently hit by cyclones from the Bay of Bengal. The prevalent winds in Kakinada are southwest throughout the most of the year, except from October to January, when they are northeast. The average annual rainfall in the city is 110–115 mm (Seatemperature.org). There is very little comprehensive research on PRMS related convective systems, that employs long-term information from across the study region. This study looks at convection-related characteristics over the Kakinada station in the Andhra Pradesh region during PRMS. These pre-monsoon convective systems are responsible for a large number of deaths and property damage in this region and so require additional research. The purpose of this research is to close that gap. Forecasting mesoscale convective activity, particularly pre-monsoon convective episodes and related rainfall, is also a key difficulty for the forecasting community. The goal of this research is to find out what factors influence convective systems above the Kakinada station during the PRMS.

MATERIALS AND METHODS

Data

The GPM IMERG (Integrated Multi-satellite Retrievals for Global Precipitation Measurement) system is a well-defined US mechanism for sending multi-satellite precipitation data to the GPM team in the United States. The Goddard Profiling Algorithm is used to grid, intercalibrate, and integrate the GPM constellation's many precipitation-relevant satellite passive microwave (PMW) sensors into half-hourly 0.1° x 0.1° (about 10 x 10 km) fields (GPROF2017). These data are accessible from any location on the globe. The URL *https://gpm.nasa.gov/data/directory/index.html* contains the GPM IMERG data. For the years 1981 to 2021, 0.25° precision ERA5 surface level and pressure level reanalysis data were obtained (Hersbach & Dee, 2018); *https://cds.climate.copernicus.eu/#!/home* is the URL where ERA5 data are collected. The National Oceanic and Atmospheric Administration's (NOAA) Global Reanalysis Products provided us with information on soil moisture, relative humidity, maximum temperature, minimum temperature, and latent heat flux. These data are available at *https://psl.noaa.gov/data/gridded/data.ncep.reanalysis.html.* The NASA Global Modeling and Assimilation Office has released MERRA-2, or Modern-Era Retrospective Analysis for Research and Applications (Gelaro *et al*., 2017). The original MERRA atmospheric reanalysis dataset has been replaced and expanded with this updated, higher-quality output of the global reanalysis (Rienecker *et al*., 2011). The Modern-Era Retrospective Analysis for Research and Applications version 2 (MERRA-2) was used to gather daily temperature data over Kakinada region from 1981 to 2021. MERRA2 data can be found at *https://goldsmr4.gesdisc.eosdis.nasa.gov/data/MERRA2*.

Methodology

We have used the calculations below to determine the CAPE and TPW parameters using the above data.

CAPE

CAPE is a unit of measurement for the potential energy of an air parcel per kilogramme of air mass, which is expressed in Joules per kilogramme (J/kg). CAPE refers to the buoyant energy necessary to lift an air packet into the air. When you combine these two numbers together, you get the total positive buoyant energy from free convection to equilibrium (Moncrieff & Miller, 1976).

$$\text{cape} = \int_x^y g\left[\frac{TV_{parcel} - TV_{env}}{TV_{env}}\right] dz \qquad \qquad \dots(1)$$

Where TV_{parcel} and TV_{env} denote the parcel's virtual temperature and the environment's virtual temperature, respectively, x and y reflect the levels of free convection and neutral buoyancy.

Cape parameter critical values (Grieser, 2012)

Cape (in J/kg)	Thunderstorm chances
Under 300	No energy for convection
From 300 to 1000	Weak convection has a low potential.
From 1000 to 2500	Convectional potential is moderate.
Greater than 2500	Convectional potential is high.

Total precipitable water (TPW)

The quantity of water that can be collected from the earth's surface to the topmost pressure level in the atmosphere is determined using TPW. When all of the water and water vapour has condensed into a liquid phase, this should satisfy the following formula, which is used to calculate it.

$$TPW = \frac{1}{g}\int_{P_1}^{P_2} W \ dP \qquad \qquad \dots(2)$$

W is the mixing ratio and P_1 and P_2 are the two pressure levels (Carlson *et al.*, 1990).
The basic arithmetic equation for the ARMA model is as follows:

$$X(t) = \sum_{i=1}^{p} \theta_i X(t-i) + \sum_{j=1}^{q} \emptyset_j e(t-i) \qquad \qquad \dots(3)$$

Where θ_i, $\emptyset_j$ are the autoregressive and moving average coefficients, respectively.
p, q: Autoregressive and Moving Average order.
X_t : Values of output parameters at time t for t = 1, 2, 3, ... t,
e_t: White noise

The numerical representation of the Autoregressive operator is as follows:

$$\theta_i = \theta_1 X(t-1) + \theta_2 X(t-2) + \cdots + \theta_p X(t-p) \qquad \qquad \dots(4)$$

In the same way, the moving average operator is defined as

$$\emptyset_j = \emptyset_e(t-1) + \emptyset_e(t-2) + \cdots + \emptyset_p e(t-q) \qquad \qquad \dots(5)$$

The autoregressive and moving average coefficients are computed using the Yule-Walker and Newton-Raphson relations (Ratnam *et al.*, 2019). The ARMA estimation model that we utilized in this work was trained and tested using the MATLAB 7.0 Toolbox.

The ARIMA (auto regressive integrated moving average) model was created as an extension or generalisation of the ARMA model (Box and Jenkins 1976). ARIMA (p, d, q) is made up of three parts: autoregressive (AR), integrated (I), and moving average (MA) (MA). The letter p stands for the AR component. It illustrates the consequences of previously stretched PRMS data. The letter d stands for the integrated (I) component. It demonstrates the wide range of differences. Finally, q is used to represent the MA component. The ARIMA (p, d, q) model is given as follows in its most basic form (Box & Jenkins, 1976; Brockwell & Davis, 2001).

$$\emptyset_p(B)(1-B)^d V_t = \theta_q(B)\varepsilon_t \qquad \qquad \dots(6)$$

Where θ_p, $\emptyset_q$ are the autoregressive and moving average coefficients, respectively.
p, q : Autoregressive and moving average order.
V_t : Forecasted output parameter values at time t
d   : The number of times the data has been changed
B   : Operator for the backward shift $BV_t = V_{t-1}$
ε_t : Error term, a normal distribution with mean 0 and standard deviation 2

It is crucial that a model be used to examine the performance of ERA5 data in order to test the significance of PRMS parameters and to create confidence intervals for the estimation. Finally, an estimation is made using the ARMA and ARIMA models. For the ARMA and ARIMA estimation methods, the PRMS parameters were used. Finding the stochastic process of the time series and properly predicting future values are the major goals of fitting the ARIMA model. First, adequate values for p, q, and d, three parameters of the ARIMA model, were identified. The statistical toolbox in MATLAB 2018 is the software utilized for ARMA and ARIMA models. Time series forecasting is a rapidly expanding field of study, offering numerous opportunities for new research in the future. One of them is the 'Combining Approach,' in which a variety of various and unrelated methodologies are combined to increase forecast accuracy.

We generated BIAS, correlation coefficient (CC), and root-mean-square error (RMSE) terms for various parameters to statistically analyse the ARMA and ARIMA model performances with ERA5 reanalysis data. Wilks (2006) gave the following formulas:

$$BIAS = \frac{1}{n}\sum_{i=1}^{n}(o_i - f_i) \qquad \qquad \text{...(7)}$$

$$CC = \frac{\sum_{i=1}^{n}(f_i-\hat{f})(o_i-\acute{o})}{\sqrt{\sum_{i=1}^{n}(f_i-\hat{f})^2}\sqrt{\sum_{i=1}^{n}(o_i-\acute{o})^2}} \qquad \qquad \text{...(8)}$$

$$RMSE = \sqrt{\frac{\sum_{i=1}^{n}(f_i-o_i)^2}{n}} \qquad \qquad \text{...(9)}$$

Where o_i and f_i are the observed and predicted values, respectively.

RESULTS AND DISCUSSION

The characteristics impacting PRMS convective systems at the Kakinada station were investigated in this study. During the period 1981–2021, we have calculated the PRMS mean rainfall for each year at the Kakinada station (Figure 1). 1990, 1995, 2016, 2010, and 2008 are the years with the five highest PRMS rainfall over the study region. 1991, 1985, 2017, 1982, and 1996 are the five lowest PRMS rainfall years over the study region. The mean PRMS daily rainfall from the GPM-IMERG satellite output is shown in Figure 1. Based on available daily rainfall data from the Kakinada station for the years 1981 to 2021, the mean seasonal rainfall across the PRMS is around 110 mm. During the PRMS month of May, the most intense convection activity is observed (see Figure 1). The years 1990, 1995 and 2016 showed rainfall higher than the normal mean rainfall. In these three years, there was cyclonic activity which led to high rainfall occurrence on the Kakinada region.
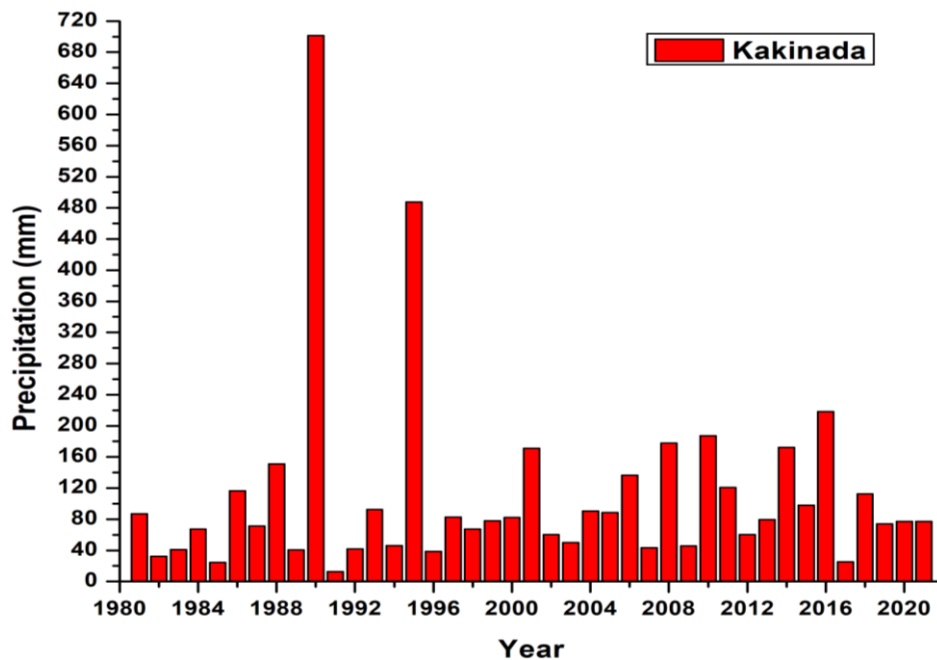

Figure 1:   Mean PRMS rainfall variations over the Kakinada station during the time period 1981 -2021.
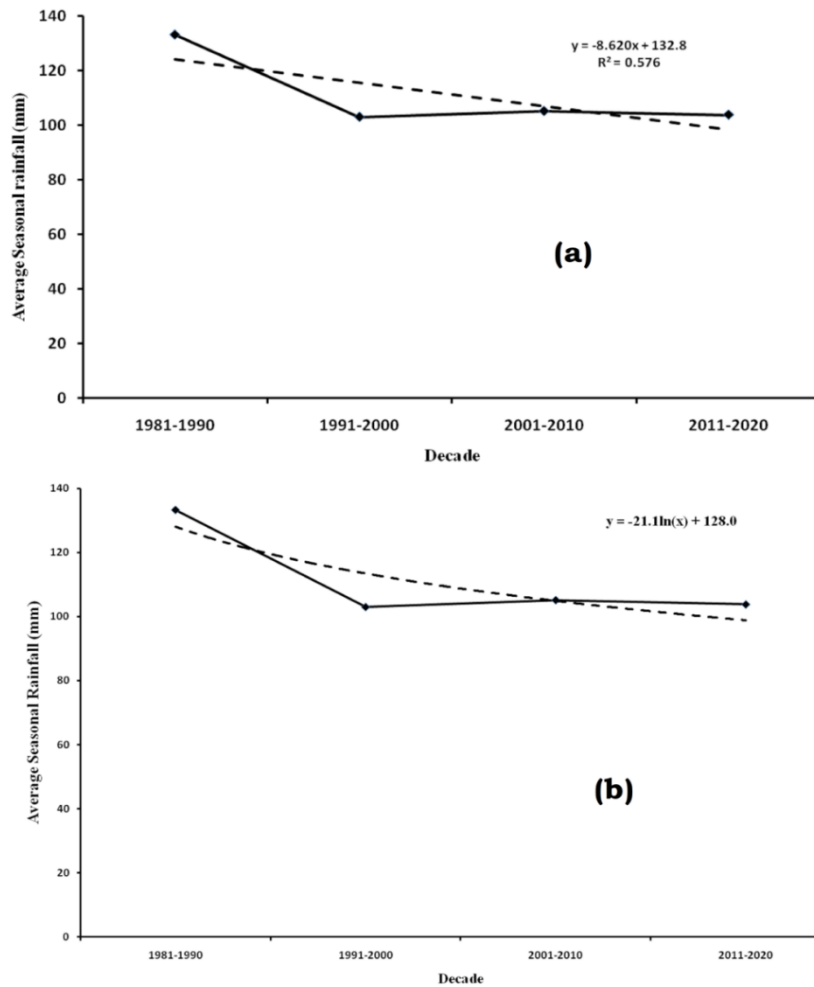
Figure 2: Decadal variation of average seasonal rainfall over the Kakinada station.

From 1991 to 1994 and 1996 to 2000, the average seasonal rainfall has decreased each year. (See Figure 1 for further information). Rainfall activity has also increased from 2005 to 2021. A deceasing trend has been noticed in the decadal variation of average seasonal rainfall during 1981-2021 (see Figure 2a and b).
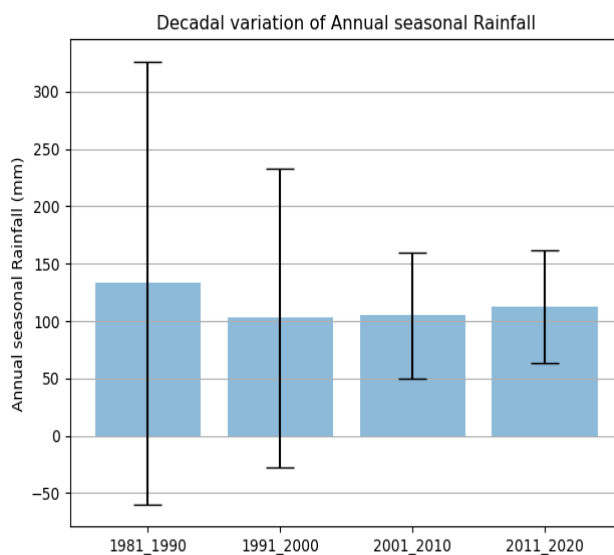

Figure 3: Bar plot of average seasonal rainfall with error bars over the Kakinada station.

Error bars are useful to problem solvers because they reflect the confidence or precision in a collection of measurements or calculated results. The generated plot has four error bars. Looking at the error by duration, we can observe that the standard deviation of seasonal rainfall during 1981-1990 is larger than the standard deviation of seasonal rainfall throughout other decades (Figure 3).
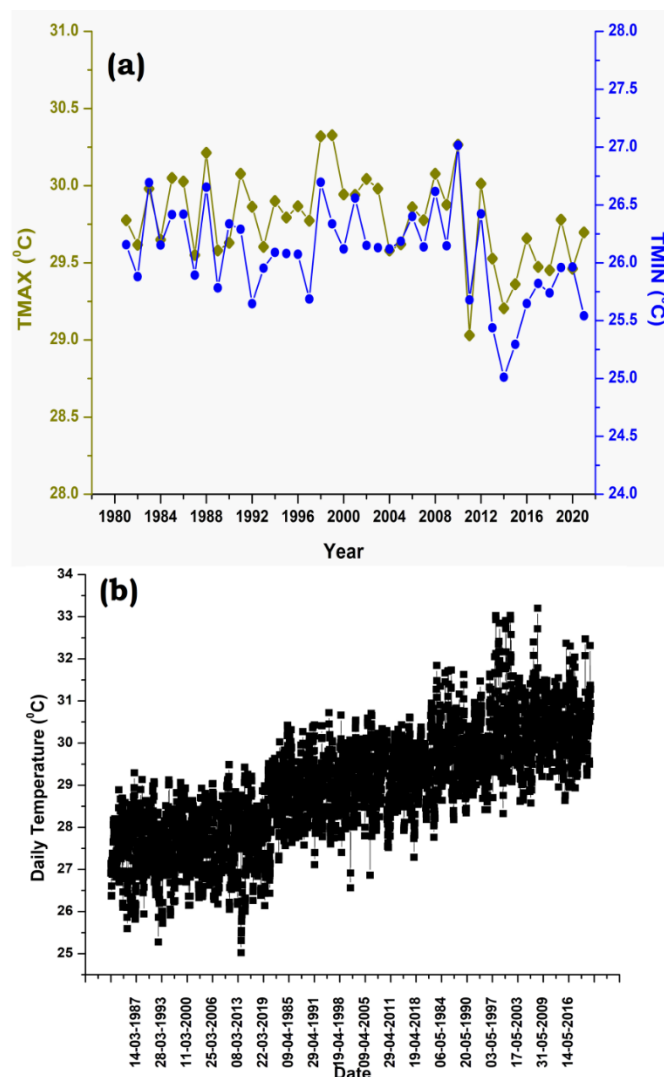

Figure 4: (a) Variations of maximum temperature parameter and minimum temperature parameter during the period 1981- 2021 of the PRMS at Kakinada region; (b) Daily Variations of temperature parameter during the period 1981- 2021 of the PRMS at Kakinada region.

The time series of maximum and minimum temperatures for the PRMS are presented in Figure 4a. The TMAX values over Kakinada station during all PRMS months range from 29 to 32 °C. It was seen that when the TMAX values are decreasing, the rainfall is increasing. The rainfall occurrence in May has been severe in the last five years, indicating strong rainfall activity over the Kakinada region. TMIN values over Kakinada station range from 25 to 27 °C for all the PRMS months. In the recent 5 years there is a drop in TMIN values which is favouring high rainfall occurrence during PRMS over the Kakinada region. Rainfall activity in the Kakinada region is higher in the months of April and May than it is in the month of March. The daily temperature values are higher in May when compared to March and April. In March, the average temperature values range between 25 °C and 29 °C. In April, the average temperature values range between 26 °C and 31 °C and between 27 °C and 33 °C in May (Figure 4b). When sunlight and infrared radiation heat the Earth's surface, water condenses as buoyant air rises, forming convective systems. As CO_2 levels rise and the land surface heats, stronger updrafts are more likely to produce lightning and rainfall.
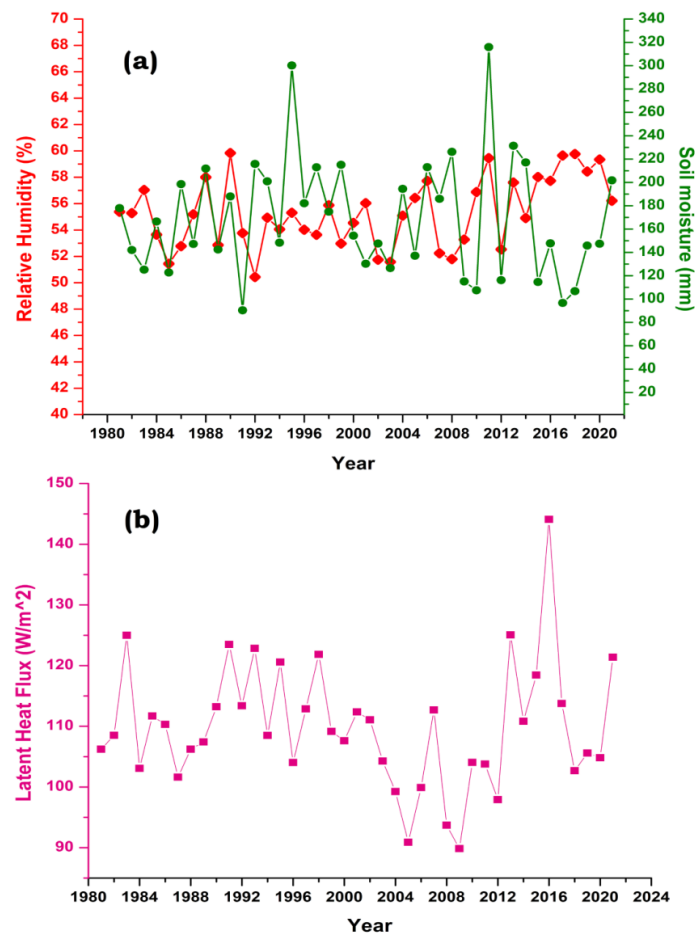
Figure 5:   Variations of (a) soil moisture and relative humidity parameter; (b) latent heat
flux parameter during the period 1981- 2021 of the PRMS at Kakinada region.

Temperature and precipitation forecasts rely heavily on soil moisture. The rate of evaporation of soil moisture increases as the temperature rises. The increased evaporation of soil moisture aids in ground cooling. Convective precipitation is influenced by soil moisture in two ways. Evaporation is aided by increased soil moisture, which cools the surface while also supplying moisture to the atmosphere. Cooling would limit convection and consequently precipitation, but adding moisture would increase precipitation. The time series of soil moisture for PRMS is displayed in Figure 5a. Over Kakinada station, soil moisture readings range from 80 to 330 mm for all the PRMS months. When the soil moisture value rises, then the rainfall rises with it. In the recent 5 years, the soil moisture values have increased significantly. This helps the high rainfall activity over the Kakinada region. Thunderstorms and convective systems thrive in high-humidity conditions. Convective systems are strengthened substantially when rising humid air cools in the higher regions of the storm, because they are tall weather systems based on columns of rising air. All of the heat energy used to evaporate that water is released as the cooling humidity condenses into liquid water in the clouds. This extra heat warms the air around it, making it more buoyant. This relative humidity parameter helps to increase the peak stage of convective formation. The time series of relative humidity for the PRMS is displayed in Figure 5a. Over the Kakinada station, the mean relative humidity values range from 50 to 60% during all the PRMS months. These percentages reached 90% on convection days. In thunderstorms and hurricanes, latent heat is extremely essential. Warm air rises, and the water vapour contained therein condenses onto cloud condensation nuclei, generating clouds. At this point, the air has become saturated. When the water vapour in this air first begins to rise, it is in the gaseous phase. Latent heat is released into the atmosphere as water vapour condenses into clouds. The latent heat then causes instability by warming the surrounding air around the nascent cloud droplet. Warm air in the vicinity of the cloud droplet will now desire to climb and condense. The time series of latent heat flow for the PRMS is displayed in Figure 5b. The latent heat flux measurements over the Kakinada station range from 85 to 150 W/m^2 during the PRMS months.
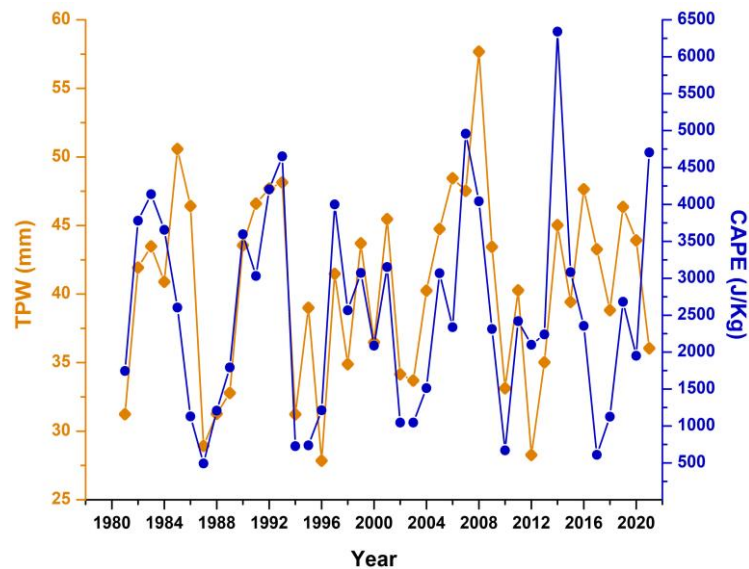
Figure 6: Variations of CAPE parameter & TPW parameter during the period 1981- 2021 of the PRMS at Kakinada region.

We have computed CAPE and TPW values over the Kakinada region using ERA5 temperature and relative humidity data at various pressure levels. Time series plots of CAPE and TPW parameters for the PRMS from 1981 to 2021 are shown in Figure 6. In recent decades, the convective available potential energy (CAPE) has gained popularity as a prominent instability indicator for analysing the atmosphere's convective potential. It has been used in a number of studies and is calculated using an integral of a vertical cloud buoyancy profile. Total precipitable water is the amount of moisture that falls over a certain place (TPW). It represents the amount of moisture in the air rather than the amount of rain that will fall. During the pre-monsoon months, CAPE values over the Kakinada station vary from 1000 to 6000 J/kg, whereas TPW values range from 25 to 60 mm. Both the CAPE and TPW parameters in the PRMS demonstrate that the thresholds for moderate to severe convection activity are good.

Around 1000 and 950 hPa, there is a small dew point dip. At 800 hPa, it climbed to 6-14 K, then began to grow to 20 K at 500 hPa. It decreased to 12K at 250 hPa in March. In April and May, the values soared even at 200 hPa. This clearly shows that moist air occurs between 1000 hPa and 800 hPa, with dry air existing above it from (800 -500 hPa), and that moist air exists between 500 hPa and 400 hPa, with dry air existing in the upper layers of the atmosphere, reflecting a highly unstable situation over Kakinada station (Figure 7a). A plot of vertical velocity (VV) across the Kakinada area is given in Figure 7b. We saw big negative vertical velocity readings on days with a lot of convection. This suggests that air mass is moving higher in the lower atmosphere. When compared to April, the month of May saw more negative VV values. When negative VV values are seen, it means the air mass is ascending. When positive VV values are detected, it indicates that the air mass is sinking. This is owing to the fact that as height increases, pressure is lowered. The substantial moisture buildup across the study region supports these VV values on heavy precipitation days.
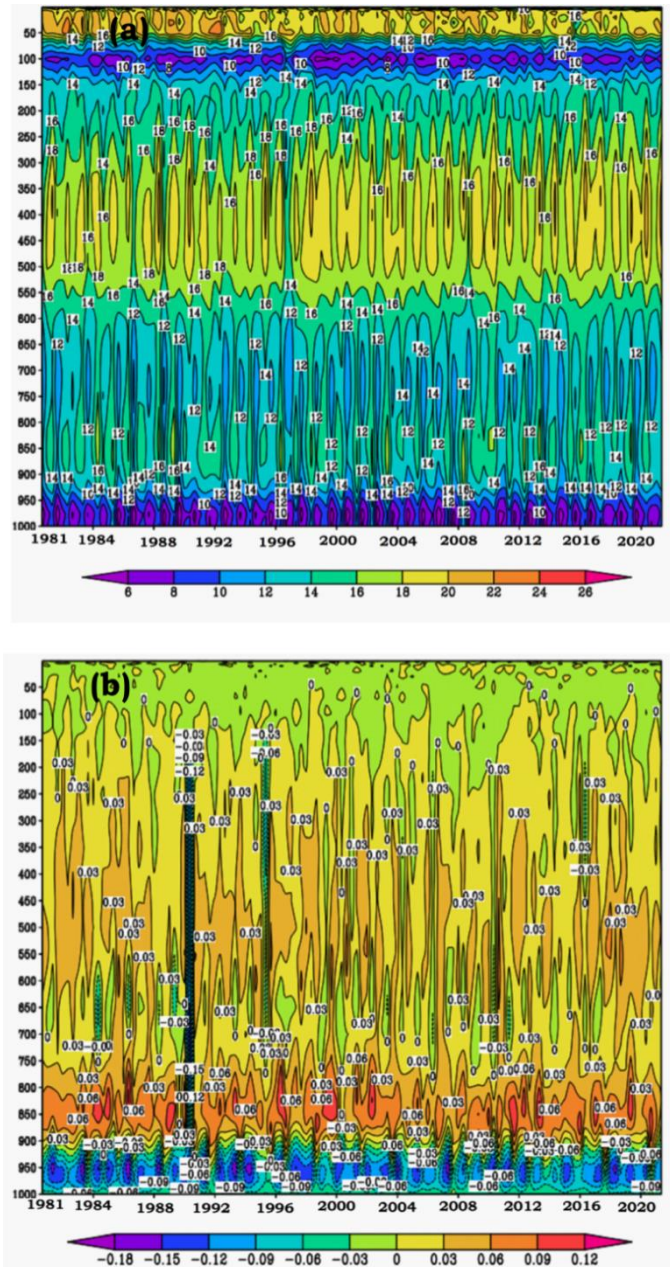
Figure 7: Time-height sections of (a) Dew point depression; (b) Vertical velocity
during the period 1981- 2021 of the PRMS at Kakinada region.

In the Kakinada region, mean temperature and humidity profiles, computed from ERA5 measurements at various isobaric levels, were displayed (Figure 8a). As a result, these profiles can reveal how convection develops. The dew point depression is around 3K at 1000 hPa, then drops to 1K at 950 hPa, then rises to 8K at 700 hPa, then drops to 5K at 500 hPa, then rises to 14.5 K at 250 hPa, then drops to 5K at 100 hPa. This clearly implies that moist air exists between 1000 and 800 hPa, and that dry air exists above this moist air from 800 to 500 hPa, and that moist air exists between 500 and 400 hPa, and that dry air exists in the top layers of the atmosphere, indicating a very unstable environment (Figure 8b).
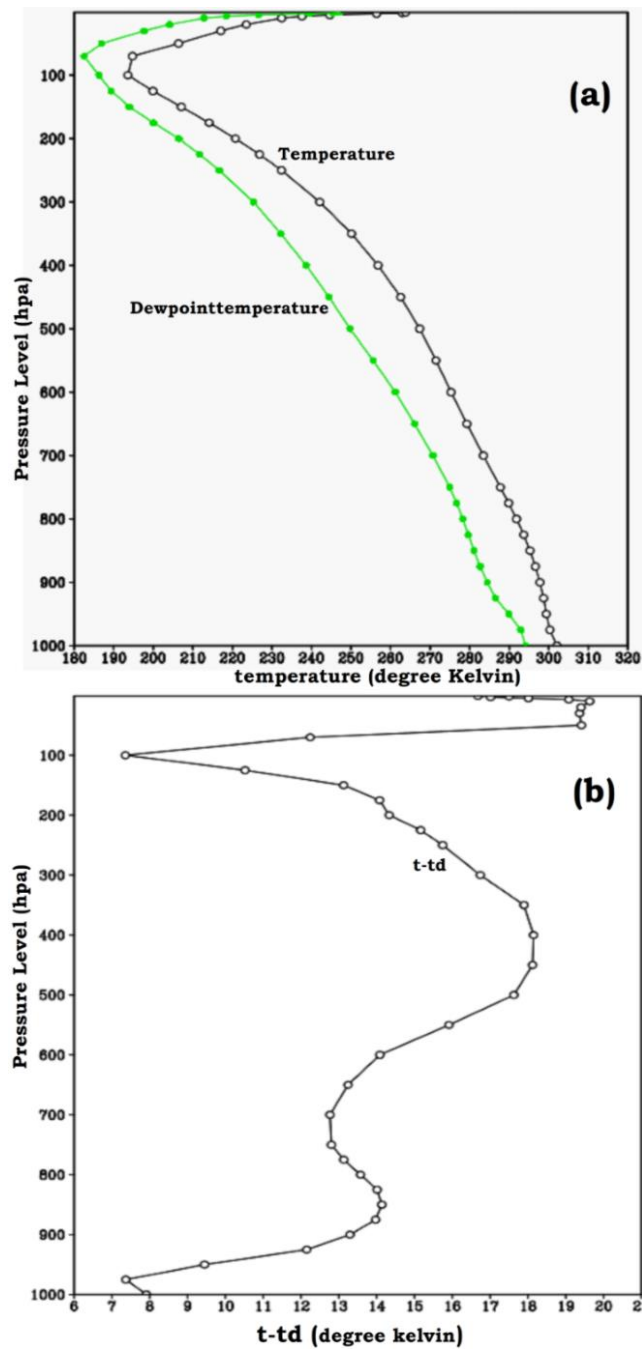
Figure 8: Time-height sections of (a) Temperature and dewpoint temperature parameters; (b) dewpoint depression during the period 1981- 2021 of the PRMS in the Kakinada region.

In the Kakinada region, the mean wind speed values from ERA5 measurements at various isobaric levels were displayed for PRMS (Figure 9a). At a height of ten metres above the Earth's surface, this value represents the greatest wind gust at the specified time. This metric is calculated by averaging the greatest wind speed over three seconds. As a result, these profiles reveal that the wind speeds increase slowly from surface to 500hpa. At the surface the wind speeds in PRMS are 4 to 6 m/s. From 500 hPa to 150 hPa, the wind speeds started increasing faster till 100 hPa. The wind speed values range in between 6 m/s and 19 m/s. This demonstrates that warm moist air is available in the lower levels whereas cold dry air is available in the upper levels. Cold dry air is related to westerly wind which we observe usually in PRMS. The warm moist air is usually linked to the Bay of Bengal. We also plotted PRMS surface wind speeds. These values range between 2.5 m/s and 4.3 m/s (Figure 9b).
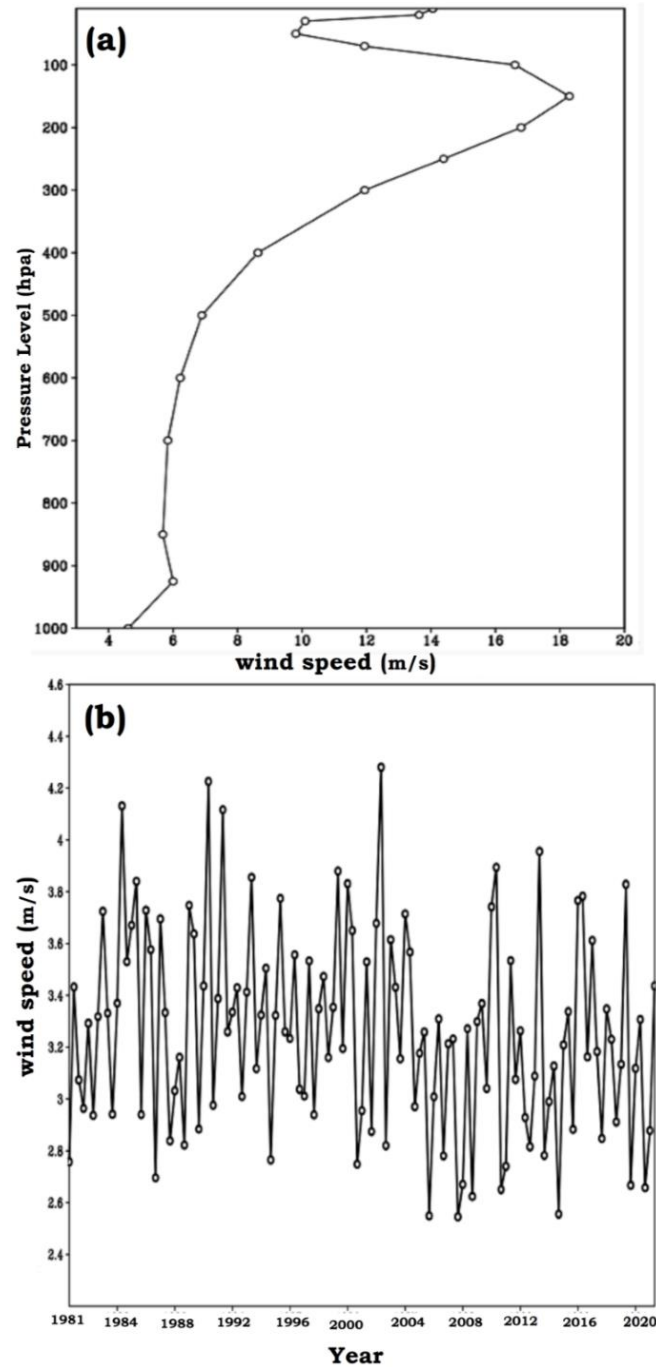
Figure 9: (a) Time-height sections of wind speed parameter; (b) Time series plot of
10 m-wind speed parameter during the period 1981- 2021 of the PRMS at
Kakinada region.

We have chosen four factors (CAPE, TPW, relative humidity, and soil moisture) for ARMA and ARIMA model
estimations based on their threshold values. As a result, we calculated those four parameters using the ARMA and
ARIMA models. The main goal of this computation, as shown in Figure 10, is to compare the precision of ARMA
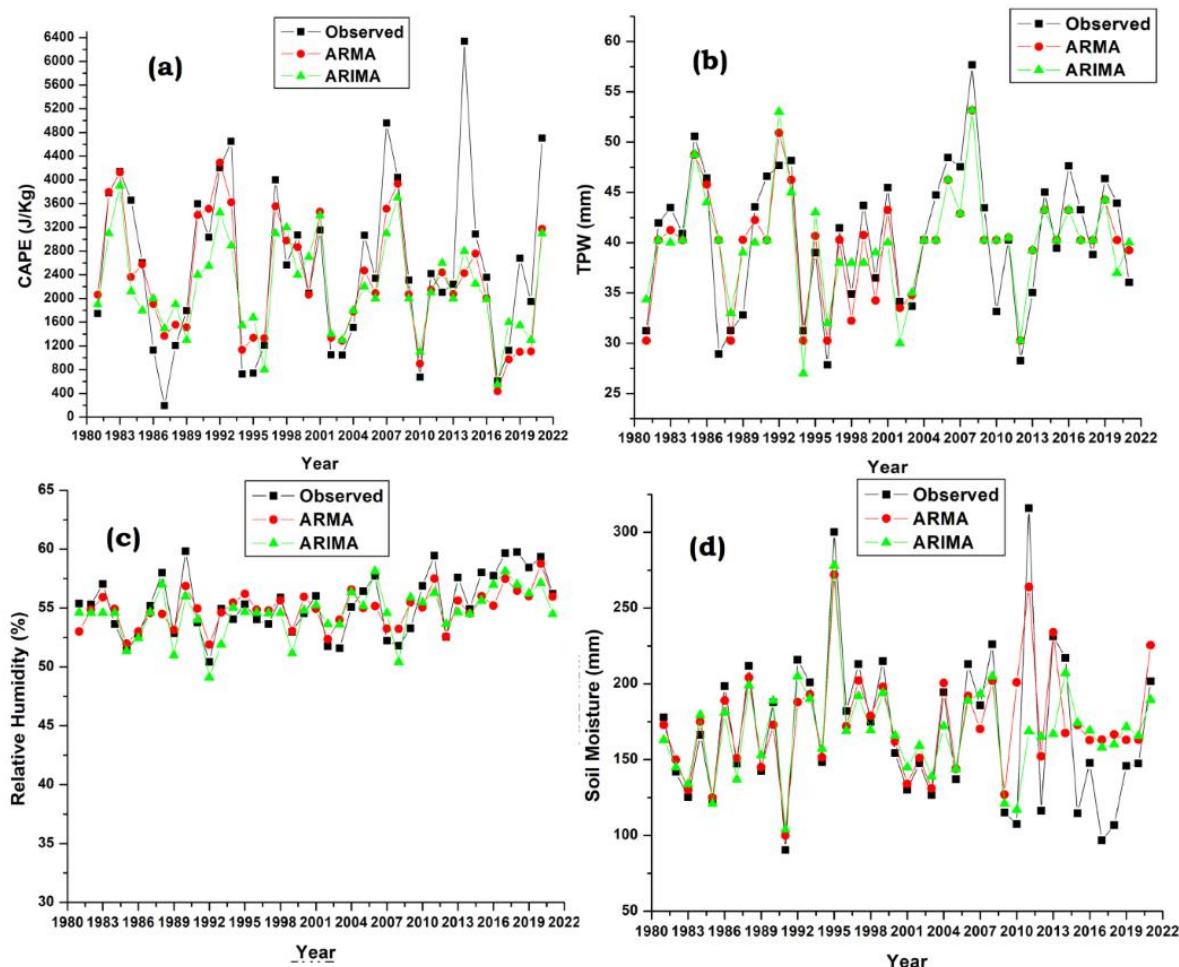and ARIMA models with ERA5 data.

Figure 10: Time series plot of observed and calculated data for PRMS parameters (a) CAPE; (b) TPW; (c) Relative Humidity and (d) Soil Moisture, at Kakinada station from 1981 to 2021.

Table 1: Statistical Based analysis of ERA5 data and ARMA model

Parameter	RMSE	CC	BIAS
TPW	3.50	0.86	0.47
CAPE	863.0	0.80	220
Relative Humidity	1.64	0.81	0.39
Soil moisture	28.09	0.84	4.34

Table 2: Statistical Based analysis of ERA5 data and ARIMA model

Parameter	RMSE	CC	BIAS
TPW	4.15	0.79	0.51
CAPE	977.5	0.77	336.8
Relative Humidity	1.73	0.78	0.70
Soil moisture	33.39	0.76	0.85

A correlation analysis was done for the Kakinada station between the ERA5 computed values and the ARMA model computed values (Table 1). The ERA5 measured parameter values (observed) were compared to the ARIMA model calculated parameter values (Table 2). We calculated the BIAS, CC and RMSE for ARMA and ARIMA models, as shown in Tables 1 and 2. The TPW parameter has the highest CC of 0.86 when compared to

other components, meaning that 86 percent of the ARMA projected TPW complement the observed data (ERA5). The CC of the CAPE parameter is 0.77, meaning that 77% of the ARMA-calculated CAPE complement the observed data (ERA5). As a result, the ARMA and ARIMA models have shown to be quite useful in obtaining precise statistical estimates of thunderstorm-related properties. In terms of estimating PRMS parameters, the ARMA model beat the ARIMA model.

CONCLUSION

The convection-related properties are studied over the Kakinada station during the PRMS. The current study is being carried out for the PRMS from 1981 to 2021. Both the CAPE and TPW metrics in the PRMS indicate that the conditions for moderate to severe convection activity are met. ARMA and ARIMA models can be used to produce a significant decision-making tool. The benefit of adopting this kind of models is that, despite many issues with their development and testing, we learn about the structure of the time series and the process that led to its production. It is fascinating to develop models for thunderstorm-related rainfall because of its intricate structure and sensitivity to environmental factors. The study demonstrates that the ARMA and ARIMA models are not only reliable but also the best models for predicting the activity of thunderstorms that produce rainfall. Policymakers are alerted by predicted outcomes to make the appropriate preparations in advance to deal with thunderstorm heavy rainfall events. As a result, the ARMA and ARIMA models have shown to be quite beneficial in obtaining precise statistical estimates of thunderstorm-related characteristics. When it comes to estimating PRMS parameters, the ARMA model outperformed the ARIMA model.

REFERENCES

Bhattacharya A.B. & Bhattacharya R. (1983). Radar observations of tornadoes and the field intensity of atmospherics. *Meteorology and Atmospheric Physics* **32**(1–2): 173–179.
DOI: https://doi.org/10.1007/BF02272722

Bharadwaj P., Singh O. & Kumar D. (2017). Spatial and temporal variations in thunderstorm casualties over India. *Singapore Journal of Tropical Geography* **38**(3): 293–312.
DOI: https://doi.org/10.1111/sjtg.12201

Box G.E. & Jenkins G.M. (1976). *Time Series Analysis: Forecasting and Control*, 2nd edition. Holden-Day Inc., San Francisco, USA.

Brockwell P.J. & Davis R.A. (2001). *Introduction to Time Series and Forecasting,* 2nd edition. Springer, New York, USA.

Carlson T.N., Perry E.M. & Schmugge T.J. (1990). Remote estimation of soil moisture availability and fractional vegetation cover for agricultural fields. *Agricultural and Forest Meteorology* **1-52**(1-2): 45–69.
DOI: https://doi.org/10.1016/0168-1923(90)90100-K

Chaudhuri S. (2008). Preferred type of cloud in the genesis of severe thunderstorms – a soft computing approach. *Atmospheric Research* **88**(2): 149–156.
DOI: https://doi.org/10.1016/j.atmosres.2007.10.008

Dhawan V.B., Tyagi A. & Bansal M.C. (2008). Forecasting of thunderstorms in pre-monsoon season over Northwest India. *Mausam* **59**(4): 107–111.
DOI: https://doi.org/10.54302/mausam.v59i4.1272

Gelaro R, McCarty W, Suárez M.J., Todling R, Molod A, Takacs L. & Zhao B (2017) The modern-era retrospective analysis for research and applications, version 2 (MERRA-2). *Journal of Climate* **30**(14): 5419–5454.
DOI: https://doi.org/10.1175/JCLI-D-16-0758.1

Grieser J. (2012). *Convection Parameters*. Selbstverl, Germany.

Hersbach H. *et al.* (15 authors) (2018). *ERA5 hourly data on single levels from 1979 to present.* Copernicus Climate Change Service (C3S) Climate Data Store (CDS). Available at *https://cds.climate.copernicus.eu/cdsapp#!/search?type=dataset.*

Kunz M. (2007). The skill of convective parameters and indices to predict isolated and severe thunderstorms. *Natural Hazards and Earth System Sciences* **7**: 327–342.
DOI: https://doi.org/10.5194/nhess-7-327-2007

Midya S.K., Pal S., Dutta R., Gole P.K., Chattopadhyay G., Karmakar S., Saha U. & Hazra S. (2020). A preliminary study on pre-monsoon summer thunderstorms using ground-based total lightning data over Gangetic West Bengal. *Indian Journal of Physics* **95**: 1–9.
DOI: https://doi.org/10.1007/s12648-020-01681-y

Moncrieff M.W. & Miller M.J. (1976). The dynamics and simulation of tropical cumulonimbus and squall lines. *Quarterly Journal of the Royal Meteorological Society* **102**(432): 373–394.
DOI: https://doi.org/10.1002/qj.49710243208

Nayak H.P. & Mandal M. (2014). Analysis of stability parameters in relation to precipitation associated with pre-monsoon thunderstorms over Kolkata India. *Journal of Earth System Science* **123**(4): 689–703.
DOI: https://doi.org/10.1007/s12040-014-0426-z

Neelin J.D. (1997). Implications of convective quasi-equilibria for the large-scale flow. In: *Physics and parameterization of moist atmospheric convection* (ed. R.K. Smith) pp. 413–446. Kluwer Academic Publishers, London, UK.
DOI: https://doi.org/10.1007/978-94-015-8828-7_17

Rafiuddin M., Uyeda H. & Islam Md. N. (2009). Simulation of characteristics of precipitation systems developed in Bangladesh during pre-monsoon and monsoon. *Proceedings of the 2nd International Conference on Water and Flood Management* (ICWFM-2009*)*, 15-17 March. Dhaka, Bangladesh, pp. 61–67.
DOI: https://doi.org/10.1002/joc.1949

Ravi N., Mohanty U.C., Madan O.P. & Paliwal R.K. (1999). Forecasting of thunderstorms in the pre-monsoon season at Delhi. *Meteorological Applications* **6**: 29–38.
DOI: https://doi.org/10.1002/met.19996103

Ratnam D.V., Otsuka Y., Sivavaraprasad G. & Dabbakuti J.K. (2019). Development of multivariate ionosphere TEC forecasting algorithm using linear time series model and ARMA over low-latitude GNSS station. Advances in Space Research **63**(9): 2848–2856.
DOI: https://doi.org/10.1016/j.asr.2018.03.024

Ray K., Sen B. & Sharma P. (2016). Monitoring convective activity over India during pre monsoon season-2013 under the SAARC STORM Project. *Vayu Mandal* **42**(2): 106–128.
DOI: http://imetsociety.org/wp-content/pdf/vayumandal/2016422/2016422_5.pdf

Rienecker M.M., Suarez M.J., Gelaro R., Todling R., Bacmeister J., Liu E. & Woollen J. (2011) MERRA: NASA's modern-era retrospective analysis for research and applications. *Journal of Climate* **24**(14): 3624–3648.
DOI: https://doi.org/10.1175/JCLI-D-11-00015.1

Roy Bhowmik S.K., Sen Roy S. & Kundu P.K. (2008). Analysis of large scale conditions associated with convection over the Indian monsoon region. *International Journal of Climatology* **28**: 797–821.
DOI: https://doi.org/10.1002/joc.1567

Schultz P. (1989). Relationships of several stability indices to convective weather events in Northeast Colorado. *Weather and Forecasting* **4**: 73–80.
DOI: https://doi.org/10.1175/1520-0434(1989)004<0073:ROSSIT>2.0.CO;2

Sen Roy S. & Sen Roy S. (2021). Spatial patterns of long-term trends in thunderstorms in India. *Natural Hazards* **107**: 1527–1540.
DOI: https://doi.org/10.1007/s11069-021-04644-6

Srinivasan V., Ramamurthy K. & Nene Y.R. (1973). Summer Nor'westers and Andhis and large scale convective activity over peninsula and central parts of the country. In: *Forecasting Manual Part - III: Discussion of Typical Synoptic Weather Situation.* India Meteorological Department, New Delhi, India.

The Hindu (2023). Lightning strikes claim 907 lives in 2022, highest toll in 14 years. Available at *https://www.thehindu.com/news/national/kerala/lightning-claims-907-lives-in-2022-highesttoll-in-14-years/article66330661.ece*.

Tyagi B. & Satyanarayana A.N.V. (2019). Assessment of difference in the atmospheric surface layer turbulence characteristics during thunderstorm and clear weather days over a tropical station. *SN Applied Sciences* **1**(8): 909.
DOI: https://doi.org/10.1007/s42452-019-0949-7

Tyagi B., Naresh Krishna V. & Satyanarayana A.N.V. (2011). Study of thermodynamic indices in forecasting pre-monsoon thunderstorms over Kolkata during STORM pilot phase 2006–2008. *Natural Hazards* **56**: 681–698.
DOI: https://doi.org/10.1007/s11069-010-9582-x

Wilks D.S. (2006). *Statistical Methods in the Atmospheric Sciences*. 2nd edition. Academic Press, London, UK.

Experimental procedure for screening rice cultivars for submergence tolerance

Seedlings impose submergence stress.
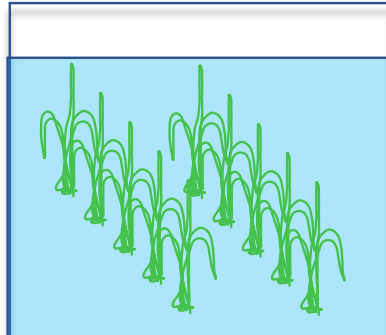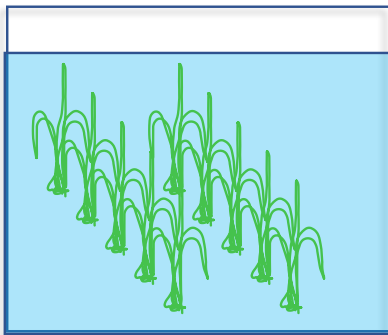
Seedlings for the control experiment.

*Control plant height
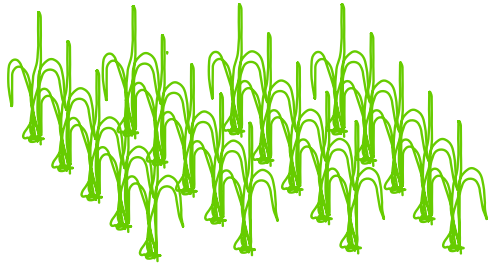
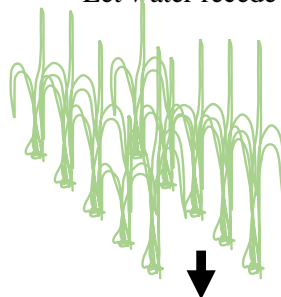*Two weeks-old seedlings were completely submerged.
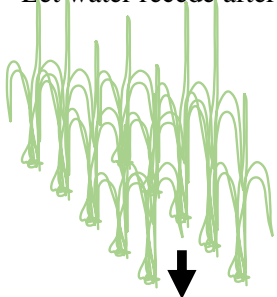*One set was submerged for nine days, and the other for 14 days.

9-day submergence
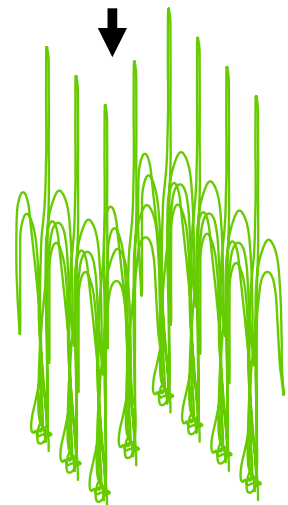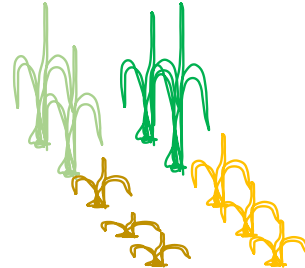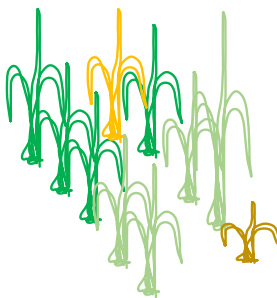
14-day submergence

*Let water recede after nine days

*Let water recede after 14 days.

Let plants survive for 14 days under the control environmental conditions (desubmerged plants).

*Survival percentage was calculated.
Plant height recording time is given by asterisk marks

*Control plants

JOURNAL OF THE
NATIONAL SCIENCE FOUNDATION OF SRI LANKA

GUIDANCE TO CONTRIBUTORS

Scope

The Journal of the National Science Foundation of Sri Lanka publishes the results of research in all aspects of Science and Technology. It is open for publication of Research Articles, Reviews, Research Communications and Correspondence.

IT related and other articles from formal sciences

The JNSF is a journal primarily devoted to natural sciences. It also considers for publication significant and novel contributions from formal sciences. Authors of emerging sub-disciplines of Computing and related areas such as Machine Learning, Artificial Intelligence and Data Sciences are requested to carefully adhere to the following guidelines when submitting manuscripts for this journal.

- Clear formulation of outcome-oriented **Research Objective/s** for targeted knowledge (sub)domain/s or (sub)discipline/s.
- Selection and comprehensive summarization of **appropriate Research Method/s** adopted to achieve the stated Research Objective/s.
- Sound reporting of research finding/s with Empirical Evaluation thereby arguing reliability, validity, and generalizability of research claim/s.

Categories of manuscripts

Research Articles: Research Articles are papers that present complete descriptions of original research. Research Articles should include an Abstract, Keywords, Introduction, Methodology, Results and Discussion, Conclusion and Recommendations where relevant. References should be prepared according to the "Guidelines for the preparation of manuscripts". Maximum length of the article should be limited to 25 pages with a word count of 10,000 including references, figures and tables. Any articles above this limit will be returned.

Reviews: Reviews are critical presentations on selected topics of Science or Technology. They should be well focused and organized and avoid general "textbook" style. As reviews are intended to be critical presentations on selected topics, reviewers need to have had substantial leadership in research supported by a publication track record in the areas covered by the review. A person/s wishing to submit a Review Article should obtain prior approval from the Editorial Board by submitting a concise summary of the intended article, along with a list of the author's publications in the related area (jnsf@nsf.gov.lk). Maximum length of the article should be limited to 40 pages with a word count of 12,000 including references, figures and tables. Any articles above this limit will be returned.

Research Communications: Research Communications are intended to communicate important new findings in a specific area of limited scope that are worthy of rapid dissemination among the scientific community. Authors are required to provide a statement justifying the suitability of the submission for a Research Communication. The article should include an Abstract, Keywords, Introduction, Methodology, Results & Discussion, Conclusion and References. Maximum length of the article should be limited to 10 pages with a word count of 2,500 including references, figures and tables. Any articles above this limit will be returned.

Correspondence: Correspondence will be accepted regarding one or more articles in the preceding four issues of the Journal, as well as Letters to the Editor. Articles covering important scientific events or any other news of interest to scientists, reviews of books of scientific nature, articles presenting views on issues related to science and scientific activity will also be considered. Publication will be made at the discretion of the Editor-in-Chief. Maximum length of the article should be limited to 05 pages with a word count of 1,500 including references, figures and tables. Any articles above this limit will be returned.

SUBMISSION OF MANUSCRIPT

Authors submitting articles to the JNSF should first create an account in the Sri Lanka Journals Online System (https://jnsfsl.sljol.info/). All manuscripts in MS Word format must be electronically submitted to the journal's online platform at https://jnsfsl.sljol.info/submit/start/. Submissions *via* emails are not encouraged. Please make sure that no author information is mentioned in the article submitted. The names and details of affiliations of all authors and contact information of the corresponding author must be fed into the system during the online submission process. Authors (at least the corresponding author) are required to provide their personal, validated ORCID ID (by obtaining an ORCID ID from https://orcid.org/) when submitting the manuscript. No change to the authors or order of authors will be accepted after the submission. All those who have made significant contributions should be listed as co-authors. The corresponding author should ensure that all contributing co-authors are included in the author list and have approved the final version of the paper and have agreed to its submission for publication.

All submissions should be in English. If the manuscript conforms to the guidelines specified, the date received will be the date that the manuscript was submitted to the online system.

Submissions are accepted for processing on the understanding that they will be reviewed and that they have not been submitted for publication elsewhere (including publication as a full paper or extended abstract as a part of Conference Proceedings). The JNSF does not accept manuscripts that have already been submitted to pre-print servers.

Suggesting potential reviewers by authors

The authors may suggest up to three names of referees when submitting their manuscript, in the Cover Letter space provided at the bottom of the page in the first stage of online submission. Referees should not be from the institution where the work was carried out and should not have been co-authors in previous publications. The address, institutional affiliation and e-mail of the suggested referees should be supplied. Please note that the JNSF is not bound to select all or any of the suggested referees for sending the manuscript for reviewing

Authorship

All authors designated as authors should be eligible for authorship. Those who have made a substantial contribution to the concept or design of the work; or acquisition, analysis or interpretation of data are recognized as Authors.

The corresponding author should be prompt and ensure adherence to timelines when responding to requests, queries and recommendation of reviewers conveyed by or on behalf of the Editor-in Chief and Editorial Board.

Supplementary materials

Any experimental data necessary to evaluate the claims made in the paper but not included in the paper should be provided as supplementary materials. Supplementary materials will be sent to the reviewers and published online with the manuscript if accepted. The supplementary materials should conform to Journal guidelines and should be uploaded as separate files. Authors should number Supplementary Tables and Figures as, for example, 'Supplementary Table S1'. Refer to each piece of supplementary material at the appropriate point(s) in the main article. Supplementary Materials may include description of the materials and methods, controls, or tabulated data presented in Tables or Figures, and programming codes.

Peer review

The manuscripts submitted to the JNSF will initially be screened by the Editorial Board and, if suitable, will be referred to at least two subject experts in the relevant field. The peer-review process of the JNSF is double-blind.

When revision of a manuscript has been requested, the revised manuscript should be submitted on or before the stated deadline. If the revised manuscript is not received on time, the manuscript will not be processed further. The authors' response to the comments of referees should be tabulated with the comment, response and the line number/s for reference. The decision of the Editorial Board shall be final.

Accepted papers are subject to editing. The date of acceptance will be the date when the Editorial Board has decided it to be acceptable for publication.

Article publication fee

A total of US$ 250 will be be levied for each accepted manuscript for publication, except when the corresponding author is affiliated to a Sri Lankan Institute, in two stages as explained below.

- A processing fee of US$ 20 will be levied for each manuscript at peer-review stage and the remaining US$ 230 will be charged for accepted manuscripts at the time of publication.

Payments can be made online via NSF Payment Portal (http://pg.nsf.gov.lk/)

Authors' declaration

When an article is accepted for publication, the authors are required to submit the Authors' Declaration signed by all the authors.

Copyright

Articles in JNSF are published under the Creative Commons License CC-BY-ND. This license permits use, distribution and reproduction of articles for commercial and non-commercial purposes, provided that the original work is properly cited and is not changed in anyway. The copyright of the article is with the National Science Foundation of Sri Lanka. Therefore, authors are requested to check with institution's copyright and publication policy before submitting an article to the JNSF. Authors secure the right to reproduce any material that has already been published or copyrighted elsewhere. When an article is accepted for publication, the authors are required to submit the Transfer of Copyright document signed by all the authors.

Post-publication corrections

The Editorial Board reserves the right to take action on publishing an erratum or corrigendum. If serious errors are identified in a published article, the Journal may consider a retraction or publishing a correction.

STRUCTURE OF MANUSCRIPT

Manuscript

The manuscript should be free of errors and prepared in single column, using double-spaced text of Times New Roman 12 font throughout with line numbers, leaving at least 2 cm margins on both sides, and liberal spacing at the top and bottom of each page. Pages should be numbered consecutively.

a. Style

The paper should be written clearly and concisely. The style of writing should conform to scholarly writing. Slang, jargon, unauthorized abbreviations, abbreviated phrasings should not be used. In general, the impersonal form should be used. Poor usage of language will result in rejection of the manuscript during initial screening.

b. Layout

Manuscripts other than review articles should be generally organized as follows: Title, Abstract, Keywords, Introduction, Methodology, Results and Discussion, Conclusions and Recommendations (where relevant), Acknowledgements and References. Pages should be arranged in the following order:

Title page should include the title of manuscript, and no author information should be mentioned in the title page. If a major part of the research has been published as an abstract in conference proceedings, it should be cited as a footnote on the title page. Authors must also indicate the **general and specific research area** of the manuscript in the title page. In order to highlight the significance of the manuscript, authors are required to provide the following highlights in brief. (1) Why was this study conducted? (2) What are the new findings? (3) Possible applications of the findings. Please limit your answers to 25-30 words for each.

Title: Should accurately and concisely reflect the contents of the article.

Running title: Should be a shortened title (limited to a maximum of 50 characters) that could be printed at the top of every other page of the Journal article.

Abstract: Should be between 200 - 250 words for full length articles and written as a single paragraph. It should not contain any references and should be able to stand on its own. It should outline objectives and methodology together with important results and conclusions. A Review Article should carry a summary of not more than 300 words.

Keywords: Include a maximum of six keywords, which may include the names of organisms (common or scientific), methods or other important words or phrases relevant to the study.

Introduction: This should state the reasons for performing the work with a brief review of related research studies in the context of the work described in the paper. Objectives of the study should be clearly stated.

Materials and Methods: This section should give the details of how you conducted your study. New methods may be described in detail with an indication of their limitations. Established methods can be mentioned with appropriate references. Sufficient details should be included to allow direct repetition of the work by others. Where human subjects are involved, they should be referred to by numbers or fictitious names. A paper reporting the results of investigations on human subjects or on animals must include a statement to the effect that the relevant national or other administrative and ethical guidelines have been adhered to, and a copy of the ethical clearance certificate should be submitted. Methods of statistical analyses used should be mentioned where relevant.

Results and Discussion: Results: the results should be concisely and logically presented. Repetition of the same results in figures, tables or text should be avoided.
Discussion: data essential for the conclusions emerging from the study should be discussed. Long, rambling discussions should be avoided. The discussion should deal with the interpretation of results. It should logically relate new findings to earlier ones. Unqualified statements and conclusions not completely supported by data should be avoided.
Molecular sequence data, such as gene or rDNA sequences, genome sequences, metagenomic sequences etc. must be deposited in a public molecular sequence repository, such as GenBank, that is part of the International Nucleotide Sequence Database Collaboration (INSDC). The accession numbers obtained must be cited in the text, Table or on Figures of phylogenetic trees of the manuscript.

Conclusion: The conclusion should be brief, highlight the outcomes of the study and should be aligned with the objectives of the study. It should not contain references.

Conflict of interest statement: All authors should include a statement on conflict of interest disclosing any financial or other substantive conflicts of interest that may be construed to influence the results or interpretation of their research. All sources of financial support for the project should be disclosed.

Acknowledgement: Should be brief and made for specific scientific, financial and technical assistance only. If a significant part of the research was performed in an institution other than in those indicated by the authors' affiliations given in the title page, this fact should be acknowledged. All those who have made substantial contribution to the research but do not qualify to be authors should be acknowledged.

References :
All research work of other authors, when used or referred to or cited, should be correctly acknowledged in the text and in the References.

Citing references in the text:
- References to the literature must be indicated in the text and tables as per the Author-Year System, by the author's last name and year, in parenthesis (i.e. Able, 1997) or (Able & Thompson, 1998).
- Citation to work by more than two authors should be abbreviated with the use of *et al*. (i.e. Able *et al*., 1997).
- Multiple publications by the same first author in the same year should be coded by letters, (i.e. Thompson, 1991a; b).
- Multiple citations should be made in chronological order and separated by a semi-colon, (i.e. Zimmerman *et al*., 1986; Able *et al*., 1997).
- Reference to unpublished work, work in preparation or work under review should be cited in italics as (*unpublished data*) or, with the author's initials and surname given; such works should not be included in the Reference section.
- Personal communications may be mentioned in the text with the date of communication as (*Personal communication, 2 June 2000*).

List of references:
- The list of References should be arranged in alphabetical order based on the last name of the first author.
- Names of all the authors should be given except when there are more than 10 authors. When there are more than 10 authors, only the name of the first author can be given followed by *et al*.
- All the initials of the author must be given after the last name and the year of publication should follow in parentheses.
- This should be followed by the full title of the referred publication.
- When journal articles are listed, the journal name should be given in full and in italics and followed by the volume number in bold type, issue number in parentheses and then the inclusive pages.
- Where there are several publications by the same author(s) and published in the same year they should be differentiated by adding a lower-case letter after the year. When books are listed, the order should be: author(s), year, book title, volume number, edition, pagination/ inclusive pages, publisher and place of publication. The book title should be in italics. When sections of a book are listed, the order should be: author(s) of chapter, year, title of the section, title of the book, edition, inclusive pages, publisher and place of publication.
- Digital object identifiers (DOIs) should be included for all references where available.
- References should only be cited as 'in press' if the paper has been accepted for publication.

Examples of correct forms of references are given below.

Journal Articles
Boutin C. & Harper J.L. (1991). A comparative study of the population dynamics of five species of *Veronica* in natural habitats. *Journal of Ecology* **79**(01): 199 – 221.
DOI: https://doi.org/10.2307/2260793

Books

Burnham K.P. & Anderson D.R. (2002). *Model Selection and Multimodal Inference*, 2nd edition, pp. 488. Springer Science and Business Media, Inc., New York, USA.

Book Chapters

Hinrichsen R.A. & Holmes E.E. (2009). Using multivariate state-space models to study spatial structure and dynamics. In: *Spatial Ecology* (eds. R.S. Cantrell, C. Cosner & S. Ruan), pp. 145 – 166. CRC/ Chapman Hall, Florida, USA.
DOI: https://doi.org/10.1201/9781420059861.ch8

Edited Books

KimatI H., Amorim L., Rezende J.A.M., Bergamin Filho A. & Camargo L.E.A. (eds.) (2005). *Manual de Fitopatologia*, volume 2. Doenças das Plantas Cultivadas, 4th edition. Ceres, São Paulo, Brazil.

Conference Papers

Weaver D. (2002). Implementation of a learning management system using an integrated approach to professional development. In: Winds of change in the sea of learning. *Proceedings of the 19th Annual Conference of the Australasian Society for Computers in Learning and Tertiary Education (ASCILITE)* (eds. A. Williamson, C. Gunn, A. Young & T. Clear), volume 2, Auckland, New Zealand, 8-11 December. Unitec Institute of Technology, Auckland, New Zealand, pp. 711-720.

Agency Publications

U.S. Census Bureau (2009). *World Population: 1950 – 2050*. U.S. Census Bureau, Washington DC, USA.
Department of Health (2008). *Health Inequalities: Progress and Next Step* (pdf). Department of Health, London, UK. Available at *http:// PublicationsPolicyAndGuidance/ DH _ 08 5307* , Accessed 9 June 2008.

Other

Robinson L.J. (2003) Spatial scale and depletion models of farmland birds in a fragmented landscape. *PhD thesis*, University of Reading, Reading, UK.
Efford M.G. (2008). Density 4.3: software for spatially explicit capture-recapture. Available at *http://www. otago.ac.nz/density* , Accessed 15 March 2009.

Abbreviations and Symbols: Unless common, these should be defined when first used, and not included in the abstract. The SI System of units should be used wherever possible. lf measurements were made in units other than SI, the data should be reported in the same units followed by SI units in brackets, e.g. 5290 ft (1610 m).

Formulae and Equations: Equations should be typewritten and quadruple spaced. They should be started on the left margin and the number placed in parentheses to the right of the equation.

Nomenclature: Scientific names of plants and animals should be printed in italics. In the first citation, genus, species and authority must be given. e.g. *Borassus flabellifer* Linn. In latter citations, the generic name may be abbreviated, for example, *B. flabellifer* L.

Tables and figures: Tables and Figures should be clear and intelligible and kept to a minimum, and should not repeat data available elsewhere in the paper. Any reproduction of illustrations, tabulations, pictures etc. in the manuscript should be acknowledged.

Tables: Tables should be numbered consecutively with Arabic numerals and placed at the appropriate position in the manuscript. If a Table must be continued, a second sheet should be used and all the headings repeated. The number of columns or rows in each Table should be minimized. Each Table should have a title, which makes its general meaning clear, without reference to the text. All Table columns should have explanatory headings. Units of measurement, if any, should be indicated in parentheses in the heading of each column. Vertical lines should not be used and horizontal lines should be used only in the heading and at the bottom of the table. Footnotes to Tables should be placed directly below the Table and should be indicated by superscript lower case italic letters ([a], [b], [c], etc.).

Figures: All illustrations are considered as figures, and each graph, drawing or photograph should be numbered consecutively with Arabic numerals and placed at the appropriate position in the manuscript. Any lettering to appear on the illustrations should be of a suitable size for reproduction and uniform lettering should be used in all the Figures of the manuscript. Scanned figures or photographs should be of high quality (**300 dpi**), to fit the proportions of the printed page (12 × 17 cm). Each figure should carry a legend so that the general meaning of the figure can be understood without reference to the text. Where magnifications are used, they should be stated.

Units of measurement

Length: km, m, mm, μm, nm
Area: ha, km^2, m^2
Capacity: kL, L, mL, μL
Volume: km^3, m^3, cm^3
Mass: t, kg, g, mg, μg

Time: year(s), month(s), wk(s), d(s), h, min, s
Concentration: M, mM, N, %, g/L, mg/L, ppm
Temperature: °C, K
Gravity: x g

Molecular weight: mol wt
Others: Radio-isotopes: 32P
Radiation dose: Bq
Oxidation-reduction potential: rH
Hydrogen ion concentration: pH